

THEORETICAL AND EXPERIMENTAL STUDIES ON  
THE INTERACTION OF NEUTRAL POLYMERS  
WITH CELL SURFACES

by

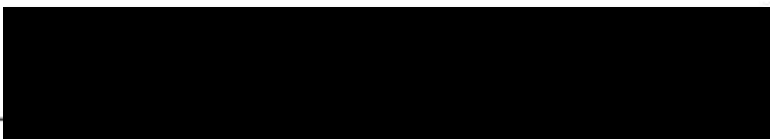
Donald Elliott Brooks, B.Sc., M.Sc.

A THESIS  
Presented to the Department of Biochemistry  
and the Graduate Division of the University of Oregon Medical School  
in partial fulfillment of  
the requirements for the degree of  
Doctor of Philosophy

March 1971

APPROVED:

  
\_\_\_\_\_  
(Professor in Charge of Thesis)

  
\_\_\_\_\_  
(Chairman, Graduate Council)

## ACKNOWLEDGEMENTS

It is a pleasure to be able to take this opportunity to thank:  
Dr. J. H. Fellman, and particularly my supervisor,  
Dr. G. V. F. Seaman, for helpful discussion, advice, and for the  
extraordinary compliment of treating me as a friend rather than a  
student; Lavelle Jackson, Bärbel Hagenberger and Matthias Kemeny  
for assistance with some of the experimental work, and for helping  
create the kind of indulgent atmosphere that made its completion so  
painless; Janet Cowan, for her cogent interpretation of a largely  
undecipherable manuscript; Dr. Alexander Silberberg, for invaluable  
comment and discussion; The New York Cancer Society, for financial  
support; and my wife, Timmie, for help, support, and an unparalleled  
ferocity of interest in the completion of this work.

To Timmie



## TABLE OF CONTENTS

<u>Chapter</u>	<u>Page</u>
1. INTRODUCTION	1
The Theory and Application of Electrokinetic Measurements on Cells	2
I. The Electrokinetic Equations	2
II. The Potential Energy of Repulsion Between Charged Plates	12
III. The Application of Electrophoretic Methods to the Study of Cell Surfaces	17
Polymer Adsorption and its Effect on the State of Aggregation of Dispersed Systems	23
I. Polymer Adsorption at the Solid-Liquid Interface	23
II. The Effect of Polymer Adsorption on the State of Aggregation of Dispersed Systems	27
III. Polymer Adsorption to Cells	32
The Effect of Neutral Polymers on the Electrokinetic Properties of Biological Surfaces	37
The Rheology of Erythrocyte Suspensions	38
Summary and Approach to Problem	53
2. PROPOSED MODELS FOR THE ERYTHROCYTE ZETA POTENTIAL INCREASE IN THE PRESENCE OF NEUTRAL POLYMERS	56
Models Based on Free Solution Properties of Neutral Polymers	56
Models Based on the Adsorption of Polymer at the Erythrocyte-Solution Interface	58
I. Ponder's Model: A Change of Dielectric Constant in the Interfacial Region	58
II. Rearrangement of the Interfacial Region to Expose Additional Charge Groups	66
III. Non-Specific Ion Adsorption to an Adsorbed Polymer Layer	71
IV. The Effect on Counterion Chemical Potentials of a Concentrated Surface Phase of Neutral Polymers	85
A. The Boltzmann Equation Modified for the Presence of a Concentrated Surface Phase of Neutral Polymer	86
B. The Theory of the Effect on the Zeta Potential of an Adsorbed Layer of Neutral Polymers	93

<u>Chapter</u>	<u>Page</u>
1. Permeable, Free Draining Layers of Finite Thickness and Constant Density	93
2. Partially Permeable, Partially Free Draining Adsorbed Layers	100
3. Permeable Partially Free Draining Layers	107
4. Adsorbed Layers of Non-Constant Density	112
The Effect of Neutral Adsorbed Layers on the Mobility-Zeta Potential Relationship	114
The Effect of Neutral Adsorbed Layers on the Electrostatic Potential Energy of Repulsion Between Two Flat Plates	117
Summary	124
 3. DIELECTRIC PROPERTIES OF AQUEOUS DEXTRAN SOLUTIONS	 127
Methods and Materials	129
Results and Discussion	133
 4. THE DEXTRAN-ERYTHROCYTE ADSORPTION ISOTHERM	 138
Materials	143
Methods	145
Results and Discussion	156
 5. ELECTROKINETIC STUDIES OF CELL AND PARTICLE SUSPENSIONS IN NEUTRAL POLYMER SOLUTIONS	 169
Methods and Materials	170
Results and Discussion	179
I. The Presence and Reversibility of Electrokinetic Effects in Particle-Neutral Polymer Systems	179
II. pH-Mobility Studies on Normal and Fixed Erythrocytes in Dextran	196
III. The Effect of Monovalent Anion and Cation Variation on the Zeta Potential of Erythrocytes in Dextran	201
IV. The Dependence of the Relative Zeta Potential on Ionic Strength	206
V. The Effect of Zeta Potential on the State of Aggregation of Normal Human Erythrocytes in Dextran Suspensions	218
VI. A Comparison Between the Adsorption and Electrokinetic Measurements	229

<u>Chapter</u>	<u>Page</u>
VII. Drainage Properties of Adsorbed Neutral Polymers	233
Summary	237
6 RHEOLOGICAL STUDIES ON SUSPENSIONS OF HUMAN ERYTHROCYTES IN DEXTRAN-SALINE SOLUTIONS	239
Methods and Materials	239
Results and Discussion	254
Summary	305
7. CONCLUSIONS	306
REFERENCES	311
APPENDICES	334
Appendix 1: The Use of Electrokinetic Measurements to Study the Properties of Neutral Adsorbed Layers	334
Appendix 2: The Effect on the Zeta Potential of a Vari- able Polymer Adsorption Factor	343

## LIST OF FIGURES

<u>Figure</u>	<u>Page</u>
2-1. The potential distribution adjacent to a charged surface in the presence of a rigid, impermeable layer.	60
2-2. The potential distribution adjacent to a charged surface in the presence of a rigid, permeable layer of low dielectric constant.	64
2-3. The absorption and difference spectra of dextran in aqueous salt solutions.	80
2-4. The potential distribution adjacent to a charged surface in the presence of a permeable adsorbed free draining layer.	95
2-5. Relative zeta potential vs. ionic strength for a free draining adsorbed layer.	99
2-6. The potential distribution adjacent to a charged surface in the presence of a partially permeable, partially free draining adsorbed layer.	101
2-7. The potential distribution adjacent to a charged surface in the presence of a permeable, partially free draining adsorbed layer.	109
2-8. Relative zeta potential vs. ionic strength for a partially free draining adsorbed layer. $\beta = 0.5$	111
2-9. Relative zeta potential vs. ionic strength for a partially free draining adsorbed layer. $\beta = 0.9$	111
2-10. Repulsive potential energy vs. $1/2$ the plate separation for two charged flat plates to which neutral polymer layers are adsorbed. $\beta = 0.6$	122
2-11. Repulsive potential energy vs. $1/2$ the plate separation for two charged flat plates to which neutral polymer layers are adsorbed. $\beta = 0.9$	123
3-1. Circuit diagram of the capacitance measurement assembly.	131

<u>Figure</u>	<u>Page</u>
4-1. Procedure used to measure the adsorption of $H^3$ -dextran to erythrocytes.	151
4-2. The dextran 77.6-erythrocyte adsorption isotherm.	160
4-3. Total supernatant activity vs. number of washes for erythrocytes exposed to $H^3$ -dextran 77.6.	163
5-1. Relative zeta potential vs. polymer concentration for erythrocytes in various neutral polymer /saline solutions.	181
5-2. Relative zeta potential vs. molecular weight for erythrocytes in various dextran fractions.	182
5-3. Relative zeta potential vs. dextran concentration for glutaraldehyde-fixed red cells (GRBC) and polystyrene latices (PSL).	183
5-4. The pH dependence of the viscosity-mobility product for normal and acetaldehyde-fixed erythrocytes in 4.39% dextran 77.6 in saline.	197
5-5. Relative zeta potential vs. ionic strength for normal (RBC) and acetaldehyde-fixed (HRBC) erythrocytes in 2.5% and 7.5% dextran 77.6.	207
5-6. Relative zeta potential vs. ionic strength for acetaldehyde-fixed erythrocytes in 2.5% and 7.05% dextran 41.	208
5-7. Relative zeta potential vs. ionic strength for acetaldehyde-fixed erythrocytes in 2.5% and 7.5% dextran 50.5.	208
5-8. Relative zeta potential vs. ionic strength for acetaldehyde-fixed erythrocytes in 2.5% and 7.5% dextran 147.	209
5-9. Relative zeta potential vs. ionic strength for acetaldehyde-fixed erythrocytes in 5% and 10% polyethylene glycol.	209

<u>Figure</u>	<u>Page</u>
5-10. Polymer adsorption factor $\beta$ vs. dextran concentration for normal erythrocytes in dextran/saline.	213
5-11. Polymer adsorption factor $\beta$ vs. dextran molecular weight for normal erythrocytes in dextran/saline.	214
5-12. Adsorbed layer thickness $d$ vs. square root of dextran molecular weight for acetaldehyde-fixed cells in dextran.	217
5-13. Degree of aggregation of normal erythrocytes induced by dextran fractions as a function of dextran concentration.	220
5-14. Degree of aggregation of normal erythrocytes induced by dextran fractions as a function of cellular zeta potential.	221
5-15. The dextran 77.6-erythrocyte adsorption isotherm on a linear coordinate system.	226
6-1. The Weissenberg Rheogoniometer.	246
6-2. Apparent viscosity vs. shear rate for erythrocytes suspended in saline/EDTA.	256
6-3. Apparent viscosity vs. shear rate for erythrocytes suspended in saline/EDTA/10% dextran 26.5.	257
6-4. Apparent viscosity vs. shear rate for erythrocytes suspended in saline/EDTA/3.00% dextran 41.	258
6-5. Apparent viscosity vs. shear rate for erythrocytes suspended in saline/EDTA/6.03% dextran 41.	259
6-6. Apparent viscosity vs. shear rate for erythrocytes suspended in saline/EDTA/10% dextran 41.	260
6-7. Apparent viscosity vs. shear rate for erythrocytes suspended in saline/EDTA/2.00% dextran 50.5.	261
6-8. Apparent viscosity vs. shear rate for erythrocytes suspended in saline/EDTA/3.00% dextran 50.5.	262

<u>Figure</u>	<u>Page</u>
6-9. Apparent viscosity vs. shear rate for erythrocytes suspended in saline/EDTA/4.01% dextran 50.5.	263
6-10. Apparent viscosity vs. shear rate for erythrocytes suspended in saline/EDTA/5.97% dextran 50.5.	264
6-11. Apparent viscosity vs. shear rate for erythrocytes suspended in saline/EDTA/10% dextran 50.5.	265
6-12. Apparent viscosity vs. shear rate for erythrocytes suspended in saline/EDTA/2.52% dextran 77.6.	266
6-13. Apparent viscosity vs. shear rate for erythrocytes suspended in saline/EDTA/5.00% dextran 77.6.	267
6-14. Apparent viscosity vs. shear rate for erythrocytes suspended in saline/EDTA/6.63% dextran 77.6.	268
6-15. Apparent viscosity vs. shear rate for erythrocytes suspended in saline/EDTA/7.58% dextran 77.6.	269
6-16. Apparent viscosity vs. shear rate for erythrocytes suspended in saline/EDTA/10% dextran 77.6.	270
6-17. Apparent viscosity vs. shear rate for erythrocytes suspended in saline/EDTA/3.48% dextran 110.	271
6-18. Apparent viscosity vs. shear rate for erythrocytes suspended in saline/EDTA/5.45% dextran 110.	272
6-19. Apparent viscosity vs. shear rate for erythrocytes suspended in saline/EDTA/7.44% dextran 110.	273
6-20. Apparent viscosity vs. shear rate for erythrocytes suspended in saline/EDTA/10% dextran 110.	274
6-21. Relative viscosity vs. hematocrit at $\dot{\gamma} = 0.68 \text{ sec}^{-1}$ for erythrocytes in saline/EDTA/dextran 41.	279
6-22. Relative viscosity vs. hematocrit at $\dot{\gamma} = 0.68 \text{ sec}^{-1}$ for erythrocytes in saline/EDTA/dextran 50.5.	280

<u>Figure</u>	<u>Page</u>
6-23. Relative viscosity vs. hematocrit at $\dot{\gamma} = 0.68 \text{ sec}^{-1}$ for erythrocytes in saline/EDTA/dextran 77.6.	281
6-24. Relative viscosity vs. hematocrit at $\dot{\gamma} = 0.68 \text{ sec}^{-1}$ for erythrocytes in saline/EDTA/dextran 110.	282
6-25. $R$ vs. $\eta_o / \eta_{sal}$ for disaggregated suspensions in various dextran fractions at $H = 50$ , $\dot{\gamma} = 0.68 \text{ sec}^{-1}$ .	288
6-26. $R$ vs. $Z$ for disaggregated suspensions in various dextran fractions at $H = 50$ , $\dot{\gamma} = 0.68 \text{ sec}^{-1}$ .	288
6-27. $R$ vs. $Z/Z_{crit}$ for aggregated suspensions in various dextran fractions at $H = 50$ , $\dot{\gamma} = 0.68 \text{ sec}^{-1}$ .	288
6-28. Relative viscosity vs. hematocrit at $\dot{\gamma} = 0.68 \text{ sec}^{-1}$ for erythrocytes in 10% dextran solutions in saline/EDTA.	294
6-29. Relative viscosity vs. hematocrit at $\dot{\gamma} = 17 \text{ sec}^{-1}$ for erythrocytes in saline/EDTA/dextran 41.	296
6-30. Relative viscosity vs. hematocrit at $\dot{\gamma} = 680 \text{ sec}^{-1}$ for erythrocytes in saline/EDTA/dextran 41.	296
6-31. Relative viscosity vs. hematocrit at $\dot{\gamma} = 17 \text{ sec}^{-1}$ for erythrocytes in saline/EDTA/dextran 50.5.	297
6-32. Relative viscosity vs. hematocrit at $\dot{\gamma} = 680 \text{ sec}^{-1}$ for erythrocytes in saline/EDTA/dextran 50.5.	297
6-33. Relative viscosity vs. hematocrit at $\dot{\gamma} = 17.1 \text{ sec}^{-1}$ for erythrocytes in saline/EDTA/dextran 77.6.	298
6-34. Relative viscosity vs. hematocrit at $\dot{\gamma} = 680 \text{ sec}^{-1}$ for erythrocytes in saline/EDTA/dextran 77.6.	298
6-35. Relative viscosity vs. hematocrit at $\dot{\gamma} = 17.1 \text{ sec}^{-1}$ for erythrocytes in saline/EDTA/dextran 110.	299
6-36. Relative viscosity vs. hematocrit at $\dot{\gamma} = 680 \text{ sec}^{-1}$ for erythrocytes in saline/EDTA/dextran 110.	299



<u>Figure</u>	<u>Page</u>
6-37. R vs. $\eta_o/\eta_{sal}$ for disaggregated suspensions in various dextran fractions at $H = 50$ , $\dot{\gamma} = 17 \text{ sec}^{-1}$ .	301
6-38. R vs. $\eta_o/\eta_{sal}$ for disaggregated suspensions in various dextran fractions at $H = 50$ , $\dot{\gamma} = 680 \text{ sec}^{-1}$ .	301
6-39. Relative viscosity vs. hematocrit at $\dot{\gamma} = 17 \text{ sec}^{-1}$ for erythrocytes in 10% dextran solutions in saline/EDTA.	302
6-40. Relative viscosity vs. hematocrit at $\dot{\gamma} = 680 \text{ sec}^{-1}$ for erythrocytes in 10% dextran solutions in saline/EDTA.	302

## LIST OF TABLES

Table	<u>Page</u>
2-1. The apparent binding of NaCl or H <sub>2</sub> O to dextran or PEG by solubility measurements.	76
3-1. Two terminal data for standard dielectrics used to calculate stray capacitance and air capacitance of cell.	134
3-2. The dielectric constants of aqueous salt-free dextran solutions.	135
5-1. Characteristics of dextran fractions.	171
5-2. Electrokinetic results for various particle-neutral polymer systems.	184
5-3. Relative zeta potential of normal human erythrocytes in 5% dextran 110 and various monovalent anions.	203
5-4. Relative zeta potential of acetaldehyde-fixed human erythrocytes in 5% dextran 77.6 and various monovalent cations.	203
5-5. Summary of model parameters of best fit to Z(c) data.	215
<u>Appendix Table</u>	
A2-1. Relative zeta potential Z(c, d) for $\beta(x) = 1 - x/d$ .	351

## CHAPTER 1

### INTRODUCTION

This thesis is concerned with the interactions of neutral polymers, in particular dextrans, with erythrocyte surfaces. The concern is focussed on two general areas:

- (i) the effects of neutral polymers on the electrokinetic properties of red cells, and therefore on the electrostatic interactions between these cells
- (ii) the effects of neutral polymers on the rheological behavior of erythrocyte suspensions and the possible influence of the cellular electrokinetic potential on this behavior.

The interest in these problems was initiated by two observations.

- (i) Ponder (1) reported in 1957 that the electrokinetically-determined surface potentials of human erythrocytes and platelets were increased when dextran was added to the suspending medium.
- (ii) Early work from this laboratory (2) demonstrated that the relative viscosities of normal human erythrocyte suspensions were markedly reduced when high concentrations (10% w/v) of low molecular weight dextran were included in the simple ionic suspending media.

The central questions with which the present work is involved, then, are what is the mechanism by which a neutral polymer can increase the surface potential of cells, and what connection, if any, does this increase have with the dextran-induced changes in the rheology of their suspensions. As an introduction to the work that follows, this chapter will outline the principles of electrokinetic measurements, describe the human erythrocyte surface region as characterized by electrophoresis, give the general properties of polymer adsorption and the effects of such adsorption on the state of aggregation of dispersed systems, discuss previous work on the electrokinetic changes neutral polymers induce in cells, and finally summarize briefly the research done to date on the rheology of erythrocyte suspensions.

### The Theory and Application of Electrokinetic Measurements on Cells

#### I. The Electrokinetic Equations

The physical bases of the electrokinetic phenomena of interest here lie in the interactions among a particle bearing a surface charge, the ions in solution which are attracted or repelled by that surface charge, and an externally applied electric field. The surface charge produces an electrostatic potential at the solid-solution interface which influences the distribution of ionic charges near the surface.

Ions of unlike sign to the surface charge (counterions) tend to accumulate near the surface, while those of like sign (co-ions) are repelled. Under the influence of thermal agitation considerable mixing takes place. The result is a diffuse layer consisting predominantly of counterions which extends some distance into solution, the distance being determined by the concentration and valence of the ions. This layer of ions is called the counterion double layer. The greater the concentration and/or valence of the counterions, the nearer to the surface is the potential due to the surface charge reduced to zero, and the thinner is the double layer. When the charged particle-double layer system is placed in an external field, the particle and double layer, being of opposite sign, tend to move in opposite directions. The result is that the particle moves in the direction dictated by its surface charge (electrophoresis), but with a terminal velocity reduced by the viscous drag exerted on it as a result of the tendency of the double layer to move in the opposite direction. The lower the ionic concentration in the bulk phase, the more diffuse the double layer, the less the drag exerted by it on the particle, and the greater the electrophoretic velocity. This velocity divided by the magnitude of the applied electric field strength is defined as the electrophoretic mobility, the experimentally determined quantity characteristic of the surface potential and the ionic atmosphere around the particle.

The quantitative relationship between the electrophoretic

mobility and the electrostatic potential at the point near or at the surface across which shearing takes place is due to von Smoluchowski (3). The derivations of this and the other electrokinetic equations have been conveniently summarized by several authors (4, 5, 6, 7).

Consider the motion of the fluid in a diffuse double layer relative to a smooth non-conducting surface bearing a fixed surface charge when an electric field  $E$  is applied tangentially to the surface. The field exerts a force  $E\rho(x)dx$  on a fluid element of thickness  $dx$  and unit area containing a charge density  $\rho(x)$ . This force is opposed by the viscous force retarding the motion of the lamina given by  $[\eta \frac{dv}{dx}]_{x+dx} - [\eta \frac{dv}{dx}]_x$ , where  $\eta$  and  $\frac{dv}{dx}$  are the viscosity and velocity gradient respectively at distances  $x$  and  $(x+dx)$  from the surface. When the fluid has attained a terminal velocity  $v$ , the sum of these forces is zero, giving:

$$E\rho(x)dx + \frac{d}{dx}[\eta(x) \frac{dv}{dx}]dx = 0 \quad (1-1)$$

The charge density is related to the potential at any point  $x$ ,  $\psi(x)$ , by Poisson's equation (assuming that the dielectric constant  $\epsilon$  does not depend on  $x$ ), which in electrostatic units is (8):

$$\frac{d^2 \psi(x)}{dx^2} = -\frac{4\pi}{\epsilon} \rho(x) \quad (1-2)$$

Substituting for  $\rho(x)$  and integrating once with respect to  $x$  between  $x$  and  $\infty$ :

$$\frac{\epsilon E}{4\pi} \frac{d\psi(x)}{dx} = \eta(x) \frac{dv}{dx} \quad (1-3)$$

since both  $\frac{d\psi(x)}{dx}$  and  $\frac{dv}{dx}$  approach zero as  $x \rightarrow \infty$ . Integrating a second time between  $x = 0$  and  $x = \infty$ :

$$\int_0^{\infty} \frac{dv}{dx} dx = \frac{\epsilon E}{4\pi} \int_0^{\infty} \frac{1}{\eta(x)} \frac{d\psi(x)}{dx} dx$$

Setting  $-v(0) = v_e$ , the velocity of the fluid relative to the surface, gives:

$$\left(\frac{v_e}{E}\right) \equiv U = \frac{\epsilon}{4\pi} \int_0^{\zeta} \frac{d\psi(x)}{\eta(x)} \quad (1-4)$$

where  $U$  is the electrophoretic mobility, and  $\psi(0) \equiv \zeta$ , the zeta potential. So long as the viscosity does not vary with  $x$ , the Smoluchowski equation relating the mobility to the surface potential is then obtained:

$$U = \frac{\epsilon \zeta}{4\pi \eta} \quad (1-5)$$

As may be seen from (1-4), the zeta potential is the potential at the surface of shear, the plane which separates the stationary and moving phases, here assumed to coincide with the smooth surface. That the

shear plane and the surface coincide, however, is an assumption. Hence, the information provided by the mobility relates only to the potential at the shear plane, and not necessarily to that at the charged surface.

The assumption that the viscosity of the ionic solutions does not vary throughout the extent of the double layer has been examined by Lyklema and Overbeek (9); these authors calculated the effect of the high electric field near the charged surface on the viscosity of water. For the low zeta potentials measured for cells, however, the effect is negligible, and in any event, their estimates of the viscoelectric effect have been criticized as being too high (10, 11).

The derivation of (1-5) given above applies only to surfaces which are everywhere parallel to the applied electric field. Henry (12) has given the derivation of an equivalent relationship for spherical particles, however, which reduces to the above equation in the limit of non-conducting particles whose radius is large compared to the double layer thickness. These conditions will virtually always apply to cells due to their size and the insulating properties of the membrane (13). Furthermore, that (1-5) applies regardless of the shape of the particle (providing that the radii of any of the areas on the particle are again much larger than the double layer thickness) has recently been shown rigorously (14). Equation (1-5), then, may be applied with some confidence to the results of cell electrophoresis.



The electrophoretic mobility, then, gives a measure of the electrostatic potential at the shear plane, which is assumed to equal the surface potential. The relationship between the surface potential and the charge density which produces it was derived by Gouy (15) and Chapman (16). These authors were the first to introduce the concept of the diffuse double layer surrounding a charged particle in an ionic solution. The assumptions under which the following treatment applies are:

- (i) the surface is assumed to be flat, of infinite extent, to bear only a fixed charge evenly smeared out over the surface, and is assumed to be impenetrable to ions
- (ii) the ions in the double layer are assumed to be point charges governed by the Boltzmann distribution
- (iii) the surface charge is assumed to be small enough that the potential  $\psi(x)$  obeys  $\left[ \frac{ze\psi(x)}{kT} \right] \ll 1$  throughout the double layer, where  $e$  = electronic charge,  $z$  = ionic valence,  $k$  = Boltzmann's constant and  $T$  = absolute temperature
- (iv) the dielectric constant is assumed to be that of the bulk liquid throughout the double layer
- (v) the solvent affects the ionic distribution only through the dielectric constant

The charge density at some distance  $x$  from the surface,  $\rho(x)$ , is related to the potential at that point by the Poisson equation in one

dimension:

$$\frac{d^2 \psi(x)}{dx^2} = \frac{-4\pi}{\epsilon} \rho(x) \quad (1-2)$$

The charges at  $x$  consist only of the dissolved ions, so:

$$\rho(x) = e \sum_i z_i n_i(x) \quad (1-6)$$

where

$z_i$  = valence of  $i$ th ion type

$n_i(x)$  = number of  $i$ th type ions per  $\text{cm}^3$  at point  $x$

The magnitudes of the ion concentrations in regions near the surface where the potential is significant, relative to their concentrations far enough away from the surface that the potential is zero, are given by the Boltzmann distribution:

$$n_i(x) = n_{i0} \exp\left[\frac{-z_i e \psi(x)}{kT}\right] \quad (1-7)$$

where  $n_{i0}$  is the number of  $i$ th type ions per  $\text{cm}^3$  in the bulk solution. Combining (1-2), (1-6) and (1-7) gives the Poisson-Boltzmann equation:

$$\frac{d^2 \psi(x)}{dx^2} = \frac{-4\pi e}{\epsilon} \sum_i z_i n_{i0} \exp\left[\frac{-z_i e \psi(x)}{kT}\right] \quad (1-8)$$

Considering now only a single symmetrical electrolyte to be present, (1-8) may be written:

$$\frac{d^2 \psi(x)}{dx^2} = \frac{8\pi z e n_0}{\epsilon} \sinh\left[\frac{ze\psi(x)}{kT}\right] \quad (1-9)$$

where the hyperbolic sine is defined by  $\sinh x = \frac{e^x - e^{-x}}{2}$ .

Applying assumption (iii), the exponentials may be expanded to give, to order of  $\left[\frac{ze\psi(x)}{kT}\right]^3$ :

$$\frac{d^2 \psi(x)}{dx^2} = \kappa^2 \psi(x) \quad (1-10)$$

where  $\kappa = \left[\frac{8\pi z^2 e^2 n_0}{\epsilon kT}\right]^{1/2}$  is the usual Debye-Hückel parameter.

The general solution of (1-10) is given by (17):

$$\psi(x) = a \exp(\kappa x) + b \exp(-\kappa x) \quad (1-11)$$

The boundary condition that  $\psi(x) \rightarrow 0$  as  $x \rightarrow \infty$  demands that  $a = 0$ . Setting  $x = 0$  gives  $b = \psi(0)$ , the surface potential, so (1-10) has the solution:

$$\psi(x) = \psi(0) \exp(-\kappa x) \quad (1-12)$$

From (1-12) it is seen that at the point  $x = 1/\kappa$ , the potential has decreased from  $\psi(0)$  to  $\psi(0) \exp(-1) = 0.37\psi(0)$ . A relative

decrease of this degree provides a convenient definition of the thickness of the double layer, equal to  $1/\kappa$ . The parameter  $\kappa$  can be expressed in terms of  $c$ , the molar ionic concentration by:

$$\kappa = \left[ \frac{8\pi e^2 N_A c z^2}{1000 \epsilon k T} \right]^{1/2} \quad (1-13)$$

or in terms of  $\mu$ , the ionic strength by:

$$\kappa = \left[ \frac{8\pi e^2 N_A \mu}{1000 \epsilon k T} \right]^{1/2} \quad (1-14)$$

where  $\mu \equiv \frac{1}{2} \sum_i c_i z_i^2$ ,  $c_i$  = molar concentration of  $i$ th ion, and

$N_A$  = Avogadro's number. It is seen from (1-13) that  $1/\kappa$  expresses quantitatively the properties ascribed to the double layer thickness earlier in this chapter. Thus,  $1/\kappa \propto \mu^{-1/2}$ , so that a decrease in either ionic valence or concentration results in an expansion of the double layer.

To derive an expression for the charge density, the electro-neutrality condition is invoked in the form:

$$\sigma A + \int_0^\infty \rho dV = 0 \quad (1-15)$$

where  $\sigma$  is the surface charge (esu) per unit area,  $A$  is the area of the surface and  $dV$  is a volume element =  $A dx$ . That is, the

total net space charge must equal but be of opposite sign to the surface charge. Substituting from (1-2), differentiating (1-12) and applying the boundary condition  $\frac{d\psi(x)}{dx} \rightarrow 0$  as  $x \rightarrow \infty$ , gives:

$$\begin{aligned}\sigma &= - \int_0^{\infty} \rho(x) dx \\ &= \frac{\epsilon}{4\pi} \int_0^{\infty} \frac{d^2\psi(x)}{dx^2} dx \\ &= \frac{-\epsilon}{4\pi} \frac{d\psi(0)}{dx}\end{aligned}$$

$$\therefore \sigma = \frac{\kappa\epsilon\psi(0)}{4\pi} \quad (1-16)$$

If again the assumption is made that the surface and zeta potentials are equal:

$$\sigma = \frac{\kappa\epsilon\zeta}{4\pi} \quad (1-17)$$

Equation (1-17) shows that for a fixed surface charge density the zeta potential depends on the thickness of the double layer,  $1/\kappa$ , and therefore on the ionic strength. The lower the ionic strength, the thicker the double layer and the greater the zeta potential. Combining (1-17) with (1-5) gives the approximate relationship between the mobility and charge density:

$$\eta U = \frac{\sigma}{\kappa} \quad (1-18)$$

Again, the further the double layer extends out into the bulk phase away from the surface, the greater the mobility of a fixed charge system.

If the approximation  $[\frac{ze\psi(x)}{kT}] \ll 1$  does not hold, equation (1-9) may still be integrated exactly to give, for a symmetrical electrolyte, (4):

$$\psi(x) = \frac{2kT}{ze} \ln \left[ \frac{1 + \gamma \exp(-\kappa x)}{1 - \gamma \exp(-\kappa x)} \right] \quad (1-19)$$

where

$$\gamma = \frac{\exp\left[\frac{ze\psi(0)}{2kT}\right] - 1}{\exp\left[\frac{ze\psi(0)}{2kT}\right] + 1}$$

and for the charge density, from (1-16):

$$\sigma = \left[ \frac{2\epsilon kT n_0}{\pi} \right]^{1/2} \sinh\left[\frac{ze\psi(0)}{2kT}\right] \quad (1-20)$$

## II. The Potential Energy of Repulsion Between Charged Plates

One of the important applications of the results of electrophoretic measurements on particles is in the study of suspension stability. Interaction between the double layers of two identical particles results in the repulsion of these particles when the double layers overlap. If this repulsion is strong enough to overcome the dispersion forces that mutually attract the particles, the particles

will not aggregate and the suspension will be stable.

Since the repulsion is generated by the overlap of counterion double layers of adjacent particles, the potential energy of repulsion can be expected to depend on the surface and solution properties that determine the magnitude and extent of the potential and ion distribution near the surface. Derivations of the expression for the repulsive potential energy between two charged plates have been given by several authors (18, 19, 20); that reproduced here is due to Derjaguin (19) as quoted by Overbeek (20).

Consider two infinite flat charged plates in contact with a reservoir at zero potential, containing  $n_0$  molecules of symmetrical electrolyte per  $\text{cm}^3$ , in which the hydrostatic pressure is  $p_b$ . Assume that the plates are held at a separation  $2s$  by a pressure  $P$ . This pressure is necessary to counteract the osmotic forces tending to dilute the counterion accumulation and separate the plates. In equilibrium, the hydrostatic and electrical forces acting on the ionic space charge must equal zero:

$$\frac{dp(x)}{dx} + \rho(x) \frac{d\phi(x)}{dx} = 0 \quad (1-21)$$

where  $\frac{dp(x)}{dx}$  is the pressure gradient at some point  $x$ , and  $\phi(x)$  is the total electrostatic potential at that point. Considering the region between the plates,  $\rho(x)$  may be expressed by (1-2) to give:

$$\frac{dp(x)}{dx} - \frac{\epsilon}{4\pi} \frac{d^2\phi(x)}{dx^2} \frac{d\phi(x)}{dx} = 0 \quad (1-22)$$

Integrating:

$$p(x) - \frac{\epsilon}{8\pi} \left[ \frac{d\phi(x)}{dx} \right]^2 = \text{constant} \quad (1-23)$$

At  $x = s$ , midway between the plates, the potential gradient  $\frac{d\phi}{dx}$  must vanish, because the potential must be symmetrical about  $x = s$ . Therefore, the right hand side (RHS) of (1-23) must be  $p(s)$ , the pressure midway between the plates tending to force them apart. The difference between  $p(s)$  and  $p_b$ , the pressure in the bulk reservoir must be  $P$ , the net "disjoining" pressure repelling the plates. Hence,  $P = p(s) - p_b$ , which may be evaluated by integrating  $dp(x)$  between the point in solution where  $\phi(x) = \phi(s)$  and the bulk reservoir, where  $\phi(x) = 0$ :

$$P(s) = \int_{\text{bulk}}^s dp(x) \quad (1-24)$$

Substituting from (1-21):

$$P(s) = - \int_0^{\phi(s)} \rho(x) d\phi(x) \quad (1-25)$$

The space charge density  $\rho(x)$  is again determined by the Boltzmann distribution, which gives from (1-6) and (1-7):



$$\rho(x) = -2ze n_o \sinh\left[\frac{ze\phi(x)}{kT}\right] \quad (1-26)$$

Combining (1-25) and (1-26), and integrating gives for the force per unit area tending to separate the plates:

$$P(s) = 2n_o kT \left[ \cosh\left[\frac{ze\phi(s)}{kT}\right] - 1 \right] \quad (1-27)$$

Approximating  $\cosh x \sim 1 + \frac{x^2}{2}$ , good to 4th order in  $x$ , (1-27)

becomes:

$$P(s) \sim \frac{n_o z^2 e^2}{kT} \phi^2(s) \quad (1-28)$$

The repulsive potential energy associated with this disjoining pressure,  $V_R$ , is given by twice the work required to bring one plate up from  $\infty$  to a distance  $s$  from the ultimate midpoint of the plate separation:

$$V_R = -2 \int_{\infty}^s P(s) ds \quad (1-29)$$

To carry out this integration, the dependence of  $\phi(s)$  on  $x$  must be specified. By definition,  $\phi(s)$  is the total electrostatic potential at the point midway between the plates. If the plates are far enough apart that the potentials in the double layers are small at  $s$ ,  $\phi(s)$  is simply given by the sum of the potentials  $\psi(x)$  of (1-12) or (1-19)

evaluated at  $x = s$ . Under the assumptions of small surface potentials, then, applying (1-12) gives:

$$\phi(s) \sim 2\psi(s) = 2\psi(0) \exp(-\kappa s) \quad (1-30)$$

Substituting (1-28) and (1-30) into (1-29) and integrating gives for the potential energy of repulsion per unit area of surface:

$$V_R = \frac{4e^2 n_o \psi^2(0)}{\kappa kT} \exp(-2\kappa s) \quad (1-31)$$

More exact expressions may be derived for  $V_R$  (20), but (1-31) is sufficient to point out its general properties.  $V_R$  is seen to depend on the square of the surface potential (or the zeta potential, making the usual assumption that  $\psi(0) = \zeta$ ) of the two plates. Further, it is seen to depend strongly on the double layer thickness,  $1/\kappa$ . Expansion of the double layer results in an increase in  $V_R$  both through the multiplicative and exponential terms. Measurement of the zeta potential through the electrophoretic mobility, then, allows an estimate to be made of the repulsive force and energy per unit area acting between the particles.

The derivation of equation (1-31) applies to flat surfaces which are large enough that edge effects are not important. For spherical particles no exact expression is available for  $V_R$ , but an approximate expression may be derived by treating the surfaces of the

spheres as series of concentric flat rings (19). These rings are then assumed to interact as flat surfaces, and the flat plate equations applied to each ring-ring interaction. Integration over the surface of the spheres then sums these interactions to give an expression for  $V_R$ . Since the basic interaction energy is still based on the flat plate equation, the qualitative effects of  $\psi(0) = \zeta$  and  $1/\kappa$  on  $V_R$  will be the same as described above.

### III. The Application of Electrophoretic Methods to the Study of Cell Surfaces

As was discussed in Section I, the zeta potential reflects the charge character at the plane of shear, a plane near or at the surface, within which no flow occurs. Changes in  $\zeta$ , then, reflect changes in a highly localized, if slightly ill-defined, region of the particle. Herein lies the strength of the electrophoretic method, in that only changes in surface parameters are detected. Hence, as applied to cells, electrophoresis allows one to study in virtual isolation charge structures at the periphery of the cell, structures which can be expected to be important in the interactions of a cell with its milieu.

In the derivation of the electrokinetic equations, the surface of shear was assumed to be impenetrable to counterions. Cells, however, are known to be permeable to ions and in fact their peripheral region has been likened more to a sieve than a solid surface (21). As

first discussed by Mitchell (22) and Heard and Seaman (23), and examined quantitatively by Haydon (24), the availability of regions interior to the shear plane to counterions can modify the observed zeta potential. Charge groups within the membrane can be detected by electrophoresis if they are roughly within a double layer thickness of the shear plane ( $\sim 8 \text{ \AA}$  in 0.145 M NaCl). In such a circumstance, the potential due to buried groups is not damped out by counterions over the distance between the internal charges and the shear plane, so some fraction of the potential due to buried charges still contributes additively to  $\zeta$ . The lower the ionic strength, the farther the double layer extends behind the shear plane, and the deeper into the membrane will the zeta potential "see." Even taking this porosity into account, however, the charge density indicated by the zeta potential is probably located within 10 or 20  $\text{\AA}$  of the shear plane in physiological saline.

An analysis of the effect of porosity on the charge density-zeta potential relationship has been given by Haydon (24). Assuming that the restricted space available to counterions within the membrane can be treated to first order in the same way as ionic self-exclusion effects, Haydon gives for the charge density  $\sigma(a)$  (for small potentials and 1:1 electrolyte):

$$\sigma(a) = (1 + \sqrt{1-a}) \frac{\kappa \epsilon \zeta}{4\pi} \quad (1-32)$$

where  $\alpha$  is defined as the fraction of total space within the shear plane which is not available to counterions and is assumed not to vary with distance from the surface. For  $\alpha < 1$ , then, equation (1-17) will underestimate the absolute value of the charge density by up to a factor of two. Unfortunately, however, no estimates of  $\alpha$ , which would allow (1-32) to be applied, are available. Attempts to measure  $\alpha$  have been unsuccessful because no independent measure of  $\sigma$  has yet been made for cells (25).

Although the absolute value of the surface charge density of cells can only be estimated with some ambiguity from zeta potential measurements, there are few other theoretical difficulties inherent in the application of the electrophoretic equations to the results of cell electrophoresis (26). Brinton and Lauffer (27) have questioned the use of (1-5) on the grounds that the local radii of curvature of portions of cell surfaces may be so small that its use is invalid. However, since changes in shape and radius of curvature have been shown to have no effect on red cell mobility (28, 29) it would seem these objections do not apply.

Because of the localization of the region under observation to the extreme periphery, electrophoretic methods have been used extensively in the study of cell surface properties. No attempt will be made here to summarize the field of cell electrophoresis, as extensive reviews are available (27, 29, 30, 31, 32). However, a brief description

of the properties of the human erythrocyte peripheral region will be given, since this is the cell on which the majority of the work presented in this thesis has been done.

At physiological ionic strength ( $0.145 \text{ gm-ions l}^{-1}$ ), all detectable charge groups at the shear plane of the human erythrocyte are anionic (33). The electrophoretic mobility in  $0.145 \text{ M NaCl}$  at  $25^\circ\text{C}$  is  $-1.08 \pm 0.03 \mu \text{ s}^{-1} \text{ v}^{-1} \text{ cm}$ , implying a zeta potential, calculated from (1-5) of  $\zeta = -14.1 \text{ mv} = -4.70 \times 10^{-5} \text{ statvolts}$ . The mobility for normal erythrocytes is constant between pH 4.5 and 9.0, the cells adsorbing detectable amounts of hemolysate outside that pH range which alters their electrokinetic properties (23). Fixation of the cells with acetaldehyde increases the range of pH over which the cells exhibit electrophoretic reversibility without altering their electrokinetic properties in the region where normal cells are stable (34). The mobility of fixed cells drops precipitously to zero below pH 4 indicating the presence of an ionogenic group with a  $\text{pK}_a \sim 2.6$ . Treatment of erythrocytes with neuraminidase (E. C. 3.2.1.18) decreases the mobility  $\sim 60\%$  (36). This observation, coupled with the isolation of N-acetylneuraminic acid from the medium in which the neuraminidase treatment took place, and knowledge of the enzyme specificity, was sufficient to identify sialic acid as the group responsible for the principal electrokinetic charge on the human erythrocyte (35, 36). The enzyme is believed to not penetrate the cell, and has

been shown to release virtually all of the sialic acid in the membrane (36). Approximately twice as much sialic acid (per cell) can be detected in the enzyme supernatant as is estimated from the calculated decrease in charge density using equation (1-17) (35). The discrepancy may be due to the assumption in the calculation that no counterion penetration occurs behind the charge plane, or it may be that some of the membrane sialic acid is located well behind the shear plane and is undetected by electrophoresis at physiological ionic strength.

The increased apparent  $pK_a$  ( $\sim 3.4$ ) of the groups remaining after neuraminidase treatment is consistent with the suggestion that these are  $\alpha$ -carboxyl groups of protein-bound amino acids (33). That the mobility of normal and fixed red cells does not depend on the monovalent anion present in the suspending medium (23), and that the mobility of esterified fixed cells is zero (33) indicates that none of the surface charge of the human red cell is due to anion adsorption or cation desorption. This property of cell surfaces renders them somewhat unique, most other surfaces acquiring at least some charge by the ion rearrangement mechanism (5). The lack of effect of aldehyde treatment on the erythrocyte mobility at all ionic strengths tested (34) indicates that there are relatively few free amino groups located within the peripheral region. Attempts to measure the  $\alpha$ -factor of equation (1-32) by obtaining an independent estimate of  $\sigma$  through titration of surface carboxyls with methylene blue have been unsuccessful

(25). Apparently methylene blue adsorbs only to non-neuraminidase susceptible acidic groups (33).

Application of equation (1-17) to electrophoretic data at physiological ionic strengths has produced the estimate that there are  $\sim 1 \times 10^7$  negative groups within  $\sim 8 \text{ \AA}$  of the shear plane of human erythrocytes at neutral pH (33). Approximately 62% of these are the carboxylic acid groups of N-acetylneuraminic acid, and the remainder have an average  $pK_a$  of 3.35 and may be due to the  $\alpha$ -carboxyl's of protein-bound amino acids. There are probably less than  $2-3 \times 10^5$  free amino groups in this region, this figure representing the relative accuracy with which cellular electrophoretic mobility determinations may be made ( $\sim \pm 3\%$ ).

The majority of the electrophoretic work on erythrocytes has been done at high (physiological) ionic strength. At lower ionic strengths, in media kept isotonic with sorbitol or glucose, the normal red cell is stable over a decreasingly narrow range of pH (23). Furthermore, the net charge density decreases below 0.02-0.05 M NaCl (25, 37). Since none of the surface charge is due to adsorbed anions, the most reasonable explanation for the decrease is that positively charged groups deep in the membrane are being detected at the plane of shear due to the expanded double layer. The low ionic strength apparent charge density is unaltered by aldehyde treatment, however, indicating that the positive group(s) are probably not



primary amines. Neither are they due to any group with a  $pK_a$  between 2.9 and 10.5, since the apparent charge density is constant over this pH range at low ( $0.0029 \text{ gm-ions l}^{-1}$ ) ionic strengths. Hence, while the charge groups detected by electrophoresis at high ionic strengths are relatively well characterized, at least one group responsible for the electrophoretic behavior of human erythrocytes at low ionic strengths has yet to be identified.

### Polymer Adsorption and its Effect on the State of Aggregation of Dispersed Systems

#### I. Polymer Adsorption at the Solid-Liquid Interface

Adsorption from solution of neutral and charged polymers at the solid-liquid interface has been studied extensively, due largely to its importance in industrial processes such as mineral extractions and fractionations, and water clearance. Although the range of conditions and materials which have been studied is very large, a degree of consistency of behavior has been found which is at first sight surprising. The bulk of the experimental evidence, obtained on both aqueous and non-aqueous systems, allows the following generalizations to be made (38, 39, 40):

- (i) Adsorption increases rapidly with bulk phase polymer concentration until a plateau is reached beyond which there is little concentration dependence. The concentration range over

which the increase occurs may be undetectably low.

- (ii) The adsorption data often fit a Langmuir adsorption isotherm (41), particularly for high molecular weight polymers.
- (iii) At a fixed weight concentration, adsorption is molecular weight dependent for a series of homologous polymers. The amount adsorbed increases with molecular weight (sometimes linearly) at low molecular weights, then plateaus for high molecular weights.
- (iv) The polymer molecule is adsorbed in a series of loops extending out into solution which are interspersed with trains of segments all in contact with the solid surface. The depth of the adsorbed layer is determined by the extent to which these loops protrude into solution. The amount of polymer adsorbed in the saturation region is frequently equivalent to more than one monolayer of close-packed monomers, while the depth will in general correspond to many times this number of monolayers. The structure of the adsorbed layer is therefore quite diffuse. There appears in general to be no reason to believe that multilayer adsorption occurs; every adsorbed molecule is in contact with the surface at one or more points in the chain.
- (v) Adsorption is increased from solvents in which the polymer is less soluble.

- (vi) The length of time required for equilibrium to be established may vary from seconds to many hours, the longer equilibration times generally being associated with high molecular weights.
- (vii) Washing an equilibrated adsorbed phase with the solvent from which the adsorption occurred may not remove the adsorbed polymer immediately.
- (viii) Temperature dependence of adsorption is small; the amount adsorbed may either increase or decrease with increasing temperature.

The method generally used to measure the adsorption of polymer from solution is to follow the decrease in bulk solution polymer concentration as the polymer adsorbs to a dispersed solid (39). Providing that the surface area of the particles is known, and an accurate method of measuring the polymer concentration is available, the amount adsorbed per unit area may be calculated. The amount of polymer adsorbed, or information on the monomer-surface interaction may also be obtained by examination of the equilibrated surface after excess solution has been removed. Radioactive tracers (41), infrared analysis (42, 43) or ellipsometry (44) have been successfully employed to this end. In general, any technique which can unambiguously identify and quantify the polymer, in solution or in association with a solid, may be used to measure adsorption isotherms.

Techniques for measuring the depth of adsorbed layers, however, are somewhat more limited. Ellipsometry (44), ultraviolet attenuated total reflectance spectroscopy (45) and various methods which determine the effective hydrodynamic thickness of the adsorbed layer (42, 46, 47) have been employed, the latter type being more prevalent since a wide variety of surfaces may be used. In general, the hydrodynamic methods measure the depth from which a fluid flowing past the surface is apparently excluded by the presence of an adsorbed layer. If normal flow is simply retarded in part of the adsorbed layer, the depth will be underestimated. The degree to which flow is excluded from the adsorbed layer has been anticipated (48) to depend on the flow rate past the surface, but apparently no thorough investigation has been made of this point.

The theoretical treatments of polymer adsorption date from the initial attempts of Frisch, Simha and Eirich (49, 50) to describe the statistical distribution of polymer segments near a wall. Subsequent, more involved treatments have been applied (38, 51, 52, 53, 54, 55), the most successful and complete being due to Silberberg (56). His statistical mechanical analysis of a two and three dimensional restricted random walk model yields numerical results which display all the equilibrium properties summarized above. The quantitative predictions made with respect to amounts of polymer adsorbed, depth of adsorbed layers and fraction of segments in contact with the surface

are in general agreement with the available data. This treatment shows that the free energy change involved in replacing a solvent molecule with a monomer molecule on a surface binding site need only be very small, of the order of  $kT$ , for strong adsorption to occur. Polymer adsorption might therefore be expected to be the rule, not the exception, when polymer solutions are exposed to solid surfaces. Further, Silberberg's analysis shows that while the total amount adsorbed depends on both the polymer-surface interaction energy and the bulk polymer concentration, the fraction of surface sites occupied is independent of the bulk concentration, and the amount adsorbed as loops is independent of the surface interaction energy. The properties of the diffuse part of the adsorbed layer, then, appear to be virtually independent of the type of surface to which adsorption occurs.

## II. The Effect of Polymer Adsorption on the State of Aggregation of Dispersed Systems

In simple ionic solutions, the state of a dispersed colloidal suspension is determined by the balance between the London-van der Waals forces of attraction and the repulsions generated by the overlap of counterion double layers associated with the suspended particles. These two opposing forces form the basis of the colloid stability theory developed by Derjaguin and Landau (57) and Verwey and Overbeek (58). Conditions which tend to suppress the double layer

extension, such as high ionic strength, will favor aggregation since the particles will approach more closely before significant double layer overlap occurs. The attractive force is increased at these smaller separations. Likewise, as mentioned earlier, expansion of the double layer will increase the repulsive forces, favoring disaggregation and suspension stability.

Addition of polymers to such a suspension, however, complicates the picture considerably. If the polymers are charged polyelectrolytes, they can in theory act as multivalent counterions and suppress the surface potential simply through an ionic strength effect. In practice, however, if the polyelectrolyte is of opposite charge to the particle, it will adsorb strongly to the surface (59, 60) and reduce (at low levels of adsorption) the magnitude of the net surface charge. More important, polymer molecules will frequently adsorb to more than one particle simultaneously, forming bridges of polymeric material which link the particles into flocs and destabilize the sol. This mechanism of flocculation (a term which, it has been proposed (61), should be reserved for this type of aggregation) was first suggested to apply to polymer-induced suspension destabilization of clays by Ruehrwein and Ward (62). The mechanism of flocculation was studied in detail by LaMer and co-workers (63, 64, 65), and it is to him that much of the credit must go for the basic delineation of the effect. Although the theory of filtration of the resulting flocs (66, 67) used by

LaMer's group to study and characterize flocculation has been strongly questioned (68), the mechanism of polymer bridging is now generally accepted.

Flocculation can be induced by polymers regardless of the relative sign of the charges of the particle and polymer (69), neutral polymers also being effective (70). It has been shown in a number of studies (41, 59, 60, 71, 72) that flocculation depends partially on the surface charge, aggregation only occurring to a significant extent when the zeta potential is reduced to a low level. Hence, the distinction between flocculation, caused by a polymer bridging mechanism, and coagulation, induced by changing the double layer parameters, becomes less clear in these instances. If concentrations of polymer are used which are greater than that required for optimum flocculation, disaggregation is frequently observed to occur (41, 59, 60, 71). In those cases where the charges of the particle and polymer are opposite, such re-dispersion generally parallels a reversal of charge on the particle due to strong polymer adsorption. The resulting high surface potential is felt to cause disaggregation by electrostatic repulsions in the overlapping double layers. In these instances, then, electrostatic repulsion seems to be sufficiently strong to prevent links from forming in sufficient numbers to induce flocculation.

In cases where neutral polymers or polyelectrolytes of the same charge as the particle are used as flocculants, higher molecular

weights or concentrations are required for maximum flocculation (41, 73). For negatively charged polymer and surface, the presence of multivalent cations is frequently (41, 61), but not always (71), a requisite for flocculation. In these systems, with or without multivalent cations, charge reversal is not observed, yet at high enough concentrations the particles are disaggregated. The zeta potential is typically unaltered by these higher concentrations of polymer, retaining the same low but non-zero value as measured under flocculating conditions. In this case, although some electrostatic repulsion will occur, the change in state of aggregation at constant surface potential clearly requires an alternate explanation. For neutral polymers, essentially similar behavior has been observed, but surface potentials have not always been measured (67, 74).

Two explanations have been proposed to account for this disaggregation at high polymer concentrations. The first assumes that with increased surface coverage there are insufficient binding sites available for bridging molecules, so too few links form to produce flocculation (67). There is an objection to this explanation, however, in that the adsorption isotherm is usually still increasing at polymer concentrations where disaggregation occurs. Hence, it is not clear why the adsorption leading to bridging should stop while adsorption to single particles continues.

The second explanation attributes the re-dispersion to steric



interactions between adjacent adsorbed layers to polymer (74). This suggestion was based on early work on non-aqueous dispersion stabilization by terminally-adsorbed hydrocarbons (75, 76, 77). Subsequent work directed towards the study of this steric stabilization has largely been carried out on systems where the adsorbed species has been anchored on the surface at one end of the molecule (78, 79, 80, 81, 82). It has been demonstrated that steric stabilization depends on the solvent power of the continuous phase for the stabilizing polymer moiety. Under conditions where the effective exclusion volume of one molecule for another vanishes (Flory's  $\theta$  condition (83)), steric stabilization breaks down and the particles aggregate under the influence of van der Waals attractions (80, 81, 82).

The theory of the steric stabilization process has been treated explicitly by Meier (84), and discussed in terms of the Flory theory (83) for non-adsorbed polymers by several authors (79, 80, 85). These theories predict that the chief contribution to the repulsive energies generated when the adsorbed layers overlap is due to the increased free energy of mixing of the adsorbed layers. Both entropic and enthalpic contributions may be significant (82). The repulsion is both anticipated theoretically and observed experimentally to depend on the amount of stabilizing polymer adsorbed, fairly high coverages being necessary for stabilization. The general expressions for the interaction free energy are difficult to assess, however, and

only the dependency on solvent power predicted by the theories has been specifically tested. The effect on the van der Waals energy of an adsorbed layer has been treated by Vold (86) and taken into account by Ottewill (78), but the predicted decrease in attraction is too small to account for the observed results.

Polymers, then, may either stabilize or destabilize colloidal suspensions. Because of the variety and complexity of the systems studied, it is very difficult to make general statements regarding these systems. To predict what will occur when a particular polymer, of given molecular weight and composition, is added at some concentration to a suspension of particles with a specific type of surface, in a medium of fixed ionic strength, is at present not possible (87). Neither are there analytical theories which can estimate, given the above information and the state of aggregation of the system, the energies of attraction or repulsion which result from the interaction of the polymer with the surface. There is, then, much work yet to be done in these areas.

### III. Polymer Adsorption to Cells

Very little analytical work has been done on the adsorption of polymers to biological interfaces. The interactions of proteins with cell surfaces has been studied in connection with, for instance, immunological reactions, but these macromolecules can not

necessarily be expected to behave like polymers in this regard because of their secondary and tertiary structure. The most thorough study of a polymer-cell system has been carried out by A. Katchalsky's group on the adsorption of polylysine to normal human erythrocytes suspended in an isotonic ionic medium (88, 89). These workers measured the uptake of polylysine, a strongly positively charged polymer at neutral pH, to red cells by following the electrophoretic mobility changes in the cell populations exposed to polymer. They found that the mobility change was a single valued function of the polymer concentration. By correlating electrophoretic changes with cell and polymer concentrations, a parabolic adsorption isotherm was constructed which appeared to approach a limiting adsorption corresponding to about six close-packed monolayers of polymer. Polylysine aggregated the cells strongly, the concentration at which aggregation first occurred being a decreasing function of molecular weight. The onset of aggregation was also characterized by a specific negative zeta potential, the magnitude of which was larger the higher the molecular weight of the polymer. Aggregation, then, took place in the face of significant electrostatic repulsion in all cases. Although charge reversal occurred, in no instance was disaggregation observed at higher polymer concentrations, although the concentration range was limited to  $\lesssim 0.01\%$  w/v due to hemolysis. Electron micrographs of the aggregated cells revealed the presence of

links in the seams which were taken to be the polybase molecules. The lengths of these links were comparable to the extended lengths of the polymers used, and varied with the degree of polymerization of the bridging molecules. Polylysine adsorption to red cells, then, appears to exhibit the same qualitative characteristics as the adsorption of polyelectrolytes to inert particles described in the previous section.

Quantitative studies on the adsorption of neutral polymers to cells have also been attempted. Hummel (90, 91) studied the binding of two molecular weights of  $C^{14}$ -labelled polyvinylpyrrolidone to human erythrocytes from buffered suspensions. The method used was to incubate equal volumes of packed cells and labelled solution, then spin the cells down and count the supernatant. He measured the interstitial fluid in the original pellet by weighing a sample, drying it down and re-weighing, then calculating the interstitial water content by assuming the ratio of water to solid in the cell was 2.0. No measurement of this ratio was made, however, even though he used concentrations of up to 50.0% w/v polymer where osmotic effects could affect it. Since the calculated amount adsorbed will depend critically on the value for the interstitial volume, the measurement of this ratio is of some importance. The resulting isotherms were approximately linear functions of concentration for both the 11,500 and 25,000 molecular weight samples, but roughly five times as much of the lower

molecular weight fraction was found to be adsorbed than the high. At 6.35% polymer, Hummel found adsorption corresponding to roughly 8 monolayers of M. Wt. 25,000 and 40 monolayers of M. Wt. 11,400. He also found that the apparent adsorption decreased with increased centrifugation speeds. These results, particularly the molecular weight dependence, are at such marked variance with observations and theoretical examinations on other systems in the literature that some doubt must be cast on their validity.

Because of its widespread use as a plasma expander (92, 93) there have been several attempts to measure the adsorption of dextran, a slightly branched  $\alpha$ -1,6 polyglucose, to red cells, platelets and blood vessel walls. Rothman and co-workers (94) measured the radioactivity associated with red cells and platelets after incubation in plasma made 1% in  $C^{14}$  OOH-dextran and six washes in cold plasma/dextran. They found  $\sim 8 \times 10^3$  molecules of dextran per cell associated with both types of blood elements. Bloom's group (95) also measured the  $C^{14}$  activity of the erythrocytes and blood vessel walls of a dog which had been infused with a 6% solution of  $C^{14}$  OOH-dextran to a total amount of 1% of body weight. After six washes in cold dextran-saline, approximately  $2.5 \times 10^4$  molecules per cell were found to be associated with the erythrocyte pellet. On the other hand, Håkansson, Östling and Zade-Oppen (96) have recently reported that, by counting the supernatants of saline and plasma suspensions of red

cells made  $0.002$  to  $0.05 \text{ gm l}^{-1}$  in randomly labelled  $\text{C}^{14}$ -dextran and allowing for interstitial fluid, adsorption of dextran to red cells in their systems was improbable.

Further studies on the interaction of dextran with cell surfaces have been made by methods which examine the interaction indirectly. Microscopic estimations of cellular aggregation (97), measurements of changes in light transmission of concentrated suspensions as a measure of aggregation/disaggregation (98) and sedimentation rate (99, 100) have all been used to examine the ability of dextran to aggregate or disaggregate cells. In general, these studies have shown that dextran induces human erythrocyte aggregation to varying degrees in saline, depending on the molecular weight. Molecular weights below about 50,000 seem to cause little aggregation, and apparently can reverse to some extent aggregation induced by higher molecular weight fractions, presumably through competition with the larger polymer molecules for binding sites on the cell surface. At high concentrations of low molecular weight dextran, and in the presence of partially diluted levels of plasma proteins, the dextran can also apparently compete with the proteins in citrated plasma which cause rouleaux formation. Experiments in plasma, however, are complicated by the appearance of protein precipitation at high concentrations of dextran (101, 102). Sedimentation studies indicate that cellular aggregation increases in degree with dextran concentration up to at

least 2.8% w/v dextran, M. Wt. ~82,000 (99, 100).

In so far as they exhibit a tendency to aggregate red cells, then, neutral polymers, as represented by dextran, appear to interact with human erythrocytes. Presumably these polymers cause flocculation by the same bridging mechanism observed in inert systems and polybase-erythrocyte interactions. No detailed examination appears to have been made of this proposed mechanism, however.

#### The Effect of Neutral Polymers on the Electrokinetic Properties of Biological Surfaces

In 1957, Ponder (1) reported that addition of dextran to saline suspensions of human erythrocytes and platelets resulted in an increase in the cellular zeta potential as measured by electrophoresis. This is a surprising result since dextran is a neutral polymer and should not affect the measured charge densities if it adsorbs to the cells. Since that time, many workers have reported similar results for dextran both in saline and plasma solutions (103, 104, 105, 106, 107). The zeta potential of arterial walls, determined from streaming potential measurements, was also shown to be elevated in the presence of dextran (108). Similarly ficoll and polyvinylpyrrolidone increased the zeta potential of erythrocytes in simple ionic media. Hence, the observation that neutral polymers can increase the zeta potentials of biological surfaces has been verified by a series of

workers under a variety of experimental conditions.

Various explanations of the cellular zeta potential increases have been advanced. Ponder (1) suggested that the dextran adsorbs to the cell with the hydroxyl dipoles oriented in such a way that removal of a hypothetical charge from the shear plane to infinity would require more energy than if the dextran were not present. Pollack and co-workers (104) attempted to explain the increase in terms of an increase in the dielectric constant of the polymer solutions. They supported their argument with capacitance measurements of dextran solutions at 100 kHz which indicated a large positive dielectric increment for the polymer in solution. The positive dielectric increment obtained for dextran was at variance with the results of other workers (109). Finally, Ross and Ebert (103) have suggested that the potential increase represents a configurational change at the cell surface, presumably exposing additional charge groups which in turn cause the increased zeta potential. As will be discussed in the next chapter of this thesis, however, none of the above suggestions offer a satisfactory general explanation for the phenomenon.

### The Rheology of Erythrocyte Suspensions

Rheology is defined as the study of deformation and flow of matter (110). For erythrocyte suspensions, the rheological property of interest is the viscosity,  $\eta$ , defined as the ratio of shear stress,



$\tau$  (the force per unit area applied tangentially to some plane of fluid), to shear rate,  $\dot{\gamma}$  (the velocity gradient in the fluid). If the viscosity so defined is constant over the range of shear rates tested, the fluid is said to be Newtonian; if the viscosity varies with shear rate, the fluid is non-Newtonian. Erythrocyte suspensions show a type of non-Newtonian behavior known as shear thinning. That is, their viscosities are monotonically decreasing functions of shear rate.

In general, the viscosity of a fluid is a measure of the rate of energy dissipation occurring during the flow process. If the fluid is a suspension of particles, this dissipation originates from any or all of:

- (i) the motion of one lamina of the liquid suspending medium relative to another (the viscosity of the continuous phase)
- (ii) the distortion of laminar stream lines around the suspended particles (111)
- (iii) the viscous drag exerted on a particle which is slowed by collision or long range interaction with another particle (112)
- (iv) the breaking of interparticle bonds (113)
- (v) the deformation of individual particles from an equilibrium configuration
- (vi) the distortion under shear of the ionic double layer surrounding a charged particle (the primary electroviscous effect) (114)

(vii) the "friction" associated with the entanglement of molecular species on different particles in contact (115)

Although these sources of viscous energy dissipation in suspensions may be identified, quantitative theoretical treatments describing their respective contributions to the overall flow behavior are less readily available. This is particularly true in the case of whole blood or erythrocytes suspensions where the ease of deformability of the cells is clearly a major factor in their rheological behavior.

For very low concentrations of non-deformable, non-interacting spherical particles, the dependence of the apparent viscosity,  $\eta$ , on the volume concentration of particles  $H$  was shown by Einstein to be (116):

$$\eta = \eta_0 (1 + 2.5H) \quad (1-33)$$

where  $\eta_0$  is the viscosity of the continuous phase. For non-spherical particles, the coefficient of  $H$  is greater than 2.5 but no higher order terms in  $H$  are required to define  $\eta$  (117). For particle concentrations over 2% v/v, higher order terms in  $H$  must be added, although universally accepted values for the appropriate coefficients are not available (118). These systems are generally Newtonian.

The flow regimes around isolated rigid particles, and around deformable particles (liquid droplets) whose shapes are determined by

surface tension forces are now fairly well understood, due mainly to the work of Mason and his associates (111). Although multiplet interactions have also been characterized, the extension to high particle concentrations has proven more difficult. The results obtained for deformable droplets would seem to have little application to erythrocyte suspensions at present, however, because of the non-spherical shape of the cells, and the uncertainty regarding the forces which operate to produce this shape (119, 120, 121, 122). Without knowledge of these forces, the energy required to deform red cells in a shear field cannot be estimated, and the viscosities of their suspensions cannot be predicted. The theoretical work that has been done on the viscosity of dilute droplet emulsions (123) apparently does not apply to erythrocyte suspensions, since this treatment predicts the presence of normal forces in the suspensions. Such forces, if present, are immeasurably small in red cell suspensions (124).

Theoretical treatments of non-Newtonian flow of suspensions have been based either on the theory of rate processes applied to the general relaxation processes believed to occur during flow (125), or on various forms of energy dissipation associated with shear-sensitive particle-particle interactions. These treatments have been conveniently summarized (126, 127). In general, none of the treatments provide a basic description of flow in terms only of system parameters, but rely on two or more empirical parameters to fit the theoretical

expressions to  $\eta - \dot{\gamma}$  data. They do not apply to concentrated suspensions, nor can they be expected to predict the behavior of suspensions of deformable particles such as cells.

The effects of changes in the electrostatic surface potentials of charged particles on their rheological behavior have been studied to some extent (114). An apparently satisfactory description of the viscosity increment due to distortion under shear of the counterion double layer has been given (128) and tested (129, 130). However, this effect only applies to very small particles where the double layer thickness is a significant fraction of the particle radius, and therefore does not apply to cells. A theory of the effect of surface potential on the energy dissipated as viscous drag when two particles interact at finite separations has been given and shown to provide a qualitative description of the viscosity variation with surface potential in dilute solutions (112, 131). In this treatment of the secondary electroviscous effect it is assumed no particle contact occurs. Increasing the electrostatic repulsive force between the particles, either through surface potential or double layer thickness, increases the minimum separation of two interacting elements and increases the attendant energy dissipation at a given rate of shear. Hence, increased repulsion causes an increase in the suspension viscosity which is a function of shear rate in these systems.

Suspensions of rigid particles in which aggregation occurs have

also been examined, experimentally and theoretically, for the effect of changes in particle-particle interaction energies on rheological properties (132, 133). Neither of these treatments predict a change in viscosity as a function of interaction energy, however. They both predict that particle-particle interactions affect only the extrapolated or true yield stress of the suspensions. That is, the minimum applied stress necessary to cause flow in the systems is increased as inter-particle repulsions are decreased, but the viscosity of the system once flow is established is not affected. It would appear, then, that in general no theory exists which predicts the rheological behavior of concentrated suspensions of deformable, charged, interacting, non-spherical cells as a function of shear rate, concentration and cellular surface properties.

Although the theoretical study of the rheology of cell suspensions is in its infancy, viscometric measurements on erythrocyte suspensions, and in particular on suspensions of erythrocytes in anti-coagulated blood plasma, have been made by many groups. It is necessary to distinguish between the rheology of erythrocytes in saline as opposed to erythrocytes in plasma, since the plasma proteins, particularly fibrinogen, have been shown to have a strong influence on red cell suspension viscosity (134, 135, 136, 137). The dependence of the viscosity on shear rate and cell volume concentration (hematocrit, H) of human erythrocytes suspended in homologous

anticoagulated plasma has been studied in vitro, such systems being considered models for whole blood. Recent reviews of the results are available (138, 139, 140). They may be briefly summarized as follows:

- (i) At hematocrits greater than about 10% v/v, red cells in plasma are non-Newtonian and exhibit shear thinning. For shear rates greater than roughly  $100\text{-}200 \text{ sec}^{-1}$  the suspensions are essentially Newtonian. At shear rates lower than  $100 \text{ sec}^{-1}$ , the apparent viscosity increases with decreasing shear rate; the increase being relatively greater, the higher the hematocrit. Even at hematocrits above the theoretical close-packing concentration for biconcave discoids (58%) flow occurs with essentially these same qualitative characteristics, indicating that the cells are highly deformable.
- (ii) At any fixed shear rate, the viscosity is a monotonically increasing function of hematocrit. The viscosity increases more rapidly with hematocrit the lower the shear rate at which the data is taken.
- (iii) Red cells in plasma exhibit a small yield stress at hematocrits above about 4 to 8% v/v. That is, a shear stress greater than the yield stress must be applied to the suspension for flow to occur. The yield stress is a rapidly increasing function of hematocrit. In normal suspensions, yield stress depends on the presence of fibrinogen, afibrinogenemic

plasma suspensions exhibiting virtually no yield stress. The yield stress appears to increase as fibrinogen concentration increases. The absolute value of the yield stress of erythrocyte-plasma suspensions is a matter of some debate, the values obtained depending on the method of measurement used (141, 142, 143, 144), but the presence of a finite yield in these systems seems well established. The yield stress shows little temperature dependence in most cases. The yield stress indicates the presence of some sort of structuring in the suspensions and is believed by some to be of physiological significance (145).

- (iv) At least part of the non-Newtonian behavior of erythrocytes in plasma arises from the presence of aggregates (rouleaux) in the suspensions, whose size decrease with increasing shear rate. The presence of rouleaux is associated with the presence of fibrinogen, larger rouleaux being formed at higher fibrinogen concentrations. The rouleaux observed at zero shear rate are probably the structural elements responsible for the yield stress. As the shear rate is increased, rouleaux are observed to break down (146, 147) until, in normal plasma, full disaggregation is seen at  $\dot{\gamma} \sim 50-100 \text{ sec}^{-1}$ . Rouleaux formation is reversible; the aggregates reform rapidly if the shear rate is reduced. This reversibility is

also mirrored in the shear dependence of the suspension viscosity, no hysteresis being observed if high and low shear rate measurements are made alternately.

- (v) Between 10° and 37°C, the temperature dependence of the viscosity of erythrocyte-plasma suspensions is identical to that of water, at moderate to high shear rates. At low shear rates there is less temperature dependence.
- (vi) There is no evidence for the presence of normal forces in the suspensions under flow conditions.

Although there are no specific theoretical treatments that apply to red cell suspensions, the characteristic shear dependent formation of linear rouleaux has been approximated in Casson's attempt to predict the flow behavior of linear pigment dispersions (132). Casson's treatment predicts that for dispersions of the type described the shear rate-shear stress data should obey:

$$\tau^{1/2} = \tau_y^{1/2} + k^{1/2} \dot{\gamma}^{1/2} \quad (1-34)$$

where  $\tau_y$  is the yield stress, and  $k$  is a constant equal to the apparent viscosity when  $\tau_y = 0$ . Although the assumptions of Casson's model are not fulfilled by whole blood, it is found empirically that plots of  $\tau^{1/2}$  vs  $\dot{\gamma}^{1/2}$  produce fairly linear graphs at very low ( $\lesssim 20 \text{ sec}^{-1}$ ) and high ( $\gtrsim 100 \text{ sec}^{-1}$ ) shear rates (148, 149). The



apparent linearity at low shear rates allows an extrapolation to  $\dot{\gamma} = 0$ , the intercept on the  $\tau$  axis giving  $\tau_y$ , the yield stress. Since the yield stress has been one of the principal parameters of interest in in vitro blood rheology, Casson plots have been widely utilized.

While the rheology of erythrocyte-plasma suspensions has been studied quite intensely in the 8 years since the introduction of very low shear rate viscometers, considerably less attention has been paid to the characteristics of suspensions of red cells in protein-free media. Some studies of the effect on the viscosity of shear rate, hematocrit and the degree of flexibility of the cells have been made however (2, 150, 151, 152, 153). The results of these studies, and of similar studies on rigid cells suspended in saline may be summarized as follows:

- (i) Above hematocrits of 20 to 25% v/v, suspensions of human red cells in saline are strongly non-Newtonian, their viscosities increasing with decreasing shear rates below about  $600 \text{ sec}^{-1}$ . The low shear rate viscosity increases are greater the higher the hematocrit. The degree of shear rate dependence at low  $\dot{\gamma}$  is less pronounced in saline than when plasma forms the continuous phase, but the non-Newtonian behavior extends to higher shear rates. Flow can occur with these same qualitative characteristics up to hematocrits

greater than 90% v/v.

- (ii) At any fixed shear rate, the viscosity of red cells in saline is a monotonically increasing function of hematocrit. The viscosity increases more rapidly with hematocrit the lower the shear rate.
- (iii) Normal or rigid (aldehyde-fixed) cells in saline exhibit no measurable yield stress, indicating the lack of three dimensional structuring in these suspensions.
- (iv) No rouleaux or aggregates of any kind can be seen in saline suspensions of fixed or normal erythrocytes.
- (v) Fixed rigid erythrocytes suspended in saline are approximately Newtonian at all volume concentrations at which flow occurs. Above about  $H \sim 56\%$  v/v, flow ceases altogether in such suspensions, due to the close packing of the rigid particles. The viscosity of a suspension of fixed cells in saline is higher than that of normal cells in saline at the same hematocrit, although the difference becomes progressively smaller the lower the shear rate or hematocrit.

Since the viscosity of plasma is roughly twice that of saline, comparisons between the rheological behavior of saline and plasma suspensions cannot be made by directly comparing their apparent viscosities. Such a comparison would probably reflect the continuous phase viscosities rather than give any insight into the interactions in

the system which determine its rheological properties. Comparisons of relative viscosity, the ratio of the apparent viscosity to the viscosity of the continuous phase, remove the first order effect of the plasma or saline viscosities, however, allowing more fundamental properties of the systems to be studied. Examination of the relative viscosities of saline and plasma suspensions of fixed and normal cells as a function of hematocrit and shear rate has suggested that some generalizations can be made regarding these systems:

- (i) The Newtonian behavior of rigid cells in saline suggests that the non-Newtonian character of normal cells results from their deformability. A distinction must be made between deformation induced by shear stresses transmitted through the medium, and deformation induced by collision with other cells. Since strong shear dependence is only found at relatively high volume concentrations, it seems that the non-Newtonian behavior of normal erythrocytes in saline is associated with deformation induced by cell-cell interactions. On the other hand, the increased cell-cell collisions at high hematocrit could result in interpenetration and entanglement of the cell surface molecules of colliding cells, in analogy to the process believed to occur in concentrated polymer solutions (115). These intercellular associations would not necessarily lead to a yield stress, but would be broken down

at higher shear rates. Both these explanations of the non-Newtonian properties of erythrocytes in saline are represented in the literature (2, 151).

- (ii) At low shear rates ( $\sim 1 \text{ sec}^{-1}$ ), the relative viscosities of plasma suspensions of normal or fixed cells are higher than the respective equivalent suspensions in saline, at least up to hematocrits of  $\sim 55\%$  normal cells. Both the normal and fixed cells in plasma are aggregated, while the saline suspensions are monodisperse. Hence, cellular aggregation, as well as producing a yield stress, causes an increase in the low shear relative viscosity of the cell suspensions.
- (iii) At high shear rates ( $> 200 \text{ sec}^{-1}$ ), the relative viscosities of plasma suspensions of normal cells are lower than saline suspensions at all hematocrits. If the only effect of the plasma proteins is to aggregate the cells and increase the relative viscosity, at high shear rates, where the aggregates are totally broken down, the relative viscosities in plasma and saline ought to be equal (at a given hematocrit). They are not equal, however, because the continuous phase viscosities in the two suspensions differ. Cellular deformation due to the shear stresses transmitted through the medium is greater in the more viscous plasma. The relative viscosity decreases at high shear rates are assigned to this

factor. Deformation induced by cell-medium interactions causes lowered relative viscosities at high shear rates.

This cell-medium deformation is greater the higher the shear stress acting on the particle, and increases with either increased shear rate or medium viscosity until no further deformation of the cell is possible.

It is seen, then, that some useful information regarding the interactions among the elements of cell suspensions undergoing flow has been obtained through studies on less complicated systems than whole blood.

Of particular interest with regard to interactions among cells during flow has been the effect of dextran on the rheology of whole blood. Dextran fractions have been used as plasma expanders since the Korean War. The osmotic pressure difference accompanying dextran infusion draws tissue fluid into the circulation, decreasing the blood hematocrit and protein concentration. Reviews of the development, properties and uses of dextran as a plasma expander are available (92, 93, 154). In vivo experimental work, which unfortunately has not always taken into account the hematocrit and plasma protein changes accompanying dextran infusions, has led to the claims that such infusions decrease blood viscosity (155) and inhibit red cell sludging and settling (156). In vitro experimentation under more stringently controlled conditions has failed to corroborate these claims, however. The apparent viscosities of anticoagulated bloods

to which dextrans of various molecular weights have been added have been shown to increase rather than decrease, when the hematocrits were held constant (157). Although exposure to low molecular weight dextran ( $\overline{M}_w \sim 4 \times 10^4$ ) has been claimed to reverse, presumably by cellular disaggregation, the high sedimentation rates induced by pathological plasmas or high molecular weight dextrans (99, 100), these findings have been disputed (158) and their relevance to observable disaggregation questioned (159). The extrapolated yield stress for red cells suspended in plasma has also been shown to be increased by all concentrations of all dextran fractions of  $\overline{M}_w$  greater than  $2 \times 10^4$  (157). Thus, most in vitro experimental parameters examined suggest there are no decreases in cellular interactions due to the presence of dextran in plasma suspensions of erythrocytes.

For suspensions of red cells in saline to which dextran has been added, however, there is much less data available. It might be expected that the fundamental effects of dextran on cellular interactions and on the rheology of cell suspensions might better be explored in protein-free media, since dextran apparently interacts with some of the plasma proteins (160, 161, 162). Some rheological studies of the effects of dextran in simple cell suspensions have been made. Two laboratories have reported that the relative viscosity of erythrocyte suspensions in saline plus dextran ( $\overline{M}_w = 4 \times 10^4$ ) is reduced below that of saline suspensions alone at all shear rates and hematocrits

(2, 163). It was proposed by one group that the decreased relative viscosity at low shear rates in the presence of dextran was a result of increased intercellular repulsions caused by the increased surface potentials associated with the presence of dextran. The mechanism of the decrease was thought to reside in reduced cell contact and reduced interpenetration of surface structures caused by the strong electrostatic repulsions induced by the polymer. If the suggestion is in fact valid, it is the first example of an electrostatic effect on cell suspension rheology. Other studies of the effects of surface charge on erythrocytes suspension rheology have been made (164, 165), but the effects have been sought only at relatively high shear rates. That no effects were found could easily be due to the shear region studied, since the largest relative viscosity decreases in the dextran-erythrocyte system occurred at low shear rates ( $\sim 1 \text{ sec}^{-1}$ ). Whether or not this somewhat unique type of electroviscous effect does in fact occur in cell suspensions in the presence of dextran has yet to be firmly established.

#### Summary and Approach to Problem

This chapter has attempted to provide a background for the problems to which the body of this thesis is addressed. The principles of electrokinetic measurements and their application to the study of cell surfaces have been given. The phenomenology of the cellular zeta

potential increase in the presence of neutral polymers has been described. The characteristics of polymer adsorption have been summarized, as well as the effects of such adsorption on the aggregation/disaggregation behavior of dispersions to which polymers are adsorbed. Finally, the rheological characteristics of erythrocyte suspensions have been outlined, the effect of dextran on the rheology of cell suspensions in protein-free media described, and one proposed explanation for the observed effect given.

The remainder of this thesis is concerned with two of the questions brought out in this Introduction:

- (i) What is the mechanism by which the cellular zeta potential is increased in the presence of neutral polymers?
- (ii) What connection, if any, does this increased zeta potential have with the effect of dextrans on the rheology of erythrocyte-saline suspensions?

The second chapter considers various models for the zeta potential increase and develops an approximate theory for one of them. Chapter 3 describes the measurement of the dielectric constant of dextran solutions. The results of these measurements eliminate the most elaborate explanation of the zeta potential increase proposed previously. In Chapter 4, a description is given of the measurement of the erythrocyte-dextran adsorption isotherm. Electrokinetic measurements on a variety of particle-polymer systems are given in



Chapter 5. The results are interpreted in terms of the theory developed in Chapter 2, and compared, where possible, with the results of Chapter 4. The effects of different concentrations and molecular weights of dextran on the state of aggregation of erythrocyte suspensions are also studied in Chapter 5, and the results interpreted qualitatively in terms of electrostatic interactions. Finally, rheological data on erythrocyte-dextran-saline solutions are presented, and the results discussed in the light of possible electrostatic interactions in these systems.

## CHAPTER 2

PROPOSED MODELS FOR THE ERYTHROCYTE ZETA  
POTENTIAL INCREASE IN THE PRESENCE OF  
NEUTRAL POLYMERSModels Based on Free Solution Properties of Neutral Polymers

In 1965, Pollack, Hager, Reckel, Toren and Singher (104) proposed that the increased zeta potentials they measured by electrophoresis for erythrocytes suspended in various polymer solutions were due to an increase in the dielectric constant of the bulk solution. The rationale behind such a suggestion is that an increase in the dielectric constant should decrease electrostatic interactions between counterions and the fixed surface charge on the particle. In the weaker electric field, the counterions should extend further away from the surface into solution, thus increasing the thickness of the double layer. Since the zeta potential is proportional to the double layer thickness, it should be increased in high dielectric constant media.

Pollack et al. supported their argument with low frequency dielectric constant measurements on concentrated solutions of dextran, polyvinylpyrrolidone, ficoll and bovine serum albumin. They found large dielectric increments for all polymers tested, obtaining for a 10% aqueous dextran solution of unspecified molecular weight a

dielectric constant of 483. Using their measured dielectric constant values and electrophoretic data obtained in similar media, they calculated charge densities for red cells. The values thus obtained were in good agreement with charge densities estimated from mobility measurements made in simple salt solutions.

Since the dielectric argument involves solution properties only, it should apply equally to all charged particles. It is shown in Chapter 5, however, that normal red cells, acetaldehyde-fixed red cells, quartz, bentonite, and  $\text{TiO}_2$  particles all show different electrophoretic characteristics when suspended in the same dextran-salt solution, the latter two particles showing decreases in relative zeta potential. Hence, an increased dielectric constant cannot explain the observed behavior, nor can any argument based on solution properties alone. Doubt might therefore be cast on Pollack's dielectric constant measurements. There would seem to be no theoretical basis for dextran solutions to have a dielectric constant greater than that of water (positive dielectric increment). Those macromolecules which do show positive dielectric increments at low frequencies such as proteins (166) and polyelectrolytes (167) are all highly charged. The high dielectric constant is believed due either to the permanent dipole moment of the molecule (168), or to the polarization of the counterion double layer around it (169). Neither mechanism should apply to neutral polymers, however. Furthermore, as shown in Chapter 3, it has

been impossible to verify experimentally the existence of a positive dielectric increment for dextran. There is reason to believe that the results reported by Pollack et al. may have been subject to a large systematic error.

Models based on the solution properties of neutral polymers then, and in particular on their dielectric properties, cannot be used to explain the increased zeta potentials measured for erythrocytes in such suspensions.

#### Models Based on the Adsorption of Polymer at the Erythrocyte-Solution Interface

To explain variations in the relative zeta potentials of different particles in the same dextran solution, it is clear that properties of the surface as well as those of the polymer solution must be considered. The most obvious interaction that can occur between the two phases is the adsorption of polymer in the interfacial region. The remaining models to be considered all assume that such adsorption occurs.

#### I. Ponder's Model: A Change of Dielectric Constant in the Interfacial Region

In Ponder's paper, which first described the relative zeta potential increase of erythrocytes and platelets in the presence of dextran (1), a proposal was made to explain the observation. He suggested

that the dextran adsorbs to the cell with the hydroxyl dipoles of the glucose monomers oriented in such a way that bringing a hypothetical charge from infinity to the plane of charge would require more energy than if the dextran were not present. That is, the electrostatic potential due to the charge plane would be increased. Ponder's proposal is essentially a dielectric argument, since it is the dipole moment of a molecule that supplies it with its dielectric properties. His description, however, corresponds to a decreased dielectric constant in the adsorbed layer. Ponder provides no quantitative theoretical discussion of his suggestion, but his model may be analyzed as follows.

There would seem to be three basic possibilities:

- (i) The presence of the adsorbed layer has no effect on the location of the plane of shear. In this case, the dielectric constant in the double layer would be decreased. If the surface charge remains constant, it can be seen from equation (1-18) that the viscosity-mobility product,  $\eta U$ , would be decreased, not increased as observed.
- (ii) The shear plane is displaced away from the plane of charge outside the adsorbed layer of low dielectric constant. The adsorbed layer is assumed rigid to shear and impenetrable to counterions (Figure 2-1).

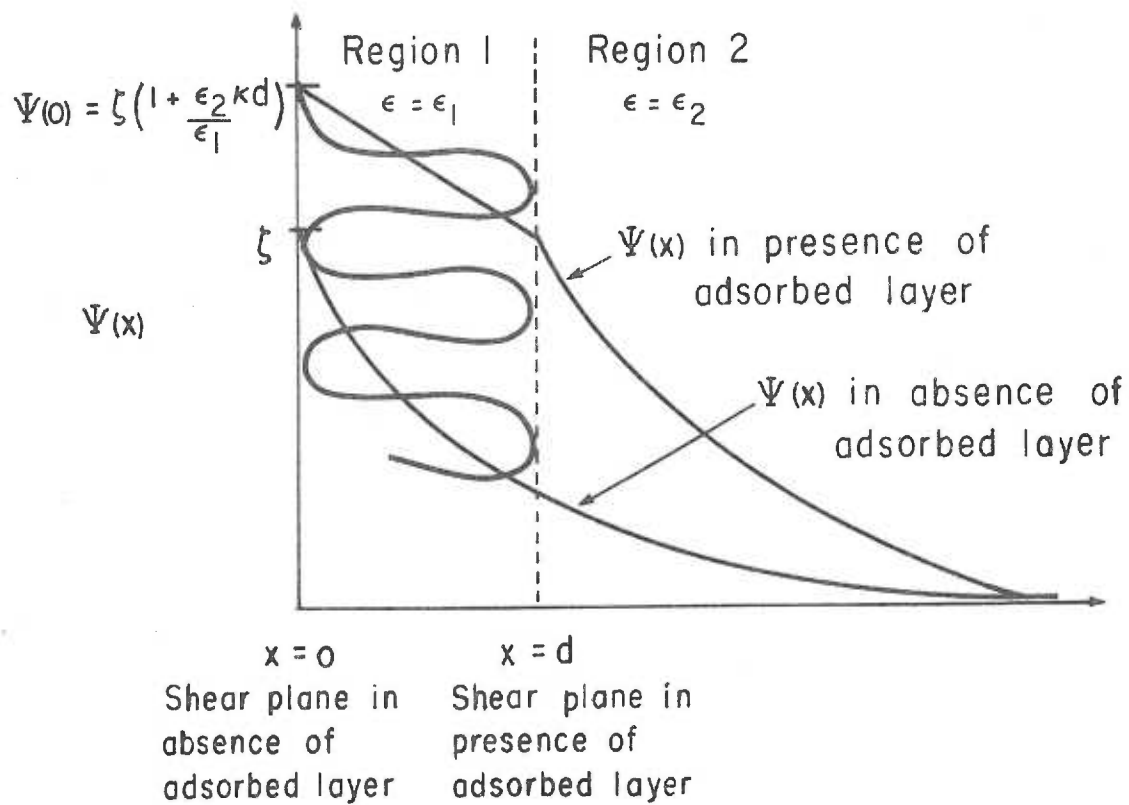


Figure 2-1. The potential distribution adjacent to a charged surface in the presence of a rigid, impermeable layer.

Let  $\epsilon_1$  = dielectric constant within adsorbed layer

$\epsilon_2$  = bulk dielectric constant

$\epsilon_r = \epsilon_2 / \epsilon_1 > 1$

$d$  = thickness of adsorbed layer

Under the same assumptions as in Section I, p. 7, the potential obeys

$$\frac{d^2 \psi_1(x)}{dx^2} = 0 \quad \text{in region 1, } 0 \leq x \leq d \quad (2-1)$$

$$\frac{d^2 \psi_2(x)}{dx^2} = \kappa^2 \psi_2(x) \quad \text{in region 2, } d \leq x \quad (2-2)$$

The potential and its first derivative must obey the following additional two boundary conditions (170), as well as those given in Section I, p. 9 :

At  $x = d$

$$\psi_1(d) = \psi_2(d) \quad (2-3)$$

$$\epsilon_1 \frac{d\psi_1(d)}{dx} = \epsilon_2 \frac{d\psi_2(d)}{dx} \quad (2-4)$$

That is, at any uncharged interface, both the potential and the normal component of the electric displacement must be continuous. The general solutions in regions 1 and 2 are:

$$\psi_1(x) = a_1 x + b_1 \quad (2-5)$$

$$\psi_2(x) = a_2 \exp(-\kappa x) \quad (2-6)$$

Applying the boundary conditions, and recognizing that in (2-5)

$b_1 = \psi_1(0)$  and  $\psi_1(d) = \zeta$ , one obtains:

$$a_1 d + \psi_1(0) = a_2 \exp(-\kappa d)$$

$$\epsilon_1 a_1 = -\epsilon_2 \kappa a_2 \exp(-\kappa d)$$

$$a_1 d = \zeta - \psi_1(0)$$

Solving for  $a_1$ ,  $a_2$  and  $\psi_1(0)$ , one obtains for the potential:

$$\psi_1(x) = -\zeta \epsilon_r \kappa x + \zeta(1 + \epsilon_r \kappa d) \quad \text{in region 1, } 0 \leq x \leq d \quad (2-7)$$

$$\psi_2(x) = \zeta \exp[-\kappa(x-d)] \quad \text{in region 2, } d \leq x \quad (2-8)$$

As in Section I, p. 11, the charge density  $\sigma$  is obtained from:

$$\sigma = - \int_0^{\infty} \rho(x) dx = - \int_d^{\infty} \rho(x) dx$$

since there are no counterions in region 1.

$$\therefore \sigma = \frac{\epsilon_2}{4\pi} \int_d^{\infty} \frac{d^2 \psi_2(x)}{dx^2} dx = \frac{-\epsilon_2}{4\pi} \frac{d\psi_2(d)}{dx} \quad (2-9)$$

since  $\frac{d\psi_2(x)}{dx} \rightarrow 0$  as  $x \rightarrow \infty$ . Differentiating (2-8), substituting for  $x = d$  and solving for  $\zeta$  gives

$$\zeta = \frac{4\pi\sigma}{\kappa\epsilon_2}$$



This is the usual expression (1-17) obtained when no adsorbed layer is present. Therefore, although it may be seen from (2-7) that the surface potential at the charge plane,  $\psi_1(0)$ , is increased in the presence of the adsorbed impenetrable layer [ $\psi_1(0) = \zeta(1 + \epsilon_r \kappa d)$ ], the zeta potential is unaffected. This result holds regardless of the value of the dielectric constant inside the adsorbed layer.

- (iii) The shear plane is displaced away from the plane of charge to  $d$ , the edge of the adsorbed layer, but the adsorbed layer remains penetrable by counterions (Figure 2-2).

The potential now obeys:

$$\frac{d^2 \psi_1(x)}{dx^2} = \kappa_1^2 \psi(x) \quad \text{in region 1, } 0 \leq x \leq d \quad (2-10)$$

$$\frac{d^2 \psi_2(x)}{dx^2} = \kappa_2^2 \psi(x) \quad \text{in region 2, } d \leq x \quad (2-11)$$

where

$$\kappa_1^2 = \frac{8\pi e^2 n_o}{\epsilon_1 kT}; \quad \kappa_2^2 = \frac{8\pi e^2 n_o}{\epsilon_2 kT},$$

again assuming only 1:1 electrolytes present.

The general solutions for the two regions are now:

$$\psi_1(x) = a_1 \exp(-\kappa_1 x) + b_1 \exp(\kappa_1 x) \quad (2-12)$$

$$\psi_2(x) = a_2 \exp(-\kappa_2 x) \quad (2-13)$$

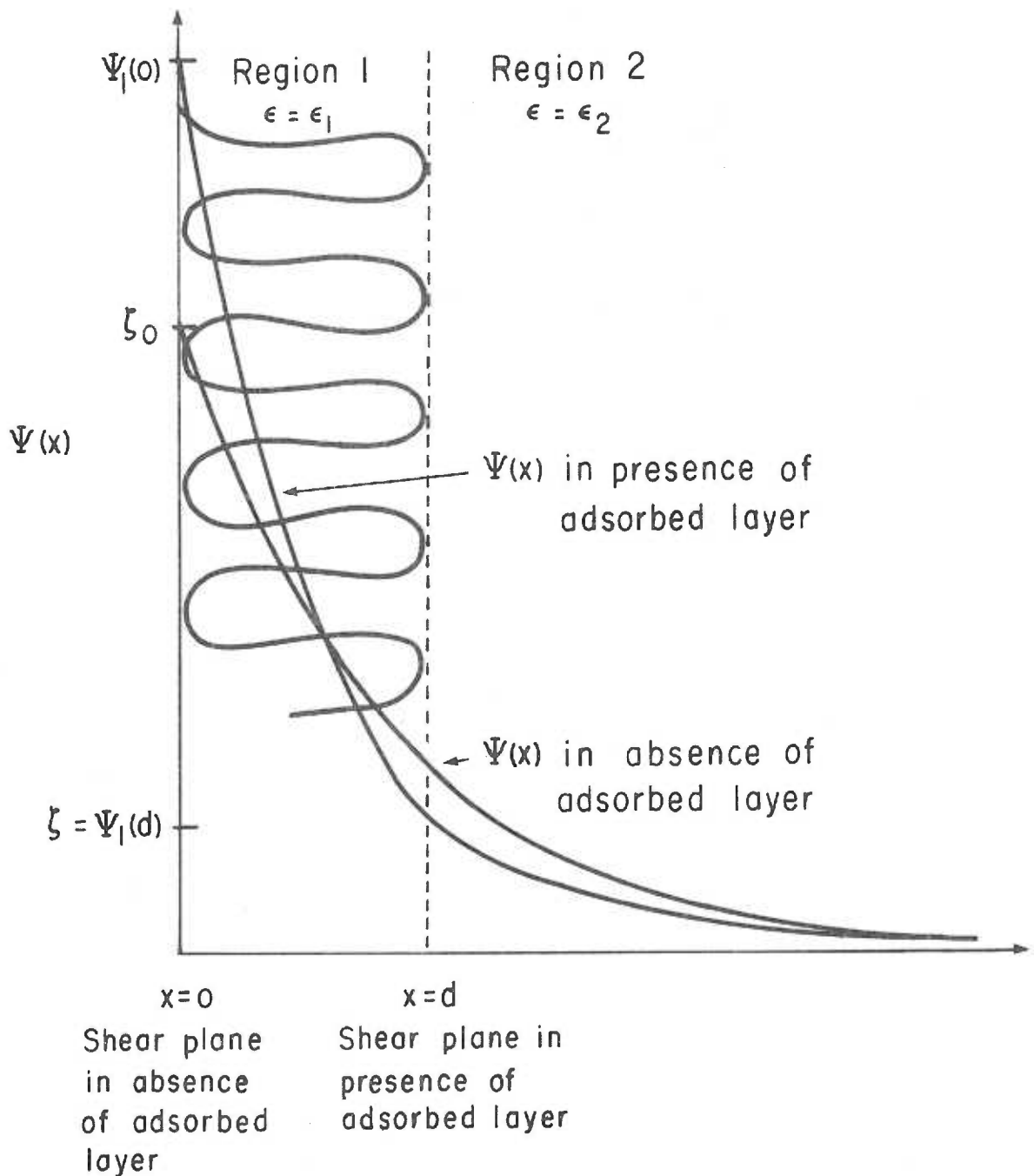


Figure 2-2. The potential distribution adjacent to a charged surface in the presence of a rigid, permeable layer of low dielectric constant.

where the second term of (2-12) must be included, since the boundary condition that  $\psi(x) \rightarrow 0$  as  $x \rightarrow \infty$  does not apply, due to the limits on  $x$  in region 1. Counterions are assumed not to penetrate behind the charge plane. Again applying (2-3) and (2-4) and noting that  $\psi_1(d) = \zeta$ , the potentials are found to be, after some algebra:

$$\psi_1(x) = \frac{\zeta(\kappa_1 + \epsilon_r \kappa_2)}{2\kappa_1} \exp[-\kappa_1(x-d)] + \frac{\zeta \exp[\kappa_1(x-d)]}{1 + \left[ \frac{\kappa_1 + \epsilon_r \kappa_2}{\kappa_1 - \epsilon_r \kappa_2} \right]} \quad (2-14)$$

$$\psi_2(x) = \frac{\zeta(\kappa_1 + \epsilon_r \kappa_2)}{2\kappa_1} + \frac{\zeta}{1 + \left[ \frac{\kappa_1 + \epsilon_r \kappa_2}{\kappa_1 - \epsilon_r \kappa_2} \right]} \exp[-\kappa_2(x-d)] \quad (2-15)$$

Equation (2-9) still applies, since its derivation does not depend on the form of  $\psi(x)$ :

$$\frac{-4\pi\sigma}{\epsilon_1} = \frac{d\psi_1(0)}{dx} = -\kappa_1 a_1 + \kappa_1 b_1$$

Substituting and rearranging gives finally:

$$\frac{1}{\zeta} \frac{4\pi\sigma}{\kappa_2 \epsilon_2} = \frac{\zeta_0}{\zeta} = \left[ \frac{1 + \epsilon_r^{-1/2}}{2} \right] \exp \kappa_1 d + \left[ \frac{1 - \epsilon_r^{-1/2}}{2} \right] \exp -\kappa_1 d \quad (2-16)$$

where  $\zeta_0 = \frac{4\pi\sigma}{\kappa_2 \epsilon_2}$  is the zeta potential in the absence of an adsorbed layer. In virtually all cases with which this thesis is concerned,  $\kappa_1 d > 1$ , so the first term dominates, and

$$Z = \frac{\zeta}{\zeta_0} \sim \left[ \frac{2}{1 + \epsilon_r^{-1/2}} \right] \exp(-\kappa_1 d) \quad (2-17)$$

Even in the limit of very large  $\epsilon_r$ , that is, in a situation where the difference in the dielectric constants is maximal, the relative zeta potential,  $Z$ , cannot be greater than  $2/e \sim 0.74$ . Therefore, none of the variants of Ponder's model can explain the experimental observations.

## II. Rearrangement of the Interfacial Region to Expose Additional Charge Groups

It has been suggested by some authors (103) and assumed by others (106) that the increased cellular zeta potentials measured in the presence of dextran actually reflect an increase in charge density at the cell surface. Since dextran is a neutral polymer, Ross and Ebert (103) have proposed that the charge increase comes about by a rearrangement of the interfacial region caused by the conjugation of adsorbed dextran molecules with cell surface proteins. The rearrangement could presumably introduce additional charge groups into that region of the cell-solution interface observable electrokinetically.

There are several difficulties with this interpretation, however.

(i) The apparent charge density as calculated from equation

(1-17) would have to be able to increase by a factor of up to

8, since this value for the relative zeta potential has been

measured for red cells in 8.9% w/v dextran 510/saline (Chapter 5). That is, 8 times as many negative charges as normal must be introduced into the interfacial region. The existence of this number of negative groups anywhere within the electrokinetically accessible surface is questionable, however. If these additional groups were near the shear plane, it might be expected that electrophoresis at low ionic strengths would give some indication of their presence. At low ionic strengths, the electrical double layer extends farther into the interior of the interfacial region, so groups buried deeper in the membrane may contribute to the mobility (23). The charge densities of erythrocytes calculated from low ionic strength mobilities, however, show no increases over the high ionic strength values (25). Instead, they decrease with decreasing ionic strength, due apparently to the presence of positively charged groups inside the membrane (171). Further, if the postulated concentration of negative charges were buried inside the membrane, it might be expected that enzymic or chemical degradative procedures could expose them. With the exception of periodate treatment (172), which presumably creates additional carboxyl groups through oxidation of surface carbohydrate, no degradative procedure causes an increase in the negative charge

density of human erythrocytes (173, 174). Hence, there would seem to be no other evidence for an extensive pool of negative groups in the red cell membrane which could be electrokinetically exposed by an adsorbed layer of dextran.

- (ii) The  $pK_a$  of the dextran-exposed groups must be the same as those groups which determine the charge in saline. Figure 5-4 shows that the apparent  $pK_a$  of an acetaldehyde-fixed human erythrocyte in 4.4% dextran 77.6 is identical to that of a fixed cell in saline and that the  $pK_a$  for the normal cell in dextran must be well below pH 4.5. Heard and Seaman (34) have shown that acetaldehyde fixation extends the pH range over which the cells exhibit electrokinetic stability (reversibility) and does not affect their electrophoretic properties in the normally stable region. Making the reasonable assumption that the apparent  $pK_a$  is independent of dextran molecular weight then, it is seen that from 2 to 8 times the normal number of  $pK_a$  2.6 groups must be present in the membrane if the rearrangement hypothesis is to apply. In the normal and acetaldehyde-fixed cell these low  $pK_a$  groups are the carboxylic acid constituents of N-acetylneuraminic acid (33). The number of these sialic acid moieties in the membrane may be determined chemically by analysis of the supernatants of neuraminidase-treated cells (35). The

amount of sialic acid present at the electrokinetic surface may also be estimated from the electrophoretic charge change upon neuraminidase treatment. The chemical determination of the amount of sialic acid released per cell is generally greater than the electrokinetic estimate by a factor of 2 to 2.5 (35). Since neuraminidase releases virtually all of the sialic acid in the normal erythrocyte membrane (36), it would seem that the membrane contains insufficient N-acetylneuraminic acid to account for the apparent charge increase seen in the presence of dextran. It cannot be ruled out that the additional groups of  $pK_a$  2.6 presumed to appear in the presence of dextran are associated with something other than sialic acid, but the possibility seems remote.

It should be noted that Ross and Ebert (103) have reported a shift in the iso-potential point of fresh platelets suspended in dextran/phosphate/saline solutions, relative to that found in the salt solution alone. The pH at the iso-potential point was 3.5 to 4, which is just at the limit of the pH range over which the platelet is electrokinetically stable (175). Since Ross and Ebert did not show that their pH-mobility curves were electrokinetically reversible over this range, it cannot be said with certainty that the apparent iso-potential shift they observed in dextran was due to the

appearance of new charge groups. An equivalent effect could have been produced by adsorption of leakage products from the cells exposed to dextran. In this connection, Robertson (176) has mentioned that dextrans of over 100,000 molecular weight can cause alterations in cell membranes demonstrable by electron microscopy.

- (iii) An increased relative zeta potential is found for some rigid particles suspended in dextran which would not be subject to interfacial charge rearrangement. Figure 5-3 shows the relative zeta potentials of suspensions of polystyrene latex in saline solutions of dextrans of various concentrations and molecular weights. The increased zeta potentials are qualitatively similar to those found for normal and fixed human erythrocytes in dextran/salt suspensions, although the magnitude of the increase is not as great. Polystyrene, however, has a rigid surface, which would not be expected to be altered by an adsorbed layer of neutral polymer.

It would seem, then, that the relative zeta potential increase in neutral polymers is not a phenomenon restricted to particles which may contain flexible interfacial regions capable of rearrangement. While exposure of additional surface charge groups may account for a portion of the increase found for normal erythrocytes in dextran, it cannot explain the effect entirely for the red cell, nor can it provide a



general explanation of the increase found with rigid particles such as fixed red cells and polystyrene latices.

### III. Non-Specific Ion Adsorption to an Adsorbed Polymer Layer

Another possible mechanism for the relative zeta potential increase of cells in neutral polymers is the adsorption of anions to an adsorbed polymer layer at the electrokinetic surface. The adsorption would have to occur at non-ionic sites on the adsorbed polymer, presumably in the case of dextran under the influence of the hydroxyl dipoles. There seems to be little information available on the feasibility of such ion binding, particularly when one considers binding to adsorbed polymers as opposed to polymers in solution. However, the following observations are pertinent to the discussion of the model:

Sieh and Sterling (177) have reported that glycogen, an  $\alpha$ 1, 4,  $\alpha$ 1, 6 highly branched polyglucose, acquires a negative charge by ion adsorption when dissolved in a variety of electrolytes. They showed, using acrylamide gel electrophoresis, that at pH's 6 to 8.5 glycogen exhibited progressively greater negative mobilities as the anion was changed, in the order:  $\text{Cl}^- < \text{Br}^- (1.3) < \text{H}_2\text{PO}_4^- (1.4) < \text{F}^- (1.5) < \text{I}^- (2.5) < \text{CNS}^- (3.6)$ , where the values in brackets are the mobilities relative to that in NaCl, all at 0.05 M salt concentration. Since the  $\text{pK}_a$  of glucose is greater than 12, their results could not be due to ionization of the hydroxyls. It is of interest that the above sequence

is not one of the predicted sequences of anion binding according to Eisenman's theory of ion selectivity (178).

The behavior of dextran in similar systems has not been examined. Although there are obviously strong structural analogies between dextran and glycogen, the glycogen molecule is more highly branched, more compact, and will therefore have a higher density of hydroxyl dipoles in free solution. If the anion association is due to ion-dipole binding, as in the case of cation-polyether (179) or  $K^+$ -nonactin binding (180), it might be expected that glycogen would be more likely to present a suitable environment for anion binding than dextran. In any case, since the configuration of an adsorbed polymer appears to differ from that in solution (56), it may be unwise to extrapolate from solution properties to those of the surface phase.

Experiments on the free boundary electrophoretic behavior of dextran in salt solutions are conflicting. Ponder and Ponder (181) have reported a slight negative mobility while Bloom (182) has found a zero mobility for dextran in a barbital buffer of 0.1 gm-ions/l ionic strength. Particle microelectrophoresis has been used to examine an insoluble bacterial dextral (183). In a phosphate buffer of 0.02 gm-ions  $l^{-1}$  ionic strength, the dextran particle had zero mobility.

A convenient particulate dextran system which can be examined electrophoretically is provided by Sephadex beads: dextran gels cross-linked with glyceryl bridges. The cross-linking reactions

require acidic conditions, resulting in the introduction of a few carboxyl groups into the gel ( $< 30 \mu\text{eq COOH per gm gel}$ ) (184). Sephadex G-100 Superfine (Pharmacia Fine Chemicals Co., Piscataway, N. J.) was allowed to equilibrate, and was washed six times in 0.1 M NaCl. After settling for  $\sim 2$  hr, the cloudy supernatant containing the "fines" was removed, spun down, and the pellet resuspended in 0.1 M NaCl, pH 6.1, in a suitable concentration for electrophoresis. The mobility of the resulting suspension of  $\sim 10 \mu$  to  $30 \mu$  diameter spherical particles was measured using the methods of Chapter 5. Approximately 20 to 50% of the particles had zero mobility, while the average mobility of the remainder of the population was  $-0.26 \mu \text{ s}^{-1} \text{ v}^{-1} \text{ cm}$ , which corresponds to a charge density of  $\sim 1.5 \times 10^3 \text{ esu cm}^{-2}$  using the modified Gouy-Chapman equation (1-32) with  $a \sim 0$  for the swollen gel. Assuming a water regain of  $19 \text{ ml gm}^{-1}$  for G-100, and a uniform volumetric charge density of  $35 \mu\text{eq gm}^{-1}$ , the theoretical surface charge density for a  $10 \text{ \AA}$  thick shell around a  $20 \mu$  diameter bead would be  $\sim 5.3 \times 10^7 \text{ esu cm}^{-2}$ .

It seems safe to say, then, that the slight negative mobility exhibited by some of the Sephadex G-100 beads does not constitute evidence for anion binding to dextran. In view of the large fraction of zero mobility particles, these results are evidence for the lack of anion binding.

Similarly, after a survey of the literature up to 1958, and after examining the electrophoretic behavior of starch granules, Seaman

(185) concludes: "Surfaces composed of neutral polysaccharide molecules evidently do not acquire any charge by the mechanism of ion adsorption in a non-complexing medium. "

Most of the work referred to thus far with regard to ion binding has been carried out at ionic strengths of  $\leq 0.1$  gm-ions  $l^{-1}$ . To see if dextran was capable of binding ions at higher salt concentrations, the solubility of NaCl was measured in concentrated dextran and polyethylene glycol (PEG) solutions. Klotz and Sloniewsky (186) have previously used this solubility method to measure small molecule binding to polymers. The PEG was included, because (i) PEG causes the relative zeta potential of erythrocytes to increase when suspended in salt solutions of this polymer (Chapter 5), and (ii) Baldwin, Raridon and Kraus (187) have shown, using the solubility method, that the ratio of the mean activity coefficient of NaCl in concentrated PEG solutions to that in water is greater than 1, where the standard state in each case is taken as that for salt in pure water. That is, the salt solubility per gm of aqueous PEG solution is lower than expected on the basis of the amount of water present. The PEG appears to be "binding" a fraction of the water, making it unavailable to act as solvent for the ions.

The experiments were carried out as follows: Concentrated dextran or PEG (Union Carbide Corp., New York) solutions were made up. Their concentrations were either measured

polarimetrically in the case of dextran, assuming  $[\alpha]_D^{20} = +199^\circ$  (188), or calculated from the weight composition of the PEG solutions, assuming the PEG powder to be dry. Aliquots of water or polymer solution were stirred with excess NaCl for at least 1 hr at  $30^\circ \rightarrow 50^\circ \text{C}$ , then equilibrated overnight at  $25^\circ \text{C} \pm 0.2^\circ$  in a water bath. Samples were spun down and duplicate  $0.100 \pm 0.0005$  ml supernatant samples weighed into tubes to each of which was added 5 ml of  $\text{H}_2\text{O}$  by weight. Triplicate chloride determinations were made on each diluted sample with an Aminco-Cotlove  $\text{Cl}^-$  Titrator, with an accuracy of about  $\pm 0.5\%$ . A 0.100 M NaCl solution, stored in polyethylene, was used as a standard throughout. Upon completion of the experiments, the  $\text{Cl}^-$  concentration of the standard was measured by  $\text{AgNO}_3$  titration and found to be 0.0995 M. The average NaCl concentration at saturation in  $\text{H}_2\text{O}$  at  $25^\circ$  was found to be 5.41 M (5 experiments). This value was converted to molal concentration using the apparent specific volume of the saturated salt solution measured pycnometrically to be  $20.74 \text{ cm}^3 \text{ mole}^{-1}$ , giving an experimental value of  $6.11 \text{ moles NaCl (Kg H}_2\text{O)}^{-1}$  at  $25^\circ$ . This is in acceptable agreement with the published value of  $6.145 \text{ moles (Kg H}_2\text{O)}^{-1}$  (189).

The theoretical ratio of NaCl solubility in the polymer solution,  $S_p$  moles salt/l solvent, to that in water,  $S_o$ , at  $25^\circ$  was calculated from the published values for the pycnometrically determined specific volumes of dextran,  $0.611 \text{ cm}^3 \text{ gm}^{-1}$  (188), and PEG,

0.837 cm<sup>3</sup> gm<sup>-1</sup> (190). Assuming that salt dissolution proceeds in the aqueous fraction of the polymer solution without regard for the polymer, the theoretical solubility ratio  $(S_p/S_o)_{th}$  is equal to the volumetric fraction of water in the polymer-water solution. The experimental value for  $(S_p/S_o)_{exp}$  is just the ratio of the salt concentrations measured in the polymer/water and water systems. The difference between the theoretical and experimental solubility ratios was expressed as  $F$ , the number of moles of salt apparently bound per gram of dextran, or the number of moles of water apparently bound per gm of PEG. The results are given in Table 2-1.

Table 2-1. The apparent binding of NaCl or H<sub>2</sub>O to dextran or PEG by solubility measurements.

Dextran Fraction	Concentration (gm/100 ml)	$\left[\frac{S_p}{S_o}\right]_{th}$	$\left[\frac{S_p}{S_o}\right]_{exp}$	$F\left[\frac{\text{moles bound}}{\text{gm dextran}} \times 10^4\right]$
Dex 40	30.17	0.819	0.875	9.54
	30.17	0.819	0.876	9.55
	30.17	0.819	0.862	9.40
	20.1	0.880	0.922	11.3
	10.0	0.940	0.968	15.1
Dex 77.6	25.77	0.843	0.881	7.98
	12.89	0.921	0.936	6.30
Dex 510	17.82	0.893	0.903	6.88
	17.82	0.893	0.929	7.08
				$\bar{F} = 9.24 \pm 2.72$
				$F\left[\frac{\text{moles H}_2\text{O bound}}{\text{gm PEG}} \times 10^2\right]$
PEG 6000	30.23	0.747	0.673	1.32
	30.23	0.747	0.676	1.33
PEG 20,000	40.01	0.665	0.575	1.28
				$\bar{F} = 1.31 \pm .03$

These results agree quite well with those of Baldwin et al. for PEG; for 25% PEG 1000 at 50°C they obtain  $1.8 \times 10^{-2}$  moles  $H_2O$  (gm PEG)<sup>-1</sup>, and indicate that at this concentration, the binding is molecular weight independent. This compares with the value of  $1.3 \times 10^{-2}$  moles  $H_2O$  (gm PEG)<sup>-1</sup> from Table 2-1 for 30% to 40% PEG 6000 to 20,000, at 25°. The slightly higher values obtained by Baldwin et al. may either reflect some hydration of the, assumed, dry PEG in the present work, or the effect of the higher temperature in the latter experiments. It would seem, then, that PEG in high concentrations effectively prevents a fraction of the water from acting as solvent for NaCl, and appears not to remove electrolyte from free solution. It is of relevance here that Couper and Stepto (191) have given evidence for the binding of water to PEG from diffusion studies as well.

The dextran results, on the other hand, indicate that the polymer effectively binds electrolyte to a degree that is roughly independent of molecular weight and concentration in the range tested (differences in  $F$  between the different molecular weights were insignificant at the 5% level using the Student t-test). Assuming that the equilibrium constant for the reaction used in the salt determinations,  $Ag^+ + Cl^- \rightarrow AgCl$ , is much higher than that for  $Dextran + Cl^- \rightarrow Dextran-Cl^-$ , the results could indicate either  $Na^+$  or  $Cl^-$  binding. No other halides or alkali metal ions were

investigated. The dextran results could not be due to salting out of dextran by the NaCl, since the dextran concentration was measured and found to be unchanged in the presence of saturation levels of salt. This is in agreement with the results of Haug and Smidsrød (192) who found that even near  $\theta$  conditions (83) in an EtOH-H<sub>2</sub>O solvent, concentrated NaCl had no effect on dextran solubility. Also, it was shown pycnometrically that the specific volume of dextran was independent of concentration up to 30%. These results are believed to be the first indication that dissolved dextran can effectively remove Na<sup>+</sup> and/or Cl<sup>-</sup> ions from solution, although it has been shown previously that dextran can bind copper (193) and iron (194). The observation of different elution volumes from Sephadex (195) for various ions need not necessarily be interpreted in this way (196).

In saturating concentration, then, NaCl appears to bind to dextran. Of more relevance to the electrokinetic experiments, however, is the possible binding at physiological ionic strengths or lower. To see if there were any effects of the apparent salt binding to dextran in its absorption spectrum, and to examine the effect of different ionic strengths, the following experiment was performed. The absorption spectrum of 12.89% dextran 77.6 was examined in H<sub>2</sub>O, 0.15 M NaCl, and saturated NaCl, between 430 and 250 m $\mu$ , on a Cary 15 spectrophotometer. Silica cuvettes with 1.0 cm light path were used, at ambient temperature of  $23 \pm 1^\circ\text{C}$ . The difference



spectra among the various solutions were also measured. The results are shown in Figure 2-3, where the second solution indicated for each curve is the blank.

The absorption spectrum of dextran in  $H_2O$  shows a peak at 259  $m\mu$  with a shoulder at 275  $m\mu$ . A similar spectrum has been obtained by Albertsson (197), only apparently without the shoulder at 275. The difference could be due to the fact that Albertsson's sample had been reduced with  $NaBH_4$  before examination. The spectrum of dextran in saturated NaCl, however, shows lower absorption in the peak regions, with the 275 peak reduced more than the 259 peak. This is more clearly seen in the difference spectrum of dex/ $H_2O$  vs dex/sat. NaCl. High salt, then, causes a decrease in the peak regions of the absorption spectrum of dextran. In 0.15 M NaCl, however, the difference spectrum of dex/0.15 NaCl vs dex/ $H_2O$  shows virtually no change at 275  $m\mu$ , and a small increase in absorption at 259  $m\mu$ . If decreased absorption in the peak region is associated with the apparent ion binding measured in the solubility studies, such binding appears to be virtually absent in the 0.15 M NaCl solutions. One interpretation of the spectral evidence, then, indicates that whatever ion binding occurs in 5.4 M NaCl may be reduced or absent at physiological ionic strengths.

The foregoing experiments and observations have largely considered the possibility of ion-polymer binding in free solution. More

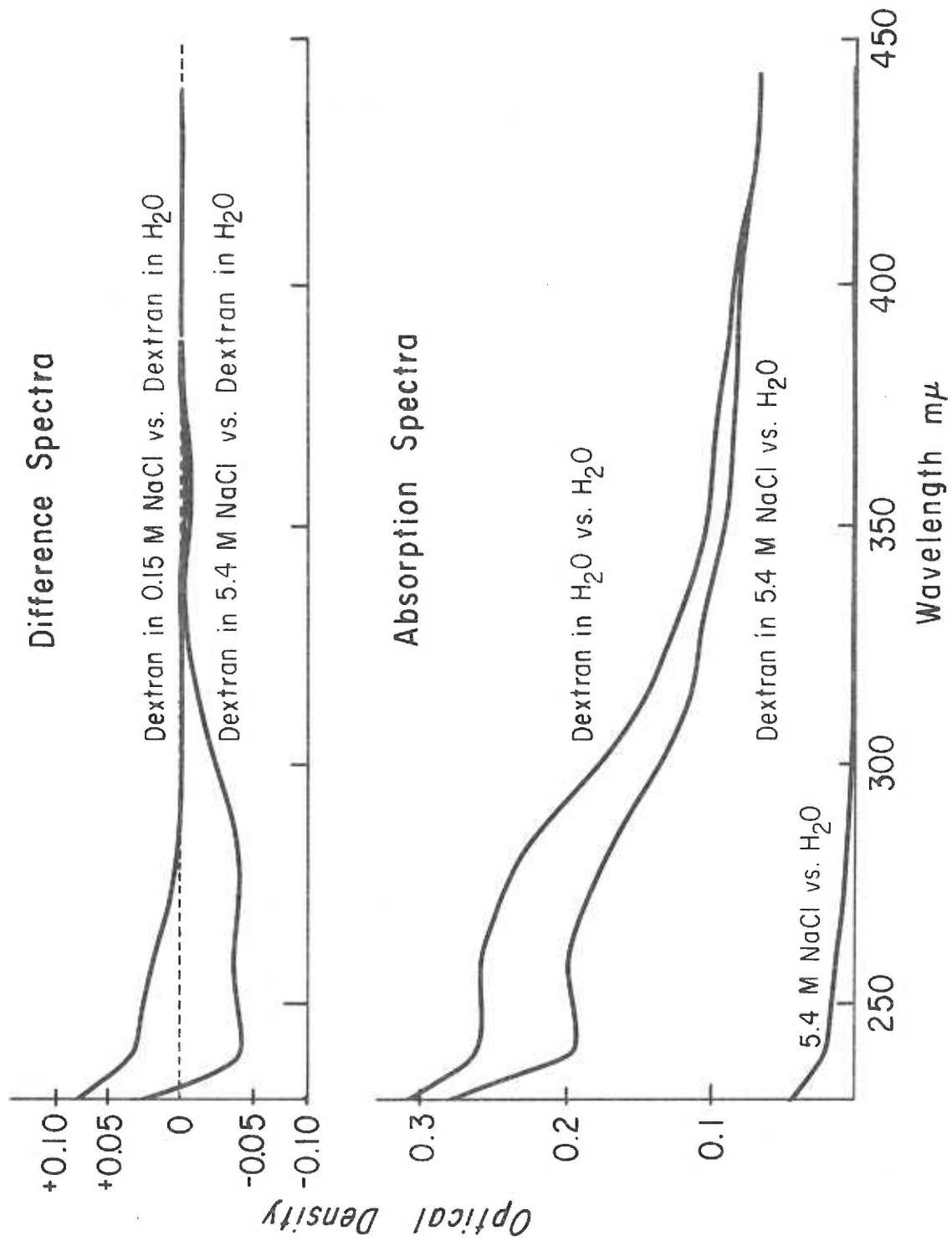


Figure 2-3. The absorption and difference spectra of dextran in aqueous salt solutions.

germane to the problem at hand are experiments on the electrophoretic behavior of particles suspended in polymer-salt solutions. None of the following observations support the anion adsorption hypothesis as an explanation for the increased zeta potentials of erythrocytes suspended in neutral polymer/salt solutions.

- (i) While the solubility studies indicate that the ion binding properties of dextran and PEG are directly opposite to each other, both these polymers produce relative zeta potential increases of fixed and normal red cells at physiological ionic strength (Chapter 5). The relative zeta potential,  $Z$ , increases with increasing molecular weight in both cases. On the basis of number of monomer units per molecule,  $Z$  is greater per monomer unit of PEG than per monomer of dextran. These results directly contradict expectations based on the ion binding studies.
- (ii) The mobility of fixed and normal erythrocytes in 4.39% dextran 77.6 is constant from pH 4.5 to 10 (Figure 5-4). Particles which acquire their charge by anion adsorption or cation desorption do not exhibit this type of behavior in general. Their mobility is almost always a continuously changing function of pH, due frequently to competitive  $\text{OH}^-$  binding (7, 198). The pH-mobility curves of Figure 5-4 are typical of surfaces composed of ionogenic groups, not of

adsorbed anions.

- (iii) The electrokinetic behavior of normal erythrocytes in dextran/salt is not a function of the anion present in the electrolyte solution (Chapter 5). The mobilities of fresh human red cells suspended in 5% dextran 110 and 0.145 M Na salts were indistinguishable if the anion was  $\text{Cl}^-$ ,  $\text{I}^-$ ,  $\text{F}^-$  or  $\text{CNS}^-$ . Thus, either the mobilities exhibit no anion spectrum, or the maximum difference is less than 5%. This independence of  $Z$  from the character of the anion also contradicts expectations based on an anion adsorption mechanism, since apparently all known binding phenomena show a preferential spectrum of activity as the ion type is changed (178).
- (iv) Shaw (7) has measured the mobility of dextran-coated oil droplets in an acetate-veronal buffer at a constant ionic strength of  $0.05 \text{ gm-ions l}^{-1}$ , and found it to be almost zero between pH 2.4 and 9.5. The oil droplets themselves with no dextran present exhibit continuously increasing mobilities from  $\sim -0.03$  to  $-6.0 \mu \text{ s}^{-1} \text{ v}^{-1} \text{ cm}$  under the same conditions. Hence, at the oil-water interface, dextran does not acquire a negative charge by ion adsorption.
- (v) Quartz, bentonite and rutile all show values of  $Z$  less than or equal to one when equilibrated with 5% dextran 110 (Chapter 5). All of these particles apparently acquire their

electrokinetic charge totally or in part through the mechanism of ion adsorption or desorption, since their charge densities decrease with decreasing ionic strength (199). That the dextran adsorbs to the particles is inferred from the fact that the zeta potential changes in dextran. Hence, adsorbed dextran at a solid particle-solution interface produces both a lower absolute zeta potential than red cells and a relative zeta potential less than one. One possible explanation of this effect is that the decrease is due to the adsorbed dextran displacing adsorbed ions from the surface. That this may not be an unreasonable suggestion is seen from the measured binding energy of  $\text{Cl}^-$  to quartz (Chapter 5). The net free energy of binding was found to be  $\sim 2.5$  KCal/mole. This value may be compared with the net free energy of a hydrogen bond, believed to be of the order of 3 to 5 KCal/mole (200). If hydrogen bonding is involved in the interaction between dextran and quartz, as seems reasonable considering their structures, this binding energy difference may be sufficient to allow the postulated displacement if the polymer monomer and ion compete for the same site. Regardless of the mechanism, adsorbed dextran is associated with a decrease in the zeta potential of bentonite and rutile. Any anion adsorption to the adsorbed dextran, if

present, is of insufficient magnitude to explain the red cell-dextran results.

Virtually all the microelectrophoretic evidence, then, indicates that adsorbed dextran does not acquire a negative charge through the mechanism of anion adsorption or cation desorption. A possible counter argument that could be applied to this conclusion is the possibility that the erythrocyte interfacial region, being porous and of unknown structure, could by its nature induce an unusual configuration on the adsorbed dextran. This configuration might encourage anion adsorption to regions of the polymer. Silberberg's (56) theoretical treatment has shown, however, that the structure of the adsorbed layer as measured by the amount of polymer adsorbed in the form of loops is practically independent of the monomer-surface interaction energy. Thus, the structure of at least the diffuse part of the layer would not be expected to vary markedly from surface to surface. In particular, the bulk of the dextran adsorbed to red cells should not take on a unique structure.

It seems, then, that ion adsorption phenomena cannot explain the experimentally observed increase in relative zeta potential of erythrocytes suspended in dextran.

#### IV. The Effect on Counterion Chemical Potentials of a Concentrated Surface Phase of Neutral Polymers

The final model to be considered treats the effect that an adsorbed layer of neutral polymer could be expected to have on the chemical potentials of counterions in the double layer. The adsorbed layer is represented analytically as simply a concentrated solution of polymer occupying a region of finite thickness adjacent to the infinite, flat, smeared charge plane of the cell. No interactions of the polymer with either the charge surface or the bulk solution interface are considered. Only through the increased concentration of polymer in the surface phase, and through the presence of an electrostatic potential in that phase is the influence of the charged surface represented. The adsorbed polymer is assumed to have no effect on the charge density at the solid-solution interface. The surface phase consisting of polymer, ions and solvent is considered to be in equilibrium with a bulk phase characterized by the free solution values for ion and polymer concentrations. Equating the chemical potentials of the ions in the two phases leads to a modified Boltzmann equation, which is used to derive relationships relating the zeta potential measured in the presence of such a surface phase with that measured in its absence. The presence of the adsorbed polymer increases the thickness of the counterion double layer. Under suitable circumstances, the zeta potential is shown to be increased when an adsorbed layer is present.

Expressions are derived for the relative zeta potential as a function of the difference in polymer concentration between the surface and bulk phases, the thickness of the surface phase, the ionic strength of the solution, and the location of the shear plane. The necessity for counterion penetration of an adsorbed layer if its presence is to be detected electrokinetically is pointed out. Finally, the effects of adsorbed polymer surface phases on the mobility-zeta potential relationship and on the electrostatic repulsive potentials between charged plates are discussed.

#### A. The Boltzmann Equation Modified for the Presence of a Concentrated Surface Phase of Neutral Polymer

The expression required must relate the concentration of ions in the surface phase to that in the bulk phase through the electrostatic potential. To obtain such a relationship, we employ the Flory-Huggins theory for concentrated polymer solutions based on the statistical mechanics of a lattice solution model (83, 201). The Flory-Huggins theory applied to the present quaternary system assumes that the volumes occupied by a solvent molecule and each of the ionic species are equal, and that the polymer molecule may be represented by  $P$  units, each of this same volume. These units need not be identified with the monomeric species making up the polymer, although it is convenient here to make this correspondence. We take  $P$ , then, to be the degree of polymerization of the polymer which is directly proportional to its



molecular weight. Assuming that the polymer is homogeneous, the free energy of mixing,  $\Delta F$ , for the polymer/ion solution making up the surface phase (assuming no specific polymer-surface interactions) is given by (83):

$$\frac{\Delta F}{kT} = n_o \ln \Phi_o + n_p \ln \Phi_p + \sum_i n_i' \ln \Phi_i + \psi \sum_i n_i' z_i + \sum_{j < k} n_j \Phi_k \chi_{jk} \quad (2-18)$$

where

$n_o$  = number of solvent (water) molecules present in the phase

$n_p$  = number of polymer molecules of degree of polymerization

$P$  present in the phase

$n_i'$  = number of ions of  $i$ th type present in the phase

$\Phi_o$  = volume fraction of solvent in phase =  $\frac{n_o}{n_o + n_p P + \sum_i n_i'}$

$\Phi_p$  = volume fraction of polymer in phase =  $\frac{n_p P}{n_o + n_p P + \sum_i n_i'}$

$\Phi_i$  = volume fraction of  $i$ th ion in phase =  $\frac{n_i'}{n_o + n_p P + \sum_i n_i'}$

$\psi = \frac{e\bar{\Psi}}{kT}$  is the electrostatic energy of a unit charge in the sur-

face phase in units of  $kT$  where the electrostatic potential

is  $\bar{\Psi}$

$\sum_{j < k} n_j \Phi_k \chi_{jk}$ : the summation is taken over all pairs of unlike species in the phase

$\chi_{jk} = \frac{z \Delta w_{jk} P_j}{kT}$  is the interaction energy parameter for the  $j$ th and  $k$ th species

$z$  = coordination number of lattice

$\Delta w_{jk}$  = change in energy resulting from replacing  $j$ - $j$  and  $k$ - $k$  contacts with contacts between the  $j$  and  $k$  species

$= w_{jk} - \frac{(w_{jj} + w_{kk})}{2}$ , where  $w_{jj}$  is the energy required to break an association between two type  $j$  molecules, etc.

$P_j$  = degree of polymerization of  $j$ th species (= 1 for solvent and ions,  $P$  for polymer)

The first three terms on the right hand side (RHS) represent the entropy of mixing for the components of the surface phase, the fourth term is the electrostatic free energy of the ions in the potential due to the surface charge, and the last term represents the heat of mixing of the various components. The chemical potential of the  $i$ th ionic species in the surface phase,  $\mu_i$ , is obtained by differentiating (2-18) with respect to  $n_i'$  (at constant  $n_j'$ , temperature and pressure):

$$\frac{\mu_i - \mu_i^0}{kT} = \frac{1}{kT} \left[ \frac{\partial \Delta F}{\partial n_i'} \right]_{n_j'}$$

where  $\mu_i^0$  is the chemical potential in the standard state. Considering now only a 1:1 electrolyte, the differentiation gives, after some

rearrangement:

$$\begin{aligned} \frac{\mu_i - \mu_i^0}{kT} = & \ln \Phi_i + \Phi_p (1-P^{-1}) + z_i \psi - \frac{n_o \Phi_p \chi_{op}}{N_T} - \frac{n_o \Phi_j \chi_{oj}}{N_T} - \frac{n_p \Phi_j \chi_{pj}}{N_T} \\ & + (n_o \chi_{oi} + n_p \chi_{pi}) \frac{(1-\Phi_i)}{N_T} + \Phi_j (1-\Phi_j) \chi_{ij} \end{aligned} \quad (2-19)$$

where  $N_T = n_o + n_p P + \sum_i n_i$  = total volume in phase, and the  $i, j$  refer only to the two ionic species. In (2-19), the first three terms on the RHS come from the entropy of mixing terms, and the last five from the heat of mixing terms. Multiplying out these last terms, considering only the interaction terms involving the polymer, and dropping all second order terms  $\Phi_k \Phi_l$  not involving the solvent (since  $\Phi_o \sim 1$ , but  $\Phi_p \Phi_i$ , for instance, will be  $\ll 1$ ) gives:

$$\frac{\mu_i - \mu_i^0}{kT} = \ln \Phi_i + \Phi_p (1-P^{-1} + \chi_{ip} - \Phi_o \chi_{op}) + z_i \psi \quad (2-20)$$

where we have used  $\frac{\chi_{pi}}{P} = \chi_{ip}$ , from the definition of  $\chi_{pi}$ . We now consider that this surface phase is in equilibrium with the bulk phase far away from the surface, where the potential is zero. The chemical potential of the  $i$ th ion type in the bulk phase,  $\mu_{io}$ , relative to the same standard state  $\mu_i^0$  as that for the surface phase ions, will then be given by:

$$\frac{\mu_{i0} - \mu_i^0}{kT} = \ln \frac{\Phi_{i0}}{\Phi_{i0} + \Phi_{p0}(1-P^{-1} + \chi_{ip} - \Phi_{o0}\chi_{op})} \quad (2-21)$$

where the second subscript  $o$  refers to the bulk phase values.

Equating these chemical potentials, assuming the volume fractions occupied by the solvent in the two phases are equal, and rearranging gives:

$$\ln \frac{\Phi_i}{\Phi_{i0}} = -z_i \psi - (\Phi_p - \Phi_{p0})(1-P^{-1} + \chi_{ip} - \Phi_o \chi_{op}) \quad (2-22)$$

The dependence of the ionic concentration on the potential is then given by:

$$\Phi_i = \Phi_{i0} \exp[-z_i \psi - (\Phi_p - \Phi_{p0})(1-P^{-1} + \chi_{ip} - \Phi_o \chi_{op})] \quad (2-23)$$

Expanding the second term in the exponential to include only first order terms in  $(\Phi_p - \Phi_{p0})$  (that is, assuming  $[(\Phi_p - \Phi_{p0})][1-P^{-1} + \chi_{ip} - \Phi_o \chi_{op}] \ll 1$ ), and identifying the volume fraction of ions with the number of ions present per  $\text{cm}^3$ ,  $n_i$ , gives the modified form of the Boltzmann equation to be used in this investigation:

$$n_i = n_{i0} [1 - \beta] \exp\left[-\frac{z_i e \Psi(x)}{kT}\right] \quad (2-24)$$

where the notation of Chapter 1 has been retained and we have defined

$$\beta \equiv (\Phi_p - \Phi_{po})(1 - P^{-1} + \chi_{ip} - \Phi_o \chi_{op}) \quad (2-25)$$

or

$$\beta = (\Phi_p - \Phi_{po})F(\chi)$$

where

$$F(\chi) \equiv (1 - P^{-1} + \chi_{ip} - \Phi_o \chi_{op})$$

The expansion of  $\exp(-\beta)$  is taken only to first order in  $\beta$  because in the derivation of the electrokinetic equations to follow, only the linearized form of equation (2-24) is dealt with.

The form of equation (2-24) is similar to the modified Boltzmann equation first proposed by Bikerman (202), and since used by a number of authors (203, 204, 205) to account for the effect of ionic size on counterion double layer distributions. In these treatments, as well as in Haydon and Taylor's (206) and Haydon's (24) treatment of the limited solvent volume available to counterions behind a charge plane, the parameter analogous to  $\beta$  is identified with the volume fraction of the solution from which the counterions are excluded due to steric limitations. The polymer adsorption factor  $\beta$ , on the other hand, is not associated with an excluded volume in this linear treatment, since exclusion effects in polymer solutions are associated with terms of second order in  $\Phi_p$  (83).

The adsorption factor  $\beta$  is seen to be proportional to the difference between the volume fractions occupied by polymer in the

surface and bulk phases. In this simple model,  $\beta$  is further seen to depend on the energy of interaction parameters,  $\chi$ , which describe the ion-polymer and solvent-polymer interactions. Since for good solvents,  $\chi_{op} \leq 0$  (83), it is seen that under conditions of equal adsorption,  $\beta$  should be larger the better the polymer solvent. Similarly, the extent of interaction between polymer and ions can be expected to affect  $\beta$  through  $\chi_{ip}$ , while the  $P^{-1}$  term indicates there should be virtually no molecular weight dependence for high polymers. The assumptions inherent in the model, however, limit the quantitative interpretation of equation (2-25). The statistical mechanical theory of polymer adsorption (56) shows that the surface phase of adsorbed polymer should not be treated as if the polymer were simply in solution. Even within the context of the present model, it is clear from work on polymer adsorption in general that  $\Phi_p$  is strongly dependent on  $P$ ,  $\chi_{op}$ , and in the cell-dextran system,  $\Phi_{po}$  (Chapter 4). Variations as a function of  $\Phi_{po}$ ,  $P$  or  $\chi_{op}$  in an experimentally determined value of  $\beta$ , then, should be initially considered to reflect changes in  $\Phi_p$ , not in  $F(\chi)$ . Although equation (2-25) cannot be expected to provide an exact description of the adsorbed polymer layer, equation (2-24) seems to be sufficiently general to produce an approximate description of the counterion distribution adjacent to a charged surface to which a neutral polymer layer is adsorbed.

## B. The Theory of the Effect on the Zeta Potential of an Adsorbed Layer of Neutral Polymers

1. Permeable, Free Draining Layers of Finite Thickness and Constant Density. Following the derivation of the Gouy-Chapman equation given in Chapter 1, the equation to be solved in order to obtain an expression for the zeta potential in terms of  $\beta$  and the ion concentrations is the modified Poisson-Boltzmann equation:

$$\frac{d^2 \psi(x)}{dx^2} = -\frac{4\pi}{\epsilon} \sum_i z_i e n_{i0} [1 - \beta(x)] \exp \left[ \frac{-z_i e \psi(x)}{kT} \right] \quad (2-26)$$

obtained by combining (2-24) with (1-2) as before. We have here included the  $x$  dependence of  $\beta$  since we assume the adsorbed surface phase to be of finite thickness. Again, assuming  $\left[ \frac{z_i e \psi(x)}{kT} \right] \ll 1$  so that the exponential may be linearized, applying the electroneutrality condition, and considering only 1:1 electrolytes gives:

$$\frac{d^2 \psi(x)}{dx^2} = \kappa^2 [1 - \beta(x)] \psi(x) \quad (2-27)$$

where  $\kappa$  is the reciprocal double layer thickness in the absence of an adsorbed layer as defined in Chapter 1. To solve (2-27) the dependence of the polymer adsorption factor  $\beta$  on  $x$ , the distance from the charge plane, must be specified. From the definition of  $\beta$ ,

it is apparent that its spatial variation should depend on the  $x$  variation of the polymer segment density in the adsorbed layer. There is no experimental data available regarding this distribution, however. Initially then, following Silberberg (56), it will be assumed that  $\beta(x)$  is a step function, having a constant value  $\beta(x) = \beta < 1$  for  $0 \leq x \leq d$ , and  $\beta(x) = 0$  for  $x > d$  (Figure 2-4). This has the advantage that (2-23) may be solved in closed form. Additional functional forms for  $\beta(x)$  will be considered subsequently.

As in Section I, p. 61, the solution must be considered in two regions: within the adsorbed layer, (region 1;  $0 \leq x \leq d$ ), and external to it (region 2;  $x > d$ ). It is assumed that no counterion penetration behind the charge plane occurs. In the two regions, (2-27) is written as:

$$\psi_1''(x) = \kappa^2(1-\beta)\psi_1(x) \quad \text{in region 1} \quad (2-28)$$

$$\psi_2''(x) = \kappa^2\psi_2(x) \quad \text{in region 2} \quad (2-29)$$

where

$$(\ )'' \equiv \frac{d^2(\ )}{dx^2}$$

The boundary conditions of p. 61 at  $x = d$  are, assuming  $\epsilon_1 = \epsilon_2$

(see Chapter 4):

$$\psi_1(d) = \psi_2(d) \quad (2-30)$$

$$\psi_1'(d) = \psi_2'(d) \quad (2-31)$$



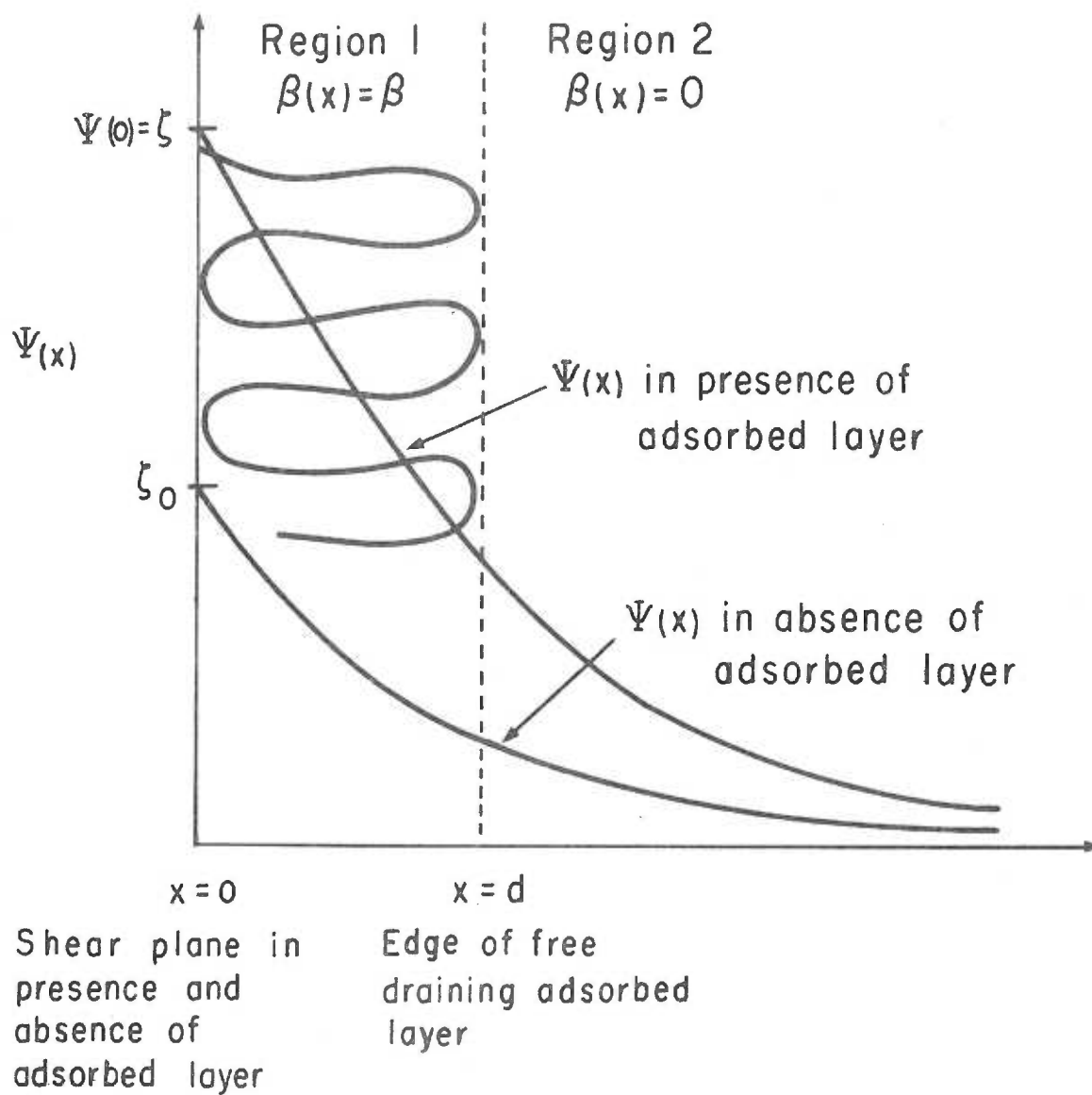


Figure 2-4. The potential distribution adjacent to a charged surface in the presence of a permeable adsorbed free draining layer.

where

$$(\cdot)' \equiv \frac{d(\cdot)}{dx}$$

The general solutions in regions 1 and 2 are:

$$\psi_1(x) = a_1 \exp(-\kappa_\beta x) + b_1 \exp(\kappa_\beta x) \quad (2-32)$$

where

$$\kappa_\beta \equiv \kappa \sqrt{1-\beta}$$

$$\psi_2(x) = a_2 \exp(-\kappa x) \quad (2-33)$$

since

$$\psi_2(x) \rightarrow 0 \quad \text{as} \quad x \rightarrow \infty$$

Applying (2-30) and (2-31), and noting that at  $x = 0$ ,  $\psi(0) = a_1 + b_1$ ,

the coefficients are found to be:

$$a_1 = \frac{\psi(0)(1 + \kappa_\beta/\kappa) \exp(\kappa_\beta d)}{2(\sinh \kappa_\beta d + (\kappa_\beta/\kappa) \cosh \kappa_\beta d)} \quad (2-34)$$

$$b_1 = \frac{\psi(0)(\kappa_\beta/\kappa - 1) \exp(-\kappa_\beta d)}{2(\sinh \kappa_\beta d + (\kappa_\beta/\kappa) \cosh \kappa_\beta d)} \quad (2-35)$$

$$a_2 = \frac{\psi(0)(\kappa_\beta/\kappa) \exp \kappa d}{\sinh \kappa_\beta d + (\kappa_\beta/\kappa) \cosh \kappa_\beta d} \quad (2-36)$$

Since  $\epsilon$  is constant throughout, the surface charge density,  $\sigma$ , is given by:

$$\sigma = -\frac{\epsilon}{4\pi} \frac{d\psi_1(0)}{dx} \quad (1-16)$$

Differentiating  $\psi_1(x)$  and setting  $x = 0$  gives:

$$\psi_1'(0) = \kappa_\beta (b_1 - a_1) \quad (2-37)$$

Substituting for  $a_1$  and  $b_1$ , recalling the definition of  $\kappa_\beta$ , and rearranging, gives:

$$\frac{4\pi\sigma}{\kappa\epsilon} = \psi(0)\sqrt{1-\beta} \left[ \frac{\sqrt{1-\beta} \sinh(\kappa d\sqrt{1-\beta}) + \cosh(\kappa d\sqrt{1-\beta})}{\sinh(\kappa d\sqrt{1-\beta}) + \sqrt{1-\beta} \cosh(\kappa d\sqrt{1-\beta})} \right] \quad (2-38)$$

Now, from (1-17) it is seen that the left hand side of (2-38) is just  $\zeta_0$ , the zeta potential of the charged surface in the absence of the adsorbed polymer layer. If it is assumed, for the present, that the presence of the adsorbed layer causes no change in location of the plane of shear, i. e., that the adsorbed layer is free draining, then  $\psi(0) = \zeta$ , the zeta potential in the presence of the adsorbed layer, and  $Z$ , the relative zeta potential in the presence of the adsorbed layer, is given by:

$$Z = \frac{\zeta}{\zeta_0} = \frac{1}{\sqrt{1-\beta}} \left[ \frac{\sinh(\kappa d\sqrt{1-\beta}) + \sqrt{1-\beta} \cosh(\kappa d\sqrt{1-\beta})}{\sqrt{1-\beta} \sinh(\kappa d\sqrt{1-\beta}) + \cosh(\kappa d\sqrt{1-\beta})} \right] \quad (2.39)$$

This expression goes to the expected limits:

(i)  $\beta \rightarrow 0 \Rightarrow Z \rightarrow 1$  as it must.

- (ii) At high ionic strength where  $c$ , the electrolyte concentration, is such that  $\kappa d\sqrt{1-\beta} \gg 1$  the bracketed term goes to 1 and  $Z \approx 1/\sqrt{1-\beta}$ . Therefore, the relative zeta potential at high ionic strength may be used to calculate a value for  $\beta$ , which should be directly related to the polymer segment density.
- (iii) At low ionic strength such that  $\kappa d\sqrt{1-\beta} \ll 1$ ,  $\sinh(\ ) \rightarrow 0$  and  $\cosh(\ ) \rightarrow 1$ , therefore

$$Z \rightarrow \frac{1}{\sqrt{1-\beta}} \left[ \frac{0 + \sqrt{1-\beta} \cdot 1}{0 + 1} \right] = 1$$

Therefore, as the ionic strength is decreased,  $Z$  decreases towards 1 in this model. This is as expected, since decreasing  $c$  increases the double layer thickness ( $1/\kappa$ ). If the double layer extends much farther into solution than the adsorbed layer, the effect of the layer would be expected to become less significant, and in the limit as  $c \rightarrow 0$  should vanish, as (2-39) indicates.

A plot of  $Z$  vs  $c$  for some representative values of  $\beta$  and  $d$ , the adsorbed layer thickness, is given in Figure 2-5.

Possibly the most debatable assumption employed in the above treatment is that involving the location of the shear plane. It has been assumed thus far that the adsorbed layer has caused no shift in

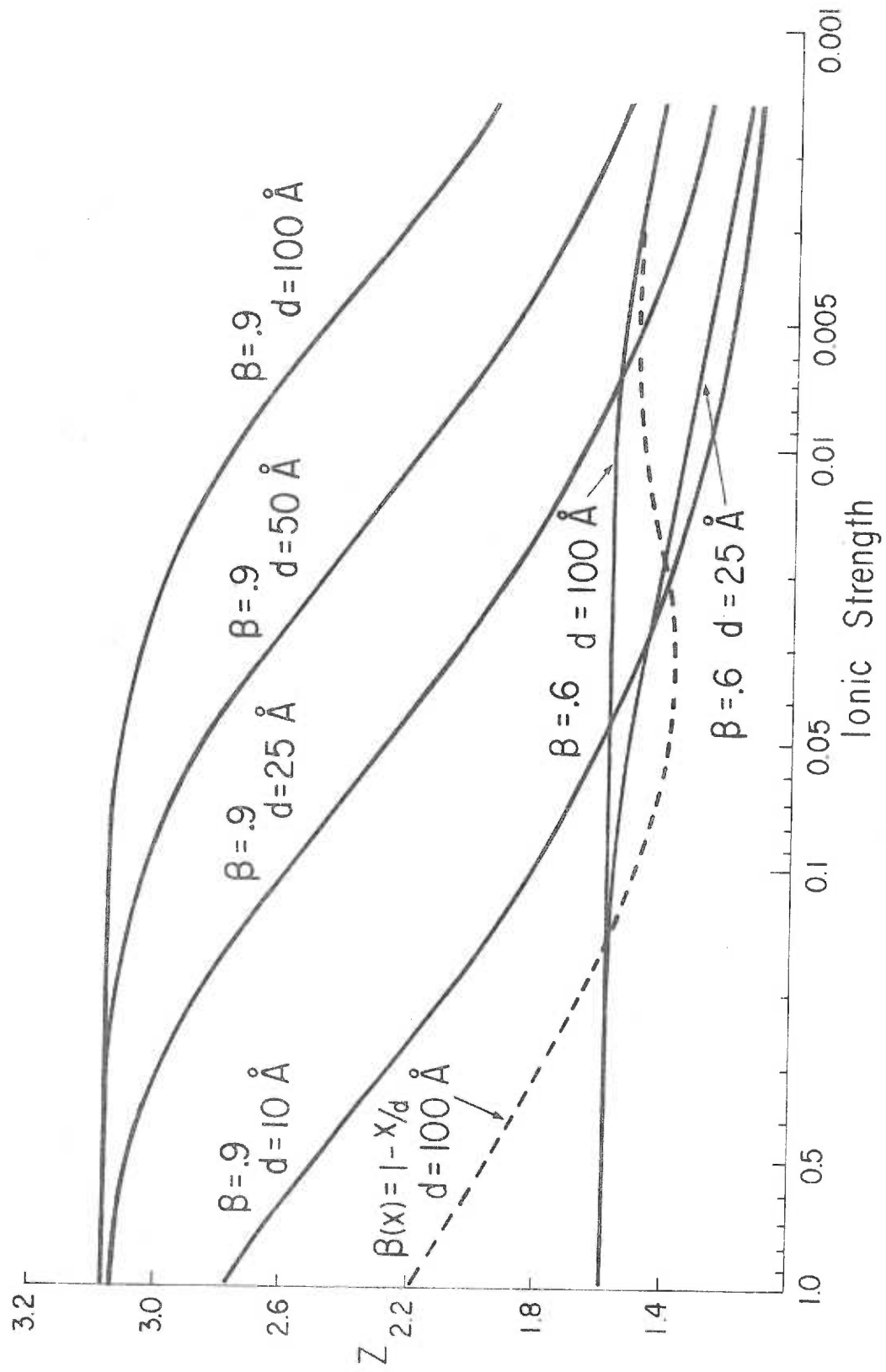


Figure 2-5. Relative zeta potential vs. ionic strength for a free draining adsorbed layer.

the shear plane. That is, the adsorbed layer has been assumed to be free draining at the velocities employed in microelectrophoresis (of the order of 1 to 10  $\mu$ /sec).

A more realistic case will now be treated.

## 2. Partially Permeable, Partially Free Draining Adsorbed

Layers. The adsorbed polymer layer is here assumed to consist of two parts: an inner, dense layer ( $\Phi_p \gg \Phi_{p0}$ ;  $\Phi_p \sim 1$ ), of dielectric constant  $\epsilon_1$ , which is impenetrable to counterions and rigid under shear (region 1), and an outer, free draining layer permeable to counterions, of the same dielectric constant as the bulk solution,  $\epsilon_2$  (region 2). It is assumed that the polymer adsorption factors for the two parts of the layer are both step functions:

$$\text{Region 1: } \beta(x) \sim 1 \quad \epsilon = \epsilon_1 \quad 0 < x \leq d_1$$

$$\text{Region 2: } \beta(x) = \beta \quad \epsilon = \epsilon_2 \quad d_1 < x \leq d_2$$

$$\text{Region 3: } \beta(x) = 0 \quad \epsilon = \epsilon_2 \quad d_2 < x$$

The shear plane, then, is assumed to occur at  $x = d_1$ , and the zeta potential will be  $\zeta = \psi(d_1)$  (Figure 2-6). The differential equations to be solved in the three regions are:

$$\text{Region 1: } \psi_1''(x) = 0 \tag{2-40}$$

since no counterions penetrate this region,

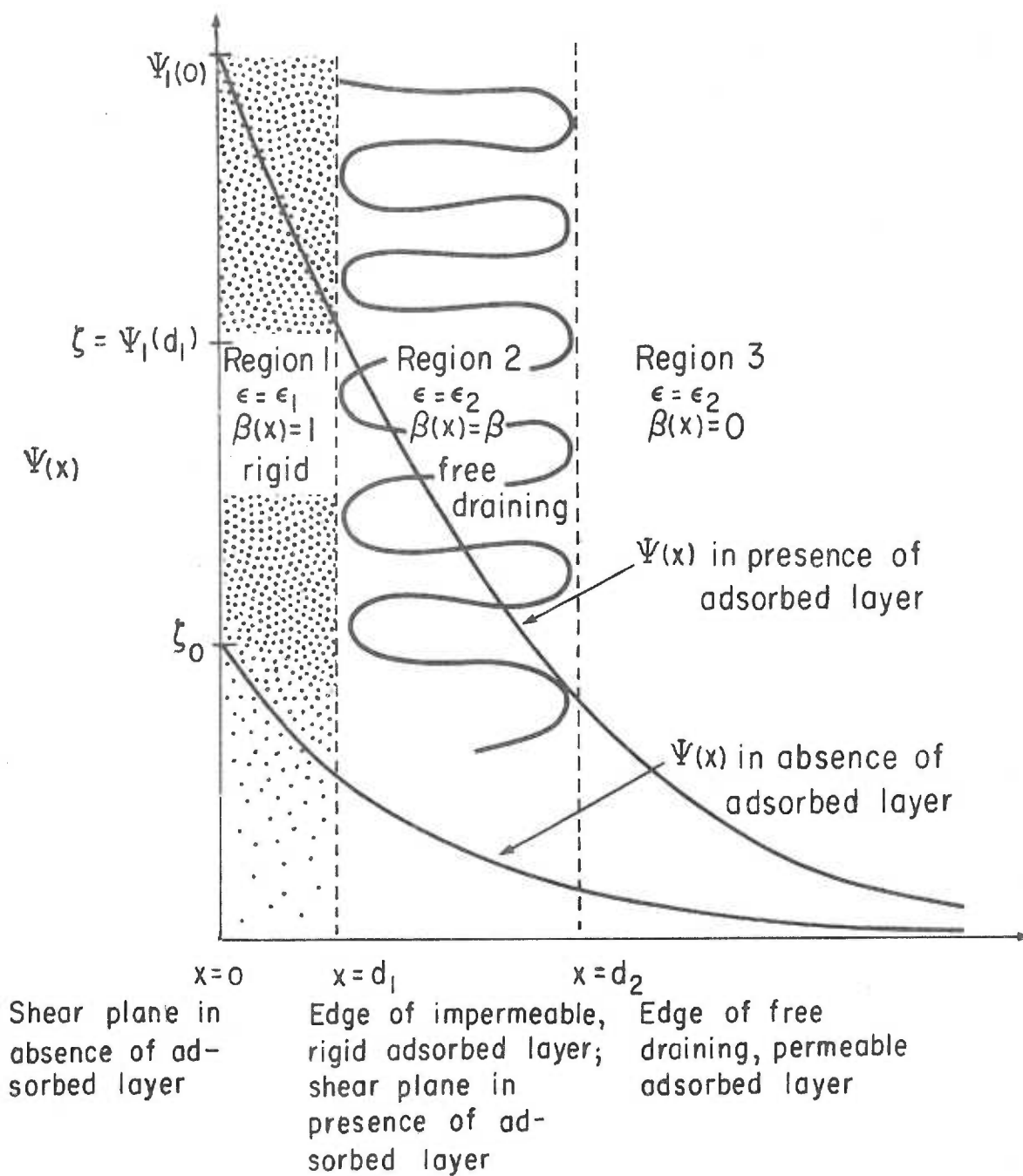


Figure 2-6. The potential distribution adjacent to a charged surface in the presence of a partially permeable, partially free draining adsorbed layer.

$$\text{Region 2:} \quad \psi_2''(x) = \kappa_\beta \psi_2(x) \quad (2-41)$$

$$\text{Region 3:} \quad \psi_3''(x) = \kappa \psi_3(x) \quad (2-42)$$

where the symbols have their previous meanings.

The boundary conditions are:

$$\text{at } x = d_1 \quad \psi_1(d_1) = \psi_2(d_1) \quad (2-43)$$

$$\psi_1'(d_1) = \epsilon_r \psi_2'(d_1) \quad (2-44)$$

where  $\epsilon_r = \epsilon_2 / \epsilon_1$ .

$$\text{at } x = d_2 \quad \psi_2(d_2) = \psi_3(d_2) \quad (2-45)$$

$$\psi_2'(d_2) = \psi_3'(d_2) \quad (2-46)$$

$$\psi_3(x) \rightarrow 0 \quad \text{as } x \rightarrow \infty$$

The general solutions which apply in the three regions are:

$$\psi_1(x) = a_1 x + b_1 \quad (2-47)$$

$$\psi_2(x) = a_2 \exp(-\kappa_\beta x) + b_2 \exp(\kappa_\beta x) \quad (2-48)$$

$$\psi_3(x) = a_3 \exp(-\kappa x) \quad (2-49)$$

Applying the boundary conditions, some algebra gives:

$$a_1 = \frac{\zeta - \psi(0)}{d_1} \quad (2-50)$$



$$b_1 = \psi(0) \quad (2-51)$$

$$a_2 = \frac{\zeta}{2} \left[ 1 - \frac{1-\psi(0)}{\epsilon_r d_1 \kappa_\beta} \right] \exp(\kappa_\beta d_1) \quad (2-52)$$

$$b_2 = \frac{\zeta}{2} \left[ 1 + \frac{1-\psi(0)}{\epsilon_r d_1 \kappa_\beta} \right] \exp(-\kappa_\beta d_1) \quad (2-53)$$

$$a_3 = \frac{\zeta \left[ 1 + \frac{1-\psi(0)}{\epsilon_r d_1 \kappa_\beta} \right]}{(1-\kappa/\kappa_\beta)} \exp(\kappa + \kappa_\beta) d_2 - \kappa_\beta d_1 \quad (2-54)$$

$$a_3 = \frac{\zeta \left[ 1 - \frac{1-\psi(0)}{\epsilon_r d_1 \kappa_\beta} \right]}{(1+\kappa/\kappa_\beta)} \exp(\kappa - \kappa_\beta) d_2 + \kappa_\beta d_1 \quad (2-55)$$

Eliminating  $a_3$  between (2-54) and (2-55) gives the relation between  $\psi(0)$  and  $\zeta = \psi(d_1)$  to be:

$$\frac{\psi(0)}{\zeta} = 1 + \frac{(F-1)}{(F+1)} \epsilon_r d_1 \kappa_\beta \quad (2-56)$$

where

$$F \equiv \frac{(1+\kappa/\kappa_\beta)}{(1-\kappa/\kappa_\beta)} \exp[2\kappa_\beta (d_2 - d_1)] \quad (2-57)$$

To express  $\zeta$  in terms of the zeta potential in the absence of any adsorbed layer,  $\zeta_0$ , we again apply (1-16):

$$\sigma = \frac{-\epsilon_1}{4\pi} \frac{d\psi_1(0)}{dx} \quad (1-16)$$

Noting that (2-47) and (2-50) give  $\psi_1'(0) = [\zeta - \psi(0)]/d_1$  and recalling

that  $\zeta_o = \frac{4\pi\sigma}{\kappa\epsilon_2}$ , we obtain:

$$\zeta_o = \frac{\zeta}{\epsilon_r \kappa d_1} [(\psi_o/\zeta) - 1]$$

Substituting for  $\psi_o/\zeta$  from (2-56) gives:

$$\zeta_o = \zeta \frac{\kappa_\beta}{\kappa} \frac{(F-1)}{(F+1)}$$

whence, by recalling the definitions of  $F$  and  $\kappa_\beta$ , and rearranging, we find finally for the relative zeta potential  $Z$ :

$$Z = \frac{\zeta}{\zeta_o} = \frac{1}{\sqrt{1-\beta}} \left[ \frac{\exp[2\kappa\sqrt{1-\beta}(d_2-d_1)] \left[ \frac{\sqrt{1-\beta}+1}{\sqrt{1-\beta}-1} \right] + 1}{\exp[2\kappa\sqrt{1-\beta}(d_2-d_1)] \left[ \frac{\sqrt{1-\beta}+1}{\sqrt{1-\beta}-1} \right] - 1} \right] \quad (2-58)$$

We note that  $Z$  is independent of  $\epsilon_1$ , the dielectric constant of the impermeable layer, and is a function only of  $(d_2-d_1)$ , not  $d_2$  alone. In other words,  $Z$  depends only on the thickness of that region of the adsorbed layer penetrable by counterions. No estimate of the total layer thickness,  $d_2$ , may therefore be made electrokinetically.

Equations 2-39 and 2-58, and the results of Section I now allow us to prove that, under the assumptions given previously, the following statement is true:

The presence of an impermeable, rigid neutral layer external to a fixed charge system is impossible to detect electrokinetically.

Proof: It has been shown in Section I that if in the region external to the impenetrable layer  $\beta = 0$ , no change in zeta potential is observed if the shear plane is moved out to the edge of the layer. To show that in the case where  $\beta \neq 0$  the presence of the impenetrable layer has no effect on the zeta potential, we must show that the two solutions (2-39) and (2-58) are identical, i. e., we must prove the identity:

$$\frac{\sinh x + \sqrt{1-\beta} \cosh x}{\sqrt{1-\beta} \sinh x + \cosh x} \stackrel{?}{=} \frac{\exp 2x \left[ \frac{\sqrt{1-\beta} + 1}{\sqrt{1-\beta} - 1} \right] + 1}{\exp 2x \left[ \frac{\sqrt{1-\beta} + 1}{\sqrt{1-\beta} - 1} \right] - 1} \quad (2-59)$$

where  $x = \kappa \sqrt{1-\beta} d$ ,  $d$  being the penetrable layer thickness  $= (d_2 - d_1)$ . Multiplying the left hand side (LHS) by  $(\sqrt{1-\beta} \sinh x - \cosh x)$  top and bottom, applying the identities  $\sinh^2 x - \cosh^2 x \equiv -1$ ,  $2 \sinh x \cosh x \equiv \sinh 2x$ ,  $2 \sinh^2 x \equiv \cosh 2x - 1$ , recalling the definition of the hyperbolic functions, and multiplying top and bottom of the RHS by  $(\sqrt{1-\beta} - 1)$ , (2-59) becomes:

$$\frac{4\sqrt{1-\beta} + \beta \exp 2x - \beta \exp(-2x)}{4 - 2\beta + \beta \exp 2x + \beta \exp(-2x)} \stackrel{?}{=} \frac{\sqrt{1-\beta} \exp 2x + \exp 2x + \sqrt{1-\beta} - 1}{\sqrt{1-\beta} \exp 2x + \exp 2x - \sqrt{1-\beta} + 1} \quad (2-60)$$

To establish (2-60) we now assume its validity, show that this

assumption leads to an obvious identity, then show that (2-60) may be regained from the obvious identity by reversible operations (no dividing by zero, etc.) (207). So, cross multiplying (2-60):

$$\begin{aligned} & (\sqrt{1-\beta} \exp 2x + \exp 2x - \sqrt{1-\beta} + 1)(4\sqrt{1-\beta} + \beta \exp 2x - \beta \exp[-2x]) \\ \stackrel{?}{=} & (\sqrt{1-\beta} \exp 2x + \exp 2x + \sqrt{1-\beta} - 1)(4 - 2\beta + \beta \exp 2x + \beta \exp[-2x]) \quad (2-61) \end{aligned}$$

Multiplying out both sides and cancelling leads to  $0 \equiv 0$ , which is the obvious identity. To regain (2-60), we can add equally to each side of  $0 \equiv 0$  the required individual terms which in turn factor to give (2-61). To regain (2-60), we must be able to divide both sides by the first factor on the LHS, and the second factor on the RHS, which requires that neither can be zero for any allowed value of  $\beta$  or  $x$ . For these to be zero:

$$\begin{aligned} \text{(i)} \quad & \sqrt{1-\beta} \exp 2x + \exp 2x - \sqrt{1-\beta} + 1 = 0 \\ \Rightarrow & \exp 2x = \frac{\sqrt{1-\beta} - 1}{\sqrt{1-\beta} + 1} \end{aligned}$$

which is impossible, since  $\exp 2x > 0$  for  $x \geq 0$ , yet the RHS is negative, since  $0 \leq \beta < 1$  in a porous layer.

$$\begin{aligned} \text{(ii)} \quad & 4 - 2\beta + \beta \exp 2x + \beta \exp(-2x) = 0 \\ \Rightarrow & \exp 2x + \exp(-2x) = 2 \frac{(\beta-2)}{\beta} \end{aligned}$$

which is again impossible, since  $\text{LHS} > 0$  for all  $x$ , but for

$0 \leq \beta < 1$ ,  $\text{RHS} < 0$ . Therefore (2-61) may be divided by (i) and (ii) above, giving (2-60) and completing the proof.

3. Permeable Partially Free Draining Layers. The adsorbed layer is here assumed to be composed of a penetrable neutral layer which is partially free draining. That is, the shear plane has here been assumed to be moved out from the plane of charge to some point within the adsorbed layer.

(i) Consider first the case where the shear plane coincides with the outer edge of the adsorbed layer, a distance  $d$  from the plane of charge. The potential distribution is then as derived in Section 1, p. 96. From (2-33) and (2-36), the potential at the point  $d$ , the zeta potential, will be:

$$\zeta = \psi(d) = \frac{\psi(0)\sqrt{1-\beta}}{\sinh \kappa\sqrt{1-\beta}d + \sqrt{1-\beta} \cosh \kappa\sqrt{1-\beta}d} \quad (2-62)$$

but

$$\psi(0)\sqrt{1-\beta} = \zeta_0 \left[ \frac{\sinh \kappa\sqrt{1-\beta}d + \sqrt{1-\beta} \cosh \kappa\sqrt{1-\beta}d}{\sqrt{1-\beta} \sinh \kappa\sqrt{1-\beta}d + \cosh \kappa\sqrt{1-\beta}d} \right] \text{ from (2-38)}$$

$$\therefore Z = \frac{\zeta}{\zeta_0} = \frac{1}{\sqrt{1-\beta} \sinh \kappa\sqrt{1-\beta}d + \cosh \kappa\sqrt{1-\beta}d} \quad (2-63)$$

Clearly  $Z \leq 1$  here, since  $\cosh x \geq 1$  and  $\sqrt{1-\beta} \sinh x > 0$  for  $x > 0$ , as we have. If no free draining occurs in the adsorbed layer, then, the relative zeta potential will be less than or equal to one, at all electrolyte

concentrations.

- (ii) Let the shear plane occur at some distance  $d_s < d$  out from the plane of charge, and let  $d_F \equiv (d - d_s)$  be the thickness of the free draining region of the layer (Figure 2-7). The zeta potential will now be given by  $\zeta = \psi(d_s)$ . From (2-32), (2-34), and (2-35):

$$\zeta = \psi(d_s) = \frac{\psi(0)}{2D} [(1 + \sqrt{1-\beta}) \exp \kappa_\beta (d - d_s) + (\sqrt{1-\beta} - 1) \exp(-\kappa_\beta [d - d_s])] \quad (2-64)$$

where

$$D \equiv (\sinh \kappa \sqrt{1-\beta} d + \sqrt{1-\beta} \cosh \kappa \sqrt{1-\beta} d)$$

Simplifying the terms in brackets:

$$\zeta = \frac{\psi(0) D_F}{D} \quad (2-65)$$

where

$$D_F \equiv (\sinh \kappa \sqrt{1-\beta} d_F + \sqrt{1-\beta} \cosh \kappa \sqrt{1-\beta} d_F)$$

Again applying (2-38) gives finally:

$$Z = \frac{\zeta}{\zeta_0} = \frac{1}{\sqrt{1-\beta}} \left[ \frac{\sinh \kappa \sqrt{1-\beta} d_F + \sqrt{1-\beta} \cosh \kappa \sqrt{1-\beta} d_F}{\sqrt{1-\beta} \sinh \kappa \sqrt{1-\beta} d + \cosh \kappa \sqrt{1-\beta} d} \right] \quad (2-66)$$

This expression goes to the appropriate limits:

$$d_F \rightarrow 0 \Rightarrow Z \rightarrow (2-63)$$

$$d_F \rightarrow 0 \Rightarrow Z \rightarrow (2-38)$$

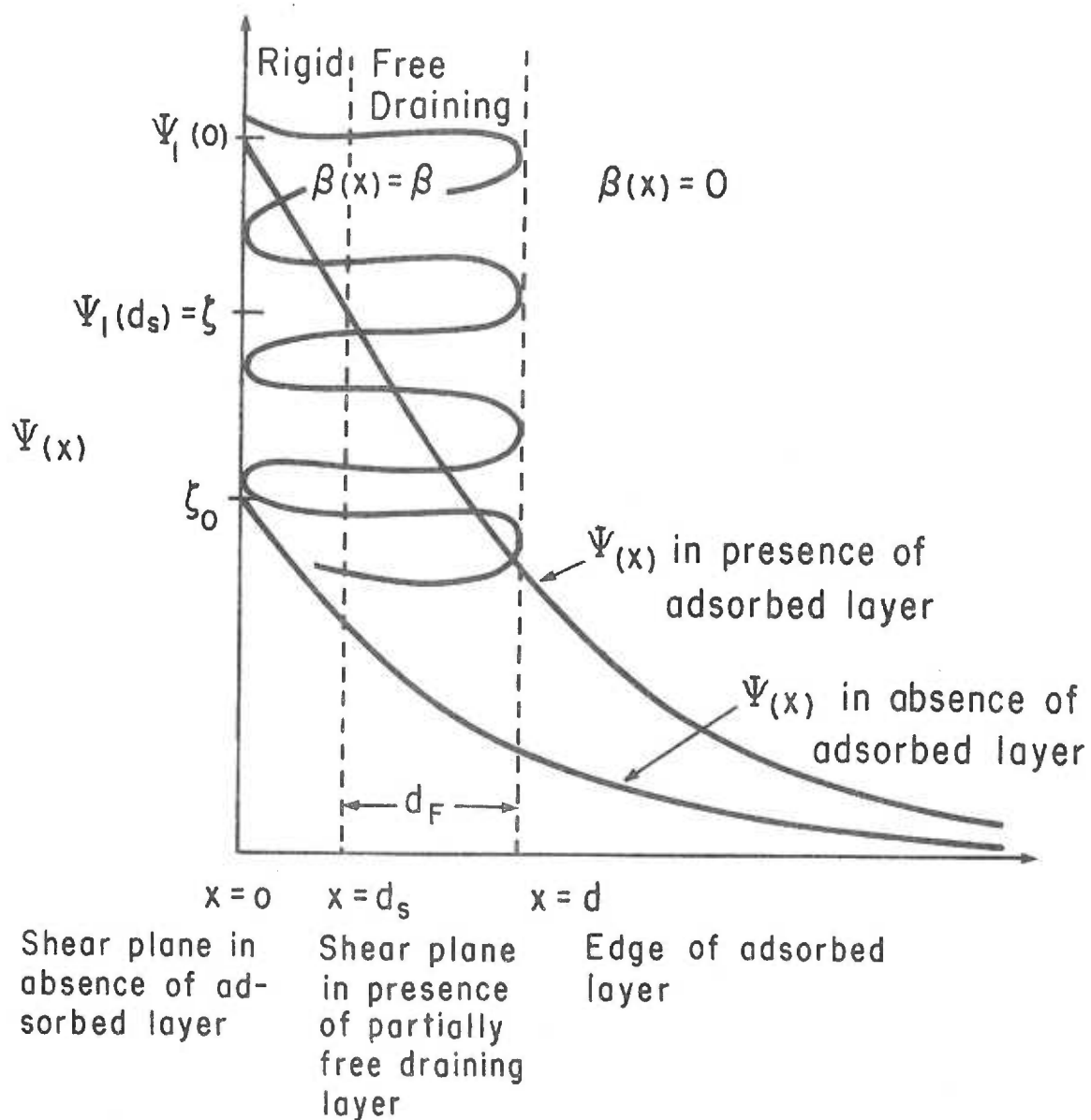


Figure 2-7. The potential distribution adjacent to a charged surface in the presence of a permeable, partially free draining adsorbed layer.

We have seen that if the entire permeable part of the adsorbed layer is free draining,  $Z \geq 1$  (Figure 2-5), and that if none of the permeable layer is free draining,  $Z \leq 1$  (2-63). The solution for the intermediate case, (2-66), must connect these two extremes. That is, there must be some value of  $d_F$  for which  $Z = 1$ . That this is in fact so may be seen from Figures 2-8 and 2-9 where  $Z(c)$ , according to (2-66), is plotted for some representative values of  $\beta$ ,  $d$  and  $d_F$ .

At high enough ionic strengths the double layer will be largely confined to that part of the adsorbed layer behind the shear plane, so the potential at the shear plane will be much lower than at the charge surface, and the relative zeta potential will be less than one. At very low electrolyte concentrations on the other hand, the double layer will extend so far out beyond the adsorbed layer that its effect will be negligible, and  $Z$  will approach 1. At intermediate ionic strengths, the double layer will occupy a significant fraction of the free draining part of the adsorbed layer so the potential will still be elevated at the shear plane and the relative zeta potential will be greater than one. The curves of  $Z(c)$ , then, will all exhibit an absolute maximum when the permeable adsorbed layer is partially free draining. If the permeable portion of the layer is totally free draining, no maximum appears, and  $Z(c)$  is a monotonically increasing function of  $c$ .



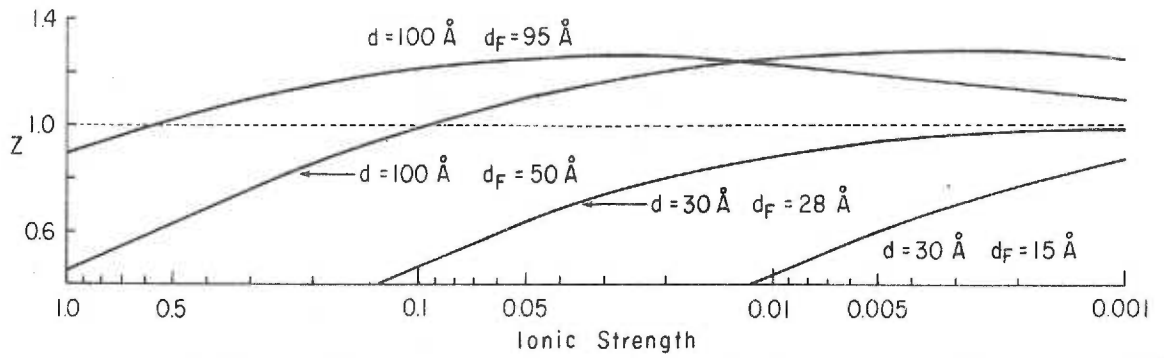


Figure 2-8. Relative zeta potential vs. ionic strength for a partially free draining adsorbed layer.  $\beta = 0.5$

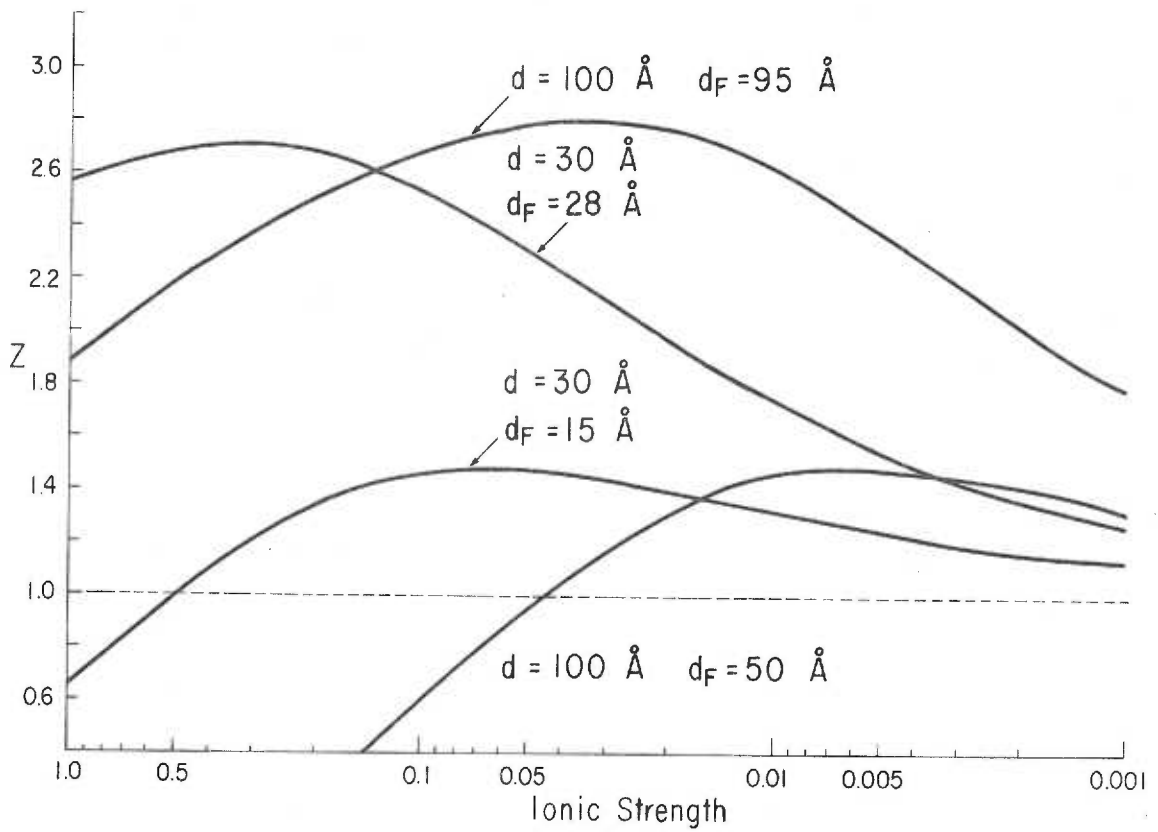


Figure 2-9. Relative zeta potential vs. ionic strength for a partially free draining adsorbed layer.  $\beta = 0.9$

Since we are here interested in the effects of an adsorbed layer on the electrokinetic behavior of cells, we shall explore the use of equation (2-66) no further. The use of  $Z(c)$  curves to examine the properties of neutral layers adsorbed to fixed charge systems is discussed in Appendix I.

4. Adsorbed Layers of Non-Constant Density. Up to this point, it has been assumed that the spatial distribution of the polymer adsorption factor,  $\beta(x)$ , has been given by one or a combination of step functions. That is, the effective density of the adsorbed layer has been constant throughout its depth. It would be useful, however, to know the theoretical dependence of  $Z$  on  $c$  for other functional forms of  $\beta(x)$ . Some functions of interest might include:

$$(i) \beta(x) = \beta_0 \exp(-x/d) \quad \text{since an isolated adsorbed} \quad (2-67)$$

polymer molecule apparently exhibits this kind of density distribution (55).

$$(ii) \beta(x) = \beta_0 [1 + (x/d)^m]^{-1} \quad \text{in analogy to many relaxation} \quad (2-68)$$

phenomena.

$$(iii) \beta(x) = \beta_0 (1 - x/d) \quad \text{a linear decrease from } \beta_0 \text{ to } 0 \text{ at} \quad (2-69)$$

$x = d$ .

The difficulty in employing such forms of  $\beta(x)$  comes in solving the differential equation (2-27) which results from their substitution. Only one case of non-constant density will be treated here, the simplest of the above cases, (iii). Let  $\beta(x) = 1 - x/d$ , i. e.,  $\beta_0 = 1$ .

The effective polymer segment density in this case would decrease linearly from one, to the bulk value at a distance  $d$  from the surface of charge. The differential equation to be solved then becomes, from (2-27):

$$\psi''(x) = \frac{\kappa^2 x}{d} \psi(x) \quad (2-70)$$

This equation has a series solution (Appendix II) which, under the appropriate boundary conditions, gives for the relative zeta potential in the presence of such a layer:

$$Z = \frac{\zeta}{\zeta_0} = \kappa \frac{F'_2(d) + \kappa F_2(d)}{F'_1(d) + \kappa F_1(d)} \quad (2-71)$$

where

$$F_1(d) = 1 + \sum_{m=1}^{\infty} \frac{(\kappa d)^{2m}}{2 \cdot 3 \cdot 5 \cdot 6 \dots (3m-1)3m}$$

$$F'_1(d) = \sum_{m=1}^{\infty} \frac{\kappa^{2m} d^{2m-1}}{2 \cdot 3 \cdot 5 \cdot 6 \dots (3m-1)}$$

$$F_2(d) = d + \sum_{m=1}^{\infty} \frac{\kappa^{2m} d^{2m-1}}{3 \cdot 4 \cdot 6 \cdot 7 \dots 3m(3m+1)}$$

$$F'_2(d) = 1 + \sum_{m=1}^{\infty} \frac{(\kappa d)^{2m}}{3 \cdot 4 \cdot 6 \cdot 7 \dots 3m}$$

A plot of  $Z(c, d)$  vs  $c$  for  $d = 100 \text{ \AA}$  is included in Figure 2-5. For equal values of  $Z$  at high ionic strength, we see that the solution for a linearly decreasing  $\beta(x)$  drops off more quickly than that for a step function factor of equal  $d$ , as would be expected. However, both models predict increased relative zeta potentials in the presence of neutral adsorbed layers, as experimentally observed.

#### The Effect of Neutral Adsorbed Layers on the Mobility-Zeta Potential Relationship

The foregoing calculations have outlined the consequences of the presence of a neutral, partially free draining layer on the zeta potential. The experimental observation of this effect is made electrophoretically in the systems under discussion. The question now to be examined is whether or not the presence of the adsorbed layer has any effect on the relationship between the electrophoretic mobility and the zeta potential of the particle.

It was shown in Section I, p. 5 that if the dielectric constant,  $\epsilon$ , is not a function of distance away from the plane of charge,  $x$ , that the relation between the particle mobility,  $U$ , and its zeta potential,  $\zeta$ , is given by:

$$U = \frac{\epsilon}{4\pi} \int_0^{\zeta} \frac{d\psi(x)}{\eta(x)} \quad (1-4)$$

If the medium viscosity is not a function of  $x$ , this gives the usual Helmholtz-Smoluchowski equation. In the presence of a free draining adsorbed layer, however, it is to be expected that the viscosity in the free draining layer,  $\eta_F$ , will be effectively higher than in the bulk medium,  $\eta_0$ . This dependence of  $\eta$  on  $x$  must then be included in the integral (1-4),

Two cases will be treated.

- (i) Free draining adsorbed layer of thickness  $d$  is sufficiently diffuse to have no effect on the counterion distribution, but has a viscosity  $\eta_F = r\eta_0$ , where  $r > 1$ . Then, transforming (1-4) to an integral over  $x$ , and converting the integration limits:

$$\begin{aligned} \frac{4\pi U}{\epsilon} &= \int_0^{\zeta} \frac{d\psi(x)}{\eta(x)} = \int_{\infty}^0 \frac{1}{\eta(x)} \frac{d\psi(x)}{dx} dx \\ &= \frac{1}{\eta_0} \int_{\infty}^d \frac{d\psi(x)}{dx} dx + \frac{1}{r\eta_0} \int_d^0 \frac{d\psi(x)}{dx} dx \end{aligned} \quad (2-72)$$

For  $\beta \sim 0$ , and under the usual assumptions, the potential distribution is given by:

$$\psi(x) = \psi(0) \exp(-\kappa x) \quad (1-12)$$

and the integrations of (2-72) give:

$$\frac{4\pi U}{\epsilon} = \frac{\psi(0)}{\eta_0} \left[ \frac{1}{r} + \left[ 1 - \frac{1}{r} \right] \exp(-\kappa d) \right]$$

Therefore the apparent zeta potential  $\zeta_{app} = 4\pi\eta_0 U/\epsilon$  is:

$$\zeta_{app} = \psi(0) \left[ \frac{1}{r} + \left[ 1 - \frac{1}{r} \right] \exp(-\kappa d) \right] \quad (2-73)$$

where the true zeta potential  $\zeta$  is assumed equal to  $\psi(0)$ .

That is,  $\zeta_{app}$  underestimates  $\zeta$  by a factor of between  $1/r$  (for large  $\kappa d$ ) and 1 (for small  $\kappa d$ ).

- (ii) Free draining adsorbed layer of thickness  $d$ , constant polymer adsorption factor  $\beta$ , having a viscosity  $\eta_F = r\eta_0$ ,  $r > 1$ .

The potential distribution is now given, from (2-33) and (2-36),

by

$$\psi(x) = \frac{\psi_0 \sqrt{1-\beta} \exp[-\kappa(x-d)]}{\sinh \kappa \sqrt{1-\beta} d + \sqrt{1-\beta} \cosh \kappa \sqrt{1-\beta} d} \quad (2-74)$$

inside the adsorbed layer. Since  $\psi(x) \rightarrow 0$  as  $x \rightarrow \infty$ , and since the potential is continuous at  $d$ , the integrations of (2-72) give:

$$\zeta_{app} = \frac{4\pi\eta_0 U}{\epsilon} = \zeta \left[ \frac{1}{r} + \frac{(1-1/r)\sqrt{1-\beta}}{\sinh \kappa \sqrt{1-\beta} d + \sqrt{1-\beta} \cosh \kappa \sqrt{1-\beta} d} \right] \quad (2-75)$$

where again we take  $\zeta = \psi_0$  to be the true zeta potential. As in the previous case, the apparent zeta potential estimated from the

mobility underestimates the true zeta potential by a factor that varies between  $1/r$  (for large  $\kappa\sqrt{1-\beta}d$ ) and  $1$  (for small  $\kappa\sqrt{1-\beta}d$ ). An increased viscosity in the double layer region, then, results in an underestimate of the zeta potential which is most severe for high ionic strengths and thick, diffuse layers. At low ionic strengths and/or for thin, dense adsorbed layers, the apparent zeta potential is less affected by the viscosity variation near the surface.

If the variation of  $\eta$  with  $x$  were known, that functional dependence could be included in the integration of (1-4), and more precise results obtained. Unfortunately, however, there appears at present to be no way to even estimate the value of  $r$  in this simple model, let alone study its spatial variation. We have to acknowledge that the assumption  $r = 1$  to be made in Chapter 5 probably leads to an underestimate of  $Z$ , and therefore of  $\beta$ , but there seems to be no other recourse open. Estimates of the thickness of the adsorbed layer, obtained by fitting (2-39) to experimental  $Z(c)$  curves, are probably less affected by this assumption.

#### The Effect of Neutral Adsorbed Layers on the Electrostatic Potential Energy of Repulsion Between Two Flat Plates

In Section II, p. 12 the derivation of an expression for the electrostatic potential energy of repulsion between two flat plates bearing a surface charge was given. We shall now extend this derivation to

include the effects of neutral adsorbed layers on the surfaces of the plates.

The "disjoining pressure,"  $P$ , midway between two plates, one situated at the origin, separated by a distance  $2s$  is given by:

$$P = - \int_0^{\phi(s)} \rho d\phi \quad (1-25)$$

The charge density,  $\rho(x)$ , in the presence of two identical adsorbed layers of thickness  $d$ , each characterized by a polymer adsorption factor  $\beta(x)$ , is given, from the sum of terms like (2-24) for a 1:1 electrolyte, by:

$$\rho(x) = -2n_o \left[ 1 - \beta(x) \right] \sinh \frac{e\phi(x)}{kT} \quad (2-76)$$

where  $\phi(x)$  is the total electrical potential at some point  $x < 2s$ . Substituting this expression into (1-25) and integrating gives for the repulsive force per unit area:

$$P(s) = 2n_o kT \left[ 1 - \beta(2s) \right] \left[ \cosh \left[ \frac{e\phi(s)}{kT} \right] - 1 \right] \quad (2-77)$$

The repulsive potential energy,  $V_R$ , can be obtained from  $P$  by applying



$$V_R(2s) = - \int_{\infty}^s P(s) d(2s) = - 2 \int_{\infty}^s P(s) ds \quad (1-29)$$

but to evaluate the integral, the dependence of  $\phi(s)$  on  $s$  must be known, and the spatial dependence of  $\beta(x)$  taken into account.

We now limit the discussion to plate separations  $2s > 2d$ , i. e., no overlap of adsorbed layers is considered, since the repulsive energy must include terms derived from the decrease in configurational entropy of the adsorbed layers if overlap is to be allowed (79, 80, 208). It does not yet seem to be clear just what form these terms should take (80). Since  $2s > 2d$ ,  $\beta(2s) = 0$ , and applying the approximation  $\cosh x - 1 \sim x^2/2$ , good to 4th order in  $x$ , (2-77) becomes:

$$P(s) = \frac{n_o e^2}{kT} \phi^2(s) \quad (2-78)$$

If we consider the case of an adsorbed layer of constant adsorption factor  $\beta$ , and assume that the plates are far enough apart that the total potential midway between them is just the sum of the potentials due to the individual plates:

$$\phi(s) = 2\psi(s) = \frac{2\Psi(0)\sqrt{1-\beta} \exp[-\kappa(s-d)]}{D} \quad (2-79)$$

where

$$D = \sinh(\kappa\sqrt{1-\beta}d) + \sqrt{1-\beta} \cosh(\kappa\sqrt{1-\beta}d)$$

as before, and  $\psi(s)$  is given by (2-74). Substituting (2-78) and (2-79) in (1-29) and integrating gives for the repulsive potential between two plates a distance  $2s$  apart:

$$V_R(2s) = \frac{4n_o e^2 \zeta^2 (1-\beta) \exp[-2\kappa(s-d)]}{\kappa kTD^2} \quad (2-80)$$

where  $V_R$  is expressed in units of  $(kT)$  per unit area. To express  $V_R$  in terms of the zeta potential, we have assumed for simplicity that the entire layer is free draining so  $\zeta = \psi(0)$ . For cases of partial free draining, the appropriate expression for  $\zeta(\psi[0])$  may be used and substituted into (2-79).

To obtain an expression for the relative change in repulsive potential caused by the presence of the adsorbed layer, the expression for  $V_R$  in the absence of adsorption,  $V_{Ro}$ , obtained using basically the same approximate form for the potential is used:

$$V_{Ro} = \frac{4e^2 n_o \zeta_o^2}{\kappa kT} \exp(-2\kappa s) \quad (1-31)$$

The relative repulsive energy in the presence of the adsorbed layer is then:

$$\frac{V_R}{V_{Ro}} = \frac{\zeta^2 (1-\beta)}{\zeta_o^2 D^2} \exp 2\kappa d \quad (2-81)$$

We have seen previously that at high ionic strengths,

$$\frac{\zeta^2}{\zeta_0^2} \sim \frac{1}{1-\beta} \quad (2-82)$$

so we may write approximately under these conditions:

$$\frac{V_R}{V_{R0}} \sim \frac{\exp 2\kappa d}{[\sinh(\kappa\sqrt{1-\beta}d) + \sqrt{1-\beta} \cosh(\kappa\sqrt{1-\beta}d)]^2} \quad (2-83)$$

Plots of  $V_{R0}$  and  $V_R$  vs  $s$ , the half plate separation are given in Figures 2-10 and 2-11 for some representative values of  $\beta$  and  $d$ . The ionic strength used is that of saline, the zeta potential in the absence of polymer is taken to be that of the human erythrocyte, and the zeta potential in the presence of polymer is assumed to be given by (2-82). As expected, the increased zeta potential due to the adsorbed layer causes an increase in the repulsive potential as well.

For large  $\kappa d$ , (2-83) may be expressed approximately as:

$$\frac{V_R}{V_{R0}} \sim \frac{2 \exp[2\kappa d(1-\sqrt{1-\beta})]}{(1+\sqrt{1-\beta})^2} \quad (2-84)$$

It is clear from this expression that for thick, dense adsorbed layers, the increase in repulsive potential can be enormous.

The absolute value of  $V_R$  is more difficult to evaluate, however, particularly for cells. The difficulties arise because the

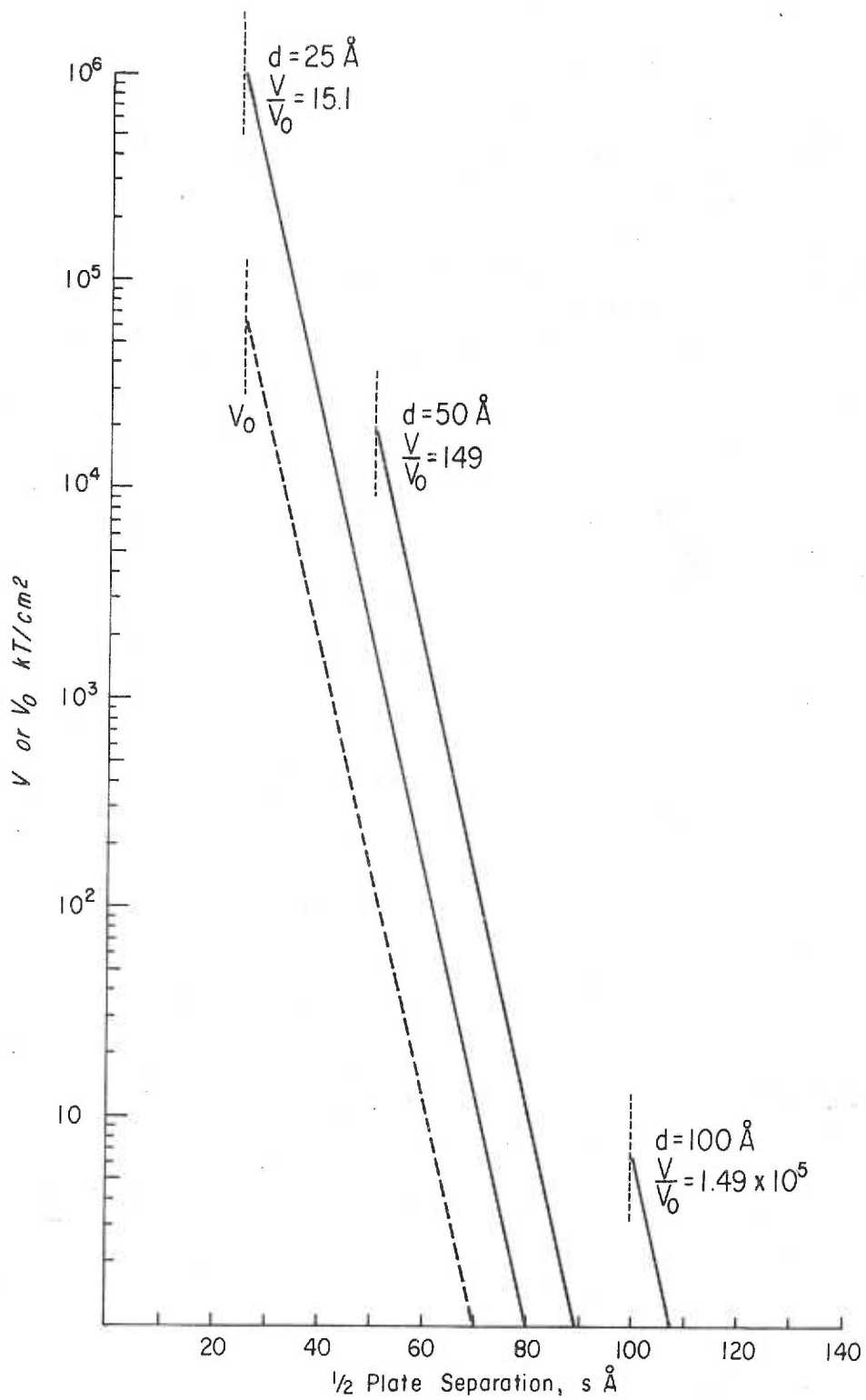


Figure 2-10. Repulsive potential energy vs.  $1/2$  the plate separation for two charged flat plates to which neutral polymer layers are adsorbed.  $\beta = 0.6$

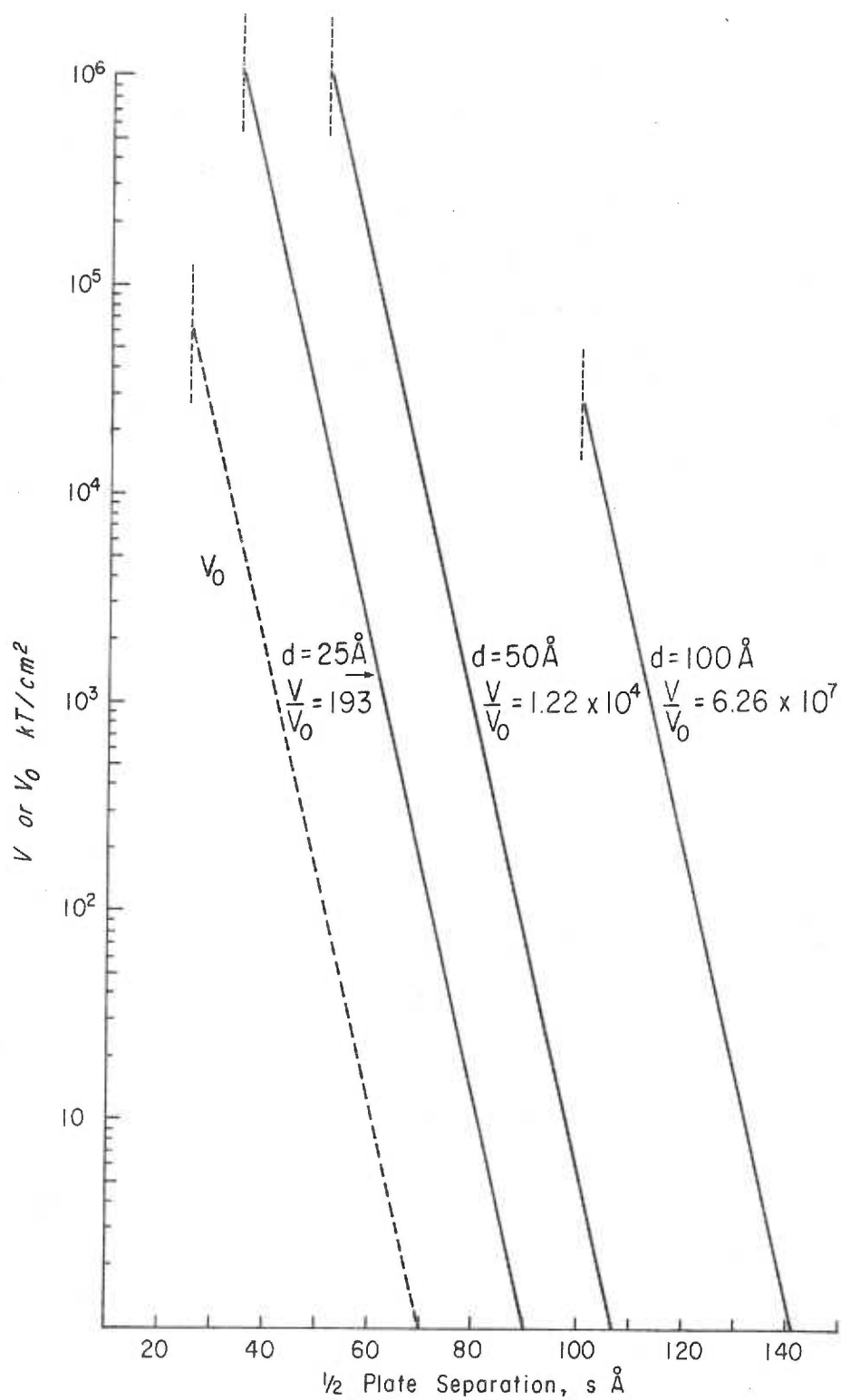


Figure 2-11. Repulsive potential energy vs.  $\frac{1}{2}$  the plate separation for two charged flat plates to which neutral polymer layers are adsorbed.  $\beta = 0.9$

approximations used in the derivation of (2-81) are such that  $V_R$  is underestimated, due both to the use of the assumption that  $\sinh x \sim x$  in deriving (2-74), and the use of  $\cosh x - 1 \sim x^2/2$  in obtaining (2-78). Further uncertainties are introduced when the geometries of the interacting bodies are considered. Treating two erythrocytes as if they were flat plates of appropriate areas is obviously only an approximation to the true case. The interaction energy for curved surfaces such as the cells would be expected to be lower than estimated here. Thirdly, the difficulty in estimating the true value of the zeta potential due to the adsorbed layer viscosity as discussed in the previous section will lead to an underestimation of  $\beta$ , which will lead to an underestimation of  $V_R$  (2-80). Within the context of the model under consideration, however, the conclusion seems inescapable that the presence of neutral polymer layers will result in increased repulsive energies between fixed charge surfaces to which they are adsorbed.

### Summary

Various models for the zeta potential increase in the presence of neutral polymers are proposed. Free solution properties such as the bulk dielectric constant are shown not to explain even qualitatively the experimental facts. Four models based on the adsorption of polymer to the charged surface are discussed. Ponder's original

dielectric argument is shown to predict a decreased, not increased, zeta potential. Charge rearrangement in the peripheral region is considered, but seems not to apply to rigid particles for which the effect is seen, and hence cannot be a general explanation of the phenomenon. Non-specific ion adsorption to the adsorbed polymer is ruled out for the dextran experiments by a variety of experimental observations on the properties of dissolved and adsorbed dextran. The final model considered is based on the effect a surface phase of adsorbed polymer will have on the chemical potential of counterions to the surface charge. The effect is analyzed assuming Flory-Huggins theory applies to the adsorbed surface phase. The analysis produces a Boltzmann equation modified by a polymer adsorption factor. This equation is used to derive several expressions for the relative zeta potential as a function of the polymer adsorption factor, the depth of the adsorbed layer, and the ionic strength, which apply under various, defined conditions. Providing the adsorbed layer is to some extent free draining, the zeta potential in the presence of the adsorbed layer is shown to be increased at some ionic strengths, the range of ionic strength over which the increase occurs being greater, the more extensive the free draining. For totally free draining layers, the zeta potential is predicted to be increased in the presence of the adsorbed layer at all ionic strengths, the increase being greater the greater the volume fraction occupied by the adsorbed layer. The

variation of the relative zeta potential with ionic strength can be used to measure the depth of a neutral polymer layer adsorbed to a fixed charge system.

The effect of an adsorbed layer on the mobility-zeta potential relationship is also discussed. It is concluded that in the presence of a partially or totally free draining polymer layer the relative zeta potential measured electrophoretically will probably be underestimated due to the assumption that the viscosities in the bulk solution and in the adsorbed layer are identical.

Lastly, the adsorption model is applied to the calculation of the repulsive electrostatic potential energy of two flat charged plates to which are adsorbed neutral polymer layers. Providing no overlap of the adsorbed layers occurs, the repulsive potential is markedly increased in the presence of the adsorbed layers.



## CHAPTER 3

DIELECTRIC PROPERTIES OF AQUEOUS  
DEXTRAN SOLUTIONS

The most detailed explanation given to date for the zeta potential increase observed for erythrocytes suspended in dextran-salt solutions is due to Pollack et al. (104). These workers suggested that dextran solutions have a much larger dielectric constant than water, and that this increased dielectric constant was responsible for the electrophoretic effects seen. It seems highly improbable that a pure solution property could be responsible for the zeta potential changes measured for a variety of particles in a given solution, as discussed in Section 2-I. Further, Allgén and Roswall (109), using a method which was not subject to some of the errors common to the capacitance measurements employed by Pollack et al., reported that up to 0.5% dextran had no effect on the dielectric constant of water. According to Pollack, on the other hand, an 0.5% dextran solution should have a dielectric constant 20 units larger than water. In view of this discrepancy, the dielectric constant measurements described below were undertaken.

The easiest and most accurate way to measure the dielectric constant of a solution is to measure the electrical capacitance of two electrodes immersed in the solution. The ratio of this capacitance to

that of the electrodes in air is the dielectric constant of the solution (209). As employed in the electrokinetic equations of Chapters 1 and 2,  $\epsilon$  refers to the dielectric constant measured at zero applied frequency, since only electrostatic effects are considered in these equations. In practice, dielectric measurements are made in an alternating field, since d. c. conditions introduce enormous errors due to the appearance of electrode polarization impedances in the circuit (210). Providing the applied frequency is low enough that no additional dispersion can occur, the low frequency dielectric constant is equal to the d. c. value.

Low frequency capacitance measurements in aqueous salt solutions are complicated by the presence of electrode polarization (210). At frequencies,  $\nu$ , of less than roughly 100 kHz, polarization impedance can cause overestimates in the measured capacitances of several orders of magnitude (211). These impedances depend on the electrode material used and on the concentration of salt in the solution. For a. c. measurements, platinum is the material of choice, since it may be coated with a porous layer of platinum black which reduces the polarization impedance of the electrodes by up to four orders of magnitude. Reduction in polarization impedance may also be obtained by reducing the ionic concentration of the solutions to as low a value as possible.

### Methods and Materials

Dielectric constant measurements were made on solutions of two dextran fractions obtained from Pharmacia Fine Chemicals, Piscataway, N. J.: Dextran T40, Batch 8687 ( $\overline{M}_w = 39,500$ ,  $\overline{M}_n = 24,000$ ,  $[\eta] = 0.196$ ) and Dextran 250, Batch 893 ( $\overline{M}_w = 236,000$ ,  $\overline{M}_n = 109,000$ ,  $[\eta] = 0.42$ ). The fractions were dissolved in, then dialyzed against, 8 changes of twice pyrex-distilled water deionized through a Barnstead standard mixed bed deionizing cartridge. The fractions were then lyophilized, made up in twice distilled deionized water to concentrations of 10% w/v, and used at this and diluted concentrations for the dielectric constant measurements. The specific conductivities of these solutions never exceeded  $2 \times 10^{-5}$  mho-cm<sup>-1</sup>. The dielectric cell used was a two terminal cell of 13.0 ml volume employing two fixed concentric cylindrical platinum electrodes, constructed by the Research Instrument Service of the University of Oregon Medical School. The electrodes were each platinized from a solution containing 1.0 gm chloroplatinic acid, 0.01 gm PbCl<sub>2</sub> and 33.3 ml H<sub>2</sub>O at a current density of 10 ma cm<sup>-2</sup> for 1 hour to give a deposition of approximately 35 coulombs cm<sup>-2</sup> (211). The electrodes were stored short-circuited for 48 hr in distilled water before use. The platinized cell had a stable air capacitance at 10 kHz of 0.4198 pF at 25.0°C. A transformer ratio arm

Type 1615-A capacitance bridge in conjunction with a Type 1310-A audio oscillator and a Type 1232-A tuned amplifier and null detector, all supplied by General Radio Co., West Concord, Mass., were used for the capacitance measurements. The circuit is shown in Figure 3-1. This bridge will measure capacitances from  $1 \times 10^{-17}$  to  $1.11110 \times 10^{-6}$  Farad and conductances of between  $10^{-12}$  and  $10^{-4}$  mho in the frequency range of 100 Hz and 10 kHz, and is useful with reduced accuracy to 100 kHz. The limits of accuracy quoted by the manufacturer at 10 kHz are  $\pm[(0.01\% + 0.00003 \text{ pF}) + (\pm 3 \times 10^{-5}\% + 2 \times 10^{-3}\% C_{\mu\text{F}} \pm 3 \times 10^{-7} \text{ pF}) \times (\nu_{\text{kHz}})^2]$  in capacitance,  $C$ , and  $\pm[(1\% \text{ of measured value} + 1 \times 10^{-5} \mu\text{mho} + 6 \times 10^{-2} \nu_{\text{kHz}} C_{\mu\text{F}} \times (1 + \nu_{\text{kHz}} + 5 \nu_{\text{kHz}} C_{\mu\text{F}}) \mu\text{mho}]$  in conductance,  $G$ . To balance the bridge with the more conductive solutions, a shielded external conductance standard of  $0.9977 \mu\text{mho}$  (1 meg $\Omega$  resistor) was used in conjunction with a General Radio Type 874-X insertion unit. The capacitance associated with the external conductance standard,  $C_x$ , was measured on the bridge to be  $7.90 \pm .04 \text{ pF}$  independent of frequency between 1 kHz and 100 kHz. Since multiples of  $C_x$  were added to the bridge capacitance,  $C_b$ , to determine the sample capacitance,  $C_s$ , whenever the external standard was required for balance, the uncertainty in the value of  $C_x$  limited the accuracy of determination of  $C_s$ .

Individual capacitance determinations were carried out as

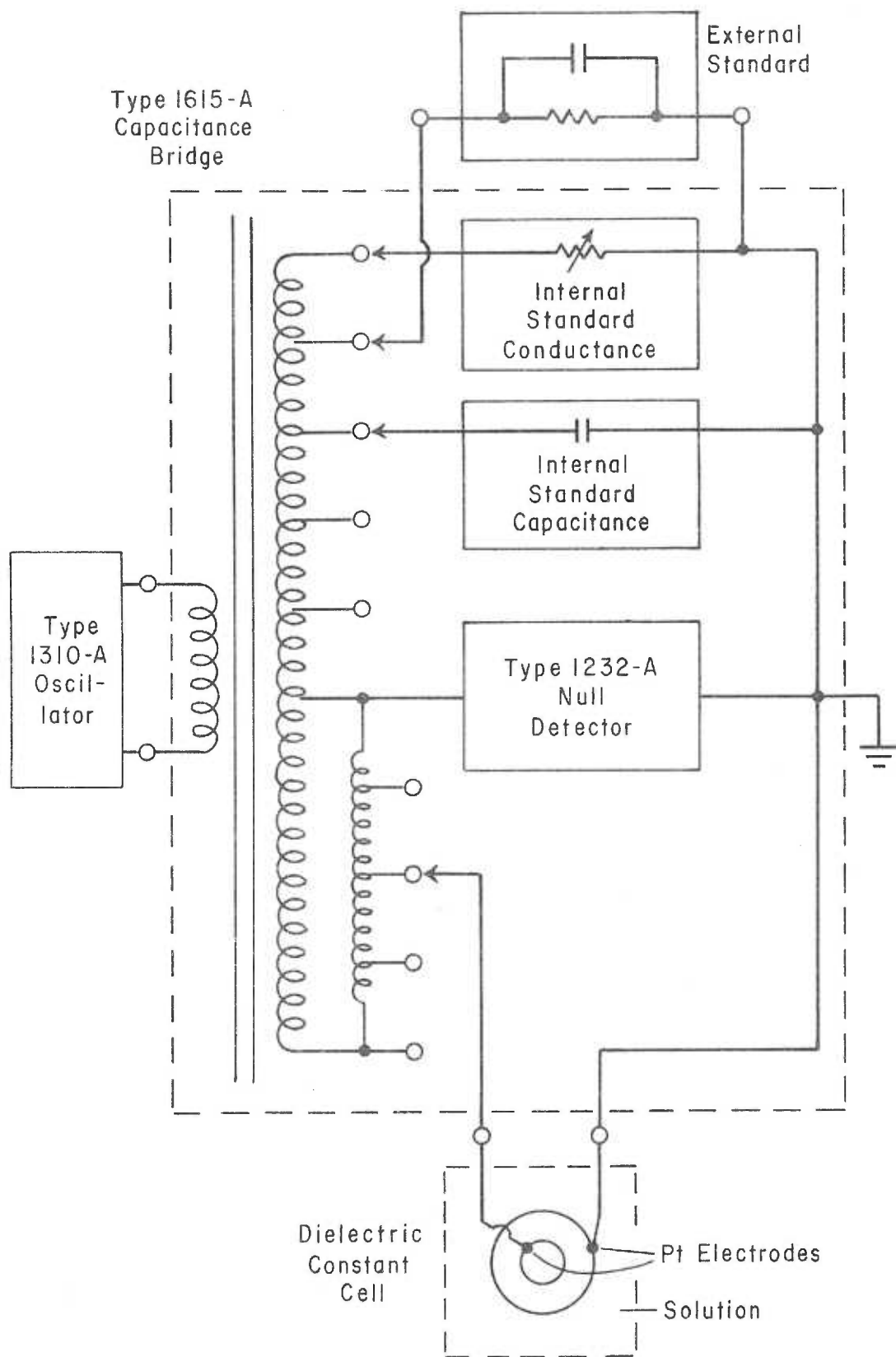


Figure 3-1. Circuit diagram of the capacitance measurement assembly.

follows: 13.0 ml of sample was pipetted into the cell, the cell was immersed in a water bath thermostatted to  $(25.0 \pm 0.2)^\circ\text{C}$ , the shielded leads from the bridge attached to the cell, and system allowed to equilibrate for 1 hr. The geometry of the leads, cell and measuring system was kept constant from run to run to avoid changes in the stray capacitances associated with two terminal measurements such as these. The bridge was sufficiently far from the cell that the hand motion associated with balancing the bridge had no effect on the measured capacitance.

The air capacitance of the cell,  $C_o$ , and the stray capacitances  $C_{st}$  were calculated by measuring the capacitance of the cell containing, air, twice distilled deionized water, reagent grade benzene and anhydrous methanol at 10 kHz and 100 kHz. The accepted values for the dielectric constants of these standards (212) were used, except in the cases of benzene and methanol, where the values were corrected for the presence of the 0.05%  $\text{H}_2\text{O}$  and 0.1%  $\text{H}_2\text{O}$  respectively present in these samples (as indicated by their purity limits). The data were fitted to equation (3-1) below using a standard linear regression program on a Hewlett-Packard 9100B calculator. The capacitances of the dextran solutions were also measured at 10 kHz and 100 kHz, the stray capacitance subtracted from the total capacitance  $(C_b + C_x)$ , and the dielectric constant  $\epsilon$  calculated from  $\epsilon = (C_b + C_x - C_{st})/C_o$  at each frequency.

### Results and Discussion

Provided the stray capacitance does not change from determination to determination, the total two terminal capacitance,  $C$ , which the bridge sees at balance is given by

$$C = \epsilon C_o + C_{st} \quad (3-1)$$

where  $\epsilon$  is the dielectric constant of the material in the cell. If a series of standards are measured for which  $\epsilon$  is known, the  $(C, \epsilon)$  data may be fitted to equation (3-1), and  $C_o$  and  $C_{st}$  determined from the slope and C-intercept of the resulting straight line. Table 3-1 gives the results of the standard measurements made at each frequency, the measured total capacitance in air at the beginning and end of the experiments, the linear regression coefficients, and the resulting values of  $C_o$  and  $C_{st}$ . The values are seen to differ slightly at the two frequencies, but the agreement is satisfactory since the accuracy of the bridge is somewhat reduced at 100 kHz (213).

The dielectric constants of a series of dextran solutions measured at 10 kHz and 100 kHz, as well as the values predicted from Pollack's results, are given in Table 3-2. The precision limits following each value represent the uncertainty in calculated  $\epsilon$  due to the  $\pm 0.04$  pF uncertainty in the capacitance of the external standard conductance. The values of  $C_o$  and  $C_{st}$  are not affected by this

Table 3-1. Two terminal data for standard dielectrics used to calculate stray capacitance and air capacitance of cell.

Dielectric	$\epsilon$	10 kHz C pF	100 kHz C pF
Air (initial)	1.00	64.54	64.42
Benzene + 0.05% H <sub>2</sub> O	2.31	65.23	65.10
Methanol + 0.1% H <sub>2</sub> O	32.68	78.75	78.70
Water	78.54	98.75	96.82
Air (post exp'ts)	1.00	64.44	64.35
Regression equation:		$C = 0.4417 \text{ pF} \cdot \epsilon + 64.14 \text{ pF}$	$C = 0.4198 \text{ pF} \cdot \epsilon + 64.18 \text{ pF}$
Regression coefficient:		$r = 1.0000$	$r = 0.9995$
Stray capacitance:		$C_{st} = 64.14 \text{ pF}$	$C_{st} = 64.18 \text{ pF}$
Cell air capacitance:		$C_0 = 0.4417 \text{ pF}$	$C_0 = 0.4198 \text{ pF}$



error since the conductivities of the calibrating fluids were low enough that no external conductance standard was necessary to balance the bridge during their measurement.

Table 3-2. The dielectric constants of aqueous salt-free dextran solutions ( $T = 25.0^{\circ}\text{C}$ ,  $\epsilon_{\text{H}_2\text{O}} = 78.54$ ).

Dextran Concentration (w/v)		$\epsilon_{10 \text{ kHz}}$	$\epsilon_{100 \text{ kHz}}$	$\epsilon_{\text{from Pollack et al.}}$
Dextran 40	2.5%	$76.9 \pm 4.5$	$84.7 \pm 4.8$	179.7
	5.0%	$79.6 \pm 9.1$	$86.3 \pm 9.5$	280.8
Dextran 250	2.5%	$77.3 \pm 5.4$	$83.2 \pm 5.7$	179.7
	5.0%	$79.2 \pm 9.1$	$85.8 \pm 9.5$	280.8
	10.0%	$78.9 \pm 10$	$109.0 \pm 11$	483.0

It is seen from Table 3-2 that in all but one case in the frequency region of reduced bridge accuracy, the uncertainties in the dielectric constants of the dextran solutions are such that the measured dielectric constants overlap with that of water. Hence, the dielectric constants of dextran solutions of up to 10% w/v concentration are indistinguishable from that of water, in agreement with Allg en and Roswall (109). It is clear from examination of the last column in the table that in no instance could the uncertainties in these measurements allow agreement with Pollack's data.

It would seem from these and Allg en's results that Pollack's results are in error. The most likely source of his apparently high

dielectric increments lies in electrode polarization. The salt concentration in his polymer solutions was significant, since they were all adjusted to pH 7.45 with 0.01 N NaOH, yet he did not employ platinized platinum electrodes. Further, many of his measurements were made at between 1 kHz and 50 kHz (214), where electrode polarization will be appreciable in such systems. His value for the dielectric increment of bovine serum albumin (b. s. a.), for instance, is roughly six times that which may be deduced from Grant's results (215) obtained in the absence of salts. Takashima's experiments (167) have shown that the pH differences in Grant's and Pollack's work should have no appreciable effect on the dielectric constants measured for b. s. a. solutions.

An explanation for the apparent internal consistency of the dielectric measurements as a function of concentration of Pollack et al. may lie in their method of correcting for electrode polarization. They state that the dielectric increment of any given polymer solution was obtained by subtracting from the capacitance of the polymer solution the capacitance measured for an aqueous NaCl solution of exactly the same conductivity, then dividing by the air capacitance of their cell. As evidenced by the currents measured during electrophoretic mobility determinations, however, the conductivities of dextran-salt solutions are lower than the conductivities of aqueous solutions at the same salt concentration but with dextran absent. Therefore, the

apparent conductivities of dextran solutions indicate falsely low salt concentrations. Salt solutions of conductivities equivalent to the polymer solutions, then, will contain lower ionic concentration. Hence, the polymer solutions will contain more salt than their controls and progressively more electrode polarization will be present in these solutions the higher the polymer concentration. The measured capacitance difference between a polymer solution and its salt solution control will therefore appear to increase in a regular way as the polymer concentration is increased. If at the salt concentrations relevant here the polarization impedance is a linear function of salt concentration, and the polymer causes a conductivity decrease which depends linearly on polymer concentration, a roughly constant apparent dielectric increment per gram of polymer would be measured, as Pollack observed. Neglect of the dependence of solution conductivity on the presence of polymer, then, would appear to be one source of systematic error in Pollack's results which could account for his apparently erroneous dielectric increments for dextran solutions.

## CHAPTER 4

## THE DEXTRAN-ERYTHROCYTE ADSORPTION ISOTHERM

All the models for cellular zeta potential increases in the presence of neutral polymers discussed in Chapter 2 assume that dextran adsorbs to the peripheral region of erythrocytes. Although adsorption to red cells from plasma solutions of dextran has been qualitatively demonstrated, dextran adsorption has not been shown to occur in the absence of plasma proteins. As discussed in Chapter 1, it is not clear from the plasma results whether the adsorbing species is dextran alone, or a dextran-protein complex. In any case, the concentration dependence of the adsorption process has not been studied. This chapter describes a direct measurement of the adsorption isotherm of a neutral polymer to cells.

The usual method of measuring adsorption from solution is to measure the concentration decrease of the adsorbent remaining in solution after equilibration with a surface. Providing it can be shown that there is no penetration of the surface by the adsorbing species (by phagocytosis, diffusion or active transport in the case of cells), the disappearance of adsorbent from solution is equated with the amount adsorbed. Knowledge of the surface area available for adsorption allows the calculation of the amount of material adsorbed per unit area. This subtraction method cannot be expected to work for the

case of dextran adsorbing to erythrocytes, however, since even in the presence of plasma proteins the uptake corresponds to less than a 1% change in the solution concentration of dextran [1% w/v (94)].

Adsorption under these conditions would be expected if anything to be higher than in the absence of plasma, since plasma proteins are known to both interact with dextran (162) and adsorb strongly to erythrocytes (216). The degree of resolution necessary to measure accurately changes of this magnitude was unlikely to be attained by normal analytical procedures. A direct measure of uptake therefore seemed to be required.

The most common method of measuring the uptake of a molecular species is by using radioactively-labelled molecules and detecting the radiation associated with their presence in the location of interest. Radioactive dextran is available, as are methods for counting labelled dextran originally associated with hemoglobin-containing cells. The primary difficulty in directly counting the labelled dextran associated with the cell involves distinguishing between the adsorbed label and label still in solution in the interstitial fluid surrounding the cell. Erythrocyte pellets, spun even at the high speeds employed in micro-hematocrit determinations (15,000 xg), contain approximately 1-2% trapped fluid (217). This amount of solution will contain more label than would be expected to be associated with the cells, on the basis of the dextran/plasma experiments. The problem, then, is to either

determine accurately the amount of interstitial fluid present in a cell pellet, or to reduce the amount of fluid to a negligible level.

The best way to estimate the volume of trapped fluid in a cell pellet is to introduce an indifferent, labelled solute to the pellet, and measure its dilution in the solvent volume available to it (218). So long as the cells do not take up this solute, the dilution factor will give an estimate of the fluid present in the pellet. The accuracy of this method, however, is very low, as may be seen from the following. Assume first that the labelled solute (sucrose, inulin, sorbitol, etc.) is added only to a concentrated pellet from which the supernatant has been removed. The volume of trapped fluid,  $V_t$ , is given by:

$$V_t = V_\ell \left[ \frac{A_o}{A_d} - 1 \right] \quad (4-1)$$

where

$V_\ell$  = volume in which the labelled solute is introduced at a specific activity  $A_o$ .

$A_d$  = specific activity of label after dilution with trapped fluid.

There will be an unavoidable error of a few percent in determining  $(A_o/A_d)$ . Since the pellet is assumed compact, the dilution will be small, and  $(A_o/A_d)$  will be not too different from 1. Hence,  $(A_o/A_d - 1)$  will be much less than 1, and the error due to the uncertainty in  $(A_o/A_d)$  will be a significant fraction of

$(A_o/A_d - 1)$  ( $\approx \pm 20\%$  at best). If on the other hand a loose pellet is used to increase  $(A_o/A_d)$  and reduce the error in  $V_t$ , the amount of trapped solvent will be so great that when the pellet is counted for dextran, the counts due to the dissolved label will be overwhelmingly greater than those due to adsorbed label. The counts due to the adsorbed label will therefore be the small difference between the total measured counts and the calculated counts due to  $V_t$ . Even small uncertainties in these two large numbers make uncertainty in their difference relatively large. Estimation of trapped fluid volumes, then, severely limits the accuracy of direct adsorption measurements made in the presence of interstitial fluid. Attempts to measure dextran uptake using the method described above were totally unsuccessful.

The other approach to dealing with the trapped fluid is to try to reduce the amount of fluid in the cell pellet to a negligible level. The normal way to accomplish such a reduction is to wash the pellet several times in an unlabelled medium. Washing in saline, however, might be expected to markedly reduce the degree of dextran adsorption, since the zeta potential increase observed in the presence of dextran in saline can be almost totally removed with one washing of normal erythrocytes. This is apparently also the case for polylysine adsorption to red cells, since Katchalsky's group showed that the electrophoretic mobility change in the presence of polylysine was a

single valued function of external polylysine concentration (88).

Dextran in plasma, on the other hand, apparently binds to red cells much more strongly, since six plasma washes do not remove it (94).

Washing with aqueous solutions in which dextran is insoluble (saturated KCl, for example) might be a possibility were it not for the observations, made in many systems, that decreased solvent power leads to greater adsorption of polymer (38).

Washing with an organic phase was attempted unsuccessfully. Washing with an organic phase (a mixture of benzyl benzoate and cottonseed oil; see below) whose density was greater than the aqueous dextran solution but less than the cells was also unsuccessful. Apparently contact of the aqueous cell suspension with the organic phase encapsulates a sufficient (variable) quantity of label-containing aqueous solution around the cell to overwhelm the counts from the adsorbed label alone. Attempts were made to separate the cells from the aqueous suspending medium by spinning them down through the organic phase of intermediate density. Again, a sufficient quantity of aqueous solution remained associated with the cells to mask the adsorbed dextran. A method was developed, however, that gave consistent and reproducible results for the adsorption of dextran to human erythrocytes from saline solutions.



### Materials

To avoid any possible complications arising from the presence of negative charges on the labelled dextran molecules, it was decided not to use the C<sup>14</sup>-carboxylated dextran employed in the previous plasma/dextran adsorption studies. Instead, a 2.0 gm sample of dextran 77.6 (Fraction FDR 403,  $\overline{M}_w = 77,600$ ,  $\overline{M}_n = 65,500$ ; kindly provided by Dr. K. Granath, Pharmacia AB, Uppsala, Sweden) was tritiated by Amersham-Searle Corp., Arlington Heights, Ill. using end group reduction with sodium borohydride-T (TRK .45 Batch 16). The dextran was received dissolved in 25 ml of H<sub>2</sub>O and contained 24.2 mC of H<sup>3</sup> activity according to the supplier's specifications. It was dialyzed against 5 changes of distilled deionized water. The fifth wash contained negligible H<sup>3</sup> activity. The dialyzed H<sup>3</sup> dextran solution was lyophilized to yield 0.7007 gm of powder. This powder was taken up in 25.02 gm of twice distilled water (2X H<sub>2</sub>O) made 0.02% in sodium azide to prevent bacterial growth and stored at 4°C until used.

The H<sup>3</sup>-dextran was checked to see if fragmentation had occurred during tritiation as follows. A (2.50 x 100) cm column was packed with Sephadex G-150 Fine to a bed volume of 458 ml and equilibrated with 0.05 M NaCl at room temperature. The column void volume was measured with a 13 ml sample of 0.15% blue dextran

$(\bar{M}_w \sim 2 \times 10^6$ , Pharmacia) and found to be 128.8 ml. All elutions were performed at room temperature. A 15 ml sample of 2.9% w/v dextran 77.6 in 0.05 M NaCl was run through the column under gravity flow of 14.9 ml/hr. The elution profile was followed by performing carbohydrate analyses on aliquots of each of the 5 ml samples collected, using the standard phenol-sulfuric acid technique (219). After eluting roughly 1 bed volume of 0.05 M NaCl, 12 ml of the  $H^3$ -dextran stock was applied to the column and the elution profile again followed with carbohydrate determinations. Both peaks eluted with a partition coefficient  $K_{av}$  (220) of 0.17. The profiles were essentially indistinguishable for the  $H^3$  and cold dextran samples in the peak region (when normalized for total applied weight). The  $H^3$ -dextran sample exhibited some tailing beyond the cold dextran peak, but the CHO analyses indicated that 97.7% of the eluted material was present under the peak. The fractions under the peak were pooled and dialyzed against 5 changes of 2X  $H_2O$ ; 192.14 mg of  $H^3$ -dextran from the dried down peak was dissolved in 24.8898 gm of 2X  $H_2O$  0.02% w/v in  $NaN_3$  and stored at 4°C. The specific activity of this solution (measured by the method described below) was  $5.07 \times 10^8$  dpm  $ml^{-1}$ , implying the specific activity of the dextran was  $6.58 \times 10^{10}$  dpm  $gm^{-1} = 29.6$  mC  $gm^{-1}$  on July 13, 1970.

$H^3$ -toluene used as an internal standard to determine counting efficiencies was supplied by New England Nuclear, Boston, Mass. and

had a specific activity of  $2.26 \times 10^6 \pm 3.1\%$  dpm ml<sup>-1</sup> on Dec. 6, 1967 (NES-004, Lot #282-222). The cottonseed oil used was once refined according to the supplier, Matheson Coleman and Bell, Norward, Ohio. The unlabelled dextran used was dextran 77.6, the parent fraction of the H<sup>3</sup>-dextran. It was made up in 2X H<sub>2</sub>O 0.02% w/v in NaN<sub>3</sub> as a concentrated solution (25.78% w/v as measured polarimetrically) and stored at 4°C. All other chemicals used were reagent grade.

Erythrocytes were obtained as in date A. C. D. -anticoagulated blood from the Red Cross Blood Bank. Cells were washed three times in standard saline (0.145 M NaCl brought up to pH 7.2 ± 0.2 with 0.5 M NaHCO<sub>3</sub>) before used in the adsorption studies. Cells were not selected as to blood group.

### Methods

A typical adsorption experiment was carried out as follows. Dry NaCl was added to an aliquot of the H<sup>3</sup>-dextran stock solution to bring its ionic concentration up to 0.145 M. Cold dextran was diluted with 2X H<sub>2</sub>O and concentrated salt solutions to bring the final solution to the desired dextran concentration. The hot and cold dextran/salt solutions were mixed by weight to give solutions of the required total dextran concentrations and specific activities. A Mettler Model P160N top loading balance which could be read to ± 0.5 mg was used

for all but the internal standard weighings. The final salt concentration of the labelled dextran solutions was either 0.145 M NaCl, brought to pH  $7.0 \pm 0.4$  with 0.5 M  $\text{NaHCO}_3$ , or that resulting from a mixture of 20% by volume 0.145 M NaCl and 80% phosphate buffer [20 parts by volume  $19.27 \text{ gm l}^{-1} \text{ NaH}_2\text{PO}_4$  plus 80 parts  $17.92 \text{ gm l}^{-1} \text{ Na}_2\text{HPO}_4$ , 287 mOsm, pH  $7.2 \pm 0.1$  (221)]. The presence of the phosphate, or the phosphate/ $\text{Cl}^-$  ratio did not appear to affect the adsorption, provided the cation was  $\text{Na}^+$ . At total dextran concentrations above about  $4 \times 10^{-4} \text{ gm ml}^{-1}$  the specific activity of the solutions was typically  $3 \times 10^7 \text{ dpm ml}^{-1}$ . Below  $4 \times 10^{-4} \text{ gm ml}^{-1}$ , either no cold dextran was used, or a mixture of cold and hot polymer was used interchangeably without influencing the results.

A mixture of roughly 2.6 parts by weight of benzyl benzoate and 1 part cottonseed oil was made up. The density of this mixture was intermediate between that of the erythrocytes and the dextran solution. That this was in fact so was always checked by shaking gently a combination of the organic phase, cells, and a sample of the most concentrated dextran solution to be used. This mixture was then spun down briefly and checked to see that the organic phase lay in between the cells and the aqueous phase. In the case of the most concentrated dextran solutions, the amount of benzyl benzoate had to be increased somewhat to increase the density of the mixture. This organic mixture has been shown to be compatible with erythrocytes, combinations

of its two components having been used to estimate erythrocyte specific gravity (222).

Approximately 3 gm of packed washed erythrocytes and 3 gm of an appropriate dextran solution were weighed into each of eight polyallomer ultracentrifuge tubes (5/8" diam. x 3", Beckman Instruments, Palo Alto, Cal.). The suspensions were mixed gently with a vortex mixer, and allowed to equilibrate for at least one hour at room temperature. Increasing the incubation time to up to four hours had no effect on the results. In those experiments where the pellets were to be washed, a total of 8 to 10 gm of the 50% cell/dextran suspension was equilibrated in 15 ml tubes, then ~6 gm of the mixture weighed into the ultracentrifuge tubes. After incubation, the tubes were spun for 15 min at 1000 xg and most of the supernatant removed from each. Samples of two or three of the supernatants were kept for trapped volume determinations and the rest discarded. Each of the tubes was then partially filled with the organic phase, fitted with tube caps and the filling then completed with organic phase. The tubes were spun for 30 min at a maximum of  $3.68 \times 10^5$  xg ( $6.5 \times 10^4$  r.p.m.) in the Type 65 fixed-angle rotor of a Beckman Model L2-65 ultracentrifuge, T = 25°C. Doubling the ultracentrifugation time had no effect on the results. All samples were then frozen overnight at ~ -25°C.

In those experiments in which part of the incubation suspension

was washed, the 2 to 4 gm of cell/dextran suspension remaining after the ultracentrifuge samples were removed was weighed, then washed 3 to 5 times in standard saline at a washing ratio of 1:10 to 14 (cells:saline). The cells were exposed to each washing solution for approximately 6 to 10 minutes. After the final wash the supernatants were removed and the washed pellets stored at 4°C until assayed. In one experiment the supernatants from 5 successive washes were assayed for  $H^3$  activity to determine the number of washes necessary to effectively dilute out from the pellet the counts from the original labelled incubation supernatant.

For each set of eight adsorption measurements, one of the original dextran/ $H^3$ -dextran/salt solutions was assayed in sextuplet for its specific activity, from which value the activities of the other solutions could be calculated from their weight compositions. The trapped volumes of unlabelled solution associated with the washed cell pellets were measured by assaying the specific activity in triplicate of at least two different incubation supernatants. The average trapped volume per gram of pellet was then calculated and this value used to calculate the corrected dextran concentrations of the incubation solutions.

The frozen cell pellets from the ultracentrifuged samples were

assayed for  $H^3$  activity as follows. \* Dry  $KMnO_4$  was used to oxidize the tritiated carbon on the dextran molecules to produce tritiated water. The tritiated water was recovered by vacuum distillation in Thunberg tubes, then counted. The specific activity of the THO was directly proportional to the specific activity of the pellet. The efficiency of the distillation-oxidation (distox) procedure (equal to the proportionality constant) was found from a series of calibration distox runs employing known amounts of cells and  $H^3$ -dextran.

The bottom of each of the polyallomer tubes was cut off slightly below the pellet-organic phase interface. The cut-off frozen pellets (~2 gm) were placed in Thunberg tubes (22 x 150 mm; Lab Glass Inc., Vineland, N. J., Catalogue No. LG10810) and allowed to thaw at room temperature. Once the pellets were thawed, the Thunberg tubes were cooled on ice, and ~2 gm of  $KMnO_4$  powder added to each tube in turn. Immediately after adding the permanganate, and while still surrounded by ice, a pyrex glass wool pad was inserted near the top of the tube barrel, the hollow bulb top placed on the tube, and the tube evacuated through the side arm and sealed. Each tube was then mixed violently with a vortex mixer, to thoroughly mix the viscous lysed pellet with the dry permanganate. The oxidation reaction was allowed to proceed spontaneously at room temperature for ~30 min before distillation.

---

\* The author would like to thank Dr. J. H. Fellman for suggesting this method of assay.

The eight Thunberg tubes were then distilled in a steam bath with the bulbs on ice for 20 min, the distilled liquid was tipped back into the body of the tube to ensure that the THO concentration was uniform throughout the tube, and the mixture redistilled for a further 20-30 min. The clear distillate (0.5 to 1 gm total) was then assayed for  $H^3$  activity. The specific activity of the pellet was calculated from the THO activity and the measured efficiency of the distox procedure. The number of dextran molecules present per gram of pellet was then calculated from the original specific activity and dextran concentration of the incubation mixture. The number of cells per gram of pellet was determined in a series of pilot runs by diluting a known weight of the recovered (unfrozen) ultracentrifuge pellet and counting the dispersed cells in a Model F Coulter Counter (Coulter Electronics Inc., Hialeah, Florida). The number of dextran molecules per cell was then calculated. A schematic diagram of the adsorption measurement procedure is given in Figure 4-1.

Between distox runs, the Thunberg tubes and bulbs were soaked overnight in a solution of 35 ml aqueous saturated sodium dichromate in 1 liter of conc. sulfuric acid, rinsed thoroughly with tap and distilled water then washed in detergent. Control distox runs on unlabelled cells and  $H^3$  assays of their distillates showed that there was no carry-over of radioactivity from run to run due to glassware contamination.



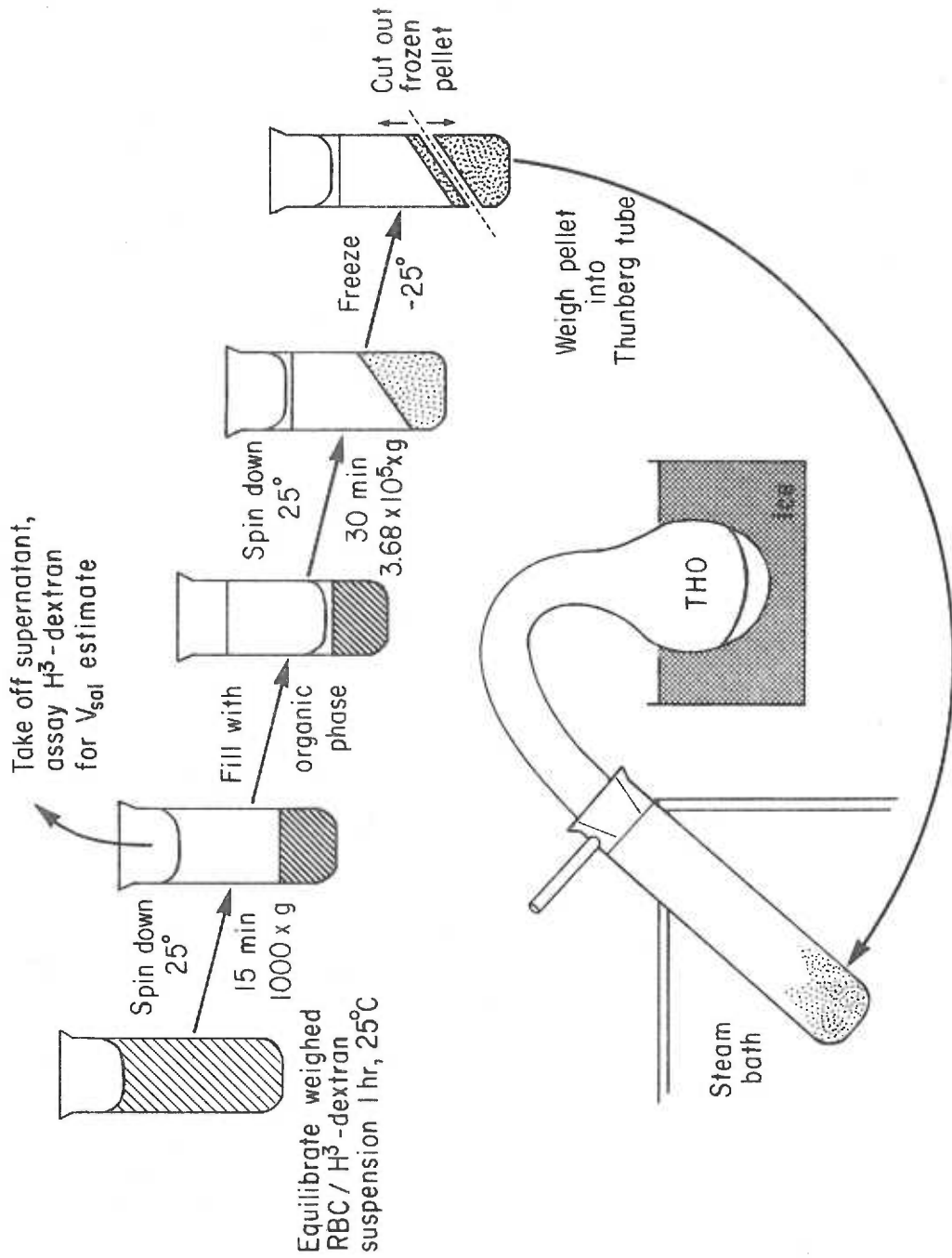


Figure 4-1. Assay pellet for  $H^3$  activity by distox procedure. Procedure used to measure the adsorption of  $H^3$ -dextran to erythrocytes.

To assay the specific activity of the washed pellets, the cells were weighed into Thunberg tubes using a peristaltic pump and 1/16" i. d. tygon tubing to transfer the cells. The tube from which the pellet was taken was repeatedly washed with small amounts of saline (less than 1.5 gm total) until all cells had been transferred. The cell suspension was then put through the distox procedure outlined above and the distillate assayed for  $H^3$  activity. From the composition and trapped volume in the incubated suspension, and the weight of that part of the suspension subjected to the washing, the number of grams of cells present in the distox assay were calculated, since a negligible number of cells were lost in the washing and transferal process. Hence the specific activity of the distox distillate could be related to the weight of cells from which the activity originated, and the number of dextran molecules per cell calculated as before.

Tritium activity was assayed by liquid scintillation counting at ambient temperature on a Beckman CPM-100 Liquid Scintillation System. The scintillation medium used contained 4.0 gm PPO (2,5-diphenyloxazole, Nuclear Enterprises, Inc., San Carlos, Cal.), 350 ml absolute ethanol and 650 ml toluene per liter. This medium dissolved at least 0.025 gm of aqueous solution per ml of cocktail at room temperature. All samples were counted at least twice to a total count each run, with a few exceptions, of not less than 40,000 cts. The efficiency of the counting procedure was measured for each

sample by weighing to 5 significant figures on a Mettler H20T balance ~0.1 ml of  $H^3$ -toluene of known activity and recounting the sample at least twice. The disintegration rate was then calculated from the counting rate and efficiency for each sample.

The aqueous dextran solutions were assayed for  $H^3$  activity by weighing 0.2 to 0.4 gm of the solution into scintillation vials, to which was added 0.1 ml of conc. HCl. The vials were then sealed, the contents hydrolyzed for 1 hr at 105°C, approximately 19 ml of scintillation fluid added and the samples counted. Increasing the acid concentration or hydrolysis time was found not to increase the specific activity measured in this way. Also, subjecting  $H^3$ -dextran samples in the absence of cells to the distox procedure gave identical results to the acid hydrolysis technique. The distillates were counted directly by weighing duplicate 0.25-0.5 ml aliquots from each Thunberg bulb into scintillation vials and adding ~19 ml of scintillation medium. A loose white precipitate formed when the oxidized pellet distillates contacted the medium. The precipitate dissolved upon heating in a water bath or standing overnight at room temperature. All activity determinations were made on samples in which the precipitate was dissolved.

The expressions used to calculate the volume of unlabelled solution trapped in the cell pellet, the dextran concentration of the incubation mixture corrected for trapped fluid in the pellet, and the

number of molecules of dextran adsorbed per cell, are:

$$V_{tr} = \frac{W_o}{\rho_o W_c} \left[ \frac{A_o}{A_s} - 1 \right] \quad (4-2)$$

where

$V_{tr}$  = volume of trapped fluid per gram of pellet,  $\text{ml gm}^{-1}$

$W_o$  = wt. of labelled solution added to pellet (wt.  $W_c$ ), gm

$\rho_o$  = density of labelled dextran solution added to pellet,  
 $\text{gm ml}^{-1}$

$A_o$  = specific activity of labelled dextran solution added to  
pellet,  $\text{dpm (gm of solution)}^{-1}$

$A_s$  = specific activity of equilibrated supernatant,  
 $\text{dpm (gm of super.)}^{-1}$

$$[\text{Dex}]_i = \frac{[\text{Dex}]_{i0} W_{i0}}{W_{i0} + V_{tr} W_{ic}} \quad (4-3)$$

where

$[\text{Dex}]_i$  = final dextran concentration ( $\text{gm ml}^{-1}$ ) of  $i$ th supernatant  
in equilibrium with  $W_{ic}$  gm of cell pellet

$[\text{Dex}]_{i0}$  = dextran concentration of  $i$ th solution before exposure to  
pellet,  $\text{gm ml}^{-1}$

$W_{i0}$  = weight of  $i$ th labelled solution added to pellet, gm

$$N_{i,Dx} = \frac{A_{i,dist} [Dex]_{io} N_A}{E_{distox} A_{io} \rho_{io} n_c \bar{M}_n} \quad (4-4)$$

where

$N_{i,Dx}$  = average no. molecules of dextran adsorbed per cell for  
ith ultracentrifuged pellet

$A_{i,dist}$  = specific activity of ith distillate dpm (gm distillate)<sup>-1</sup>

$N_A$  = Avogadro's number,  $6.02 \times 10^{23}$  mole<sup>-1</sup>

$E_{distox}$  = efficiency of distox procedure; equal to specific activity  
of distillate ÷ specific activity of sample oxidized

$A_{io}$  = specific activity of ith solution prior to exposure to  
pellet, dpm (gm sol'n)<sup>-1</sup>

$\rho_{io}$  = density of ith solution prior to exposure to pellet,  
gm ml<sup>-1</sup>

$n_c$  = average number of erythrocytes per gram of ultracentrifuge pellet

$\bar{M}_n$  = number average molecular weight of dextran

$$N_{i,Dx}^w = \frac{A_{i,dist} [Dex]_{io} N_A W_{i,T}}{E_{distox} A_{io} \rho_{io} n_{cw} \bar{M}_n W_{ic}} \quad (4-5)$$

where

$N_{i,Dx}^w$  = no. molecules dextran adsorbed per cell for ith washed  
pellet

$W_{i,T}$  = weight of cells plus saline put through distox procedure

$W_{ic}$  = weight of cell pellet in ith sample put through distox  
procedure

$n_{cw}$  = no. erythrocytes per gram of original pellet  
=  $(1 - V_{tr})n_c$

The above expressions assume that the density of trapped saline is 1.00 to three significant figures. The densities of the dextran solutions were calculated from the concentrations and specific volume of dextran,  $0.611 \text{ ml g}^{-1}$ . The decrease in specific activity and dextran concentration due to adsorption to cells is assumed to cause no significant change in these parameters within the limits of accuracy with which they may be determined.

### Results and Discussion

Upon completion of ultracentrifugation, the organic phase was situated between the cell pellet at the bottom of the tube, and a small amount of  $H^3$ -dextran solution floating at the top of the tube as anticipated. The pellet was observed to be compact and highly translucent, looking more like a clear hemoglobin gel than a cell pellet. There appeared to be no light scattering centers present in the pellet, as judged by eye. This transformation, of an opaque erythrocyte pellet compressing into a translucent, gel-like material in high centripetal fields, is known as Koeppel's criterion, according to

Ponder (223). It is supposed to indicate complete packing, the lack of light scattering being due to the loss of cell-fluid interfaces. However, Ponder claims that up to 5% of the pellet could be fluid while still meeting Koeppe's criterion. He also states that the appearance of translucency corresponds to greater packing, the greater the diameter of tubes in which the cells are spun. Under the experimental conditions applied here, even if all the counts associated with the cell pellets were due to trapped fluid, the packing must have been at least 99.4% complete.

In a pilot ultracentrifuge run, the erythrocyte pellet was recovered by decanting the aqueous and organic phases. The translucent pellet was somewhat elastic, but flowed down from the side of the tube over a period of approximately 30 minutes. When a small piece of the pellet was scraped off the tube wall and examined under a light microscope, the closely apposed cell-cell interfaces were clearly visible. No regions were ever seen where adjacent membranes were not in total contact over their entire visible surfaces. No indication of the presence of interstitial fluid was ever observed. When bits of pellet were suspended in saline and sheared gently, however, the cells were easily dispersed into normal-appearing flexible biconcave discoids. Little or no hemolysis accompanied the ultracentrifugation procedure. These observations are in agreement with those of Parpart and Ballantine (224).

The efficiency of the distox procedure was measured by adding varying amounts and concentrations of  $H^3$ -dextran of known activity to erythrocyte pellets, putting them through the distox procedure and assaying the distillates for  $H^3$ . Up to the maximum cell:solution ratio measured (2:1), any systematic variation in efficiency due to composition variation was found to be smaller than the statistical variation measured from run to run. From duplicate  $H^3$  assays of 24 efficiency determinations, the efficiency of the distox procedure was found to be  $0.788 \pm 0.139$ , where the confidence limits represent  $\pm$  the standard deviation. As an absolute measurement, then, the statistical error in the distox efficiency limits the accuracy of the adsorption isotherm to at least  $\pm 14\%$ . Further errors are introduced into the calculation of  $N_{Dx}$  through the measurement of the distillate and  $H^3$ -dextran solution activities, and the number of cells per gram of pellet. Hydrolyzed samples were counted at rates of  $2-5 \times 10^4$  cpm, at an efficiency of  $\sim 15\%$ , while the distillate counts were generally  $> 10^4$  cpm, and never less than 2X background. The efficiency for distillate counting was  $\sim 20\%$ . Under these conditions the measured activities were reproducible to  $\pm 3\%$ . The number of cells per gram of pellet was measured repeatably to  $\pm 2\%$ . In spite of the large relative error in determining the trapped volume in the pellet, the correction for trapping when applied to the dextran concentration produced only a  $\pm 2\%$  uncertainty in the equilibrium supernatant dextran concentration.



The errors in calculating solution compositions, dilution factors, etc. were negligible compared to the other errors, since all manipulations were done by weight to at least an estimated fourth significant figure. The value of  $\overline{M}_n$  for the low concentrations must be very close to that of the parent fraction, judging by the elution behavior of the H<sup>3</sup>-dextran, and the fact that varying the ratio of cold to hot dextran produced no inconsistencies in the results. The molecular weight distribution is therefore essentially that of the reasonably homogeneous parent dextran 77.6 ( $\overline{M}_w/\overline{M}_n = 1.18$ ), for any of the labelled solutions used. As an absolute measurement, then, assuming only a homogeneous polymer population, the accuracy of  $N_{Dx}$  can be expected to be about  $\pm 23\%$ , with more than half the uncertainty due to the standard deviation of the distox efficiency determination. As a relative measurement of adsorption as a function of dextran concentration, however, the experimental data should be internally consistent to approximately  $\pm 8\%$ , due to the uncertainties in  $A_{i,dist}$ ,  $A_{i0}$  and  $[Dex]_{i0}$  of equation (4-4).

The dextran 77.6-erythrocyte adsorption isotherm determined by the above procedure is given in Figure 4-2. The isotherm is linear on a log-log plot for dextran concentrations between  $6.8 \times 10^{-6} \text{ gm ml}^{-1}$  and approximately  $7 \times 10^{-2} \text{ gm ml}^{-1}$ , at which point the adsorption increases somewhat. Linear regression analysis of the data in log form gives the equation of the line of best fit to be:

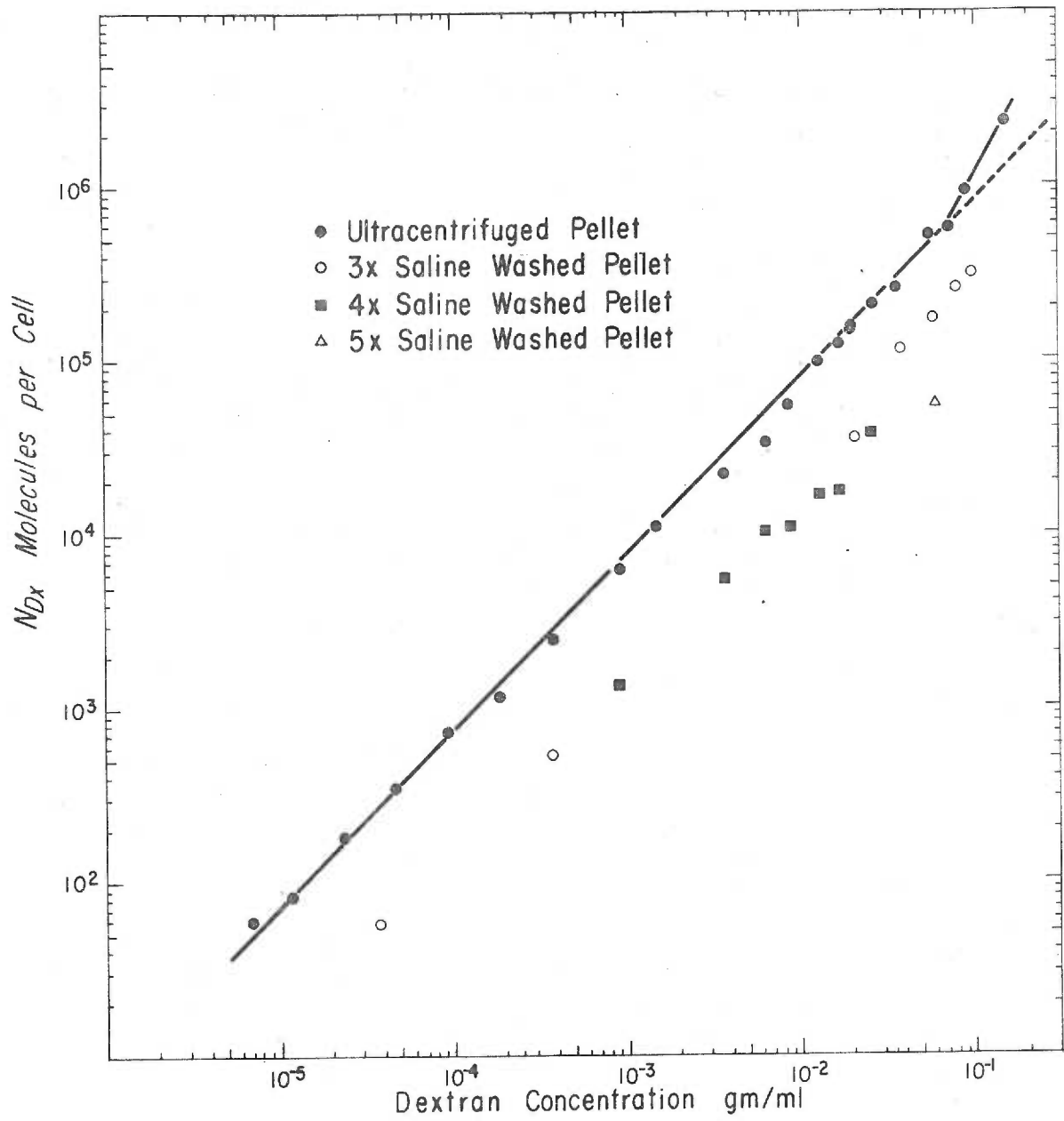


Figure 4-2. The dextran 77.6-erythrocyte adsorption isotherm.

$$\log N_{Dx} = 1.013 \log[Dex] + 6.92$$

$$r = 0.998, \quad 6.75 \times 10^{-6} \text{ gm ml}^{-1} \leq [Dex] \leq 7.16 \times 10^{-2} \text{ gm ml}^{-1}$$

In linear form, the regression equation for the same concentration range is:

$$N_{Dx} = 8.34 \times 10^6 [Dex] - 4.64 \times 10^3$$

$$r = 0.993$$

The  $N_{Dx}$ -intercept of the  $N_{Dx}$ -[Dex] regression line is not significantly different from zero, so for  $[Dex] < 7\%$  w/v, the adsorption of dextran 77.6 from saline to human erythrocytes is directly proportional to the dextran concentration. Above 7%, adsorption increases, again apparently linearly, although too few points were taken above 7% to adequately define the concentration dependence.

The linearity of the measured points immediately suggests that the results represent a small constant fraction (~0.6%) of trapped fluid per gram of pellet rather than adsorption of label to the cells. That the linearity of the results do not represent only trapped fluid can be seen from the results of the washing experiments, also shown in Figure 4-2. It is clear that washing the pellets either 3 or 4 times in saline leaves an amount of dextran adsorbed per cell which again varies linearly with dextran concentration. The log-log regression lines for each of the 3X and 4X washed cells have slopes of  $1.0 \pm 0.1$ .

These results cannot be due to the presence of a small amount of the original solution still being present in the cells, since the cumulative dilution factor after washing is too great to account for the results. That this is in fact true may be seen from Figure 4-3, where the total supernatant activity for each of five washes of a pellet equilibrated with 5.8% dextran is given as a semi-log plot. If each washing results in dilution by a factor  $F$ , after  $n$  washes the activity  $A(n)$  of the supernatant, in terms of the original supernatant activity  $A(o)$ , will be:

$$A(n) = F^n A(o)$$

$$\therefore \log A(n) = n \log F + \log A(o) \quad (4-6)$$

Therefore a plot of  $\log A(n)$  vs  $n$  should be linear for simple dilution. Such linearity is seen in Figure 4-3 for the first two washes. By the third wash, however, the slope of the line has changed sharply, and the  $n = 3, 4$  and  $5$  points fall on a distinct, much less rapidly changing line. If these latter points were produced by dilution, they should clearly be orders of magnitude lower. It is probable instead that they represent slow desorption of polymer from the cell membrane. Hence, the counts associated with 3X and 4X washed pellets must be due to adsorption of dextran.

A further indication that the linearity of the isotherm is not due to fluid trapping is given by the behavior above 7% dextran. The sharp

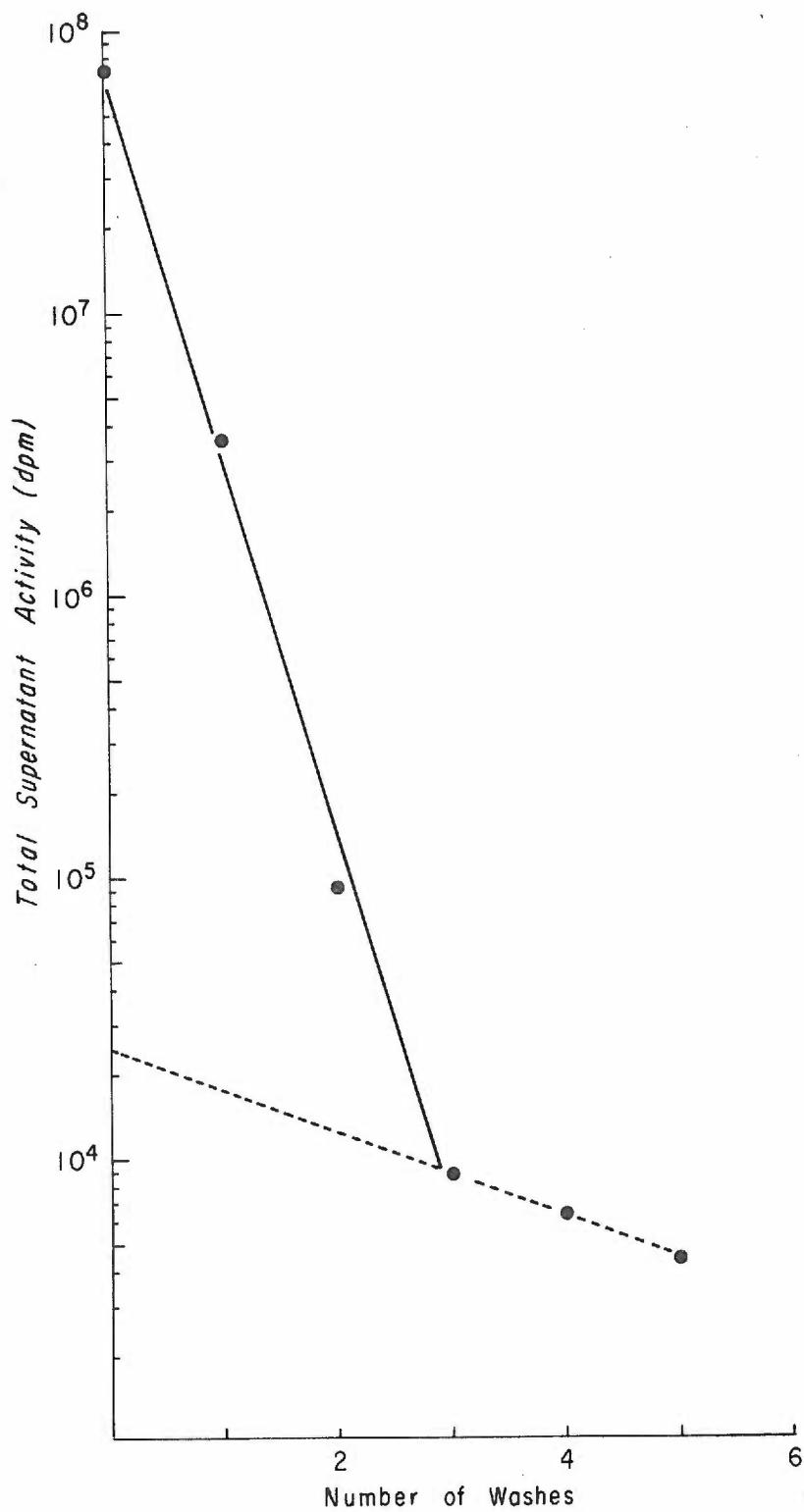


Figure 4-3. Total supernatant activity vs. number of washes for erythrocytes exposed to  $H^3$ -dextran 77.6.

apparent increase in adsorption would not be expected to appear if the data were a measure of the trapped solution. Were this the case, a featureless straight line would be seen for all dextran concentrations. The rationale behind the adsorption increase will be discussed in Chapter 5.

Since the adsorption appears to be linear over an extended concentration range, there is a possibility that only a portion of the counts associated with each pellet are due to adsorption, the remainder being due to label trapped in the pellet. There are two pieces of evidence, however, which suggest that at least 85% of the counts are due to adsorption.

- (i) The anticipated concentration at which an adsorption increase would be observed, on the basis of independent evidence, is  $[\text{Dex}] \geq 6.9\%$  (see Chapter 5). The line extrapolated from data at the three highest concentrations cuts the 6.9% division approximately 15% below the lower concentration regression line (see Figure 5-15). Hence, the true adsorption would appear to contribute at least 85% of the counts measured in the pellets.
- (ii) The number of counts lost in the first three washes of the pellet of Figure 4-3 may be estimated by extrapolating the desorption part of the plot back to 0 washes. The sum of the counts given by this extrapolation through 2, 1 and 0 washes

is a measure of the total activity lost by the pellet in the washing, assuming that the desorption proceeds exponentially at the higher surface concentrations. If the total counts lost are added to the counts measured for the pellet after three washes, the result is only 13% lower than indicated by the regression line at that concentration. Again, then, it appears that the adsorption isotherm lies within 15% of the regression line. Since the absolute location of this line is only known to within  $\pm 23\%$ , it is concluded that the regression line for the measured data points represents the true adsorption isotherm of dextran in this system within the limits of experimental error of the method.

It is noteworthy that the adsorption isotherm shows no indication of saturation even at very high polymer concentrations. This is in marked contrast to almost all other polymer adsorption isotherms in the literature (38), where generally the adsorption is found to be roughly independent of polymer concentration over an extended range. The experiments on which this generalization is based, however, have virtually all been performed on solid, non-biological surfaces. As far as the author is aware, the only accurate studies on polymer adsorption to cells have been made on polylysine adsorption to erythrocytes (88). In the polylysine work the isotherm for polymer of molecular weight  $\sim 4640$  (D. P.  $\sim 36$ ) was found to saturate in an

amount equivalent to about 6 to 10 monolayers of close packed polymer, at a concentration of 5 to  $10 \times 10^{-5}$  gm ml<sup>-1</sup>. Even at  $10^{-1}$  gm ml<sup>-1</sup>, however, the dextran adsorption corresponds to about 1.3 monolayers of polymer [assuming an area per glucose monomer of  $46 \text{ \AA}^2$ , an area per red cell of  $163 \mu^2$  (225) and a degree of polymerization of 404]. At concentrations of  $10^{-5}$  gm ml<sup>-1</sup> of polymer, roughly  $8 \times 10^4$  times as many monomer units of polylysine adsorb as dextran. Hence the adsorption of the positively charged polymer to red cells is vastly stronger than dextran, as would be expected for the negatively charged cell surface. Weaker adsorption is apparently accompanied by much stronger concentration dependence.

Qualitatively, this concentration dependence is not unexpected theoretically. The simplest treatment of adsorption in general, the Langmuir isotherm, predicts that the lower the adsorption energy, the greater the concentration range over which adsorption is concentration dependent. If  $A$  is the amount adsorbed at a concentration  $C$ ,  $a$  is an association constant, and  $\gamma$  is a constant proportional to the number of binding sites on the surface, the Langmuir expression is (226):

$$A = \frac{a\gamma C}{1+aC} \quad (4-7)$$

If  $aC \ll 1$ ,  $A = a\gamma C$  and the amount adsorbed is strongly concentration dependent. The lower the association constant  $a$ , the



greater the range of  $C$  over which  $aC \ll 1$ , and the more extensive the region of concentration dependence. Similarly, Silberberg's statistical mechanical treatment of polymer adsorption indicates that the lower the net free energy change per monomer associated with a monomer-surface site interaction, the greater the concentration dependence of adsorption from good solvents. The observed concentration dependence for dextran-erythrocyte adsorption, however, greatly exceeds that predicted for a solid, uniform surface.

Finally, it should be noted that the literature contains some indirect evidence that adsorption of dextran to erythrocytes is an increasing function of dextran concentration at high concentrations, and does not show saturation behavior in this region. Thorsén and Hint (100) showed that the sedimentation rate of an approximately 30% (v/v) suspension of washed erythrocytes in a solution of dextran (viscosity-average mol. wt. ~82,000) increased linearly with dextran concentration between 1.5% and 2.8% w/v. Their results were not corrected for the increasing viscosity and density of the suspending media as the dextran concentration was increased. There is no detailed theory of erythrocyte sedimentation rate in aggregating media; it is an enormously complicated problem. Qualitatively, however, it seems that the increased aggregation, as reflected in the sedimentation rate, was caused by increasing amounts of dextran adsorbing to the cells, causing progressively larger flocs to form as the dextran

concentration was raised. If the amount of dextran adsorbed were constant over this concentration range, it is difficult to see how aggregation, and therefore the sedimentation rate, would increase the higher the polymer concentration. Since Thorsén and Hint's data was not corrected for viscosity and density changes, the corrected sedimentation rate should increase even more rapidly with dextran concentration than they indicate.

Hardwicke and Squire (227) performed a series of sedimentation experiments in which corrections for the suspending medium viscosity and density were applied. Using suspensions of 30% v/v red cells in a medium 35% v/v serum and 65% v/v dextran/saline they showed that three dextran fractions of molecular weights 1.5, 3.0 and  $8.0 \times 10^5$  increased the corrected sedimentation rate as a function of concentration. They found that between 0.1% and 1.4% w/v the corrected sedimentation velocity increased as the 2.15th power of the dextran concentration, independent of molecular weight.

These sedimentation results, then, argue strongly that dextran adsorption to erythrocytes is an increasing function of concentration at the relatively high concentrations examined, in agreement with the measured isotherm.

## CHAPTER 5

ELECTROKINETIC STUDIES OF CELL AND PARTICLE  
SUSPENSIONS IN NEUTRAL POLYMER SOLUTIONS

As has been discussed previously, several workers have shown that the cellular zeta potential is increased when the electrophoretic mobility of cells is measured in the presence of neutral polymers. In this chapter, the effect is delineated for a variety of particle-polymer systems. The dependence of the relative zeta potential of human erythrocytes on concentration and molecular weight of a series of dextran fractions is given. The effect of pH, ionic strength, and monovalent ion type is examined. The variation of relative zeta potential with ionic strength is interpreted in terms of the model developed in Chapter 2. Values for the polymer adsorption factor  $\beta$ , and the adsorbed layer thickness  $d$  are estimated from this electrokinetic data, and their variation with dextran molecular weight given. The effect of the zeta potential on the state of aggregation of red cells in the presence of various dextrans is noted. The increased adsorption of dextran 77.6 above  $\sim 7\%$  concentration described in Chapter 4 is interpreted in terms of a change in the state of aggregation at this concentration. The results of the adsorption and electrophoretic measurements are compared, and the polymer adsorption model discussed critically in the light of this comparison. Finally,

the drainage properties of neutral adsorbed layers are considered in the context of the present results.

### Methods and Materials

All chemicals were of reagent grade unless noted. All aqueous solutions were made up with twice pyrex-distilled water. Sharply cut dextran fractions were generously supplied by Dr. K. Granath of Pharmacia AB, Uppsala, Sweden. The fractions used and their specifications were as given in Table 5-1. Polyethylene glycol (PEG) or polyethylene oxide was obtained from Union Carbide Corp., New York as three fractions: PEG 6 (Carbowax 6000), PEG 20 (PEG compound 20-M) and Polyox 100 (Polyox WSR N-10), where the designation in brackets is the commercial specification. All dextran and PEG samples are hereinafter referred to by chemical species, and by their nominal molecular weight, given by  $10^3$  times the number indicated for each fraction. Methyl cellulose was obtained from Dow Chemical Co., Midland, Mich. as Methocel MC, 25 cps Premium Grade (viscosity of 2% aqueous solution  $\sim 25$  cps at  $20^\circ\text{C}$ ). Polyacrylamide was supplied by American Cyanamid, Wayne, N. J. as Magnifloc 990-N, mol. wt.  $\sim 4 \times 10^6$ . Block co-polymers of polypropylene oxide and polyethylene oxide were generously donated by Wyandotte Chemicals Corp., Wyandotte, Mich. as Pluronic F-68 (mol. wt. 8750; 20% w/w polypropylene oxide, 80% w/w polyethylene

oxide) and Pluronic F-108 (mol. wt. 16,250; 20% w/w polypropylene oxide, 80% w/w polyethylene oxide).

Table 5-1. Characteristics of dextran fractions.

Dextran Fraction	Pharmacia Designation	$\overline{M}_w$	$\overline{M}_n$	$\overline{M}_w/\overline{M}_n$
Dextran 26.5	RMT 726	26,500	19,700	1.35
Dextran 41	FDR 858	41,000	26,000	1.58
Dextran 50.5	RMT 829	50,500	37,500	1.35
Dextran 77.6	DR 776	77,500	50,800	1.53
	FDR 403	77,600	65,500	1.18
Dextran 110	III A 1	110,000	83,000	1.33
Dextran 147	II A 1	147,000	114,000	1.29
Dextran 510	4376	510,000	185,000	2.76

Human erythrocytes were obtained either from unexpired blood bank whole blood originally taken into ACD, or by drawing blood from healthy, fasting volunteers into 1/10 volume of 3.8% w/v  $\text{Na}_3$  citrate. The blood was spun down, the buffy coat removed, and the red cell pellet washed three times (3X) in 0.145 M NaCl adjusted to pH  $7.0 \pm 0.2$  with 0.5 M  $\text{NaHCO}_3$  (standard saline) then once in the appropriate suspending medium. Human platelets were obtained by spinning fresh citrated blood at room temperature for 12 min at 60 xg, taking off the platelet-rich plasma and washing the platelets from this plasma 3X with standard saline. Human peripheral lymphocytes were obtained from whole blood, made ~1% w/v with gelatin, which was allowed to sediment for 45 min at 37°C. The resulting

supernatant was diluted 1:4 with standard saline, spun for 15 min at ~700 xg, and the pellet washed twice with 0.156 M  $\text{NH}_4\text{Cl}$  (10 min incubation at room temp.; 10 min spin at 110 xg), then once with standard saline. One half of each of the washed platelet and lymphocyte pellets was washed once in the polymer solution before electrophoresis.

Acetaldehyde-fixed cells were prepared from unexpired blood bank ACD blood using the method of Heard and Seaman (34). Cells were used after fixation periods of between two months and three years. Glutaraldehyde-fixed cells were prepared by suspending one volume of washed human erythrocytes in at least ten volumes of a solution of 2% w/v glutaraldehyde (Polysciences Inc., Warrington, Pa., supplied as 8% aqueous solution, pH 7.0, sealed under  $\text{N}_2$ ) in standard saline for 60 min at room temperature. The cells were then spun down, the supernatants replaced with fresh fixing solution, and the cells stored at 4°C. Before use all fixed cells were washed 3X in standard saline.

Two samples of polystyrene latex particles (PSL) were obtained from the Dow Chemical Corp. that had a mean diameter of 1.099  $\mu$  (both Lot LS-1028-E). They were either washed 3X in standard saline, or 3X in phosphate-buffered saline (PBS), pH 7.3, composed of 100 volumes 0.145 M NaCl, 5 volumes 0.067 M phosphate buffer (8 parts 0.067 M  $\text{Na}_2\text{HPO}_4$ , 2 parts 0.067 M  $\text{KH}_2\text{PO}_4$ ), then once in the

appropriate dextran solution.  $\text{TiO}_2$  (rutile; Titanox RA 42) obtained from Titanium Pigment Corp., bentonite obtained from American Colloid Co. Skokie, Ill. as Volclay BC-USP, and quartz powder were all washed 3X in standard saline and once in the dextran solution before use.

For all but the dextran solutions the polymers were made up as concentrated aqueous salt-free stock solutions whose concentrations were taken to be that indicated by the weight of (presumed) dry powder used. The dextran fractions were also made up, initially with heating, in 2X distilled water as concentrated (15 to 20% w/v) salt-free stocks. The concentrations were determined polarimetrically as described by Albertsson (197). All solutions were stored at 4°C until used. In some cases where the stocks were initially cloudy the solutions were filtered under negative pressure through 0.49  $\mu$  Millipore filters before storage. The viscosities of the dextran stock solutions did not vary over the period of storage, indicating negligible depolymerization due to bacterial contamination. The polymer-salt solutions used throughout these experiments were all made up by weight from stock polymer and concentrated salt solutions to  $\pm 0.0005$  gm on a Mettler P160N top-loading balance whose pan was shielded from air currents with an inverted 2 l. beaker. The densities used to convert the solution weights to volumes were calculated from the specific volumes of dextran ( $0.611 \text{ gm cm}^{-3}$ ), and the known densities of the aqueous salt

solutions. All dextran-salt solutions were made  $5 \times 10^{-4}$  M  $\text{NaHCO}_3$  to bring the pH up to  $\text{pH } 7.4 \pm 0.4$ . The contribution of this concentration of bicarbonate was included in all ionic strength determinations.

In those experiments where the mobility was measured as a function of pH at constant ionic strength and dextran concentration, the pH was varied by adding either a 4.39% w/v dextran, 0.134 M NaCl, 0.011 M HCl solution, pH 1.2, or a 4.39% w/v dextran, 0.134 M NaCl, 0.011 M NaOH solution, pH 11.6, to a 4.39% w/v dextran 0.145 M NaCl solution. The pH of each mixture was measured on an aliquot of the cell suspension to be examined electrophoretically after the cells had been added. The pH meter used was a Radiometer Model 28 standardized before each experiment with pH 4 and pH 10 standard buffers (Matheson Coleman & Bell). Mobility measurements were made immediately after pH adjustment, so the mobilities measured represented the behavior of cells exposed to acid or base for about 15 or 20 minutes. Electrokinetic reversibility was established by measuring the mobility of a cell suspension at a given pH, adding sufficient acidic or basic dextran solution to the remaining suspension to bring the pH back to  $\text{pH } 7.0 \pm 0.5$ , then repeating the mobility measurement. If the resulting mobility was within  $\pm 5\%$  of the usual mobility at pH 7, the mobility at the original pH value was considered to be electrokinetically reversible. The amount of water formed from the acid



and base mixtures was insufficient to affect the ionic strength significantly. The mixtures of the acidic, basic, and neutral dextran solutions used all had the same viscosity, and the viscosity of the acidic solution did not change over the course of the experiment, indicating negligible depolymerization due to hydrolysis during this period.

For the experiments involving the measurement of mobilities at low ionic strengths in the presence of constant concentrations of polymer, the suspending solutions were made up from aqueous solutions of salt and polymer, both at twice the final concentration required. Equal volumes of each were then weighed out to give the final mixtures. The salt solutions of the same final ionic strength, required for the control mobility determinations (in the absence of polymer), were made up from the same stock salt solutions, but with distilled water replacing the polymer stocks. In this way it was ensured that the mobilities in both the presence and absence of polymer, used to calculate the relative zeta potentials, were measured at the same ionic strength. When the mobilities of unfixed cells were measured in the presence of dextran as a function of ionic strength, the cells were washed one additional time in saline,  $\text{pH } 7.4 \pm 0.1$ , just before exposure to the low ionic strength media to remove any trace of hemoglobin which could adsorb to the cell surface. The low ionic strength solutions to which unfixed cells were exposed were all made approximately isotonic with sorbitol as described by Heard and

Seaman (23). The pH of all normal cell suspensions of low ionic strength was never less than 7.2.

Cell electrophoresis was performed using the apparatus and techniques described by Seaman (228), and Seaman and Heard (229). The apparatus used employs a cylindrical chamber of approximately 1 ml volume, and a Ag/AgCl electrode system. All measurements at ionic strengths  $\leq 0.145$  gm ions  $l^{-1}$  were made with 50 volts applied across the electrodes (corresponding to a field strength of approximately  $5v\text{ cm}^{-1}$ ). At higher ionic strengths, 30 volts were applied to reduce heating and convection in the chamber (230). The effective field strength and equipment factor were calculated from the currents measured with KCl solutions in the chamber, as described by Seaman and Heard (229). All measurements were made at  $25.0 \pm 0.2^\circ\text{C}$ . Except for those measurements of relative zeta potential as a function of polymer concentration at constant ionic strength (Figure 5-1 and 5-3), the results of mobility measurements are based on a minimum of two separate mobility determinations, each of which consisted of measuring the velocity of ten cells, alternating the direction of the applied field after each timing. Some of the points of Figure 5-1 and 5-3 are based on single mobility determinations (10 cells). Before each set of electrophoretic measurements, the mobility of normal washed human erythrocytes suspended in standard saline was measured as a check on the apparatus and equipment factor. Only if this

checkpoint mobility determination gave  $-1.08 \pm 0.03 \mu s^{-1} v^{-1} cm$  (23) was the equipment considered satisfactory. At ionic strengths  $\leq 0.0145 \text{ gm-ions } l^{-1}$  the equipment factor was observed to decrease slightly, presumably due to leakage of KCl from the electrode chambers in the vicinity of the sintered glass discs. It was not necessary to correct for this effect, however, since all the low ionic strength results are expressed as zeta potentials in polymer solutions relative to salt controls. Since the factor decrease was not significantly different in the presence of polymer (allowing for viscosity differences), the relative zeta potentials quoted are independent of the absolute values of the mobilities calculated using a constant equipment factor. Virtually all the electrokinetic results, then, are expressed in terms of  $Z$ , the relative zeta potential defined as (for constant applied voltage):

$$Z = \frac{\eta U}{\eta_o U_o} = \frac{\bar{\eta} \bar{t}_o}{\eta_o \bar{t}} \quad (5-1)$$

where

$U$  = mobility of particle in salt-polymer solution in

$$\mu s^{-1} v^{-1} cm$$

$U_o$  = mobility of particle in salt solution alone in  $\mu s^{-1} v^{-1} cm$

$\eta$  = viscosity of salt-polymer solution, in centipoise (cp)

$\eta_o$  = viscosity of salt solution alone, in cp

$\bar{t}$  = average migration time over fixed distance for particle

suspended in salt-polymer solution

$\bar{t}_o$  = average migration time over same fixed distance for  
particle suspended in salt solution only

Viscosity measurements were made at  $25.0 \pm 0.1^\circ\text{C}$  with an Ostwald capillary viscometer of 5 ml volume and a flow time for water of 84.5 sec. At least for dextran, the polymer solutions used have been shown to be Newtonian (231), so the viscosities measured at the relatively high shear rates found in this viscometer ( $>100 \text{ sec}^{-1}$ ) may be assumed to apply at the lower (of the order of  $1 \text{ sec}^{-1}$ ) shear rates operative in cell electrophoresis. The flow time for water was determined before and after each set of viscosity measurements, to be sure that all the polymer solution had been rinsed out after each run. Viscosities were calculated from the expression:

$$\eta = \frac{t}{t_w} \frac{\rho}{\rho_w} \eta_w \quad (5-2)$$

where

$\eta$  = viscosity in centipoise of solution measured

$\eta_w$  = viscosity of water at temperature used ( $\eta_w = 0.8937 \text{ cp}$   
at  $25^\circ$ )

$t$  = flow time for solution

$t_w$  = flow time for water

$\rho$  = density of solution at temperature used

$\rho_w$  = density of water at temperature used ( $\rho_w = 0.9970 \text{ gm cm}^{-3}$   
at 25°)

The degrees of aggregation of the erythrocyte-dextran suspensions were estimated by observation with light microscopy. Approximately 30% v/v cell suspensions in dextran were mixed well, a drop of suspension placed on a new glass slide, covered with a plastic coverslip, allowed to stand 10 minutes, then examined at X 300 magnification. The degree of aggregation in the center of slide was estimated on a scale of 0  $\rightarrow$  +++, with the appearance of a 30% v/v saline suspension of erythrocytes graded as 0.

All calculations were made on a Hewlett-Packard 9100-B calculator equipped with a Model 9120-A printer. Theoretical curve fitting was carried out by programming the appropriate function on the 9100-B and having a series of the appropriate parameters surveyed. Curve fitting to data points was then carried out by eye.

## Results and Discussion

### I. The Presence and Reversibility of Electrokinetic Effects in Particle-Neutral Polymer Systems

The relative zeta potentials of fresh washed human erythrocytes suspended in neutral solutions of various dextran fractions, PEG, and

Pluronic F-68, all 0.145 M with respect to NaCl, are given as a function of polymer concentration in Figure 5-1. The dependence of  $Z$  on number average molecular weight for the dextran fractions is given in Figure 5-2. It is seen that the relative zeta potential is a smooth function of molecular weight, levelling off at high molecular weight as might be expected for a polymer adsorption-related phenomenon. The points for dextran 510,  $\overline{M}_n = 185,000$  do not fall on the curves defined by the lower molecular weight, more sharply defined fractions, probably because of the polydispersity of this fraction. ( $\overline{M}_w / \overline{M}_n = 2.8$ ). The relative zeta potentials of glutaraldehyde-fixed human erythrocytes and PBS-washed PSL in 0.145 M NaCl plus various molecular weights and concentrations of dextran are given in Figure 5-3. Table 5-2 lists the results of relative zeta potential determinations on a variety of other particle-neutral polymer systems, all of which are 0.145 M in NaCl. It is seen that all the neutral polymers tested produce a relative zeta potential greater than one for normal and fixed human red cells. Not all particles exhibit the same relative zeta potentials in the same solutions, however. After extended incubation in 5% dextran 110, for instance, normal erythrocytes exhibit a relative zeta potential greater than one, quartz a  $Z$  of approximately one, and bentonite and rutile a  $Z$  of less than one. Furthermore, not all samples of the same type of surface exhibit the same behavior in virtually identical solutions. Figure 5-3 shows that the

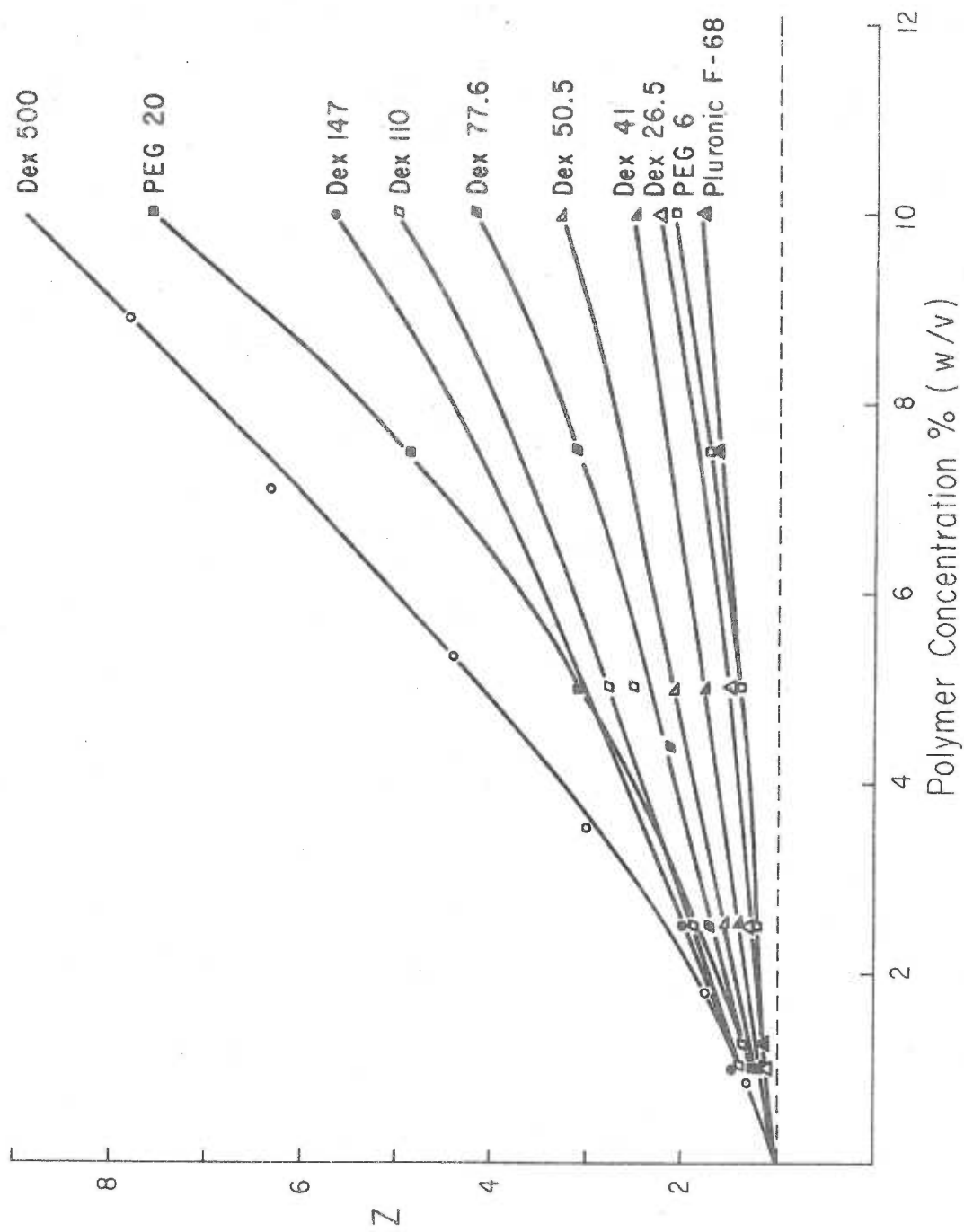


Figure 5-1. Relative zeta potential vs. polymer concentration for erythrocytes in various neutral polymer/saline solutions.

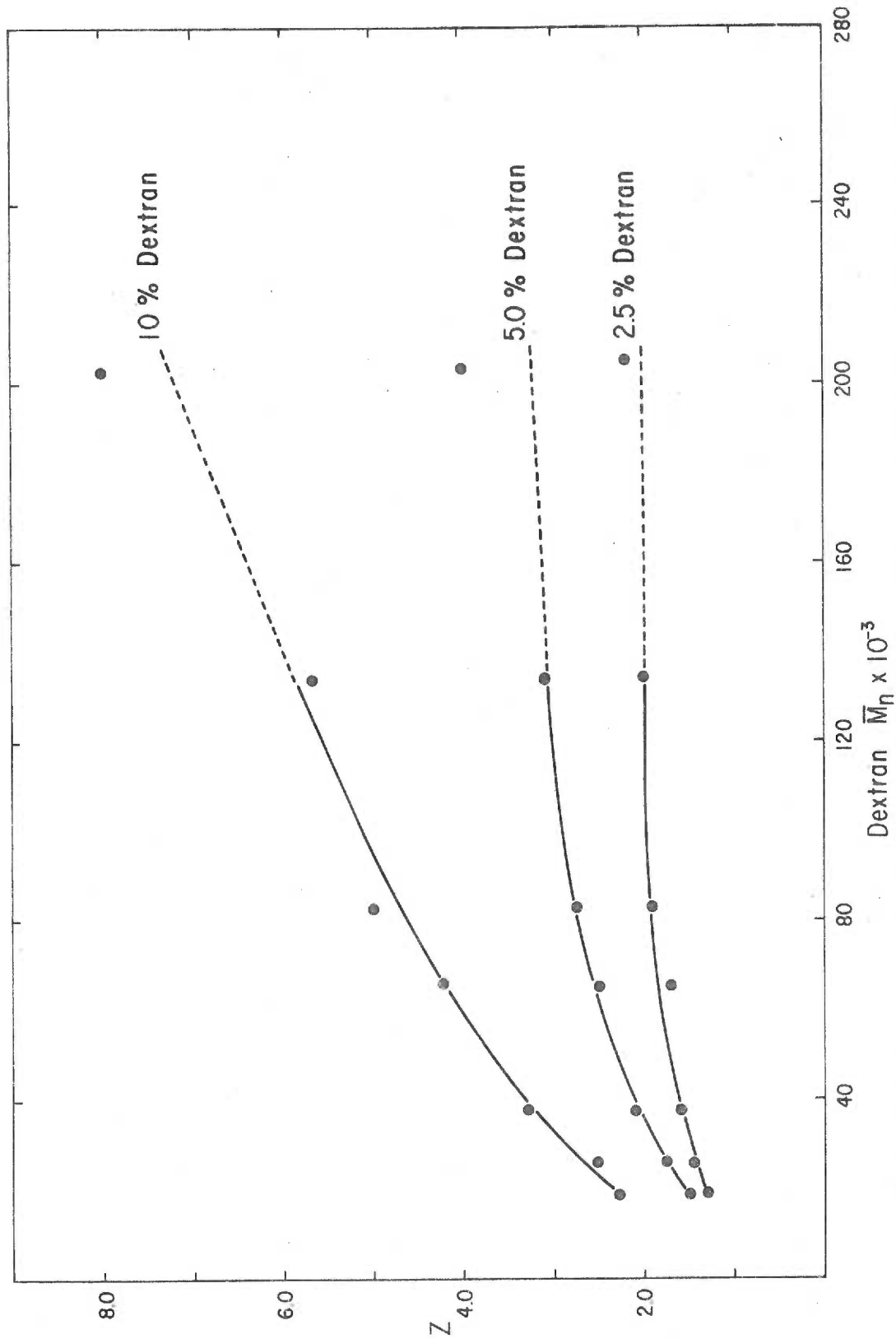


Figure 5-2. Relative zeta potential vs. molecular weight for erythrocytes in various dextran fractions.



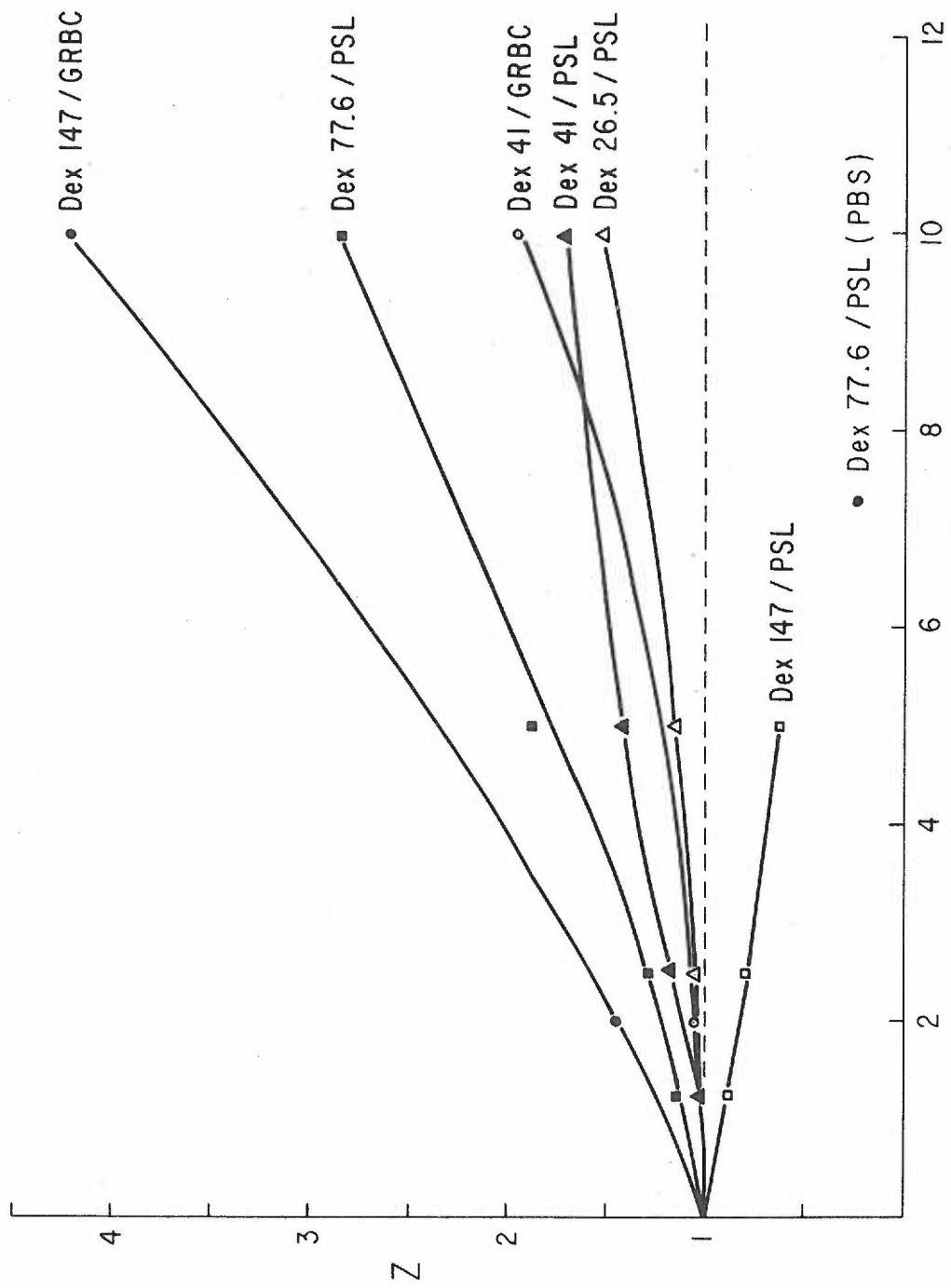


Figure 5-3. Relative zeta potential vs. dextran concentration for glutaraldehyde-fixed red cells (GRBC) and polystyrene latices (PSL).

Table 5-2. Electrokinetic results for various particle-neutral polymer systems (ionic concentration = 0.145 M NaCl).

Particle	Control Mobility ( $\mu \text{ s}^{-1} \text{ v}^{-1} \text{ cm}$ )	Treatment or Suspending Medium	Z
Normal platelet	-0.88	5% dextran 77.6	2.00
Normal lymphocyte	-0.97	5% dextran 77.6	1.59
Normal RBC	-1.08	0.045% polyacrylamide	1.37
Normal RBC	-1.08	0.18% methyl cellulose	1.43
Normal RBC	-1.08	0.45% polyethylene oxide	1.38
Normal RBC	-1.08	4.0% pluronic F108	1.75
Bentonite	-2.83	5% dextran 110	0.49
		3X saline washed post dextran 110	0.83
Rutile	-0.73	5% dextran 110	<0.6
		3X saline washed post dextran 110	0.38
Quartz	-1.67	5% dextran 110	
		(i) 5 min incubation	1.63
		(ii) 30 min incubation	1.35
		(iii) overnight incubation	1.04
		2X saline washed post dextran 110	0.67
		4X saline washed post dextran 110	0.84

relative zeta potential of a PSL sample washed three times in standard saline instead of PBS, gave  $Z = 0.26$  in a 6.6% dextran 77.6-saline solution. The control mobilities in the two cases differed only by 10%, indicating that no gross changes in surface charge properties were caused by the two washing procedures. It seems possible that organic contaminants or surface active molecules remaining from the polymerization of the PSL could have been responsible for some change in surface properties. Polystyrene latices are notoriously difficult to get, and keep, electrokinetically clean (232).

The relative zeta potential of some particles in neutral polymers is time dependent. Table 5-1 shows that quartz particles exhibit a relative zeta potential that decreases slowly with time when the particles are suspended in 5% dextran 110 in saline. Fresh erythrocytes, on the other hand, exhibit little or no measurable time dependence of their electrokinetic properties when suspended in dextran-saline solutions, as is seen from the following experiment. The mobilities of fresh washed erythrocytes after a one hour incubation in the appropriate solution, were measured in 5% and 2.5% dextran 77.6-saline solutions to be  $-0.82 \mu s^{-1} v^{-1} cm$  and  $-1.02 \mu s^{-1} v^{-1} cm$ , respectively. The suspension of RBC's in 5% dextran/saline was then diluted 1:1 with a suspension of RBC's in saline, mixed thoroughly, and an aliquot used for a mobility determination immediately after mixing (completed within 7 min). The resulting erythrocyte mobility was

$-1.02 \mu s^{-1} v^{-1} cm$ , indicating that any time effects in these systems were too rapid to be seen electrokinetically.

The experimental results described above effectively eliminate two of the possible models for the erythrocyte zeta potential increase in the presence of neutral polymers, as discussed in Chapter 2. The strong dependence of  $Z$  on the type and state of particle surface indicates that no pure solution property can be responsible for the observed electrokinetic behavior. Such a dependence on surface properties might be expected, however, if the zeta potential were related to fairly weak polymer adsorption, as the model requires. The time dependence of  $Z$  for the quartz/dextran system is also consistent with this model, since polymer adsorption often takes several hours to come to equilibrium (38). That  $Z$  decreases with time for quartz and that both bentonite and rutile show  $Z < 1$  in dextran argues strongly against the anion adsorption model of zeta potential increase. If the zeta potential increases were due to anion adsorption to an adsorbed dextran layer, neither  $Z < 1$  nor  $Z$  decreasing ought to have been observed.

There are at least two explanations for these results, however. The first involves the location of the shear plane in the vicinity of an adsorbed dextran layer. That  $Z \neq 1$  for these three systems strongly suggests that such an adsorbed layer is present. It was shown in Chapter 2 that values of  $Z < 1$  occur when the shear plane

is displaced away from the effective plane of charge by a dense adsorbed layer. The decreasing value of  $Z$  for quartz could be an indication that the adsorbed layer becomes less free draining as it equilibrates. One might expect that a dense layer would be more likely to occur, the more strongly the polymer adsorbed. That the binding of dextran to quartz, bentonite and rutile is stronger than to erythrocytes is demonstrated by the washing experiments also summarized in Table 5-2. Even after three or four washes, the zeta potential has not returned to the control value for these particles, while at most two washes are required to make  $Z = 1$  for fresh erythrocytes (see below). Hence, polymer adsorption to erythrocytes is apparently less tenacious than to the rigid particles.

The second explanation for the low or decreasing  $Z$  values is based on the apparently low adsorption energy of anions to quartz. The variation in surface charge as a function of ionic strength may be used to estimate the net free energy of binding of potential-determining ions to a surface if a suitable expression for the adsorption isotherm is available. The Stern equation (233) supplies such an estimate, and was applied as follows. The electrophoretic mobility of quartz was measured at  $\text{pH } 7.0 \pm 0.2$  (in the absence of polymer) in 0.145 M and 0.0145 M NaCl, and the corresponding charge densities,  $\sigma(c)$ , calculated using the Gouy equation (1-17). The Stern equation relates  $\sigma \text{ esu cm}^{-1}$  to the monovalent ion concentration  $c \text{ M}$ :

$$\frac{1}{\sigma(c)} = \frac{1}{en_a} + \frac{1}{c} \frac{1}{en_a \exp(-G/kT)} \quad (5-3)$$

where

$e$  = electronic charge in esu

$n_a$  = no. adsorption sites per  $\text{cm}^2$

$G$  = net free energy of adsorption of one ion

$k$  = Boltzmann constant

$T$  = absolute temperature

A plot of  $1/\sigma(c)$  vs  $1/c$  allows the determination of  $G$  from the slope and intercept, which may be estimated from just two pairs of  $(\sigma, c)$ . The mobilities and calculated charge densities in 0.145 M and 0.0145 M NaCl were respectively  $U = -1.67 \mu \text{s}^{-1} \text{v}^{-1} \text{cm}$ , corresponding to  $\sigma = 5.87 \times 10^3 \text{ esu cm}^{-2}$ , and  $U = -2.95 \mu \text{s}^{-1} \text{v}^{-1} \text{cm}$ , corresponding to  $\sigma = 3.43 \times 10^3 \text{ esu cm}^{-2}$ . Substituting these values in equation (5-3) gave for the free energy of adsorption of a potential determining ion  $G \sim -4.4 \text{ kT}$ , corresponding to  $G \sim -2.5 \text{ K Cal mole}^{-1}$ . This is a typical value for such adsorption processes (233), and indicates that the ion binding is relatively weak. This binding energy may be compared to that of a hydrogen bond, which is generally found to be of the order of 3 to 5  $\text{K Cal mole}^{-1}$  (200), somewhat higher than the ion value.

It seems possible, considering the hydrophilic nature of the silicate surface of quartz and the abundance of hydroxyl groups in

dextran, that hydrogen bonding could be an important factor in dextran adsorption to quartz. Such bonding would be consistent with the results of Griot and Kitchener (70) who give evidence for the binding of polyacrylamide to quartz through H-bonding. It seems not unreasonable, then, to expect that dextran could compete favorably with anions for dipolar or charged sites on the quartz surface capable of both hydrogen bonding and ion binding. Such competition, as the polymer adsorption approaches equilibrium, could result in a gradual decrease in surface charge due to displacement of anions by polymer segments, accounting for the decreasing  $Z$  observed in these systems. Some support for this explanation is provided by the values of  $Z$  found after washing the quartz. After two saline washes, the relative zeta potential was lower than when the dextran was present in solution. If the decreasing  $Z$  values in dextran were due only to the changing location of the shear plane, it is difficult to see why washing the surface should increase this effect. It seems more reasonable to expect that the observed behavior was due to a combination of the effect of the adsorbed polymer on the counter ion activity, causing the initially observed  $Z > 1$ , and anion desorption, resulting in the decreasing  $Z$  values with time. The low, but increasing values of  $Z$  upon washing would then reflect the desorption of polymer and the slow replacement of depleted potential-determining anions.

Washing experiments on fresh erythrocytes, as mentioned above,

indicate that dextran adsorption is more readily reversible in these systems. Washed fresh erythrocytes were incubated one hour in 10% dextran 77.6-saline, spun down and the supernatant removed. Approximately 0.05 ml of the pellet was added to 40 ml of standard saline, the contents mixed, and two mobility measurements made immediately (completed within 15 min). The cells were then spun down, the viscosity of the supernatant measured, and the relative zeta potential calculated to be  $Z = 1.05$ . After a second wash in standard saline, the value of  $Z$  was 1.00. A similar experiment performed on cells exposed to 5% dextran 110 gave  $Z = 1.00$  after one wash. Fresh erythrocytes, then, exhibit almost complete reversibility of the electrokinetic effects of exposure to dextran after one washing. Erythrocytes which have been stored in vitro for some time, however, maintain part of the zeta potential increase associated with neutral polymers through several washes, as is seen from the following experiment.

Washed human erythrocytes were prepared from blood bank ACD whole blood which had been stored at 4°C for 48 days. One volume of these washed stored cells, and one volume of washed fresh cells were incubated in 10 volumes of 4% PEG 6 for one hour at room temperature, spun down, each washed three times in standard saline, and their mobilities measured along with control mobilities for the two populations which were not exposed to the PEG. The control



mobilities of both the fresh and stored cells, as well as the mobility of the fresh cells which had been exposed to PEG, then washed, were all  $-1.07 \mu s^{-1} v^{-1} cm$ . The stored cells which had been incubated in PEG, however, had a mobility of  $-1.18 \mu s^{-1} v^{-1} cm$  after three washes. Stored erythrocytes, then, apparently retain the electrokinetic effects associated with neutral polymers to a greater extent than fresh cells. These observations are consistent with the concept of an association between polymer adsorption and the zeta potential increases seen, so long as the polymer adsorption is not directly controlled by charge groups responsible for the electrophoretic mobility of the cells. The equality of the mobilities of fresh and stored cells suggest, as in the case of PSL, that subtle differences in surface properties may strongly influence the adsorption of polymers in these systems.

One inconsistency in the polymer adsorption model which merits some discussion appears when the results of the  $H^3$ -dextran uptake measurements of Chapter 4 are considered. It is apparent from Figure 4-2 that after exposure to high concentrations of dextran 77.6 and three saline washes, there should be enough dextran left adsorbed to the cell to cause a larger  $Z$  value than was observed. This discrepancy could be due to a variety of factors:

- (i) The  $H^3$  associated with the washed cells could have represented  $H^3$  which had penetrated the cell membrane, either

still associated with dextran molecules, or with a hydrolysis product of dextran liberated by an erythrocyte or bacterial enzyme. This explanation seems unlikely for a variety of reasons, however. There was no other evidence of bacterial contamination present in the suspensions. There appears to be no suggestion in the literature that human erythrocytes are capable of hydrolyzing,  $\alpha$ -1,6 glycosidic linkages, although they do degrade glucose via anaerobic glycolysis (234). Dextranase (E. C. 3. 2. 1. 11) is reported to occur in humans only in the intestinal mucosa (235). Furthermore, apparently the largest  $\alpha$ -1,6 polyglucose capable of penetrating the red cell is isomaltose (236), so the enzyme would have to hydrolyze either the  $\alpha$ -1,6 linkage of the terminal glucopyranosyl- $\alpha$ -1,6- $H^3$ -sorbitol group, producing  $H^3$ -sorbitol, or the next linkage up the chain. Sorbitol, as opposed to glucose, apparently does not penetrate the membrane significantly (237), while glucopyranosyl- $\alpha$ -1,6-sorbitol has not been tested. Penetration of the membrane by a  $H^3$ -labelled molecule, then, seems unlikely to occur in this system.

- (ii) The erythrocytes used in the electrophoresis and  $H^3$ -dextran adsorption studies, while having been stored for roughly the same period of time (7 and 8 days respectively), were of different blood type, the former being A(+) and the latter

B(+). It is conceivable that the blood group antigens, being partially carbohydrate (238) could affect the adsorption of dextran. No experimental examination of this possibility was carried out, however.

- (iii) The dextran associated with the red cell could be adsorbed inside the membrane as well as on its surface, rendering a portion of it less susceptible to removal by washing, yet invisible to electrophoretic examination. Precedent for this idea is found in the studies on polylysine adsorption to human erythrocytes made by Nevo et al. (88). These authors made the suggestion that intramembrane polymer adsorption occurred, based on their findings that the equivalent of six monolayers of polylysine adsorbed per cell, and that the number of charge groups adsorbed was almost two orders of magnitude greater than was observed electrophoretically. At the very low concentrations of polybase used, however, ( $<40 \mu\text{g ml}^{-1}$ ) the electrokinetic changes, on which were based their uptake measurements, were completely reversed by saline washing. In a later paper, on the other hand, Katchalsky et al. (89) found that red cell agglutination caused by intercellular polybase bridging was not reversed by washing, in spite of the fact that the mobility of the aggregates returned to the control value. The observations suggest that

polymer molecules, which had to be present to cause the agglutination, were located either within the membrane, or only between the cells in such a way that they could not be detected electrophoretically. Intramembrane polymer adsorption, which is not easily reversed by washing, would therefore seem to be a possible explanation for the dextran washing results.

- (iv) Dextran may bind more strongly to regions of the membrane which bear no charge groups. The electrophoretic mobility would then be virtually unaffected by the presence of polymer in these neutral regions, unless the polymer were located within roughly 1 double layer thickness ( $\sim 8 \text{ \AA}$  in saline) of the charge groups. Since even assuming a uniform charge distribution the erythrocyte surface charges are an average of 28 to 36  $\text{\AA}$  apart (33), there would seem to be room for such electrokinetically invisible adsorption. Furthermore, there is some evidence that the (presumably charged) sites of polylysine adsorption to adjacent cells are rather localized spatially, since Katchalsky et al. observed with the electron microscope isolated "islands of adsorbed polybase" linking the surfaces of agglutinated cells. If adsorption in regions some distance from charged groups resisted desorption upon washing, the observed results would be obtained.

Some support for the idea that adsorption to neutral regions is stronger than to charged regions is found in the following. In a single experiment, the adsorption of  $H^3$ -dextran 77.6 was measured, using the methods in Chapter 4, to fresh red cells which had been treated with neuraminidase. Washed human erythrocytes were treated with neuraminidase (Behringwerke, from Vibrio cholerae) as described by Seaman and Uhlenbruck (174), washed twice in standard saline, then the adsorption of dextran 77.6 from a 2% solution measured using the ultracentrifugation-distox procedure. The adsorption to an untreated washed control suspension from the same fresh blood sample was measured using an identical dextran concentration. Adsorption to the control suspension differed from the regression line of Figure 4-2 by only 5%, while the neuraminidase-treated cells, in spite of incomplete reaction as judged by their mobility ( $-0.61 \mu s^{-1} v^{-1} cm$ ) adsorbed roughly 20% more dextran than the control. Hence, partial removal of sialic acid from the cells, and a 40% reduction in surface charge, caused significantly greater dextran adsorption to occur. The neutral regions created by neuraminidase treatment, then, probably bind dextran more strongly than do the charged sialic acid moieties, lending some credence to the above explanation.

## II. pH-Mobility Studies on Normal and Fixed Erythrocytes in Dextran

Figure 5-4 gives the variation of the viscosity-mobility product ( $\eta U$ ) with pH for normal and acetaldehyde-fixed human erythrocytes suspended in solutions of 4.39% dextran 77.6 at a constant ionic strength of  $0.145 \text{ gm-ions l}^{-1}$ . The curves have several noteworthy features.

- (i) Over the pH range for which the normal red cell in saline is electrokinetically stable, pH 4.5 to 9.0 (23), the three curves are all parallel and level. That is, there is no pH dependence of mobility between pH 4.5 and 9.0 for any of the systems. Hence, rigid control of pH is seen to be unnecessary for the examination of electrokinetic properties in these polymer solutions.
- (ii) The presence of adsorbed dextran has a strong stabilizing effect on normal red cells exposed to basic solutions. The range of electrokinetic stability, defined to be that range of conditions over which the mobility may be altered reversibly, is extended from pH 9.0 for red cells in saline, to pH 11.5 for red cells in dextran/saline. Stability in acid solutions, however, is not affected by dextran, since the decrease in mobility of normal cells in dextran at pH 4.1 could not be reversed by bringing the suspending medium pH back to

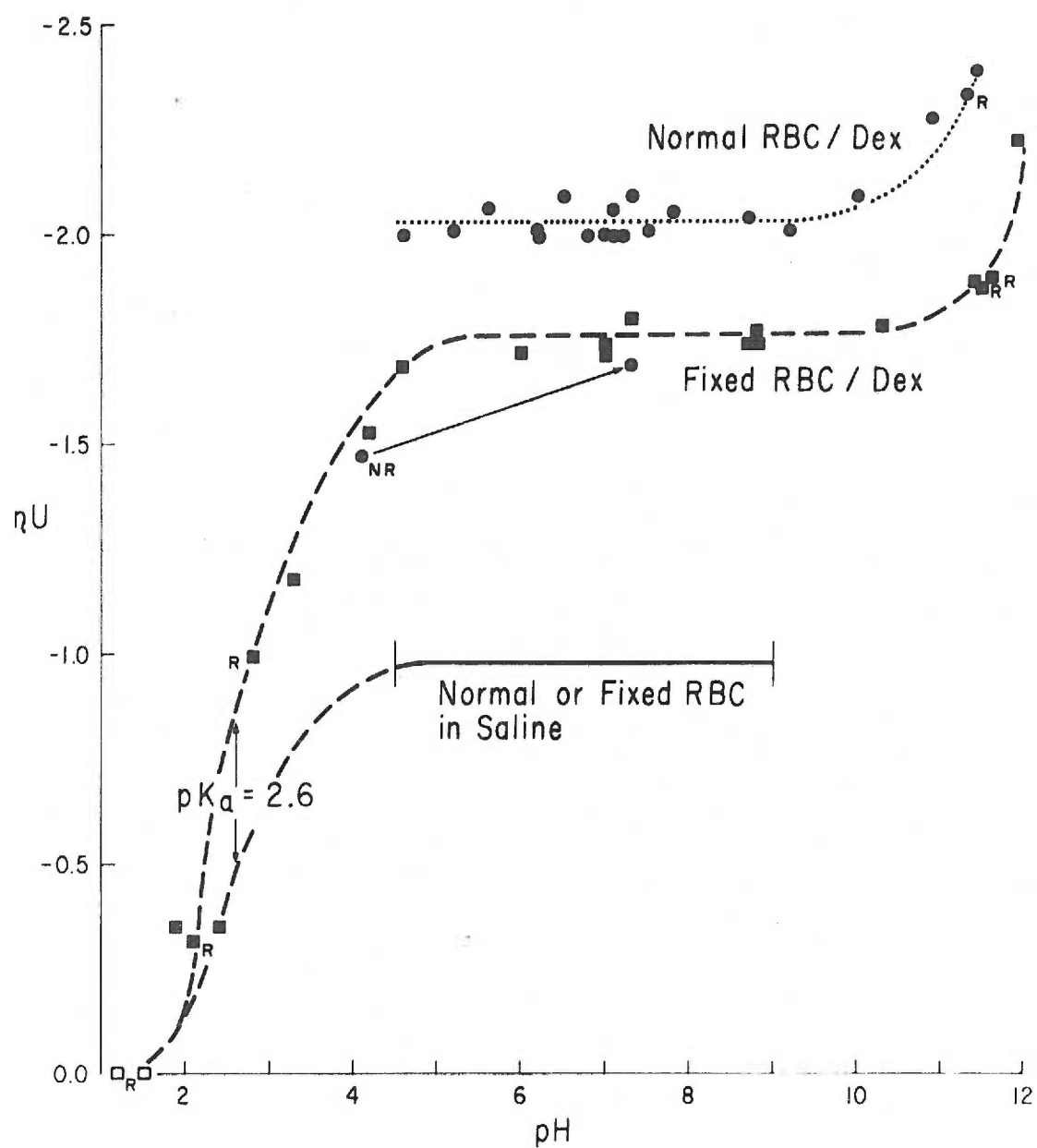


Figure 5-4. The pH dependence of the viscosity-mobility product for normal and acetaldehyde-fixed erythrocytes in 4.39% dextran 77.6 in saline. R => reversible; NR => not reversible

neutrality. It is not clear why the presence of dextran should stabilize the membrane in this way. The stabilization extends well beyond the region of metastability delineated by Heard and Seaman (23). One possible explanation of this effect is that dextran protects surface or membrane structures normally labile in the presence of significant concentrations of  $\text{OH}^-$  ions, or the absence of protons. A second possibility might be that the adsorbed dextran layer renders the membrane less permeable of  $\text{OH}^-$  ions, which normally penetrate freely. Apparently hemoglobin leakage and lysis, believed to be responsible for electrokinetic irreversibility (34), depend on the accumulation by the cell of  $\text{OH}^-$  ions at basic pH's, since lysis proceeds with the same time course after 5 min exposure to base whether or not the cells are washed or left in the high pH medium (239). Were the dextran layer to slow the entry of  $\text{OH}^-$  ions into the cell, it is possible that the internal  $\text{OH}^-$  concentration necessary for lysis might not be reached within the time needed to complete a mobility determination and return the pH to neutrality (less than 15 min).

- (iii) The zeta potential (proportional to  $\eta U$ ) of normal cells in dextran is 2.1 times that for normal cells in saline, while for acetaldehyde-fixed cells, the zeta potential in dextran/saline



is 1.8 times that in saline. That the relative zeta potential of normal cells is higher than that of fixed cells when they are suspended in identical neutral polymer solutions is an observation that has been found to hold for all polymer solutions tested. There seem to be at least two reasonable explanations for this. One possibility is that polymer adsorption is more extensive to normal cells than to fixed cells, and that the difference in  $Z$  is due to a more extended double layer caused by the adsorbed polymer surface phase associated with normal cells. No adsorption measurements on fixed cells were made to examine this suggestion. A second explanation for the difference could be that polymer adsorption to unfixed cells causes a rearrangement of surface groups to electrophoretically expose some additional negative charges at the shear plane. Strong arguments have been presented in Chapter 2 against the interpretation that all of the zeta potential increase seen in neutral polymer solutions is due to charge rearrangement at the cell surface. However, it is not inconceivable that some rearrangement could occur in normal cells that would not occur in the rigid fixed cells, causing the differences in  $Z$  observed. The results of Cook, Heard and Seaman (35) indicate that there are a sufficient number of sialic acid moieties in the cell membrane to

account for the zeta potential differences between fixed and normal erythrocytes.

(iv) The pH- $\eta$ U curves for both normal and fixed cells in dextran indicate the presence of a group at the shear plane with a  $pK_a > 11$ . Since there are no detectable basic groups present on the surface of normal or fixed cells suspended in saline (33), these groups are presumably associated with the adsorbed dextran layer. The mobility increase at high pH could not be due to exposure of primary amines from deeper in the membrane because reaction with acetaldehyde would block such groups. It seems reasonable to assume that the increase is associated with the deprotonation of glucose monomers of dextran, since the  $pK_a$  of glucose is 12.4 (240). Support for this suggestion is found in Sieh and Sterling's measurements of the mobility of glycogen in polyacrylamide gels (177). These authors observed a roughly 10 fold increase in glycogen mobility above pH 12 which they also assigned to the ionization of glucose hydroxyls.

(v) The pH- $\eta$ U curve for fixed cells in dextran in acid solutions indicates the presence of an ionizable group near the shear plane with a  $pK_a$  of 2.6, identical to that of the fixed cell in saline alone. The curves for fixed cells in the presence and absence of dextran are indistinguishable except for a

multiplying factor. They suggest strongly that the charge group responsible for the mobility of fixed cells in dextran/saline below pH 11 is identical to that which dominates the electrokinetic characteristics of fixed cells in the absence of dextran: sialic acid (35). There is absolutely no evidence from these curves for the presence of potential-determining ion adsorption to an adsorbed dextran layer. That the mobility was zero at both pH 1.2 and 1.5 argues strongly that ionogenic groups are responsible for the surface charge, not adsorbed anions or desorbed cations.

The results of these pH- $\eta$ U studies are in complete agreement with the predictions of the model developed in Chapter 2 for zeta potential increases in the presence of neutral polymers.

That model predicts that, providing the neutral polymer adsorption is unaffected by pH, the relative zeta potential of cells in polymer solutions should not be affected by the acidity of the medium, as observed.

### III. The Effect of Monovalent Anion and Cation Variation on the Zeta Potential of Erythrocytes in Dextran

The relative zeta potentials at neutral pH of fresh washed human erythrocytes suspended in 5% dextran 110 made 0.145 M with respect to NaF, NaCl, NaI or NaCNS are given in Table 5-3. It is seen that

there are no significant differences among the values of  $Z$  for the various monovalent anions used. These results agree with those of studies on normal erythrocytes in the absence of polymer, where no mobility dependence on monovalent anion type was found (23). They are taken to imply the absence of a significant degree of anion binding at the electrokinetic shear plane, since apparently all ion binding phenomena thus far observed show some sensitivity to monovalent ion type (178). They provide further evidence against the involvement of anion binding to an adsorbed polymer layer in the zeta potential increases seen in neutral polymer solutions.

In Table 5-4 are given the results of relative zeta potential measurements on acetaldehyde-fixed red cells in 5% dextran 77.6 solutions made 0.0145 M in NaCl, LiCl,  $(\text{CH}_3)_4\text{NCl}$  (TMACl) and  $(\text{C}_3\text{H}_7)_4\text{NBr}$  (TPABr), and  $5 \times 10^{-4}$  M in  $\text{NaHCO}_3$ . These studies were made at low ionic strength, where the mobility is more sensitive to ionic strength effects. The anion effects were sought at high ionic strength, since these conditions should maximize any anion binding present. The results of Table 5-4 are noteworthy in two respects. First, the control zeta potentials (proportional to  $\eta U$ ) of the fixed red cells at low ionic strength seem to depend to some extent on the monovalent cation counterion present. In fact, they are seen to increase in the same order as the radii estimated from conductivity data and molecular models of the hydrated cations present (241). Variations

Table 5-3. Relative zeta potential of normal human erythrocytes in 5% dextran 110 and various monovalent anions (ionic strength = 0.145 gm-ions  $l^{-1}$ , pH  $7.2 \pm 0.4$ ).

Salt	Relative Zeta Potential
NaCl	3.08
NaF	3.04
NaI	3.04
NaCNS	3.12

Table 5-4. Relative zeta potential of acetaldehyde-fixed human erythrocytes in 5% dextran 77.6 and various monovalent cations (ionic strength = 0.015 gm-ions  $l^{-1}$ , pH =  $8.0 \pm 0.4$ ).

Salt	Hydrated			Z
	Radius ( $\text{\AA}$ )	Control $\eta U$	5% Dex $\eta U$	
NaCl	3.3	-2.01	-3.32	1.65
LiCl	3.7	-2.12	-3.58	1.69
$(\text{CH}_3)_4\text{NCl}$	3.5	-2.05	-3.74	1.82
$(\text{C}_3\text{H}_7)_4\text{NBr}$	4.5	-2.24	-4.15	1.85

in the amount of water associated with the dry salt, and therefore in the ionic strength of the stock salt solutions, could conceivably have caused the observed differences. Some mobility dependence on the cation at low ionic strength is not unexpected, however, when the permeability of the membrane to counterions is considered. Within the context of Haydon's model (24), if smaller counterions have access to more space in the membrane than do larger ions, the greater exclusion of the larger counterions will result in a bigger  $\alpha$  factor (equation 1-32) for these ions. The cellular mobility might then be expected to be greater the greater the hydrated radius of the counterion, as observed.

The second noteworthy feature of the results in Table 5-4 is the dependence of the relative zeta potential of fixed cells in dextran on the cation present. Again, the largest cation,  $\text{TPA}^+$ , is associated with a greater  $Z$  than are the smaller alkali metal cations. The difference is statistically significant, the Student  $t$  value being 7.27 for  $d.f. = 7$ , implying  $p < 0.001$ . The difference between  $\text{TMA}^+$  and  $\text{Na}^+$  is only marginally significant due to the large standard deviation ( $\pm 7\%$ ) of the mobilities in  $\text{TMA}^+$ :  $t = 2.78$ ,  $d.f. = 8$ , implying  $0.05 < p < 0.01$ . This dependence of the relative zeta potential on counterion size is also expected in the context of the model developed in Chapter 2. Different counterions can be associated with different  $\beta$  factors, either through the ion-polymer interaction term  $\chi_{ip}$  of

equation (2-25) or through exclusion terms occurring in higher order expansions of equation (2-23). In the latter case, larger counterions exhibiting greater exclusion would correspond to higher  $\beta$ 's, which would in turn be seen experimentally as increased relative zeta potentials for the particle in the presence of the larger counterions. In these experiments the variation in  $Z$  with ion type cannot be explained by possible decreased ionic strengths in solutions of the more hygroscopic salts. Although the concentrated salt stock solutions could be at a lower ionic strength than the weight of salt used would indicate, there would be no difference in the ionic strengths of the dextran and control solutions, since these were both made up from equivalent dilutions of this same stock. The differences in control mobilities are consistent with expectation only if the ionic strengths of the stocks were lower the greater the hydrated radius of the cation, assuming the explanation based on ionic size is not to be accepted. However, as shall be demonstrated in the next section, if the ionic strength of the  $\text{TPA}^+$ /dextran solution were lower than that of the  $\text{Na}^+$ /dextran solution, the  $Z$  value for  $\text{TPA}^+$  should if anything be lower than the  $Z$  for  $\text{Na}^+$ , not significantly higher as observed. Hence, the relative zeta potential of fixed red cells in dextran is significantly greater when a large counterion,  $\text{TPA}^+$ , is present than when smaller cations such as  $\text{Na}^+$  and  $\text{Li}^+$  act as counterions to the negative surface charge.

The dependence of the relative zeta potential of cells in dextran on the type of cation and anion present in the medium is as might be expected from the polymer adsorption model. Since the cell surface is negatively charged, the dependence of  $Z$  on the species of ions present in the cellular suspending media should be limited to cations, the dominant species in the double layer, as is observed experimentally. Qualitatively, then, the expectations of the polymer adsorption model appear to be fulfilled by these anion/cation dependency experiments.

#### IV. The Dependence of the Relative Zeta Potential on Ionic Strength

The relative zeta potential of fresh, washed human erythrocytes suspended in 2.5% w/v and 7.5% w/v dextran 77.6 as a function of ionic strength is given in Figure 5-5. Similar data for acetaldehyde-fixed cells in 2.5% dextran 77.6, with and without sorbitol present, is given in the same figure. The points represent experimental data, while the solid lines are plots of equation 2-39 using the values of  $\beta$  and  $d$  indicated to the right of the curves. Similar data and curves for acetaldehyde-fixed cells in various dextran fractions and PEG 6 are given in Figures 5-6, 5-7, 5-8 and 5-9. The upper solid curve in Figure 5-8 is a plot of equation (2-66) for the parameter values indicated, while the dotted curve is a comparative plot of equation



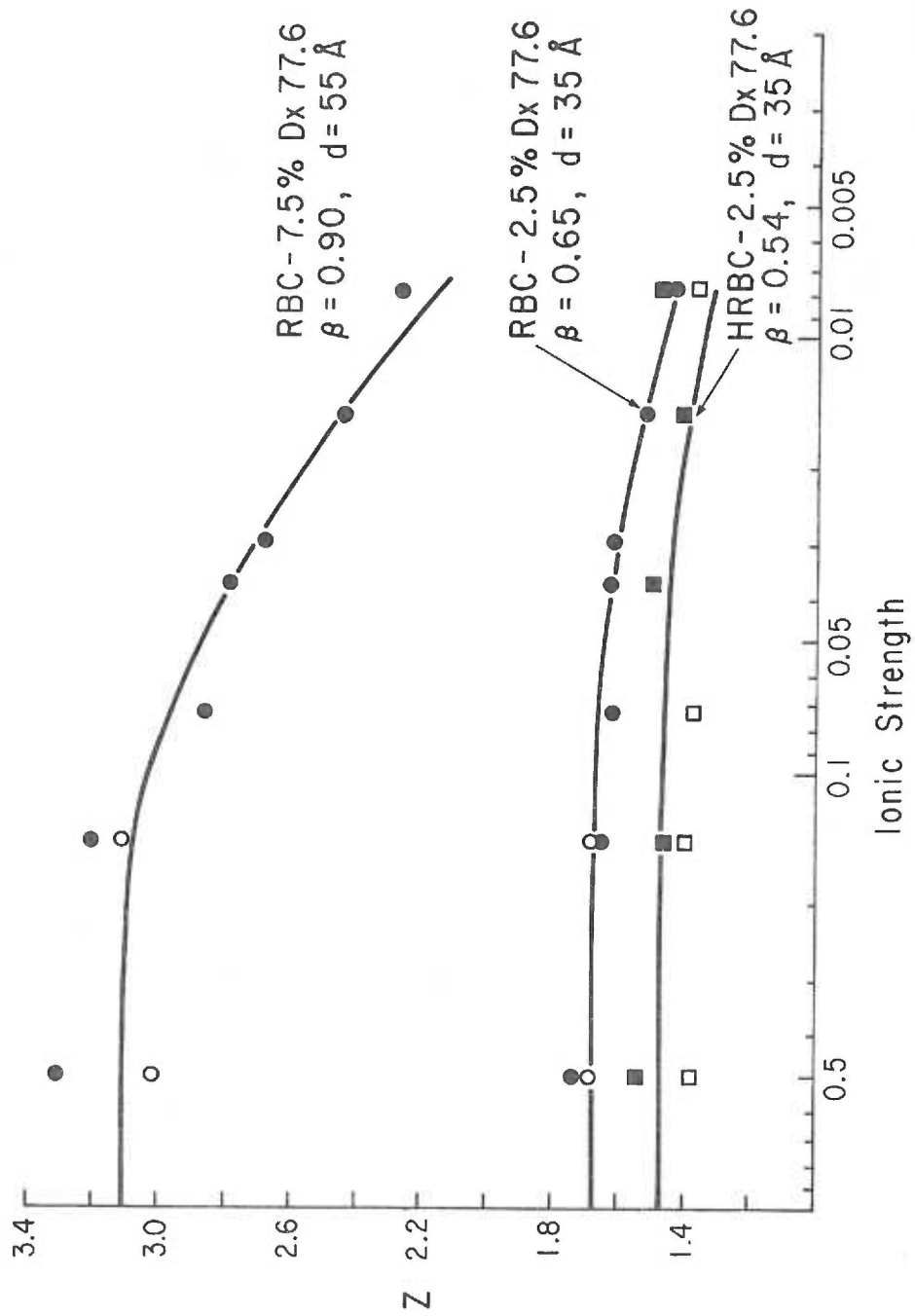


Figure 5-5. Relative zeta potential vs. ionic strength for normal (RBC) and acetaldehyde-fixed (HRBC) erythrocytes in 2.5% and 7.5% dextran 77.6.

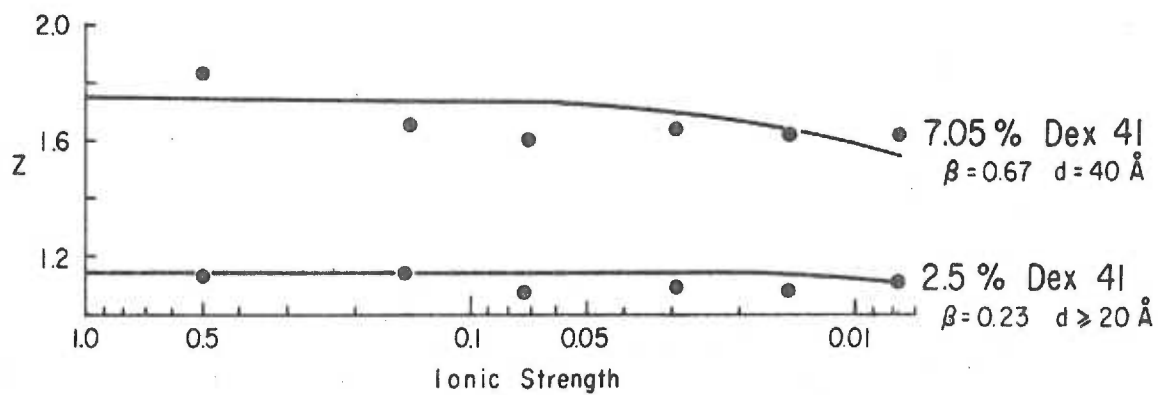


Figure 5-6. Relative zeta potential vs. ionic strength for acetaldehyde-fixed erythrocytes in 2.5% and 7.05% dextran 41.

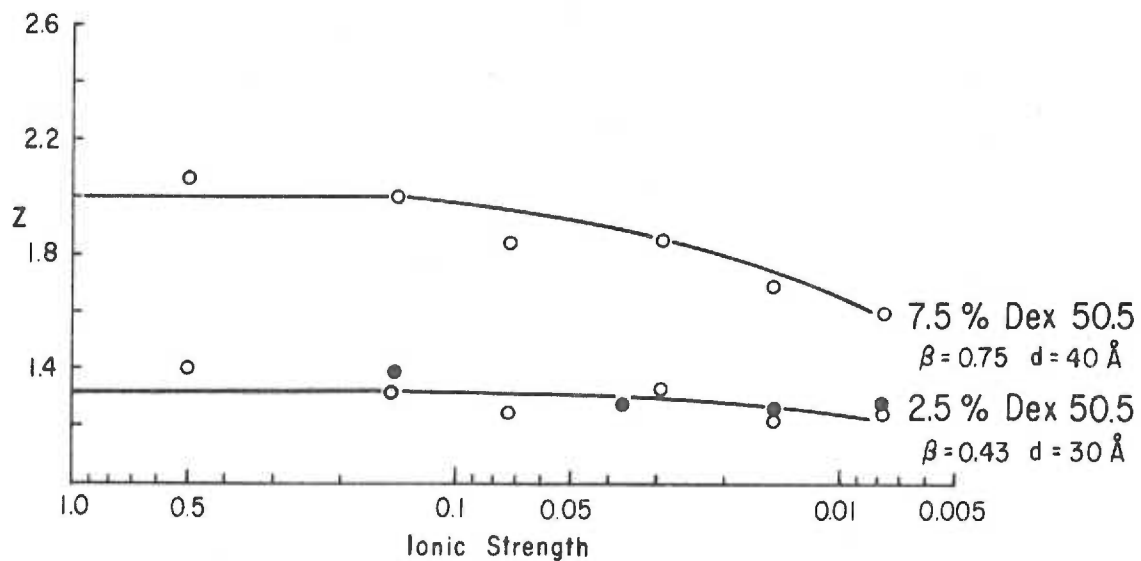


Figure 5-7. Relative zeta potential vs. ionic strength for acetaldehyde-fixed erythrocytes in 2.5% and 7.5% dextran 50.5.

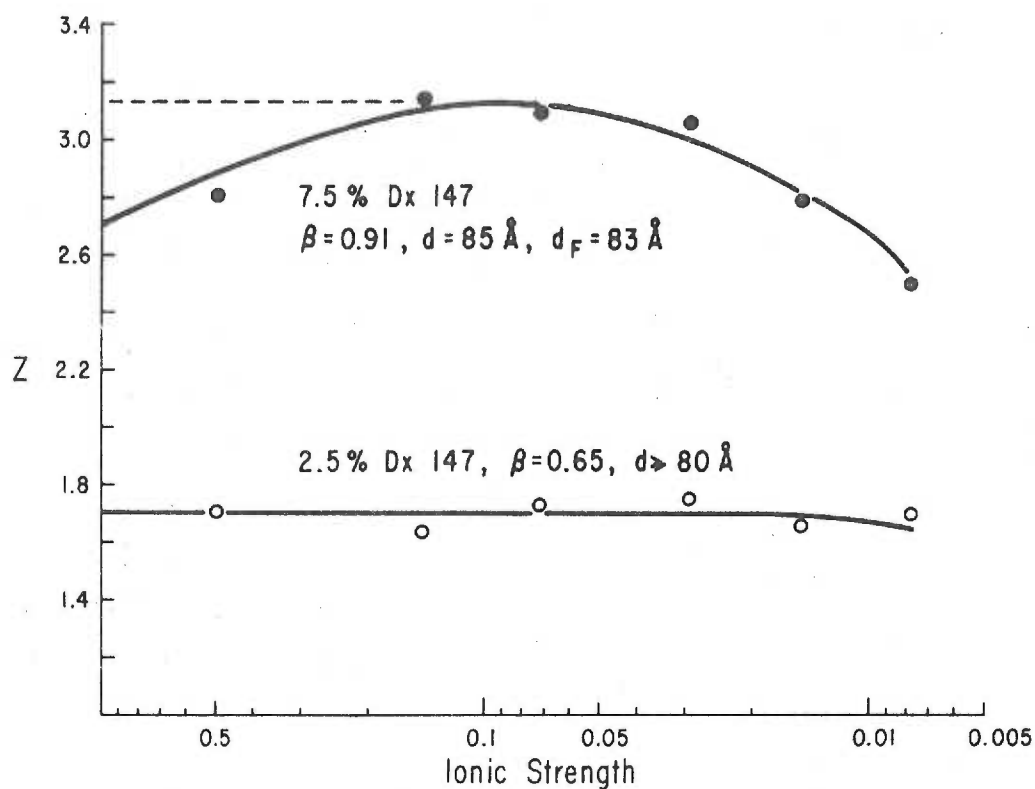


Figure 5-8. Relative zeta potential vs. ionic strength for acetaldehyde-fixed erythrocytes in 2.5% and 7.5% dextran 147.

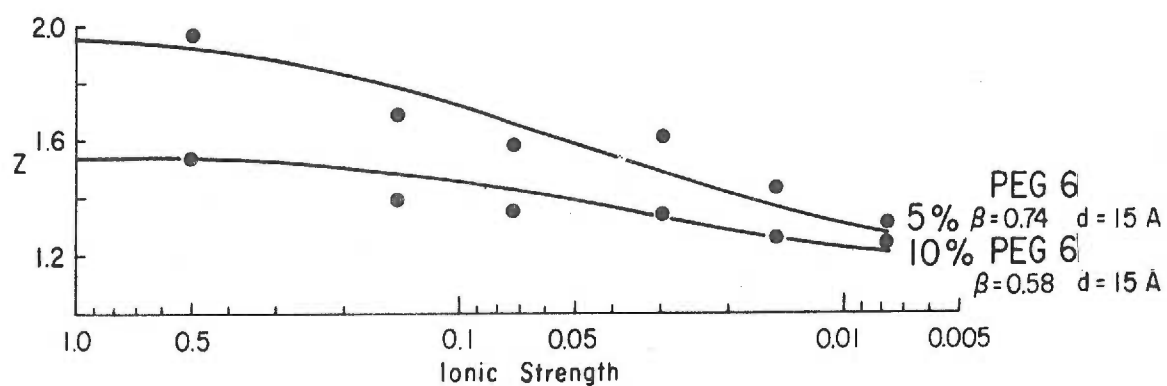


Figure 5-9. Relative zeta potential vs. ionic strength for acetaldehyde-fixed erythrocytes in 5% and 10% polyethylene glycol.

2-39 using the same parameters. The parameters quoted for each curve represent the values which produced the best fit to the experimental data, as judged by eye. It is seen that the equations based on the polymer adsorption model, with appropriate choice of parameters, fit the data quite nicely.

The uncertainties in the data points in these figures are quite high for the highest ionic strength points measured (0.5 M NaCl). The necessity of using low voltages to measure these points, plus the high viscosities of some of the polymer solutions resulted in very low velocities, with a large scatter in timings. Hence, the uncertainties in  $Z$  (equal to the sum of the standard deviations of the control and polymer mobility determinations) at 0.5 M NaCl were as high as  $\pm 25\%$  for the high polymer concentrations and high molecular weight. The 0.5 M points for the lower polymer concentrations were generally good to  $\pm 15\%$ , the improvement being due to the lower viscosity of the solutions. At salt concentrations  $c = 0.145$  M, high voltages were used in the mobility measurements, with a consequent increase in accuracy. For  $c = 0.145$  M, the uncertainty in the high polymer concentration points was less than 10%, and was less than 8% for the low polymer concentrations. At lower ionic strengths, the uncertainties in all points were less than 7%.

It is conceivable, considering the errors discussed above, that the decrease in  $Z$  at  $c = 0.5$  M for 7.5% dextran 147 relative to

the 0.145 M point (Figure 5-8) is due only to statistical variation in the data. The difference was consistently found in a series of separate measurements, however. Testing the data, the difference was found to be statistically significant ( $t = 4.39$ , d.f. = 78, implying  $p < 0.001$ ). Hence, the decrease was considered to be a true property of the system. It was interpreted as evidence for the presence of a partially free-draining layer of adsorbed polymer, justifying the use of equation (2-66) to fit the data. Some support for this interpretation is seen in the dextran 147 curve in Figure 5-3. The relative zeta potential of PSL, measured in the same series of experiments and from the same stock suspension as the other curves in the figure, was less than one at a salt concentration of 0.145 M. One interpretation of this observation is that the high molecular weight dextran adsorbs more strongly to the PSL than the lower molecular weight fractions, and the resulting adsorbed layer is effectively less free draining. Hence, at the relatively high ionic strength of saline, the relative zeta potential is less than one, as predicted by equation (2-63) or (2-66). No measurements of  $Z$  as a function of salt concentration were made to further examine this possibility, however.

Interpreting Figure 5-1 and the  $Z(c)$  data in terms of equations (2-39) and (2-66) provides values for the depth and polymer adsorption factor of the adsorbed layer in each of the systems studied. These parameters show some regularity in their dependence on the

concentration and molecular weight of the polymer fractions used. They are summarized in Table 5-5 along with the values of  $V_R/V_0$  for each suspension, calculated from equation (2-83). Figure 5-10 gives the dependence of  $\beta$ , the polymer adsorption factor, on polymer concentration for the dextran fractions used. The values of  $\beta$  plotted were calculated from the data of Figure 5-1 using the expression  $\beta = 1 - Z^{-2}$ , derived from the high ionic strength approximation of equation (2-39). It is seen that  $\beta$ , which should be proportional to the difference between the densities of segments in the adsorbed layer and bulk phase, increases rapidly with increasing dextran concentration below about 3% w/v, then levels off to a limiting value at high concentration which is a function of the molecular weight of the fraction. The plateau is more pronounced for the higher molecular weight fractions. The dependence of  $\beta$  on the number-average molecular weight of the dextran fractions is given in Figure 5-11. A strong dependence of  $\beta$  on molecular weight is seen at low molecular weights which is rapidly attenuated at high molecular weights, regardless of the polymer concentration. In fact,  $\beta$  is virtually independent of molecular weight at the extreme end of the high concentration curve. The behavior of  $\beta$  with respect to its independence from molecular weight and concentration dependence at large values of these parameters is qualitatively similar to polymer adsorption in general.

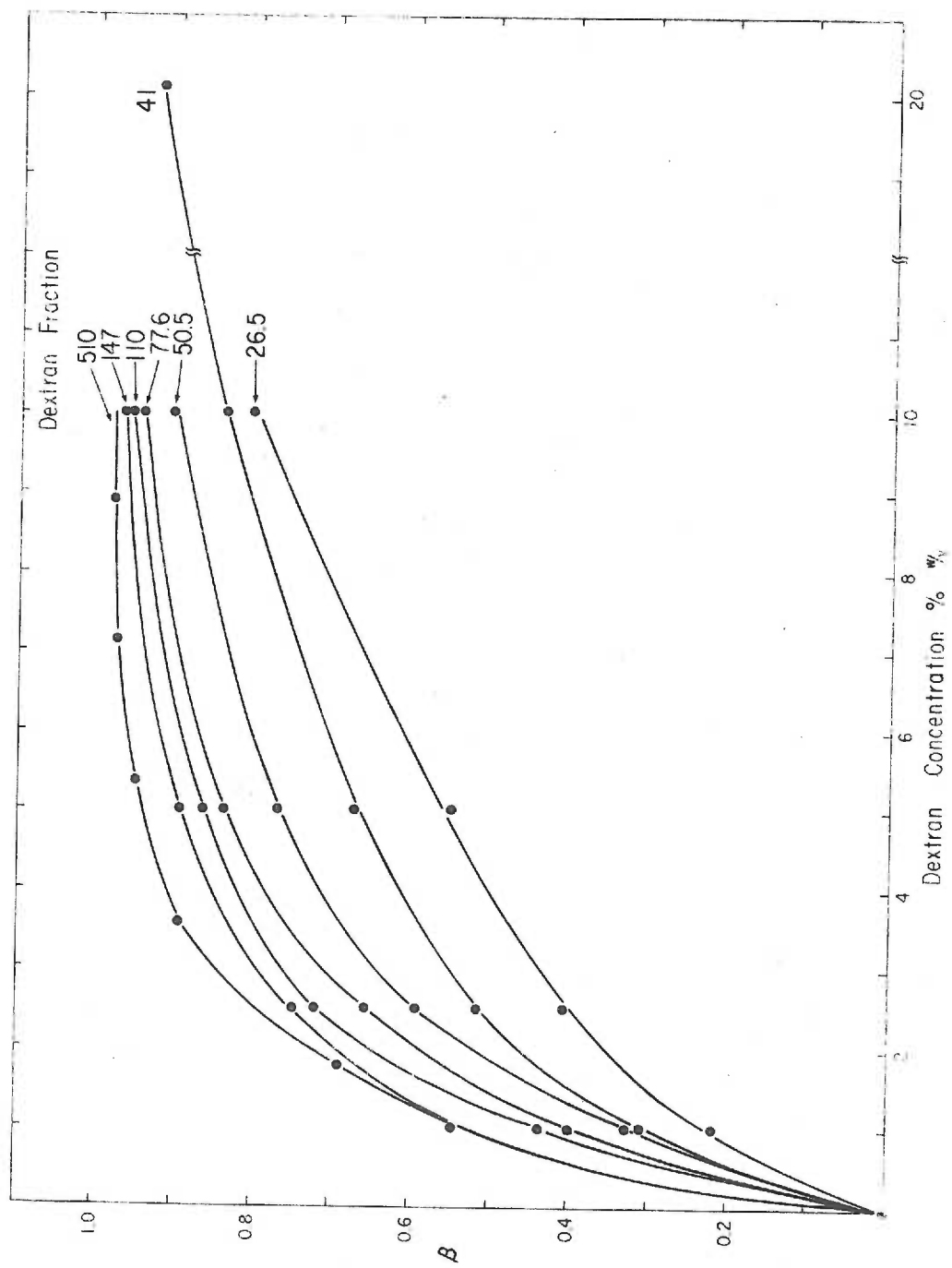


Figure 5-10. Polymer adsorption factor  $\beta$  vs. dextran concentration for normal erythrocytes in dextran/saline.

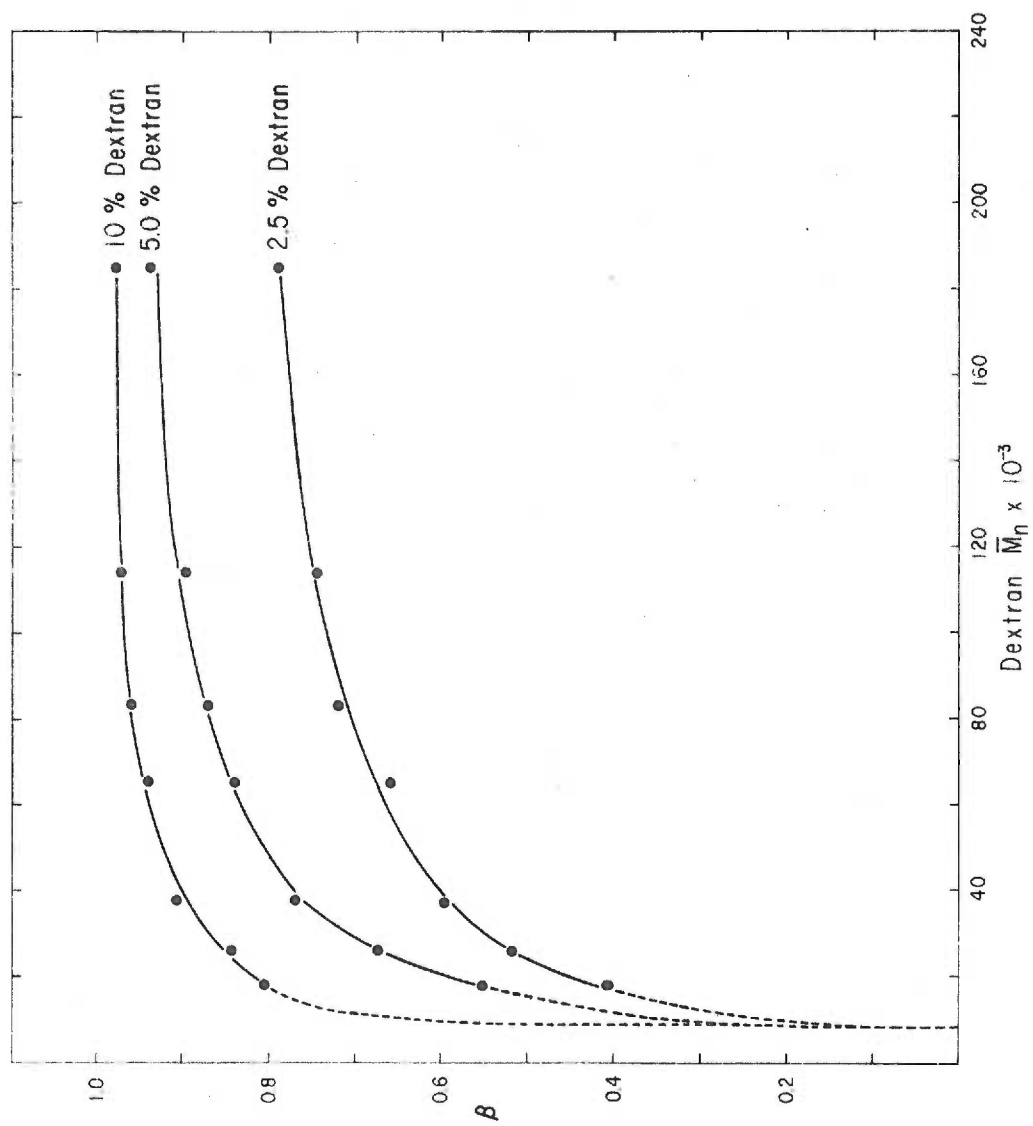


Figure 5-11. Polymer adsorption factor  $\beta$  vs. dextran molecular weight for normal erythrocytes in dextran/saline.



Table 5-5. Summary of model parameters of best fit to  $Z(c)$  data (acetaldehyde-fixed cells unless noted).

Polymer	Conc. % w/v		$\beta$	$d(\text{\AA})$	$V_R/V_o$
Dextran 41	2.5%		0.23	20 → 70	4.5 (avg)
	7.05%		0.67	45	195
Dextran 50.5	2.5%		0.43	30	8.2
	7.5%		0.75	40	267
Dextran 77.6 $\bar{M}_n = 50,800$	2.5%	Fixed RBC:	0.54	35	23.8
	2.5%	Normal RBC:	0.65	35	56.7
	7.5%	Normal RBC:	0.90	55	$1.2 \times 10^5$
Dextran 147	2.5%		0.65	90	$1.56 \times 10^4$
	7.5%		0.91	85	$1.13 \times 10^7$
				$d_F = 83$	
PEG 6	5.0%		0.58	15	5.7
	10.0%		0.74	15	12.2

The total depth of the adsorbed layer,  $d$ , as estimated from the decrease in  $Z$  at low ionic strengths also varies with molecular weight in a regular way. The dependence of  $d$  on concentration is more difficult to assess, however, because at low polymer concentration the absolute value of the decrease of  $Z$  at low  $c$  is quite small. The range of values of  $d$  for which equation (2-39) fits the data is consequently large, so the uncertainty in this parameter, and therefore in the concentration dependence of  $d$ , is quite large. Some of this uncertainty would have been removed if mobility measurements could have been made at lower ionic strengths. For such measurements, the electrophoresis apparatus should be equipped with

platinum or palladium electrodes, to avoid contamination of the sample with ions leaking from the electrode chambers. No such suitable apparatus was available for these studies. The uncertainty in  $\bar{d}$  at the higher concentrations is  $\pm 10 \text{ \AA}$ , as estimated by the fit to the data of curves computed for  $(\bar{d} \pm 10) \text{ \AA}$ . It would appear from the data in Table 5-5, however, that there was little concentration dependence of the absorbed layer thickness in the systems studied.

The adsorbed layer thickness has been shown in a variety of systems to depend linearly on the square root of the polymer molecular weight (39). This type of dependence has also been predicted by at least two of the theoretical treatments of polymer adsorption (56, 242). A plot of the electrokinetically determined  $\bar{d}$  vs  $\bar{M}_n^{1/2}$  for 7.5% dextran data is given in Figure 5-12. The data for dextran 77.6 and normal cells was included with the fixed cell data, since the value for  $\bar{d}$  at 2.5% dextran 77.6 was identical for the fixed and normal erythrocytes. It is seen that the fit to a straight line is satisfactory, the regression coefficient being 0.97 over the range of molecular weight studied. The use of equations (2-39) and (2-66) to analyze the data, then, seems to produce reasonable values for the thickness of the absorbed layer.

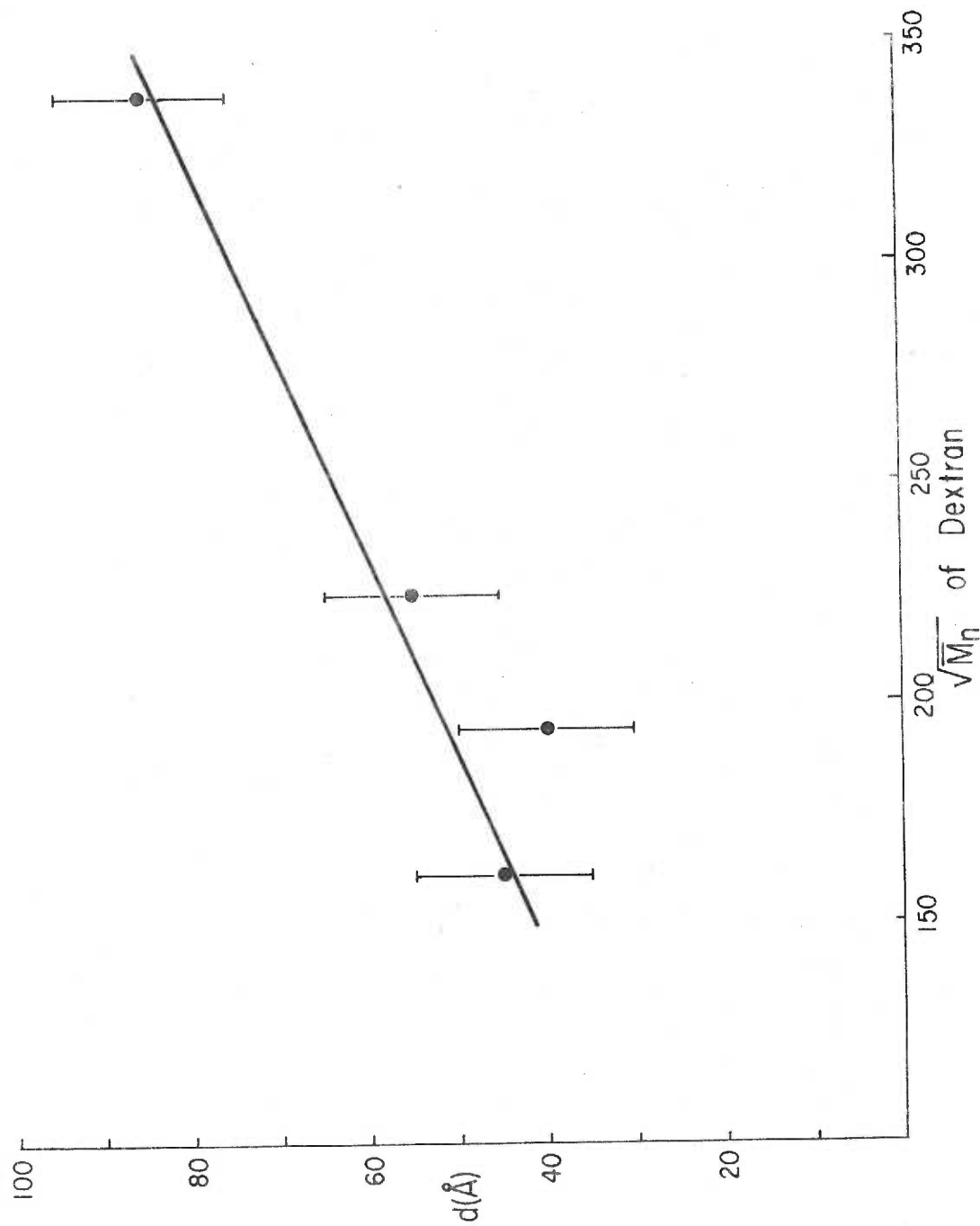


Figure 5-12. Adsorbed layer thickness  $d$  vs. square root of dextran molecular weight for acetaldehyde-fixed cells in dextran.

## V. The Effect of Zeta Potential on the State of Aggregation of Normal Human Erythrocytes in Dextran Suspensions

In the suspensions of normal washed erythrocytes in dextran-saline studied, if the number average molecular weight of the dextran was over roughly 30,000 it was found that the presence of the polymer above a certain (low) concentration but below a particular, well-defined high concentration, caused the cells to aggregate. The polymer concentrations which defined the region of aggregation, and the degree of microscopic aggregation within each region, were found to be a function of the molecular weight of the dextran fraction used. The zeta potential of the red cells in these solutions was also a function of concentration and molecular weight of the polymer fraction used as shown in Figure 5-1. Hence, the concentration of dextran at which disaggregation occurred for a given molecular weight corresponded to a critical zeta potential for each system. Above this critical cellular zeta potential, the cells would not aggregate, and the suspensions were observed under the light microscope to be monodisperse. Below this critical zeta potential, as long as there was a sufficient concentration of cells present, the cells were found to be aggregated. The aggregation was more severe, the higher the molecular weight of the dextran. In dextran 110, for instance, the aggregation was extremely heavy between 1% and 6% dextran. There were no single cells seen after 10 minutes exposure to the polymer. The cell

aggregates were very large, bulky, roughly symmetrical globs in which individual cells were frequently seen to be grossly distorted by packing. The forces responsible for the severe (++++) aggregation were clearly stronger than those responsible for maintaining the biconcave shape of the cell, since disturbances in the solution caused by pressing the cover slip were frequently seen to partially separate aggregates at the expense of extensive elongation and distortion of cells in the region of the separation. At lower molecular weights, however, the aggregates were more regular, linear, and rouleaux-like, and the individual cells were seen to be less distorted by the forces causing aggregation. Individual aggregates could often be dispersed by shear in the suspensions.

The concentration ranges over which 30% v/v cell suspensions were aggregated for various dextran fractions are given in Figure 5-13, along with the state of aggregation of the cells and their relative zeta potential. The region which is cross-hatched is that in which aggregation of some degree could be established by microscopic observation. It is seen that for the two lowest molecular weight dextran fractions examined, no aggregation was found at any concentration. The same data is plotted in Figure 5-14 with the relative cellular zeta potential as the abscissa, emphasizing the critical zeta potential variation with molecular weight.

It seems clear from work on a variety of particle-polymer

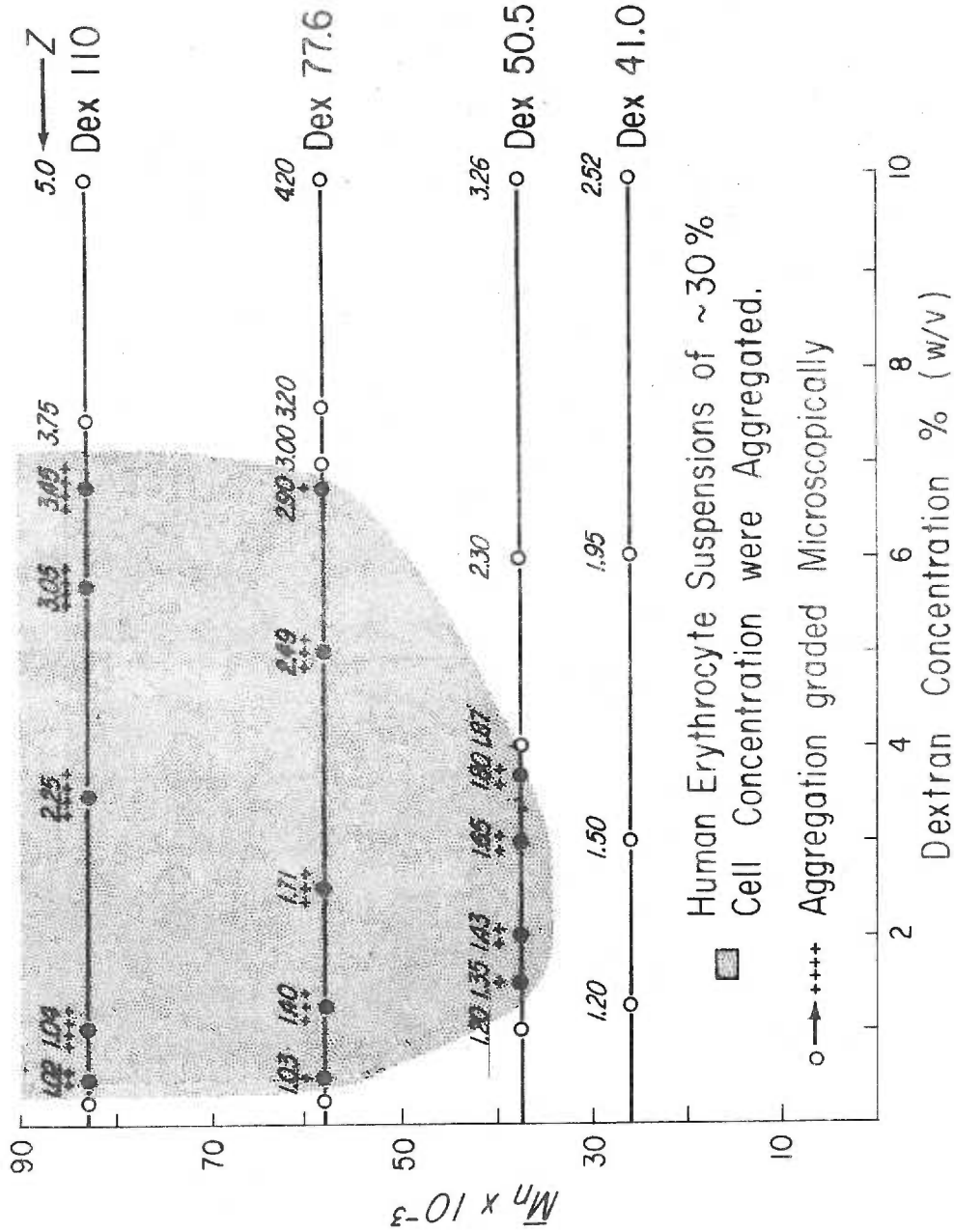


Figure 5-13. Degree of aggregation of normal erythrocytes induced by dextran fractions as a function of dextran concentration.

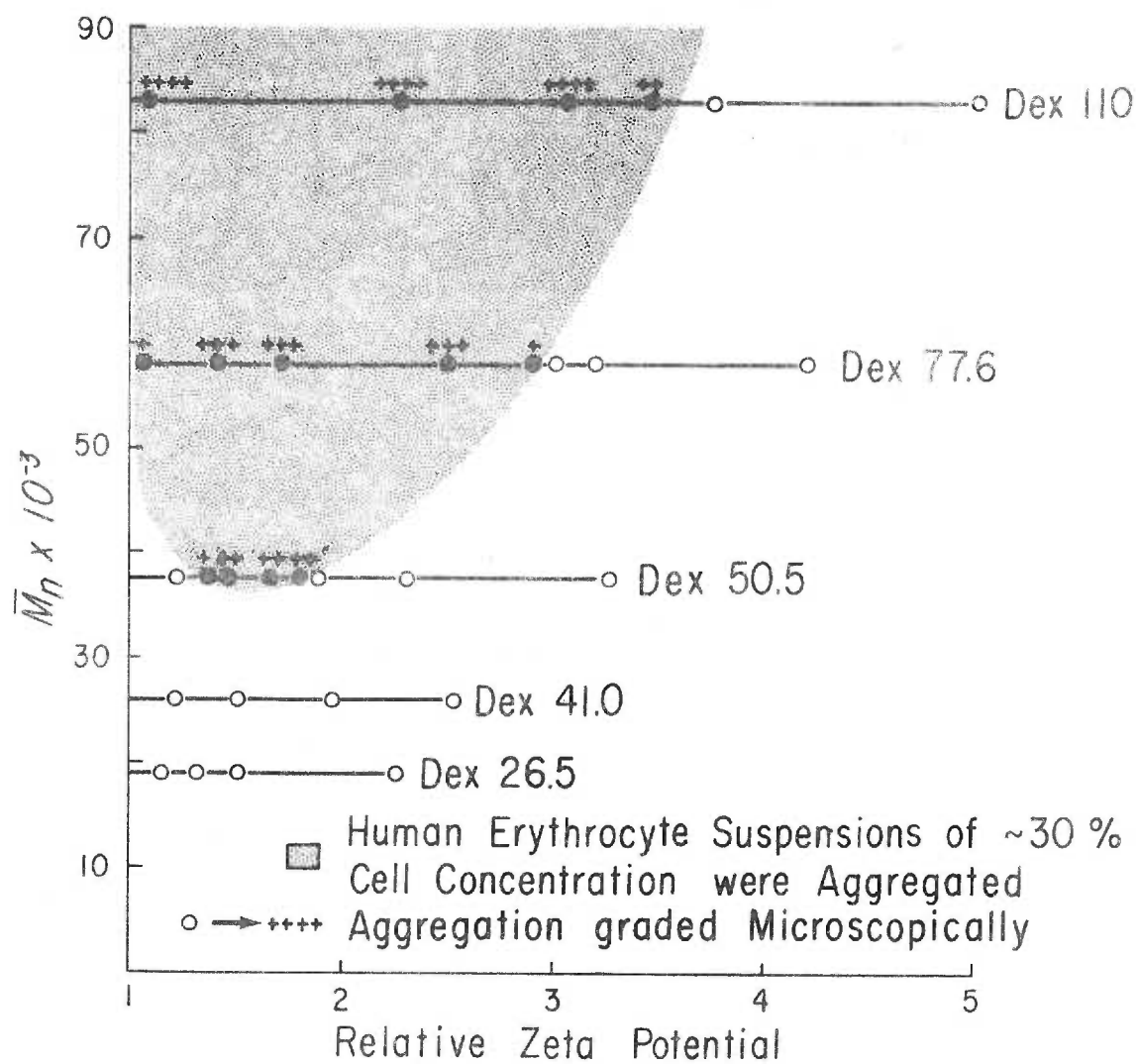


Figure 5-14. Degree of aggregation of normal erythrocytes induced by dextran fractions as a function of cellular zeta potential.

systems that the aggregation frequently observed in such systems, which is not present in the absence of polymer, is due to simultaneous adsorption of the same polymer molecules to two adjacent particles (Chapter 1). The multiple links thus formed between the particles tend to bind them together. Any attempts to disaggregate such systems must be carried out in the face of this strong tendency towards flocculation induced by the polymer molecules. In the red cell-dextran systems, the adsorption of dextran and the attendant aggregation (above dextran 41) is also accompanied by an increase in zeta potential. It was shown in Chapter 2 that the polymer adsorption model for these increased zeta potentials predicts very large increases in the forces of repulsion acting between cells in these circumstances. Regardless of the model for the increased zeta potential, however, the repulsive potential energy will be increased by at least a factor of  $Z^2$ , as may be seen from equation 1-31. It seems reasonable, then, to assume that the disaggregation observed at high dextran concentrations is due to the increased electrostatic repulsions between the cells caused by the elevated zeta potentials. That the disaggregation is not a direct result of some form of steric stabilization resulting from the close apposition of polymers adsorbed to separate cells (82) is indicated by the results of the following preliminary experiment (243). The electrokinetic surfaces of glutaraldehyde-fixed cells were chemically modified by  $\text{SOCl}_2$ -MeOH treatment and their



electrophoretic characteristics measured in saline and in saline made 10% w/v in dextran 110. The relative zeta potential of the cells under these conditions was much less than one, indicating the presence of a tightly bound layer of dextran. Microscopic observation showed the cells to be monodisperse in saline, but heavily aggregated in 10% dextran 110. Hence, in the presence of tightly bound layers of neutral polymer which would be expected to maximize any steric stabilization, but in the absence of electrostatic stabilization, the cells were totally aggregated. Steric stabilization, then, would not seem to be of major importance in these systems.

The critical zeta potential necessary to disaggregate the cells is an increasing function of molecular weight, implying that larger repulsive energies are required to disperse systems flocculated by higher molecular weight polymers. This dependence accords well with measures of the degree of aggregation which show that the higher molecular weight dextrans increase the degree of aggregation, estimated subjectively from the size and shape of the aggregates and the amount of distortion seen in the individual cells they contain. Apparently the repulsive potential present in the dextran 26.5 and 41 suspensions is sufficiently large to keep the cells far enough apart to prevent individual molecules from linking cells. The low molecular weights of these two fractions would both limit the separations over which they could link cells, and limit the number of binding sites per

molecule with which the dextran interacts with the cell surfaces.

Either or both of these effects apparently reduces the potential energy responsible for flocculating the cells below the level of the repulsive potential energy at all concentrations of dextran 26.5 and 41.

If more were known about the molecular mechanism of this polymer-mediated flocculation process, it might be possible to estimate the magnitude of the force responsible for linking the cells together. Without an indication of the distances over which such links can be established, the relationship between these distances and polymer molecular weight, and the number of binding sites per molecule necessary to establish such a link, it is not possible at present to estimate these forces. Progress in the theory of these two particle adsorption processes is now being made, however (244).

Some support for the concept of electrostatic repulsions causing the disaggregation in these systems is found in a recent report by Chien and co-workers (245). These workers found that the intercellular separation distances of cells flocculated by dextran increased as the molecular weight of the dextran was increased, in spite of increasing degrees of aggregation as estimated by the aggregate sizes. These observations are consistent with the above discussion, since higher molecular weights produce higher zeta potentials at equal polymer concentrations. Hence, intercellular repulsions at a given cell separation will be larger when higher molecular weight dextrans are

present, causing the cell separation to increase as observed. Increasing the dextran concentration can be expected to increase cell separation also, until the concentration reaches the level corresponding to the critical zeta potential for that molecular weight. At this point the cell separation should just exceed the maximum length of the polymeric links which are still strong enough to hold the cells together. It is to be expected that this distance will more nearly equal the end-to-end chain length of the molecule, the stronger the binding energy between the monomeric segments and the particle surface. Hence, the separations observed by Katchalsky et al. (89) for polylysine-linked cells were only slightly less than the extended lengths of the polylysine fractions used. It is to be expected, however, that much smaller separations relative to chain length would be found for the dextrans, since the binding energies are evidently so much lower.

The observation that red cells are aggregated in dextran 77.6 up to a concentration of about 6.8% w/v of the polymer, but are disaggregated above this concentration suggests an explanation for the abrupt change in slope in the  $H^3$ -dextran adsorption curve (Figure 4-2). The adsorption data at high concentrations is replotted on a linear scale in Figure 5-15. It is seen that the change in slope occurs very close to the concentration at which disaggregation is first seen. The increase in adsorption rate above 7% dextran can be explained if it is assumed that disaggregation frees some binding sites on each cell

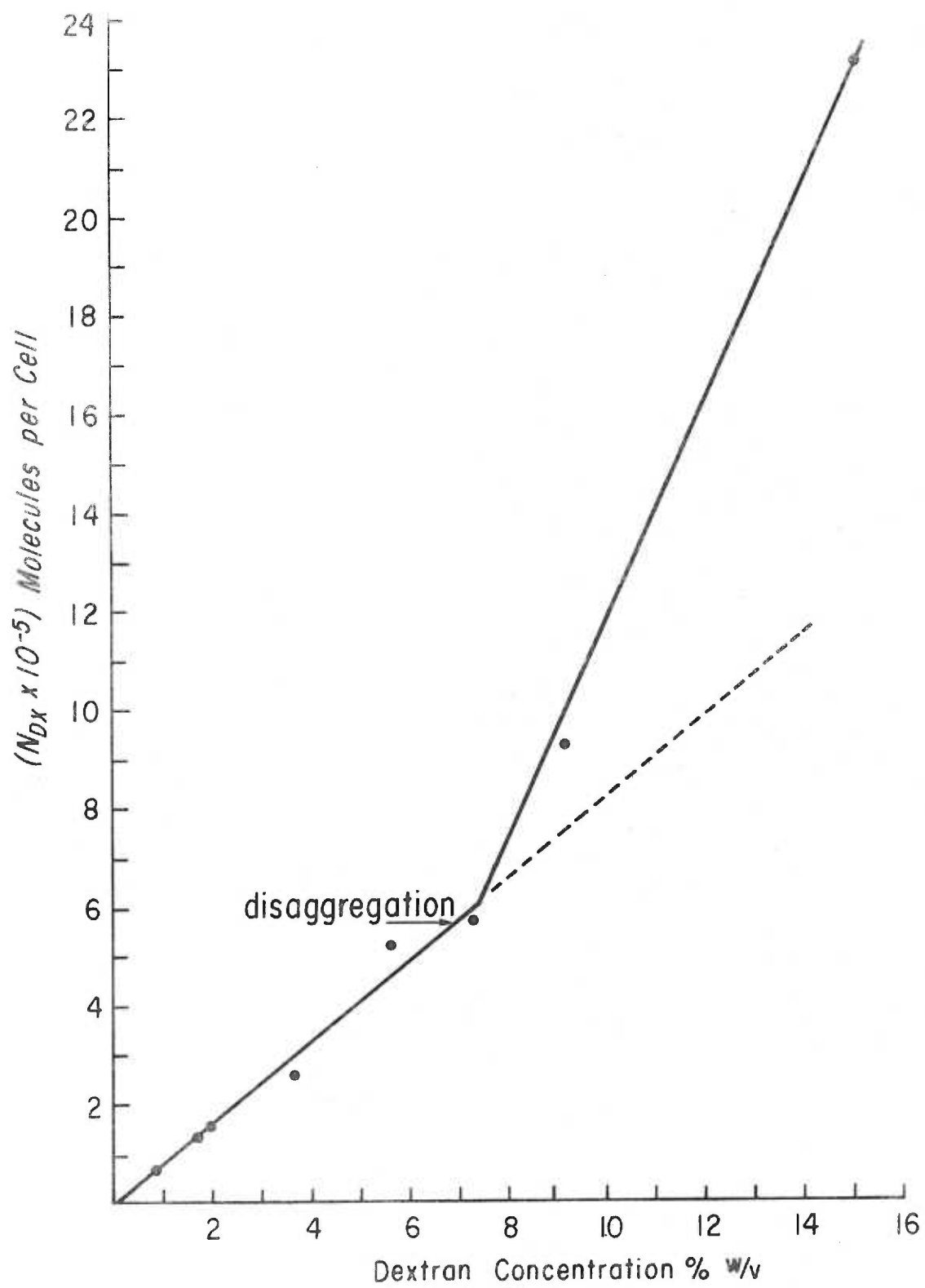


Figure 5-15. The dextran 77.6-erythrocyte adsorption isotherm on a linear coordinate system.

which were previously occupied by molecules adsorbed to two cells at once. Occupation of these free sites by polymer molecules from solution increases the total number of molecules bound per cell, causing the increase seen in Figure 5-15. Were adsorption uniform between all cells and the dextran fraction completely monodisperse, a precipitous jump in adsorption would occur upon disaggregation. The level of adsorption immediately after aggregate dispersal would be just twice that before dispersal, and the adsorption would then proceed at twice the previous rate (assuming no other change occurs in the adsorption process). That the increase at 7% is not steeper can be attributed to the non-uniformity of the adsorption process and the materials used. It is to be expected that, had adsorption been measured at higher dextran concentrations, the isotherm would have decreased in slope again and eventually continued with twice the initial slope. The concentrations necessary to extend the measurements to this range were prohibitively high however. The fact that the change in slope occurs at very nearly the dextran concentration corresponding to the critical zeta potential for disaggregation infers that the adsorption isotherm measurement is essentially correct, as discussed in Chapter 4.

It is of interest that the increased adsorption upon disaggregation was seen in spite of the very high packing forces operative in packing the cell pellets before assaying them for  $H^3$ -dextran. If the

correct interpretation of these results is that the cells remained separated in the face of the ultracentrifugal compression forces, the repulsive energies required would be enormous, many orders of magnitude larger than those predicted by equation 2-76. On the other hand the packing of the cells, the possible replacement of interstitial fluid by organic phase, the kinetics of dextran desorption or re-adsorption, and the effect of the organic phase on the adsorption itself are all factors which complicate interpretation of the results. Estimating repulsion energies from these packing experiments would therefore appear to be unwise.

If in fact the change in slope of the adsorption isotherm is due to disaggregation, and not to some intrinsic property of the adsorption process, it would appear that the number of molecules adsorbed to a single, isolated cell should be larger than is implied by the isotherm. Under the conditions of the adsorption measurements, the cells were aggregated at dextran 77.6 concentrations below 6.8%. Hence, the bulk of the isotherm refers to the number of molecules adsorbed per two cells, not one. Assuming that the sites freed upon disaggregation can all bind one molecule, the number of molecules bound per isolated cell would be  $2N_{Dx}$ . The factor multiplying  $N_{Dx}$  will be smaller if the freed sites bind fewer molecules than were released. That the value of  $N_{Dx}$  at 15% dextran is nearly twice the value expected from extrapolating the low concentration data suggests that this

factor may be not much less than two, however.

### VI. A Comparison Between the Adsorption and Electrokinetic Measurements

A test of the model developed in Chapter 2 is provided by a comparison between the number of molecules adsorbed per unit area determined by  $H^3$ -dextran uptake and the electrokinetic measurements. Using the notation defined in Chapter 2, the number of molecules adsorbed per unit area of cell  $N_a$ , will be given by:

$$N_a = \frac{\Phi_p d}{V_p} \quad (5-4)$$

where  $V_p$  is the molecular volume of one polymer molecule. Substituting (5-4) into the definition of  $\beta$  (2-25) and rearranging gives:

$$F(\chi) = \frac{\beta d}{N_a V_p - \Phi_{po} d} \quad (5-5)$$

Since all the parameters on the RHS have been determined experimentally, a comparison between the electrokinetic and  $H^3$ -dextran adsorption measurements is provided by calculating the value of  $F(\chi)$  as a function of  $\Phi_{po}$ , the bulk polymer concentration. If the resulting value for  $F(\chi)$  is constant, as equation (2-25) predicts, some support for the proposed model may be inferred.

The values of  $\beta$  and  $d$  for 2.5% and 7.5% dextran 77.6 with normal cells are taken from Table 5-5. Since for the very low cell concentrations used in electrophoresis ( $\sim 0.05\%$  v/v) the cells were monodisperse, to compare the electrokinetic estimates of adsorption with the  $H^3$ -dextran measurements the adsorption values found by the latter method will be doubled, as discussed above. The number of molecules adsorbed per unit area of cell will then be:

$$N_a = \frac{2N_{Dx}}{A_{RBC}} \quad (5-6)$$

where  $N_{Dx}$  is the number of molecules adsorbed per cell as measured in Chapter 4, and  $A_{RBC} = 163 \mu^2$  is the area of a human red cell. Taking  $V_p = 6.75 \times 10^{-20} \text{ cm}^3$ , estimated from the molecular weight and specific volume of the  $H^3$ -dextran, and  $\Phi_{po} = 0.611 \text{ cm}^3 \text{ gm}^{-1} \times [\text{Dex}] \text{ gm cm}^{-3}$ , where the first term is the specific volume of dextran and  $[\text{Dex}]$  is the bulk phase concentration, the values calculated for  $F(\chi)$  at 2.5% and 7.5% dextran are:

$$2.5\%: F(\chi) = 20.2$$

$$7.5\%: F(\chi) = 19.6$$

The close agreement is probably fortuitous, since there is considerable uncertainty in some of the terms of equation (5-5). The constancy of  $F(\chi)$ , however, lends some further support to the form



of the treatment applied in Chapter 2.

The feature of the above calculation which does not support equation (2-25), however, is the magnitude of  $F(\chi)$ . According to its definition  $F(\chi)$  should be of the order of one. That it is an order of magnitude greater than this figure may be attributed to a variety of causes, the most compelling being the original assumption that Flory-Huggins theory can be applied directly to an adsorbed surface phase. Accepting this assumption, however, there are several other sources of uncertainty which could lead to an overestimate of  $F(\chi)$ . The value for  $d$  is probably not grossly wrong, since its estimate is subject to fewer errors than is  $\beta$ , as mentioned earlier. Also,  $N_{Dx}$  in (5-6) is probably a reasonably good number, as discussed in Chapter 4. It is possible that  $N_a$  could be somewhat underestimated if adsorption to the cell were non-uniform in the region of the discrete charge groups. In order to decrease  $F(\chi)$ , adsorption would have to be concentrated in the region of the sialic acid moieties, effectively reducing the value of  $A_{RBC}$  in (5-6). The fact that neuraminidase treatment apparently causes an increase in  $H^3$ -dextran adsorption, however, argues against this suggestion, although even stronger adsorption to groups exposed by neuraminidase cannot be entirely ruled out.

It seems most likely that the chief source of uncertainty in (5-5) lies in the assumption that the only mechanism operative in

producing relative zeta potentials greater than one is that on which the model is based. For normal cells, charge rearrangement due to adsorbed polymer could produce an increase in  $Z$  by up to a factor of about 2. Furthermore, if there is counterion penetration behind the apparent charge plane, as the low ionic strength electrokinetic studies on cells would imply (171), and if adsorbed polymer can occupy regions behind the charge plane as well, then the activity of counterions in this region will be affected by the polymer according to equation (2-20). This effect could produce an additive contribution to  $Z$  of up to one additional unit. However, neither of these mechanisms can provide general explanations for the increased  $Z$  for PSL or quartz, nor for the very high values of  $Z$  found for normal cells at high concentrations of high molecular weight polymers.

An additional source of overestimation of  $\beta$  could be found in ionic self-exclusion effects (203). These effects could be of considerable importance in the region near the charge plane under conditions of high  $Z$ , since the apparent counterion concentration adjacent to the surface is proportional to  $\exp\left[\frac{e\zeta_o Z}{kT}\right]$ . The first order treatment of ionic self-exclusion results in a modified Boltzmann equation identical in form to equation (2-24) (246). Hence, any effects of counterion self-exclusion would be included in the experimentally determined values of  $\beta$ , resulting in an overestimate of  $F(\chi)$ .

The remaining assumptions inherent in the development of

equation (5-5) would all tend to produce a larger value for  $F(\chi)$  than estimated above. Thus, the linearization of equation (2-23), the assumption that the adsorbed layer has an effective viscosity equal to the bulk solution, and the presumed lack of dependence of dielectric constant and viscosity on the electric field in the double layer all are factors which might tend to increase  $F(\chi)$ . However, there would seem to be no obvious way to circumvent these difficulties at the present time.

#### VII. Drainage Properties of Adsorbed Neutral Polymers

A feature of the polymer adsorption model which warrants discussion is the necessity for flow to occur within the region of the adsorbed layer if an elevated zeta potential is to be observed. This is of particular interest, considering that the usual ways of measuring the thickness of an adsorbed layer assume the exclusion or at least retardation of flow in the adsorbed layer. The methods typically measure apparent increases in size of suspended particles, or decreases in effective diameter of capillary pores, as observed by changes in flow properties of the appropriate suspension or fluid. An increase in the relative viscosity of a particle/polymer suspension, for instance, is interpreted in terms of the increased volume fraction occupied by particles to which polymer has adsorbed. Such increased volumes demand that flow be either excluded completely from the

layer, or that the viscosity in the layer be sufficiently high, relative to the surrounding solution, to cause a measurable increment in energy dissipation. In the polymer adsorption model, on the other hand, if flow were completely excluded from the adsorbed layer, only values of  $Z$  less than one would be observed. If flow were retarded in the adsorbed layer, but not excluded, values of  $Z > 1$  would be measured but underestimated. It has had to be assumed in the interpretation of the electrokinetic data that the viscosity in the layer is equal to that in free solution, as discussed in Chapter 2. This assumption may not be too severe, however, since the differences in viscosity between the adsorbed layer and polymer solution may not be a large fraction of the latter, considering its elevated values. Also,  $\beta$  is less sensitive to changes in  $Z$  for high values of the relative zeta potential, so its estimate may not be greatly affected.

One explanation of this apparent paradox could involve the shear rates at which the two types of measurement are made. In order to accurately measure the changes in relative viscosity related to particle volume increases, high rates of shear are generally employed ( $10^2$ - $10^3$   $\text{sec}^{-1}$ ). Conversely, the maximum shear rate at the surface of a cell moving at electrophoretic velocities ( $\sim 4 \mu \text{sec}^{-1}$ ) is only about  $1 \text{sec}^{-1}$ . [ $\gamma_{\text{max}} = 3v/2r$  where  $\gamma_{\text{max}}$  = maximum surface shear rate at particle velocity  $v$ , radius  $r$  (247)]. Hence, if the

hydrodynamic thickness as measured by the suspension viscosity is shear dependent, the electrokinetic and viscometric results may not be at variance. That this may not be an unreasonable explanation is suggested by some results in the literature. Based on measurements of the hydrodynamically-effective thicknesses of a series of strongly adsorbed polymers, Eirich (39) has stated that the adsorbed layer thickness appears to increase more rapidly with concentration than does the amount of polymer adsorbed. These thickness estimates, made at high shear rates, are therefore apparently sensitive to less than saturated coatings. On the other hand, using the sedimentation rate in an ultracentrifuge as a basis for measuring the hydrodynamic radius, Ottewill and Walker (79) have given adsorption and layer thickness data for an aqueous system in which roughly 30% of neutral polymer adsorption is complete before any effective particle volume change is evident. Under the conditions of their layer thickness measurement, however, the particle velocities would have been of the same order of magnitude as electrophoretic velocities,  $3-4 \mu \text{ sec}^{-1}$ , and the maximum surface shear rate less than  $100 \text{ sec}^{-1}$ . They obtained thicknesses of  $50 \text{ \AA}$  for adsorption to latices  $500 \text{ \AA}$  in diameter, of the same order of magnitude as those found in the dextran/erythrocyte system. The configuration of the adsorbate was probably different in the former experiments, however. In this system, then, (n-dodecyl hexaoxyethylene monoether on polystyrene

lattices) it appears that the adsorbed layer was free draining at significant surface coverages.

Other work from Ottewill's group also may be interpreted as indicating that adsorbed layers, if not too dense, can be free draining at electrophoretic velocities. Mathai and Ottewill (78) have reported that the adsorption of alkyl polyoxyethylene glycol polymers to silver iodide particles proceeds to approximately 40% of maximum before large shifts in the location of the shear plane are observed. The shift in location of the shear plane was seen as a sudden decrease in particle mobility at an adsorbate concentration where sudden adsorption increases were observed. That no increased zeta potential was observed in these systems could have been due to the low molecular weights of the molecules used (<650). The interpretation of the above results in terms of free draining of the adsorbed layers is in contrast with the authors' interpretation that the adsorbed molecules lay flat at the surface up to a critical concentration. No thickness estimates were made on this system, which could distinguish between these possibilities.

Considering the above results, then, it may not seem too unreasonable to expect diffuse adsorbed layers to exhibit some degree of free draining behavior at low shear rates. In fact, considering the analysis of the ion exclusion model, it would appear that some free draining must occur under these conditions, since polymers are known

to adsorb at interfaces in systems where increased zeta potentials are measured. That the adsorbed layers in the systems used in the present work were in fact diffuse may be seen by comparing the amount of polymer adsorbed with the thickness estimates of the adsorbed layer. The amount of  $H^3$ -dextran adsorbed at 2.5% w/v dextran 77.6 corresponds to about 0.5 monolayers of polymer (assuming an area per glucose molecule, estimated from molecular models, of  $46 \text{ \AA}^2$ ), while the depth of the layer is equal to about 7 monolayers.

Although the quantitative interpretation of some of the derived parameters may be questioned (for instance the high  $\beta$  values and the impossibly low value of  $d_F$  in Figure 5-8) this analysis strongly suggests that some free draining occurs in adsorbed polymer layers, in apparent contrast to the situation in free solution (248).

### Summary

The variation of the relative zeta potential of a variety of cell and particle systems suspended in neutral polymers is given as a function of the concentration and molecular weight of several polymeric species. All neutral polymers tested produced an increase in the zeta potential of human erythrocytes. The effect of pH, ionic strength and monovalent ion type of the relative zeta potential of erythrocytes suspended in dextran is examined and the results found to be consistent with the model developed in Chapter 2. The variation

with polymer concentration and molecular weight of the experimentally determined parameters defined by the adsorption model is found to be in good agreement with the properties of polymer adsorption in general. The aggregation/disaggregation behavior of erythrocytes in dextran is interpreted in terms of a balance between the tendencies for polymers to adsorb to adjacent cell surfaces, causing their aggregation, and the elevated electrostatic repulsions resulting from such adsorption tending to cause their disaggregation. Critical zeta potentials for red cell disaggregation are defined for the dextrans studied. The increased adsorption of dextran 77.6 above ~7% concentration is interpreted in terms of the disaggregation which occurs at this concentration. The results of the  $H^3$ -dextran uptake and electrokinetic experiments are compared, and the concentration dependence of  $\beta$ , the polymer adsorption factor, found to be correctly predicted by the theory of Chapter 2. The failure of the treatment to predict correctly the values of all the parameters introduced is discussed in terms of the assumptions made in the model's development. Finally, the drainage properties of neutral adsorbed polymer layers are considered. In the light of the theoretical and experimental results obtained in the present work, it is concluded that such layers are at least partially free draining at the shear rates operative in electrophoretic measurements.



## CHAPTER 6

RHEOLOGICAL STUDIES ON SUSPENSIONS OF HUMAN  
ERYTHROCYTES IN DEXTRAN-SALINE SOLUTIONS

As was discussed in Chapter 1, when normal human erythrocytes are suspended in saline solutions containing high concentrations of low molecular weight dextran, the relative viscosities of these suspensions, measured at low rates of shear ( $\sim 1 \text{ sec}^{-1}$ ), are markedly lower than those of equivalent suspensions in pure saline. In this chapter, the viscosities of red cell suspensions in saline solutions of dextrans of various molecular weights and concentrations are given as a function of shear rate and hematocrit. The variations in relative viscosity as a function of hematocrit at low shear rates for different concentrations of dextran are correlated with the state of aggregation of the system, the zeta potential of the cells and the viscosity of the continuous phase. Similar correlations are made for higher rates of shear. The results are discussed in terms of the interactions among the elements of the systems studied.

Methods and Materials

The dextran fractions used were those described in Table 5-1. Blood was obtained and washed cells prepared as described in Chapter 5, except that all saline solutions used in the rheological studies

were composed of 0.137 M NaCl, 0.005 M NaHCO<sub>3</sub> and 0.001 M Na<sub>2</sub>EDTA (disodium salt of (ethylene-dinitrilo) tetraacetic acid). The EDTA was included to remove the possibility of abnormal membrane rigidity induced by intramembrane Ca<sup>++</sup> chelation (249, 250). The presence of EDTA had no effect on the electrokinetic properties of the cells. Dextran-saline solutions were made up and their viscosities measured with an Ostwald capillary viscometer as described in Chapter 5. The dextran/saline/EDTA solutions were neutral and essentially isotonic (152). Cell samples were prepared by suspending packed washed cells in saline/EDTA containing the appropriate amount and molecular weight of dextran, spinning the suspensions down, removing the supernatant, and resuspending the appropriate volume of packed cells in fresh dextran/saline/EDTA. Hematocrits were determined either by spinning samples in Wintrobe tubes for 45 min at 2000 xg, 25°C, or in micro-hematocrit capillaries for 10 min at ~15,000 xg, 25°C. All hematocrits were corrected for trapped fluid by multiplying the apparent hematocrits by 0.96 or 0.99, respectively (217).

Viscosity measurements of all cell suspensions and suspending media were made on a Model R17 Weissenberg Rheogoniometer (Sangamo Controls Ltd., Bognor Regis, England) (251) equipped with combined concentric cylinder-cone plate measuring elements (252). The cylinders were machined from plexiglass to allow visual

examination of the samples in situ. The base of the inner cylinder (bob) consisted of a slightly truncated  $1^\circ$  cone which was positioned with the gap setting mechanism so that the calculated location of the apex of the cone coincided with the flat base of the outer cylinder (cup). The bob was 8.84 cm in diameter and 4.41 cm high, while the inner diameter of the cup was 9.00 cm. The dimensions were such that the mean shear rate across the cylindrical gap was equal, for Newtonian fluids, to that in the cone-plate portion of the cup. The surfaces of all measuring elements were ground and polished. No guard ring was employed, but the air-sample interface was exposed to an atmosphere of saturated water vapor which originated from a reservoir of distilled water on top of the bob, enclosed by a cover plate, as described by King (253). Since the suspensions were essentially free of dissolved protein, there was little danger of artefacts being introduced by denatured surface films.

The temperature was maintained to  $25 \pm 2^\circ\text{C}$  by use of a constant temperature water jacket consisting of concentric plexiglass cylinders split in the middle and sealed on all edges. The two halves of the cylinder could be placed around the cup to enclose it in a constant temperature atmosphere. There was sufficient room above the bob to allow it to be partially raised and lowered without removing the water jacket. Water was circulated through the two halves of the jacket using a Haake Model F Constant Temperature Circulator. The

sample temperature was monitored to  $\pm 0.1^\circ\text{C}$  by two thermistors imbedded just below the surfaces of the cone and wall of the bob, and the signals detected with a Yellow Springs Instruments Model 46 Tele-thermometer.

In the Rheogoniometer, the outer cylinder is rotated at a series of constant speeds by a synchronous motor and logarithmic gear box. The gear box enables the rotation to be varied over a relative range of 1 to  $10^{-5.9}$  in steps of  $10^{-0.1}$ . Hence, the shear rate may be varied over six orders of magnitude. Since the mean shear rate in the coaxial cylinder and cone plate portions of the cup are nominally equal, the shear rate,  $\dot{\gamma}$  was simply calculated from (254):

$$\dot{\gamma} = \frac{360}{at} \quad (6-1)$$

where  $a$  = cone angle in degrees and  $t$  = period of revolution of cup in seconds.

When the cup is rotated, the torque transmitted through the sample deflects the bob. The bob deflection is counteracted by the torque of the torsion bar from which the bob and shaft are hung. The shaft is accurately centered on the axis by two air bearings. The arm of a variable inductance displacement transducer is locked to the top of the shaft and the tangential linear movement of the arm measured 5.0 cm for the torsion bar. A hydraulic damping paddle

immersed in a reservoir containing ~1 poise oil is locked to the transducer arm to reduce the effect of external vibrations. The torsion bar constant of the bar used throughout this work was 94.3 dyne-cm micron<sup>-1</sup>. The displacement of the linear transducer is proportional to the torque exerted by the torsion bar against the torque transmitted through the sample to the bob when the sample is sheared. The displacement could be read in microns from a Boulton Paul Aircraft Transducer Meter. The machine constant,  $k$ , was determined from the transducer displacements measured when a series of silicone oils (Brookfield Engineering Laboratories Inc., Stoughton, Mass.), sucrose, and salt solutions of known viscosity were run at a series of shear rates. The constant thus determined was  $k = 0.208 \text{ poise sec}^{-1} \text{ micron}^{-1}$ , and the viscosities at any  $\dot{\gamma}$  were therefore calculated from the expression:

$$\eta = \frac{k\Delta}{\dot{\gamma}} \quad (6-2)$$

where  $\Delta$  is the transducer displacement in microns and  $(k\Delta)$  is the shear stress in dyne cm<sup>-2</sup>.

The output of the transducer meter could either be monitored visually on the meter face, or fed through a low frequency filter and amplifying unit to a Type SE 2005 Ultraviolet Recorder (S. E. Laboratories Ltd., Feltham, England). Although the most sensitive range

on the meter was  $\pm 5 \mu$ , full scale (center zero), a 20x increase in sensitivity was available using the filter unit. Hence, the maximum sensitivity available was  $\pm 0.25 \mu$ , center zero, displayed on a 15 cm wide chart. The natural frequency of the torsion head assembly was 8.7 Hz, and that of the galvanometer unit in the uv recorder was 100 Hz. The time constant of the deflection measuring system was therefore determined by the low frequency filter unit, and was set to give an overall time constant of 2 sec for all measurements made using the recorder. In general, at all shear rates below about  $10 \text{ sec}^{-1}$ , the recording system was employed.

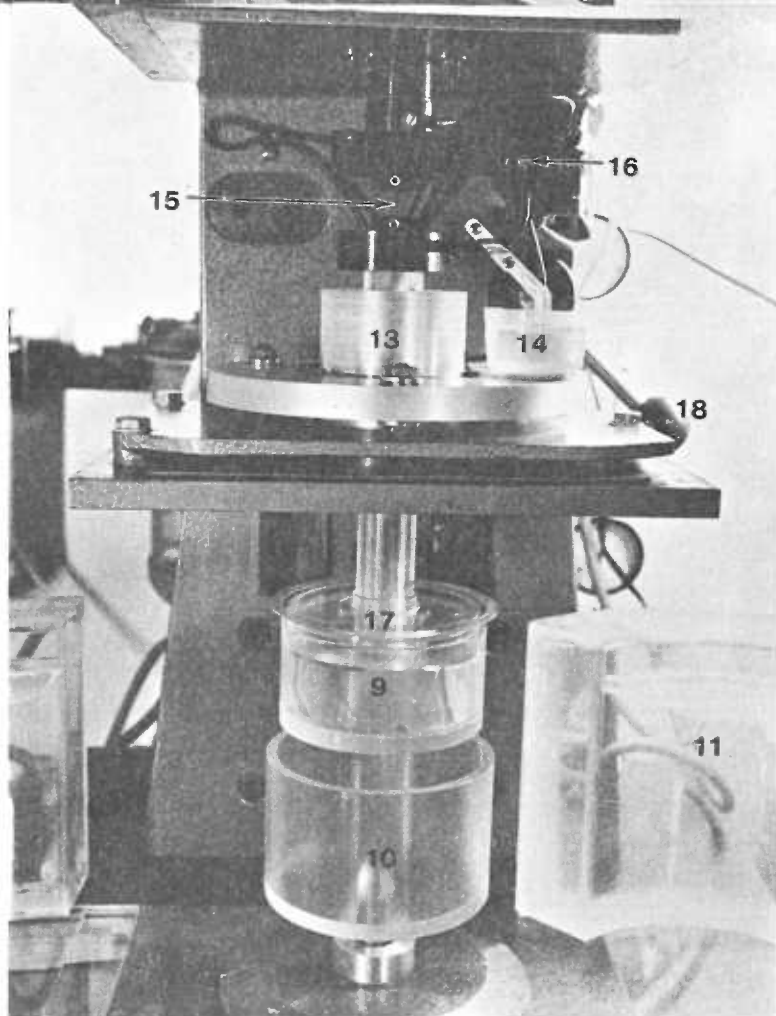
The Weissenberg Rheogoniometer used in the present work is illustrated in Figure 6-1.

The protocol followed in making a typical set of viscosity measurements as a function of shear rate was as follows. The machine constant was checked at the beginning of each day's runs; it was found to remain constant to within  $\pm 2\%$  from day to day. The gap between the truncated tip of the cone and the base of the cup was set at  $50 \mu$  with the gap setting device. A 15 ml sample was pipetted into the cup, and the bob lowered slowly into the sample using the hydraulic torsion head lifting system. Once the cone was immersed, the head was lowered rapidly to the stop, and the base and sides of the cup examined for bubbles. Bubbles were frequently found at the intersection of the sides and base of the cup, but could generally be removed

Figure 6-1. The Weissenberg Rheogoniometer.

- (1) motor
- (2) gear box
- (3) hydraulic head control
- (4) motor controls
- (5) low frequency filter unit
- (6) transducer meter
- (7) thermometer
- (8) recorder
- (9) bob
- (10) cup
- (11) thermostated water jacket
- (12) head
- (13) air bearing
- (14) hydraulic damper
- (15) torsion bar
- (16) linear transducer
- (17) water reservoir
- (18) head lock







by repeatedly raising and lowering the bob while shearing the sample at moderate shear rates. The detection of the bubbles through the clear cup and their removal was of critical importance, since the bubbles caused greatly elevated shear stress values at low shear rates. Once the bob was in place and bubbles removed, the water reservoir on top of the bob was filled, the lids placed on the cup to enclose the water vapor, and the clear water jacket placed around the cup. The sample was allowed to come to thermal equilibrium over a period of about 15 min while being sheared at  $\sim 40 \text{ sec}^{-1}$ . A slide of the cell suspension was made and examined microscopically for the degree of aggregation present 10 minutes after the cover slip had been placed on the sample drop.

For preparations in which aggregation was absent, the sample was mixed by raising and lowering the bob a few times, then torque measurements were made at a series of increasing shear rates. The torque values taken were the averages of the values obtained by shearing in both directions at each shear rate. The sample temperatures at the wall and bottom of the bob were recorded at each shear rate. The sample was re-mixed after every third shear rate increment. Once the series of shear rates had been covered, several low and medium shear rate measurements were repeated to make sure there was no time dependence in the determinations. The sample was then aspirated out of the cup, and a slide was made of the sheared

sample to check for any changes in the state of the suspension induced by the measuring procedure. The cup and bob were washed with saline and distilled water, dried in an air stream, and the next sample introduced.

For suspensions in which any degree of aggregation was present, a different protocol was used. Before every torque measurement, the sample was thoroughly mixed by rapidly raising and lowering the bob several times. Exactly 30 seconds after the bob was lowered to the stop for the final time, the electromagnetic clutch was engaged and the torque measured as a function of time on the recorder until a relatively steady value was reached. An interval of 30 sec between stirring and mixing allowed time to lock the torsion head in place and zero the recorder before shearing commenced. Allowing the time interval to vary produced results which were less reproducible than those obtained with the 30 sec interval, particularly for the heavily aggregated samples. Sample temperatures were again recorded at every shear rate, and the rest of the measuring procedure carried out as for non-aggregating suspensions.

The mean shear rate was calculated for any rotational speed from equation (6-1). This calculation applies strictly only for Newtonian fluids, or for non-Newtonian fluids in the cone-plate region where the shear rate is constant across the gap between the bob and base of the cup. In the gap between the concentric cylindrical walls

of the bob and cup, however, the shear rate varies. Hence, for non-Newtonian fluids, whose viscosity is a function of shear rate, the shear rate corresponding to the shear stress measured at the bob wall will depend on the properties of the fluid. For fluids which exhibit shear thinning, such as erythrocyte suspensions, the true shear rate at the bob wall will be higher than the apparent shear rate calculated from the geometry of the system and the angular velocity of the outer cylinder. For any fluid in which the shear rate is only a function of the shear stress, Krieger and Elrod (255) have derived an expression for the shear rate at the bob wall,  $\dot{\gamma}_b$ , as a function of the angular velocity of the cup,  $\Omega$ , and the shear stress measured at the bob,  $\tau_b$ :

$$\dot{\gamma}_b = \frac{\Omega}{\ln s} \left[ 1 + \ln s \frac{d \ln \Omega}{d \ln \tau_b} + \frac{(\ln s)^2}{3\Omega} \frac{d^2 \Omega}{d(\ln \tau_b)^2} + \dots \right] \quad (6-3)$$

where  $s$  is the ratio of the radius of the outer to the inner cylinder.

Cokelet (134) has applied this expression to viscometric data on whole blood and shown that, for his G. D. M. Couette viscometer, the shear rates calculated assuming a Newtonian liquid were significantly in error below about  $20 \text{ sec}^{-1}$ . However, the viscometer he used was equipped with cylinders whose radius ratio was  $s = 1.096$ . The cup and bob of the Rheogoniometer are more than three times as great in diameter and have a smaller gap width, giving a radius ratio of

$s = 1.018$ . Hence,  $\ln s$  is five times smaller on the Rheogoniometer and the correction terms in equation (6-3) are therefore much smaller. That the error in the apparent value of  $\dot{\gamma}$  is much less significant for the apparatus used here than for the G. D. M. viscometer may be seen by applying (6-3) to Cokelet's data for whole blood, ( $H = 47.4$ ,  $T = 24.8^\circ\text{C}$ ) but using the geometric factor of the Rheogoniometer. Using his tabulated data for the derivatives at apparent shear rates of  $0.124 \text{ sec}^{-1}$  and  $0.491 \text{ sec}^{-1}$ , the true shear rates in the Rheogoniometer would have been  $0.130 \text{ sec}^{-1}$  and  $0.501 \text{ sec}^{-1}$  respectively, representing errors of 5% and 2% over the apparent values compared to 29% and 16% errors calculated for the G. D. M. data.

The error for the present apparatus becomes even less significant when the contribution of the cone-plate portion of the bob is considered. The cone-plate contributes about 25% of the total torque measured by the displacement transducer. This 25% is subject to none of the uncertainties regarding shear rate that apply to the concentric cylinders' torque. Hence, considering that the cone-plate expression (6-1) gives the correct shear rate for a given viscosity measurement will be even less subject to error than calculations based on equation (6-3) would indicate. The errors will be smaller, the less shear dependent is the suspension viscosity. For preparations whose shear thinning characteristics are no more severe than

normal blood, then, the uncertainties in shear rate determination are insignificant over the range of  $\dot{\gamma}$  employed in this work.

For non-aggregating suspensions, the shear stress measured at a given shear rate was given simply by the average of the steady state torsion head displacement when the sample was sheared in the forward and reverse directions. The steady state displacement was also used for aggregating preparations when the measurements were made at shear rates so high that the torque-time records were flat-topped. At low shear rates, however, the time-dependence of the torsion head displacement complicated interpretation of the data. In general, aggregating suspensions measured at low shear showed an initial peak in their torque-time records which decayed to a lower, roughly constant value. The peak was never seen for suspensions which did not show microscopic evidence of aggregation. The width of the peak varied with the hematocrit and aggregating tendency of the suspending medium. When present, it was wider at the lower shear rates. In severely aggregated systems, the peak was apparent at hematocrits as low as 15% v/v, while in less heavily aggregated suspensions it appeared only at hematocrits of 30% and above. On the other hand, in some systems of moderate aggregating tendency the torque was observed to build up to a steady state value over a period of 10 to 30 seconds and show no peak over ~60 seconds. In general, the qualitative impression obtained was that the initial behavior of the

torque-time records reflected the presence, kinetics of formation, and degree of cellular aggregation present in the suspensions. No quantitative study was made of any possible relationships between the initial torque-time behavior and conditions determining the aggregation behavior of the preparations, however.

When an initial peak was present, the procedure used to obtain a shear stress measurement was that described by Cokelet (134, 141). The descending slope of the peak was extrapolated back to the point at which the shear was applied to the suspension, and the resulting displacement used to calculate the shear stress and viscosity at that shear rate. In contrast to the behavior of whole blood in the G. D. M. viscometer, where the low shear rate peak develops over a period of 1 or 2 minutes, the peak height occurred within 3 seconds of the time that shear was applied at all shear rates, and was therefore controlled to some degree by the time constant of the detection system. As the shear rate was increased, the peak narrowed from a width of 30-90 sec at low shear, to only a few seconds at high rates of shear. The peak was frequently observed to persist up to shear rates of between 10 and 50  $\text{sec}^{-1}$  in heavily aggregated, concentrated suspensions. Where the peak was very narrow, even its detection on the chart recorder depended on the time constant of the low frequency filter, since at some shear rates where the peak was no longer present on the chart, its presence could still be observed, although not

measured, on the Transducer Meter. In general, however, the extension of the peak above the steady state value was small when the peak width was of the order of the time constant of the filter. The relative error involved in extrapolating from the recorded peak was therefore not large. In those cases where the torque was seen to build up slowly to a steady-state value, the steady state reading was taken in order to calculate the viscosity.

Using the procedures described above, the apparent viscosity at the sample temperature was calculated for each shear rate from equation (6-2). These viscosities were then corrected to the viscosity at 25°C using the temperature dependence of water (256). The raw data displacement values  $\Delta(T)$  and corresponding gear settings, which determined the shear rates, were converted to values of viscosity at 25°C and shear rate using a program written for the Hewlett-Packard 9100B Calculator. The program generated values of  $\dot{\gamma}$  from the gear setting  $G$  using the expression:

$$\dot{\gamma} = 4278.6 \exp(-2.3026 G) \quad (6-4)$$

and generated the viscosity values at 25°,  $\eta(25^\circ)$  from the values at a temperature  $T$ ,  $\eta(T)$ , using the expression:

$$\eta(25^\circ) = \frac{0.8937 \eta(T)}{\exp[-0.022546 T + 0.45161]} \quad (6-5)$$



The expression in the denominator gives the viscosity of water at any temperature  $23^{\circ} \leq T \leq 28^{\circ}$  to an accuracy of  $\pm 0.06\%$ .

### Results and Discussion

The apparent viscosities of all suspensions were unique functions of the rate of shear when the measurement procedures outlined above were employed. That is, the  $\eta(\dot{\gamma})$  values obtained were independent of the history of the sample and did not depend on the order of shear rates in which the measurements were made. The reproducibility of all measurements at hematocrits greater than about 30% v/v was better than  $\pm 5\%$  except in the very heavily aggregated suspensions measured at  $\dot{\gamma} < 1 \text{ sec}^{-1}$  where the reproducibility was  $\pm 10\%$ . At low hematocrits and low shear rates ( $H < 30\%$ ,  $\dot{\gamma} < 1 \text{ sec}^{-1}$ ) the electrical and mechanical noise produced a signal which was a significant fraction of the total transducer displacement recorded. The uncertainty in the viscosities measured in this region is therefore somewhat larger than at higher shear rates and hematocrits, but was never larger than  $\pm 15\%$  for the data reported here.

In no instance was any change in the state of the suspension detected microscopically when the slides were examined upon completion of shearing. In general the cells appeared to be normal when monodisperse, although a small, variable amount of hemolysis was present in some of the dextran/saline suspensions. The presence or



absence of hemolysis of the degree observed in these samples had no measurable effect on their flow properties.

The degree of aggregation present was estimated on a 0 to ++++ scale, as discussed in Chapter 5. Saline suspensions were graded as 0. The presence of doublets or small multiplets of cells which flowed as single units under very low shear indicated + aggregation. Roughly linear aggregates of four or more cells in which little cell distortion was seen were graded as ++ aggregation. Larger, more globular, three dimensional clumps which were more resistant to shear and which caused noticeable cell distortion were denoted +++. The ++++ aggregates were very large, three dimensional elastic networks of cells in which all cells were severely distorted and which were more resistant to shear than lower grades. Normal red cell rouleaux formed in plasma would be graded ++  $\rightarrow$  +++ on this scale.

The apparent viscosities of washed human erythrocytes suspended in either saline/EDTA, or saline/EDTA to which various amounts of dextrans of differing molecular weights had been added are give as a function of shear rate between 0.2 and 1,000  $\text{sec}^{-1}$  in Figures 6-2 to 6-20. The viscosities of the suspending media as determined in the Rheogoniometer are given for each suspension. All dextran solutions were Newtonian over the ranges of shear rate and concentration examined, and their viscosities agreed with the values determined with the Ostwald viscometer to  $\pm 2\%$ . Qualitatively, the

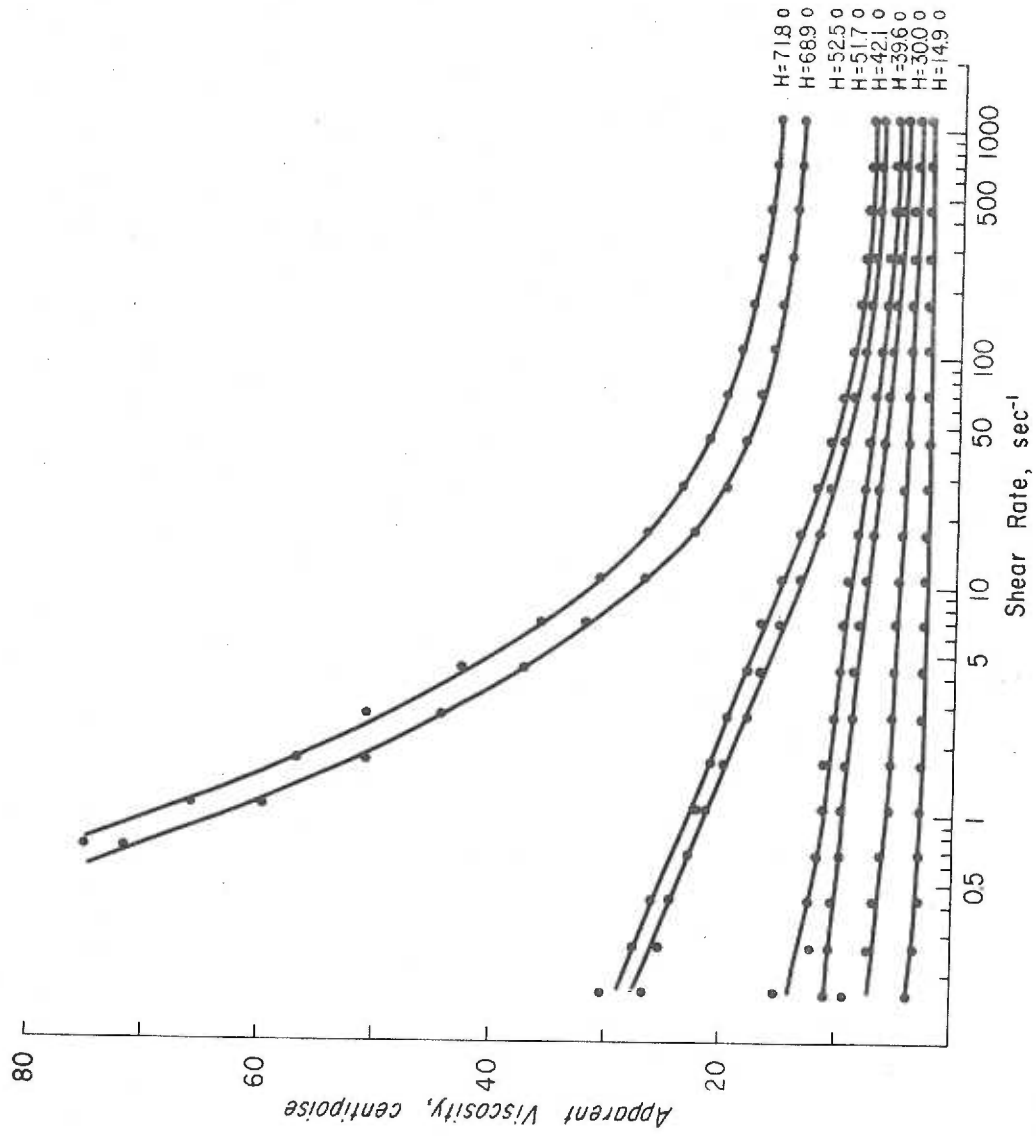


Figure 6-2. Apparent viscosity vs. shear rate for erythrocytes suspended in saline/EDTA.

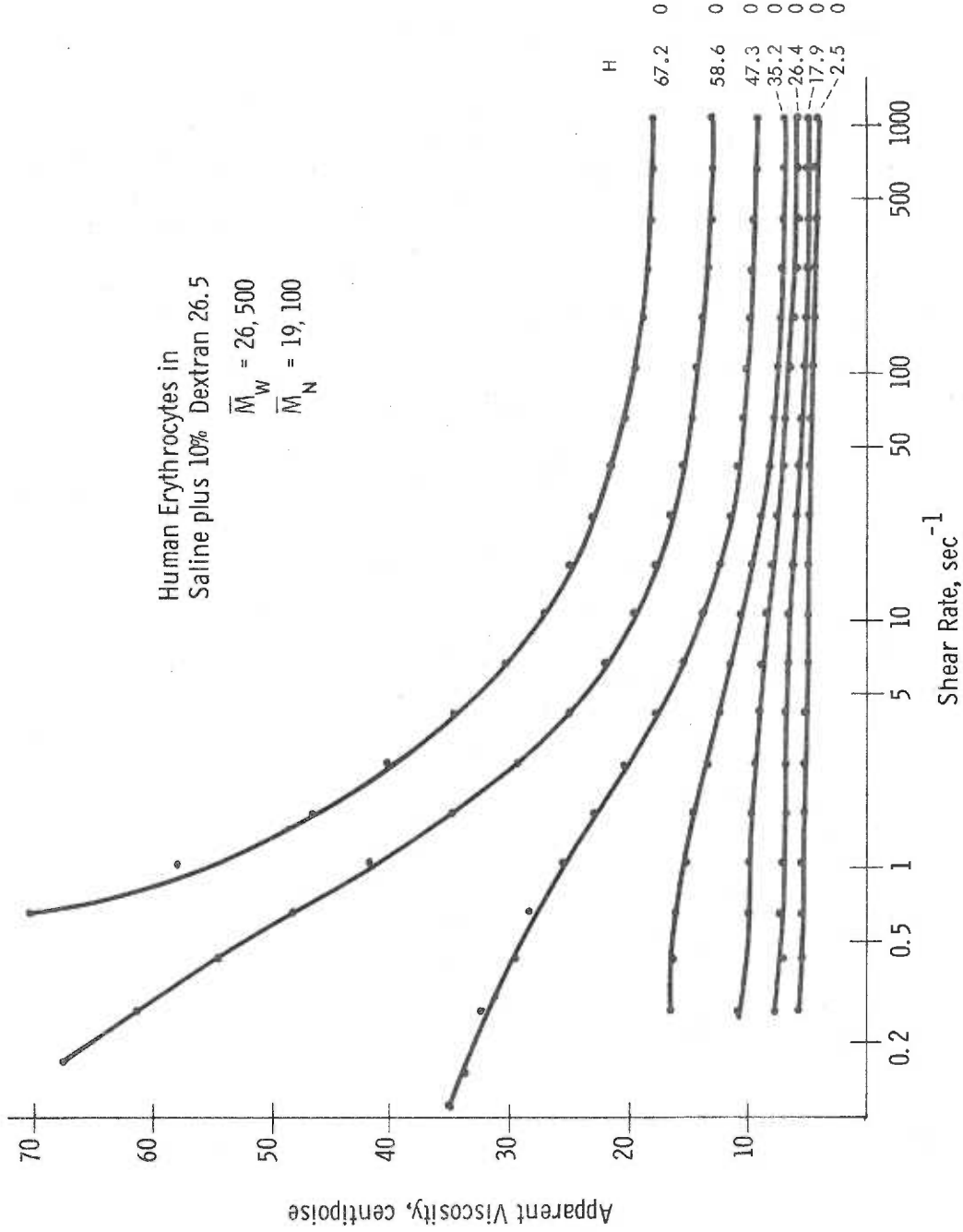


Figure 6-3. Apparent viscosity vs. shear rate for erythrocytes suspended in saline/EDTA/10% dextran 26.5.  $\eta_0 = 4.02$  cp

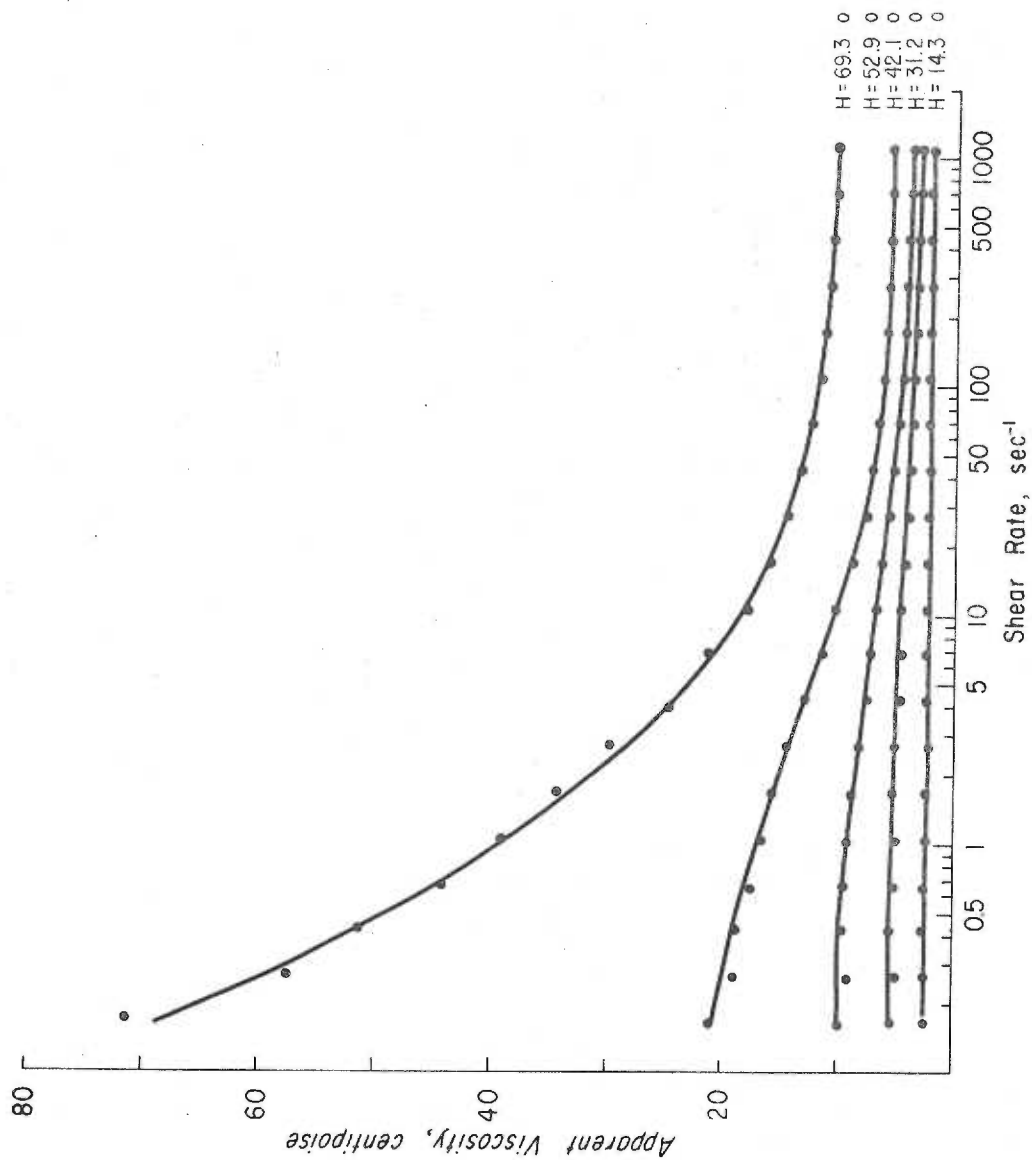


Figure 6-4. Apparent viscosity vs. shear rate for erythrocytes suspended in saline/EDTA/3.00% dextran 41.  $\eta_0 = 1.63$  cp

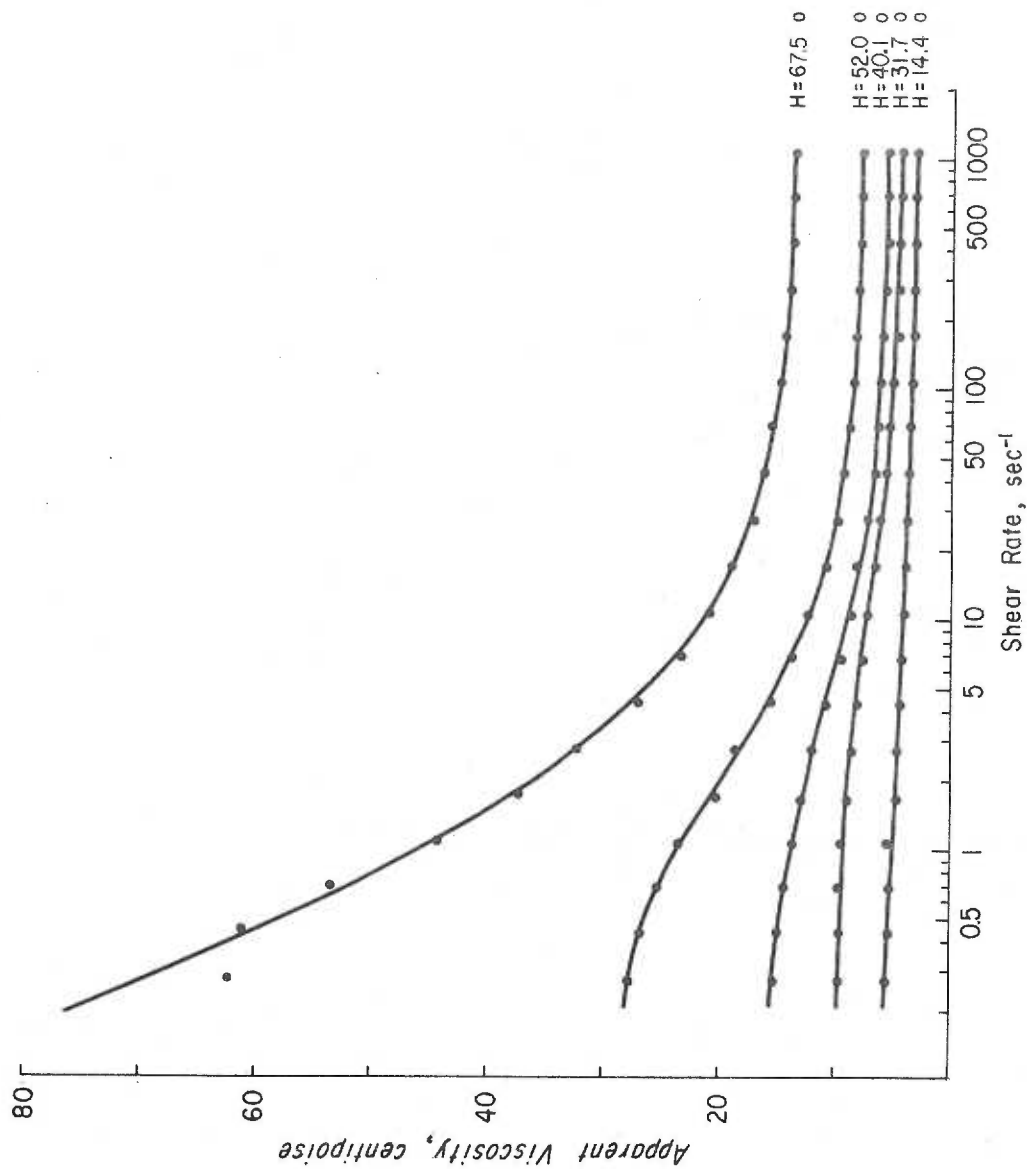


Figure 6-5. Apparent viscosity vs. shear rate for erythrocytes suspended in saline/EDTA/6.03% dextran 41.  $\eta_0 = 2.57$  cp.

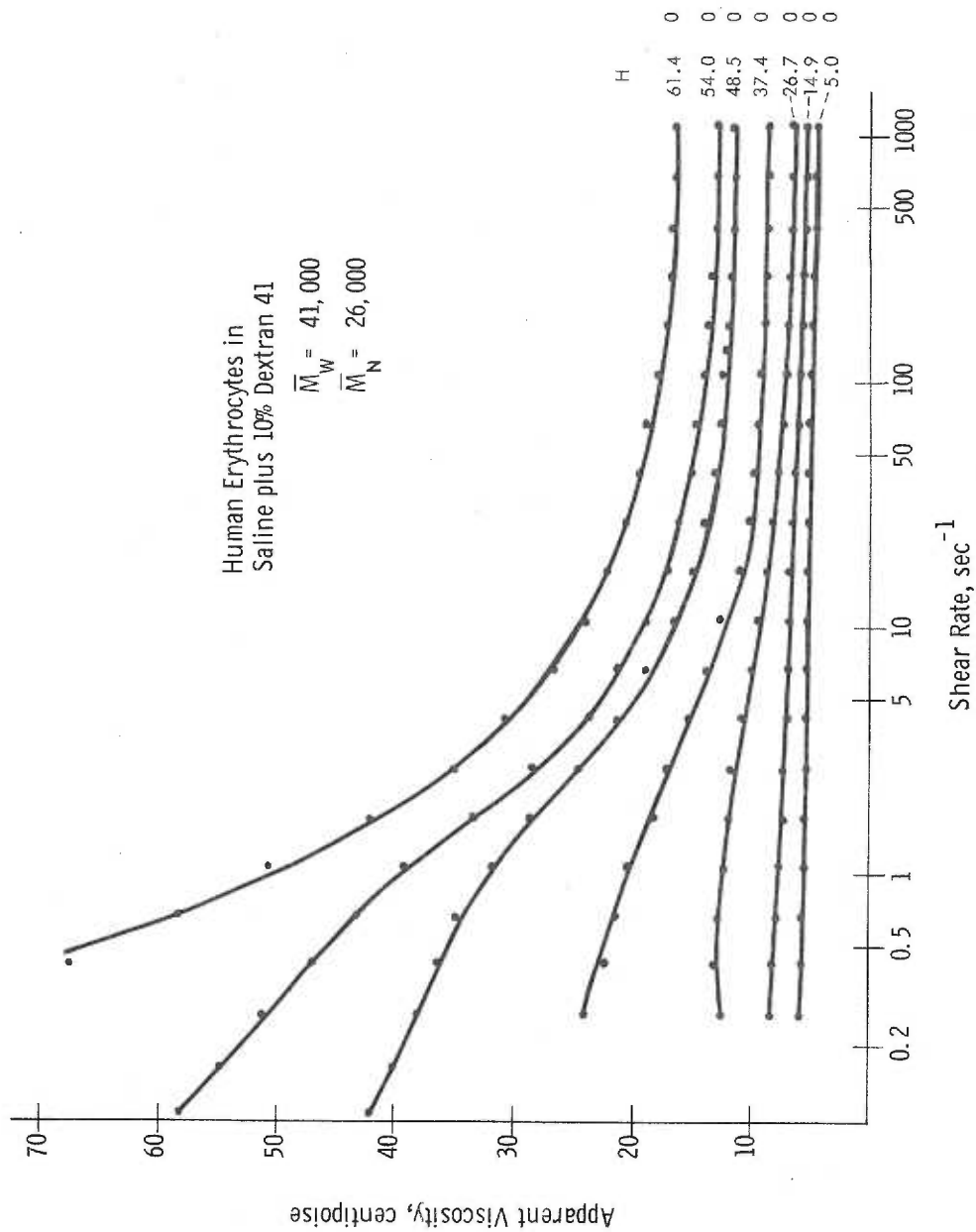


Figure 6-6. Apparent viscosity vs. shear rate for erythrocytes suspended in saline/EDTA/10% dextran 41.  $\eta_0 = 4.43$  cp

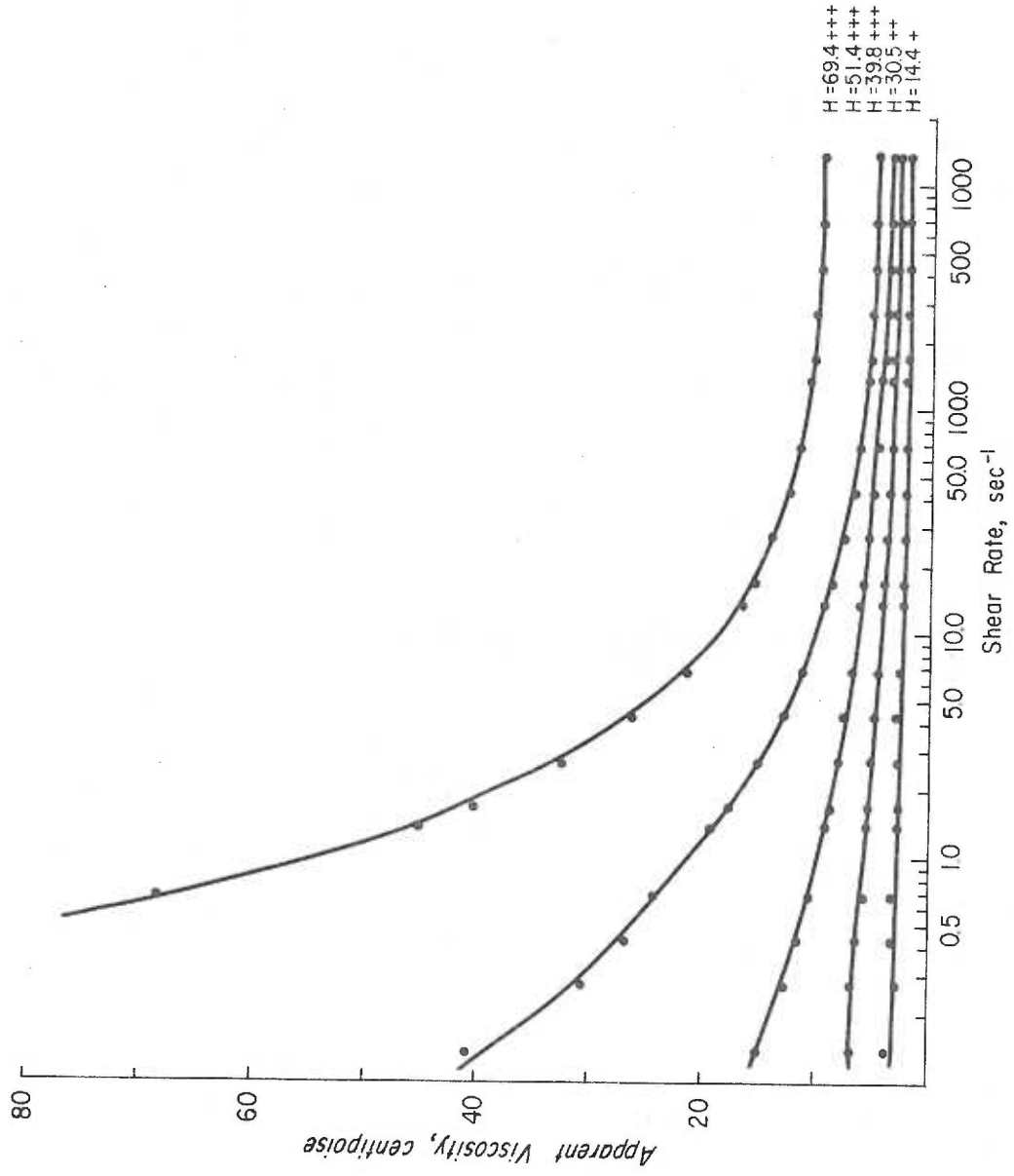


Figure 6-7. Apparent viscosity vs. shear rate for erythrocytes suspended in saline/EDTA/2.00% dextran 50.5.  $\eta_0 = 1.46$  cp

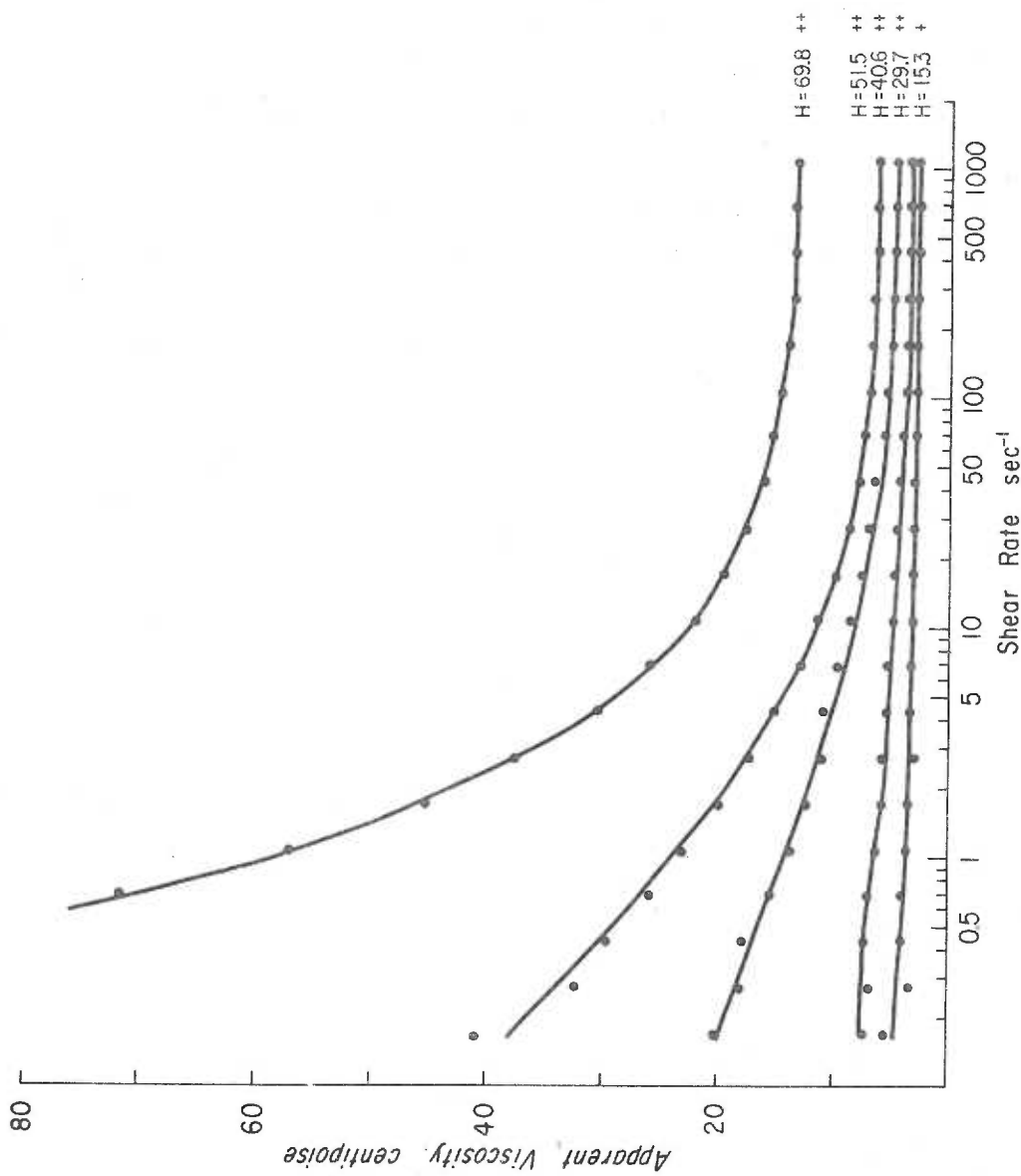


Figure 6-8. Apparent viscosity vs. shear rate for erythrocytes suspended in saline/EDTA/3.00% dextran 50.5.  $\eta_0 = 1.85$  cp



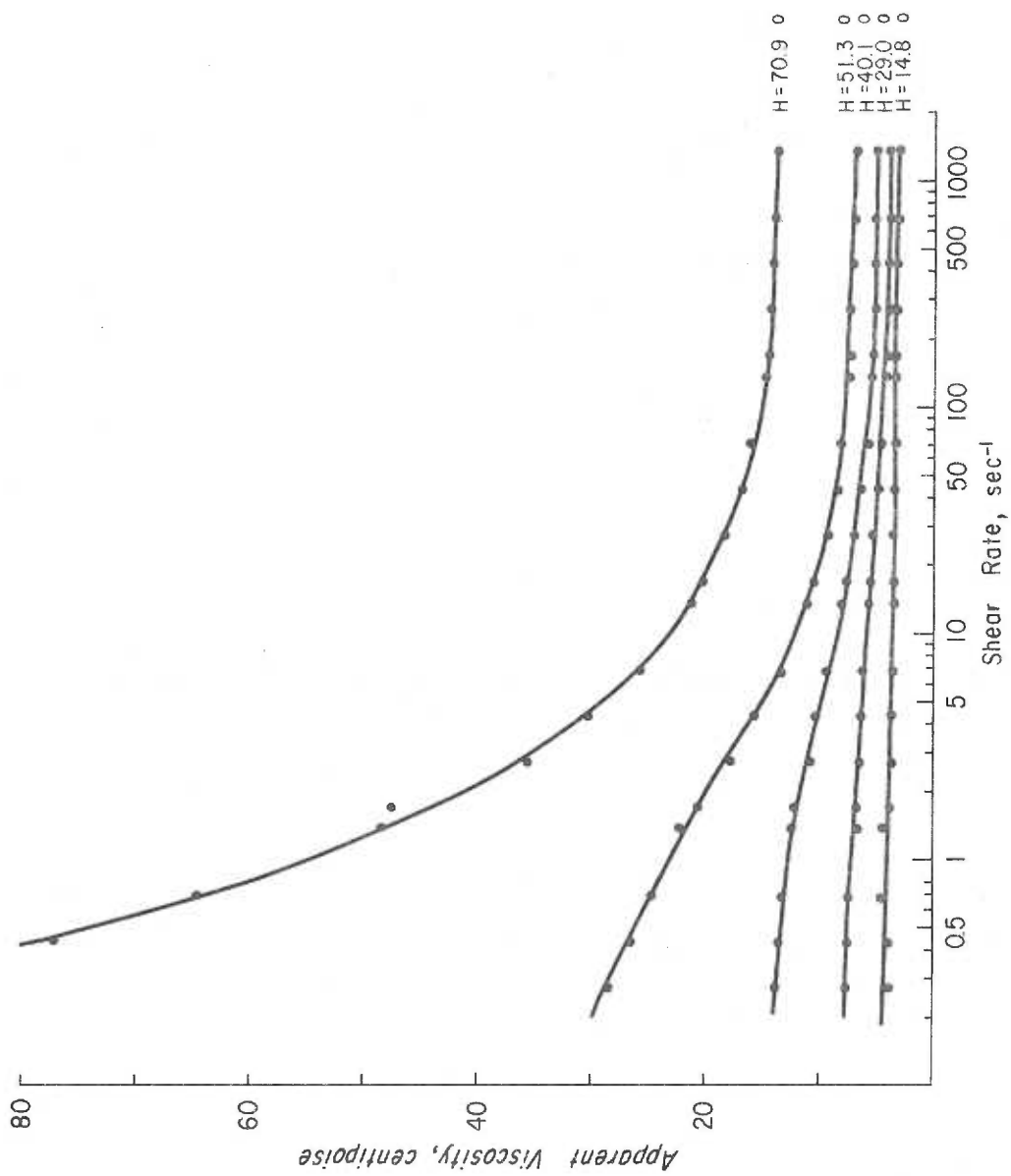


Figure 6-9. Apparent viscosity vs. shear rate for erythrocytes suspended in saline/EDTA/4.01% dextran 50.5.  $\eta_0 = 2.21$  cp

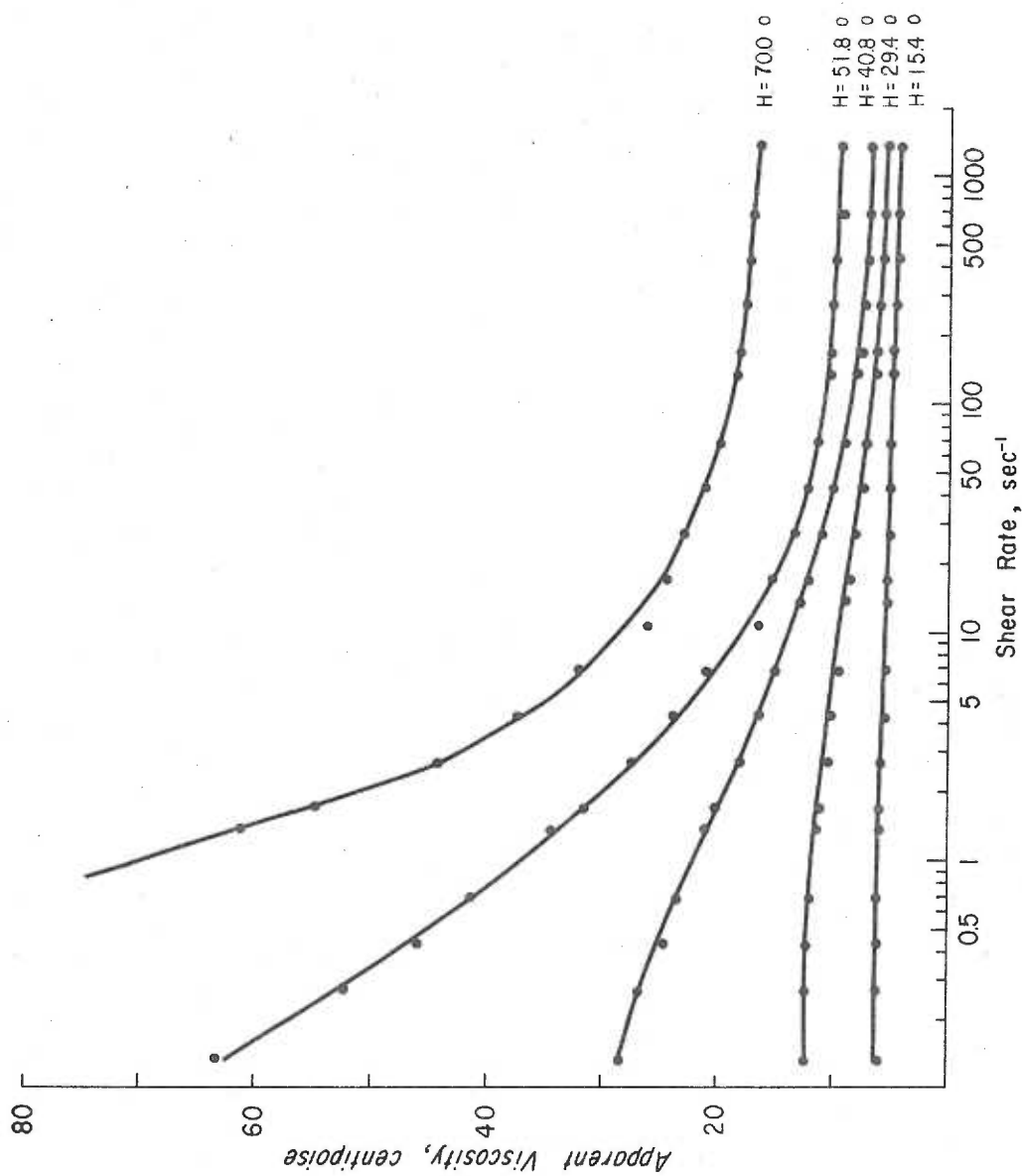


Figure 6-10. Apparent viscosity vs. shear rate for erythrocytes suspended in saline/EDTA/5.97% dextran 50.5.  $\eta_0 = 3.49$  cp

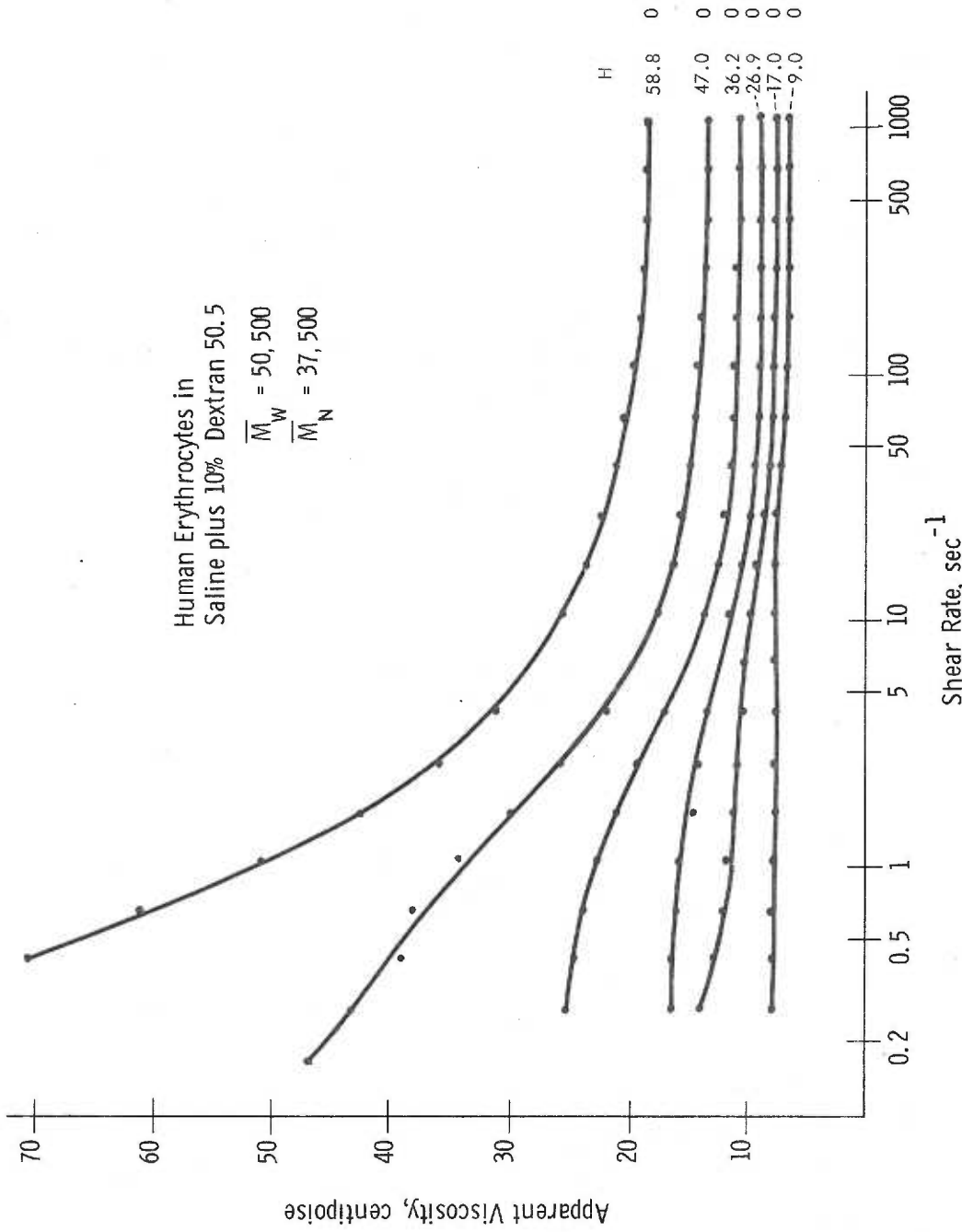


Figure 6-11. Apparent viscosity vs. shear rate for erythrocytes suspended in saline/EDTA/10% dextran 50.5.  $\eta_0 = 5.86$  cp

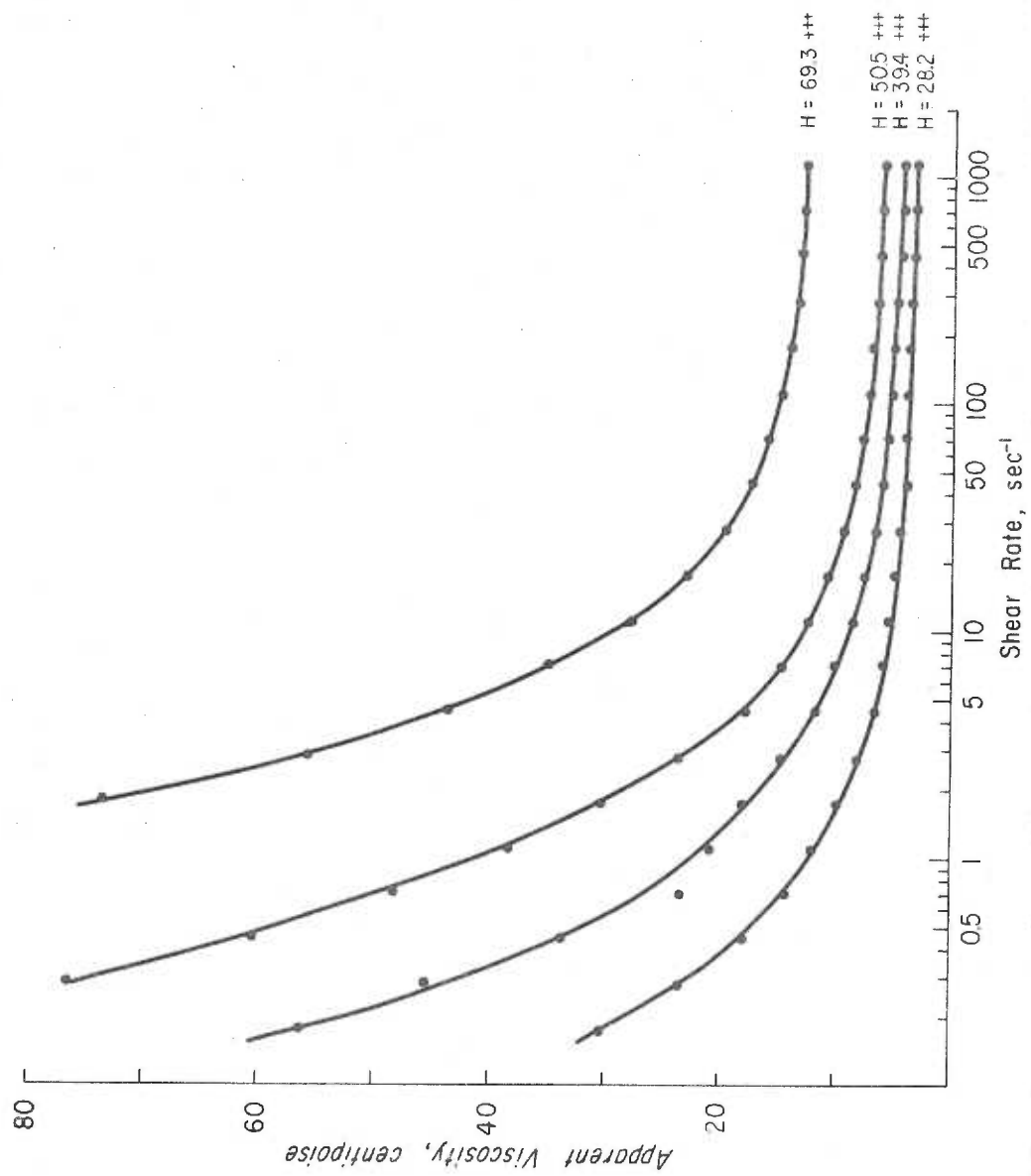


Figure 6-12. Apparent viscosity vs. shear rate for erythrocytes suspended in saline/EDTA/2.52% dextran 77.6.  $\eta_0 = 1.76$  cp

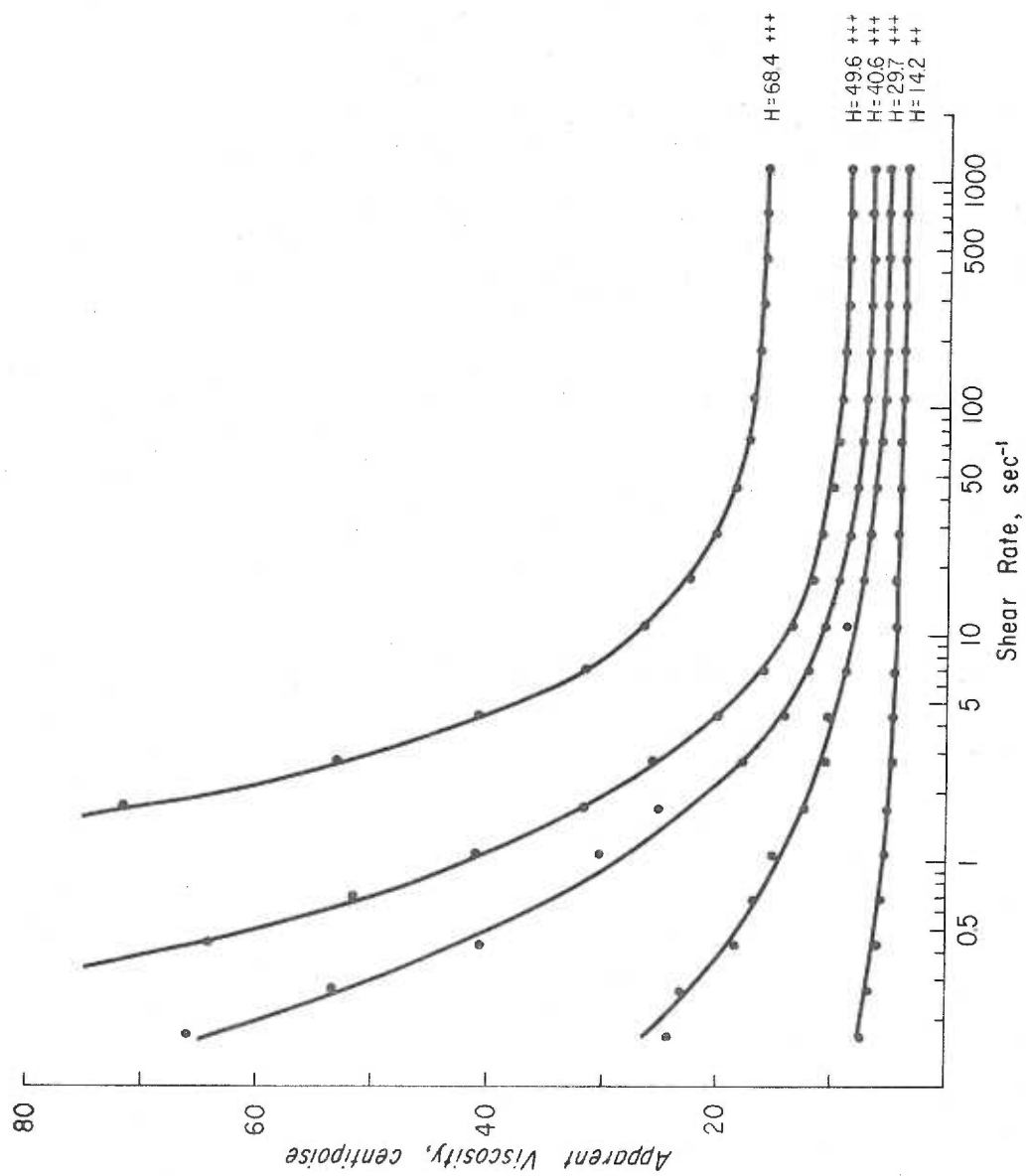


Figure 6-13. Apparent viscosity vs. shear rate for erythrocytes suspended in saline/EDTA/5.00% dextran 77.6.  $\eta_0 = 3.04$  cp

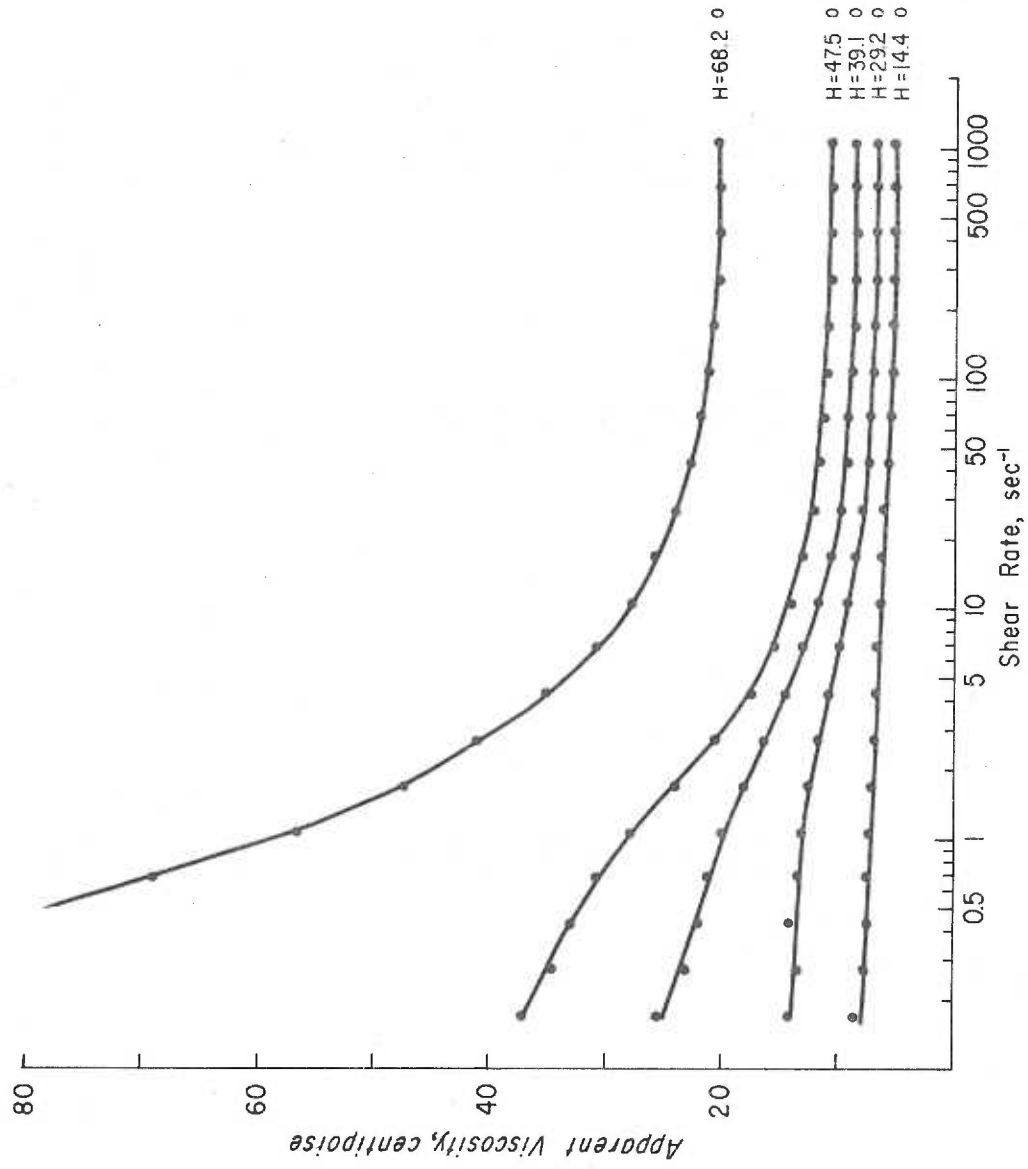


Figure 6-14. Apparent viscosity vs. shear rate for erythrocytes suspended in saline/EDTA/6.63% dextran 77.6.  $\eta_0 = 4.43$  cp

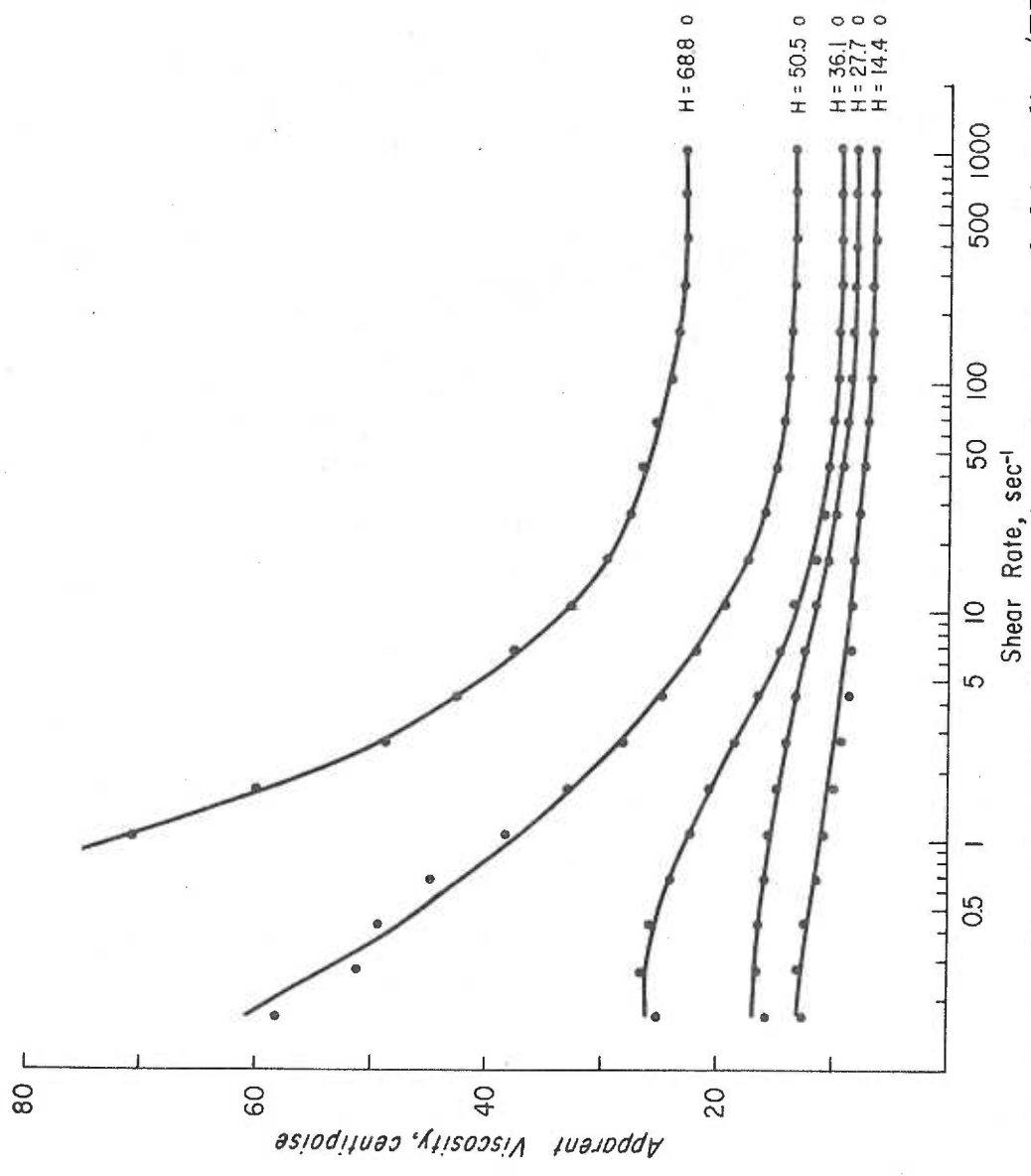


Figure 6-15. Apparent viscosity vs. shear rate for erythrocytes suspended in saline/EDTA/7.58% dextran 77.6.  $\eta_0 = 5.30$  cp

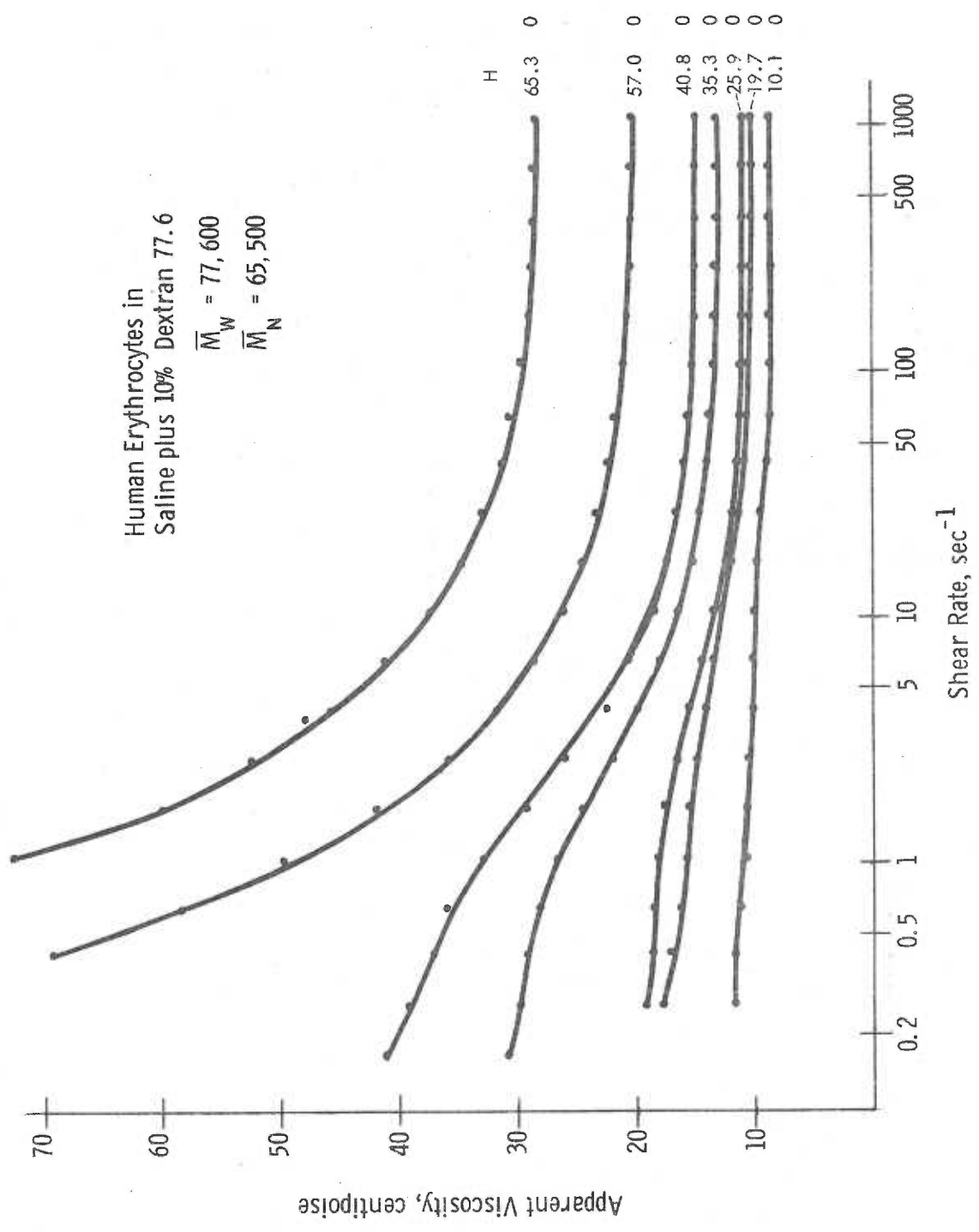


Figure 6-16. Apparent viscosity vs. shear rate for erythrocytes suspended in saline/EDTA/10% dextran 77.6.  $\eta_o = 7.89$  cp



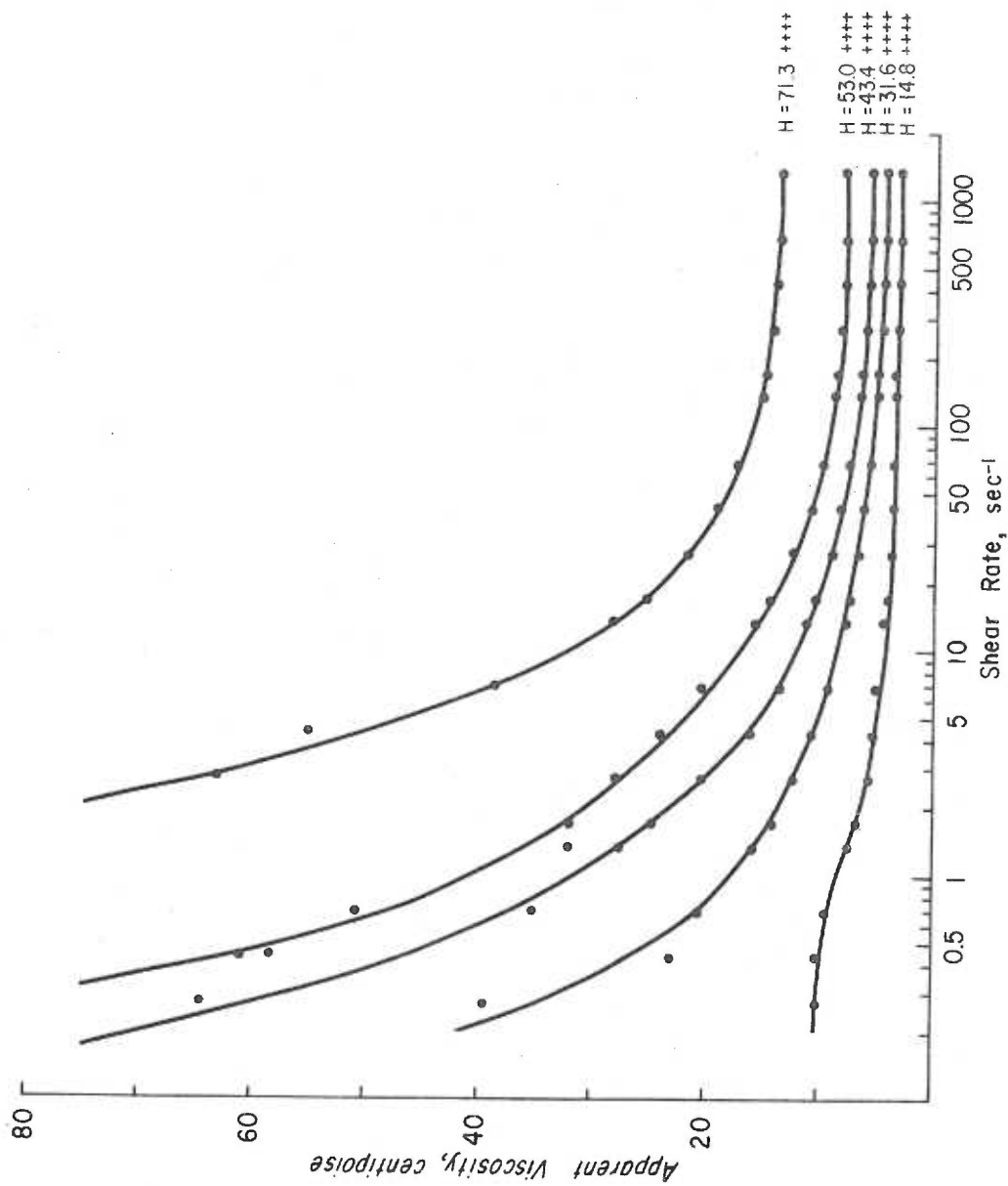


Figure 6-17. Apparent viscosity vs. shear rate for erythrocytes suspended in saline/EDTA/3.48% dextran 110.  $\eta_0 = 2.46$  cp

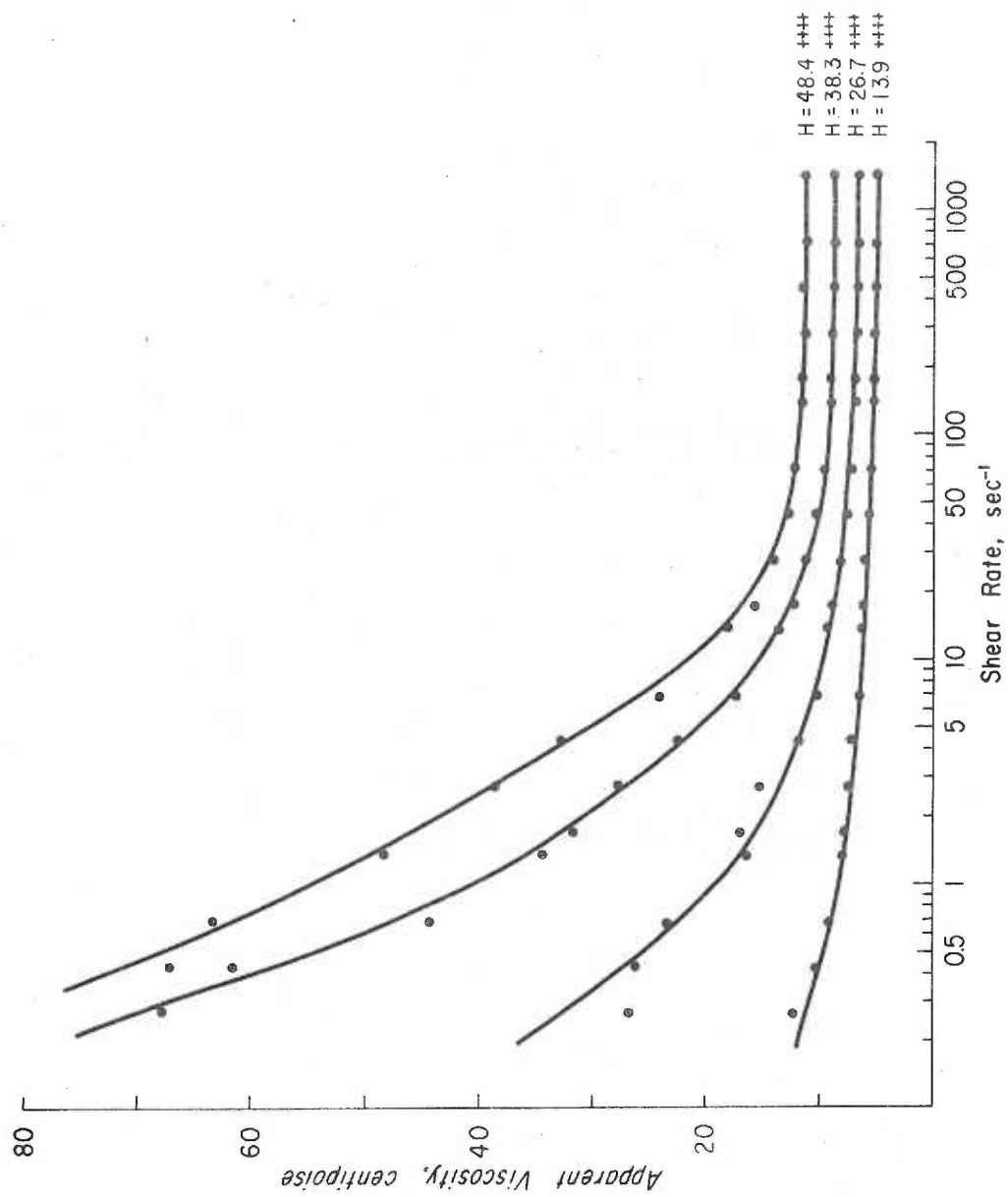


Figure 6-18. Apparent viscosity vs. shear rate for erythrocytes suspended in saline/EDTA/5.45% dextran 110.  $\eta_0 = 4.14$  cp

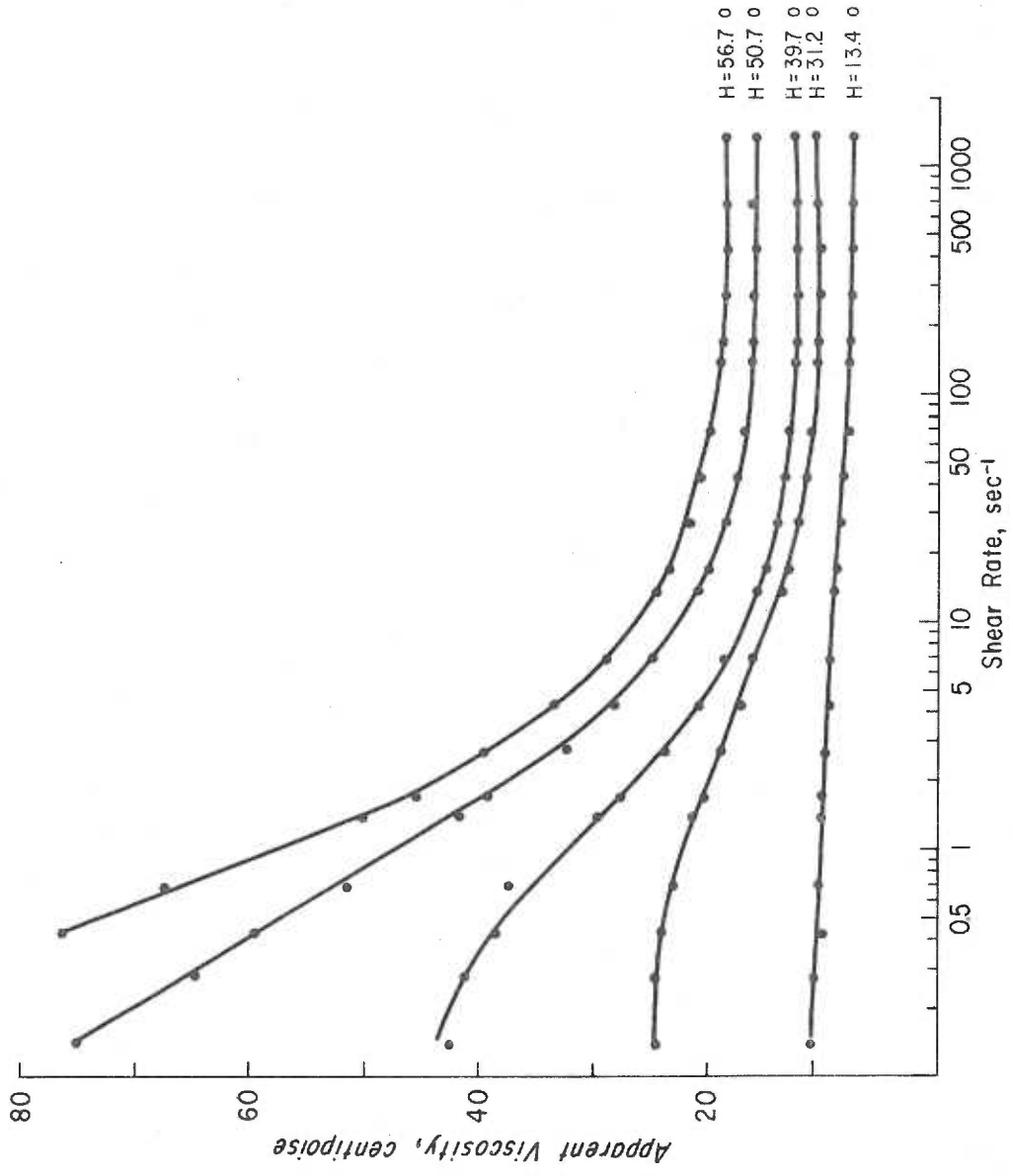


Figure 6-19. Apparent viscosity vs. shear rate for erythrocytes suspended in saline/EDTA/7.44% dextran 110.  $\eta_0 = 6.35$  cp

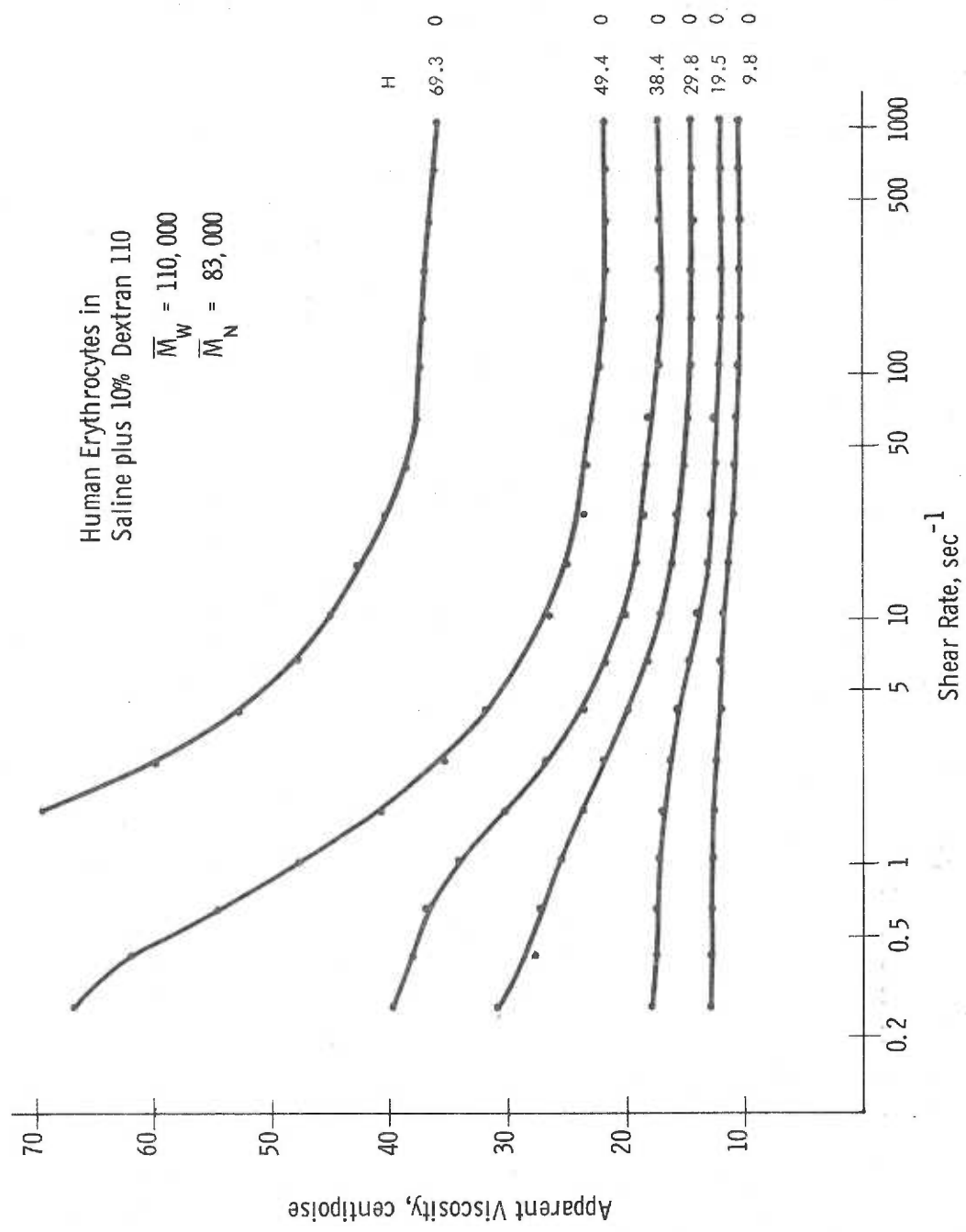


Figure 6-20. Apparent viscosity vs. shear rate for erythrocytes suspended in saline/EDTA/10% dextran 110.  $\eta_0 = 9.09$  cp

sets of viscosity-shear rate curves appear similar in that at low cell concentrations the shear rate dependence is small but becomes more marked as the hematocrit is increased. There are striking differences in the low shear rate regions, however, depending on whether or not the suspensions were aggregated. At hematocrits near 50% v/v, the aggregated samples such as 3% dex 50.5 (Figure 6-8), 2.5% dex 77.6 (Figure 6-12) or 3.5% dex 110 (Figure 6-17) show much stronger increases in viscosity at low shear rate than do the non-aggregated systems in saline (Figure 6-2) or 3% dex 41 (Figure 6-4). The viscosities at all shear rates are elevated in the dextran solutions, as a result of the increased viscosities of the suspending media. Thus, increases in  $\eta(\dot{\gamma})$  are to be expected as the concentration and molecular weight of the dextrans are increased. This dependence of the apparent viscosity on the continuous phase viscosity,  $\eta_0$ , limits the usefulness of  $\eta(\dot{\gamma})$  as a parameter for describing the interactions among the elements of the system.

In general, the dependence of the apparent viscosity of any suspension at a fixed shear rate on the volume concentration of particles,  $H$ , may be expressed as an extension of the Einstein equation (1-33) to higher order terms in  $H$ :

$$\eta = \eta_0 (1 + a_1 H + a_2 H^2 + \dots) \quad (6-6)$$

As was mentioned in Chapter 1,  $a_1 = 2.5$  for non-interacting rigid spheres, and in general is a measure of the shape of the particles, not their interactions. For colloidal suspensions of rigid particles the higher order coefficients  $a_2, a_3, \dots$  are observed to be larger, the greater the degree of aggregation or structuring in the system (257, 258). A comparison of the flow behavior of red cells suspended in plasma and saline has shown that at low shear rates ( $\sim 1 \text{ sec}^{-1}$ ) such a relationship also applies to erythrocytes, in spite of their great deformability (152). One quantitative measure of aggregation, then, would seem to be provided by the values of  $a_2, a_3, \dots$  obtained in various suspending media. These coefficients should be determined at a series of shear rates, and the values found at  $\dot{\gamma} = 0$  by extrapolation. The problem in determining coefficients such as these is that very high accuracy is required in the determination of low shear rate viscosities on suspensions of low volume concentration; the necessary precision is extremely difficult to achieve.

For instance, consider the error likely to apply to the determination of  $a_2$  from data such as that in Figures 6-2 to 6-20. To estimate  $a_2$  at  $\dot{\gamma} = 0$ , the reduced viscosity,  $\eta_{\text{red}} = \frac{\eta/\eta_0 - 1}{H}$ , is plotted as a function of  $H$  at a series of shear rates. At low  $\dot{\gamma}$  and  $H$ , the uncertainty in  $(\eta/\eta_0)$  is  $\pm 15\%$ . Hence, for a typical value of  $(\eta/\eta_0) = 1.3$  at  $H = 5\% \text{ v/v}$ , the uncertainty in the reduced viscosity is  $\pm 65\%$ . Since the first coefficient,  $a_1$  (the

intrinsic viscosity), is given by  $\lim_{H \rightarrow 0} \eta_{red}$ , and  $a_2$  is the slope of the  $\eta_{red}$ -H curves at  $H = 0$ , it is clear that the values obtained will be subject to considerable error, particularly when  $a_1(\dot{\gamma})$ ,  $a_2(\dot{\gamma})$  are extrapolated to  $\dot{\gamma} = 0$ . The determination of  $a_3(\dot{\gamma} \rightarrow 0)$  will be subject to much larger errors, since its value will depend on  $a_1$  and  $a_2$ . Attempts to evaluate the coefficients of equation (6-6) for the data of Figures 6-2 to 6-20 were unsuccessful.

One parameter which has been used as an indication of the degree of structuring in plasma suspensions of red cells is the yield stress (141). There are several disadvantages to the use of the yield stress as a generalized measure of cell-cell interactions, however. It is not a dimensionless quantity, and its value seems to depend strongly on the method used in its measurement (141, 142, 143, 144). When measured using a viscometer, the value of the yield stress is determined by extrapolating  $\tau^{1/2} - \dot{\gamma}^{1/2}$  or  $\tau - \dot{\gamma}$  plots to  $\dot{\gamma} = 0$ . Since the shape of these curves, and of the torque-time records from which they are derived, vary depending on the type of viscometer used (124, 141, 253), the extrapolation procedure appears somewhat uncertain. In any case, the yield stress can only indicate the degree of structuring in the system, not the degree of dispersion. It could therefore not be expected to give information on, for instance, the postulated "frictional" interactions which might be occurring in non-aggregating saline suspensions. The yield stress, then, was not

examined for the suspensions studied here.

Although it was not possible to evaluate the coefficients of (6-6) for the  $\eta(\dot{\gamma}, H)$  data obtained, at least the first order effect of the continuous phase viscosity on the results could be eliminated by calculating relative viscosities,  $\eta/\eta_0$ , for the systems studied. At low shear rates, where the effects of cell-cell interactions are maximized, the form of the  $\eta/\eta_0 - H$  curves should give some qualitative information regarding the fundamental interactions occurring in the suspensions. Figures 6-21 to 6-24 give plots of  $\eta/\eta_0$  as a function of  $H$  at  $\dot{\gamma} = 0.68 \text{ sec}^{-1}$ . The dextran concentration, continuous phase viscosity, and degree of aggregation are indicated for each curve. The data for saline/EDTA is included on each plot as a basis for comparison.

It is seen that, in every case, those suspensions which show detectable aggregation at zero shear rate on a microscope slide have relative viscosities greater than saline over a considerable hematocrit range at  $\dot{\gamma} = 0.68 \text{ sec}^{-1}$ . Hence, as in the plasma suspensions mentioned earlier, cellular aggregation is associated with increases in  $\eta/\eta_0$  relative to saline suspensions, and therefore increased values of at least some of the coefficients of equation (6-6) at this rate of shear. For suspensions in which no aggregation is observable, however, the relative viscosities are less than or equal to those for saline suspensions at all hematocrits. This is the effect discussed in



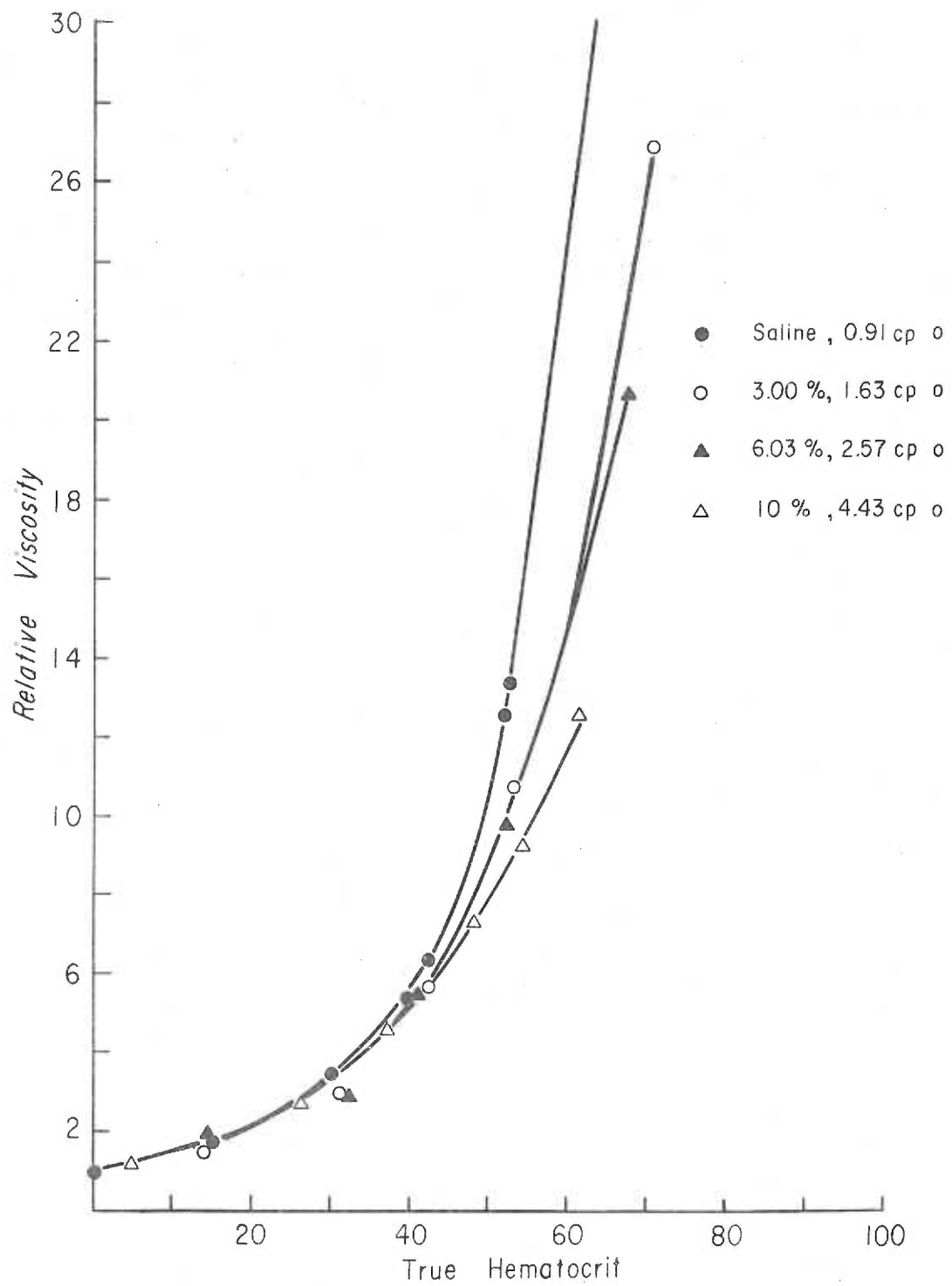


Figure 6-21. Relative viscosity vs. hematocrit at  $\dot{\gamma} = 0.68 \text{ sec}^{-1}$  for erythrocytes in saline/EDTA/dextran 41.

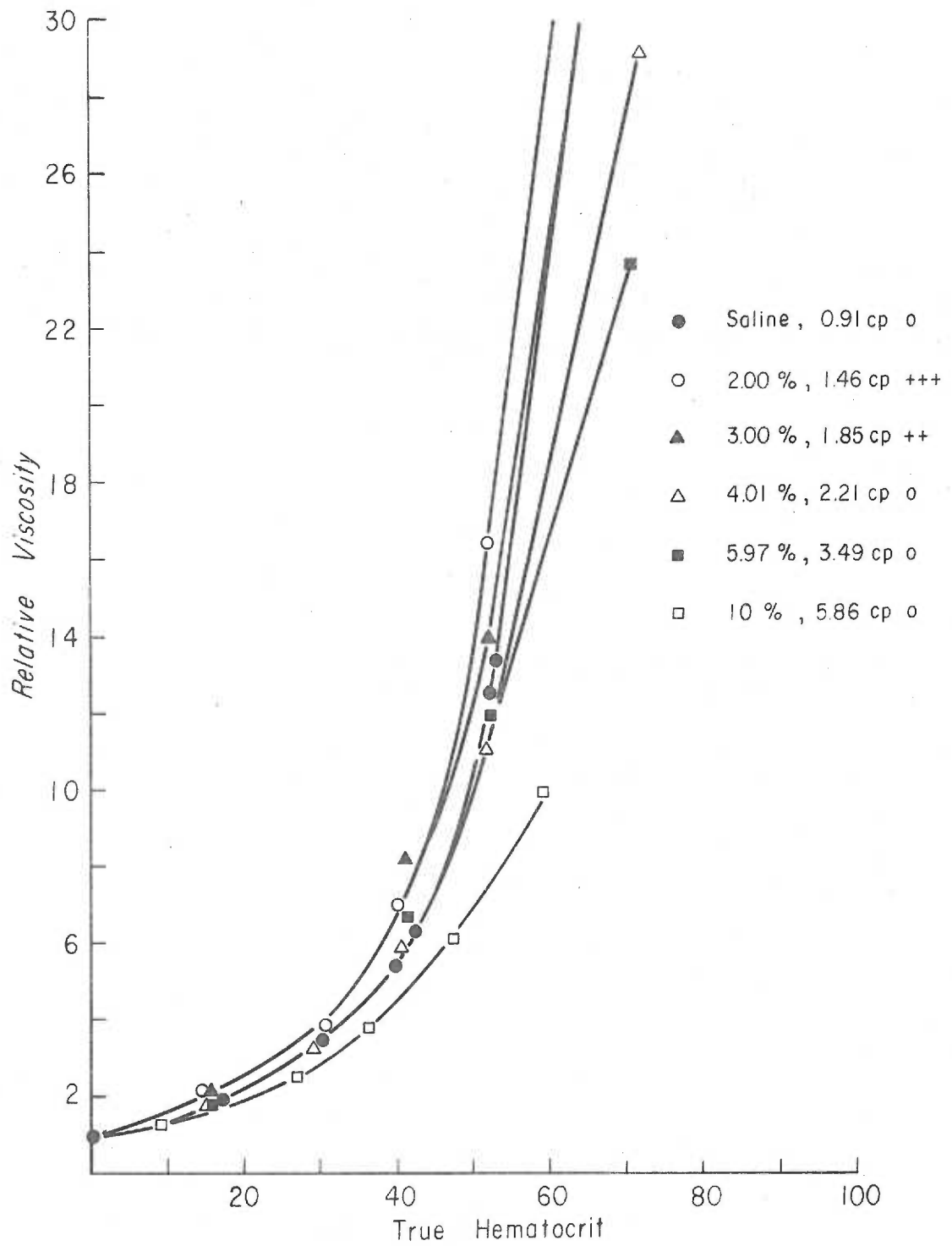


Figure 6-22. Relative viscosity vs. hematocrit at  $\dot{\gamma} = 0.68 \text{ sec}^{-1}$  for erythrocytes in saline/EDTA/dextran 50.5.

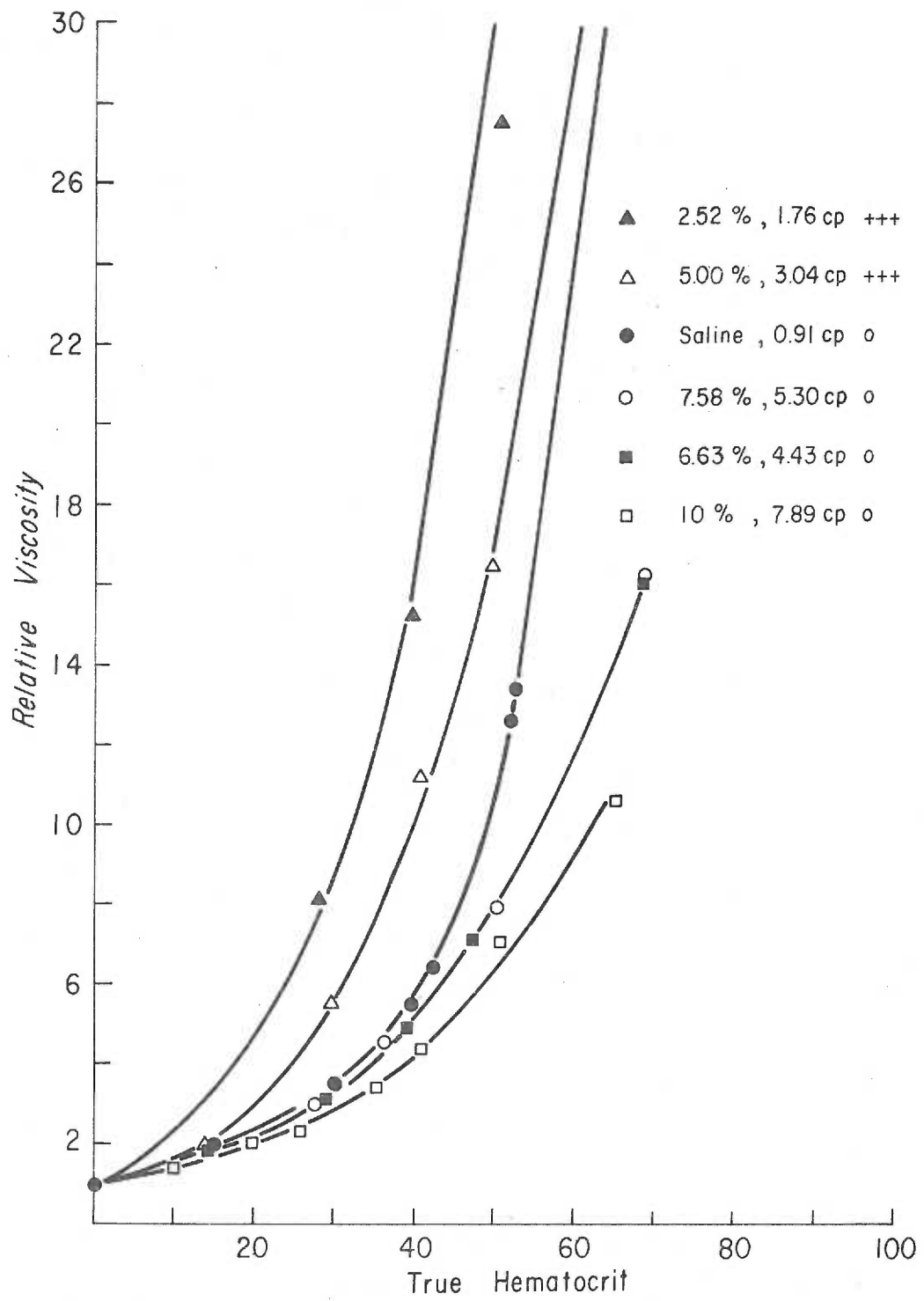


Figure 6-23. Relative viscosity vs. hematocrit at  $\dot{\gamma} = 0.68 \text{ sec}^{-1}$  for erythrocytes in saline/EDTA/dextran 77.6.

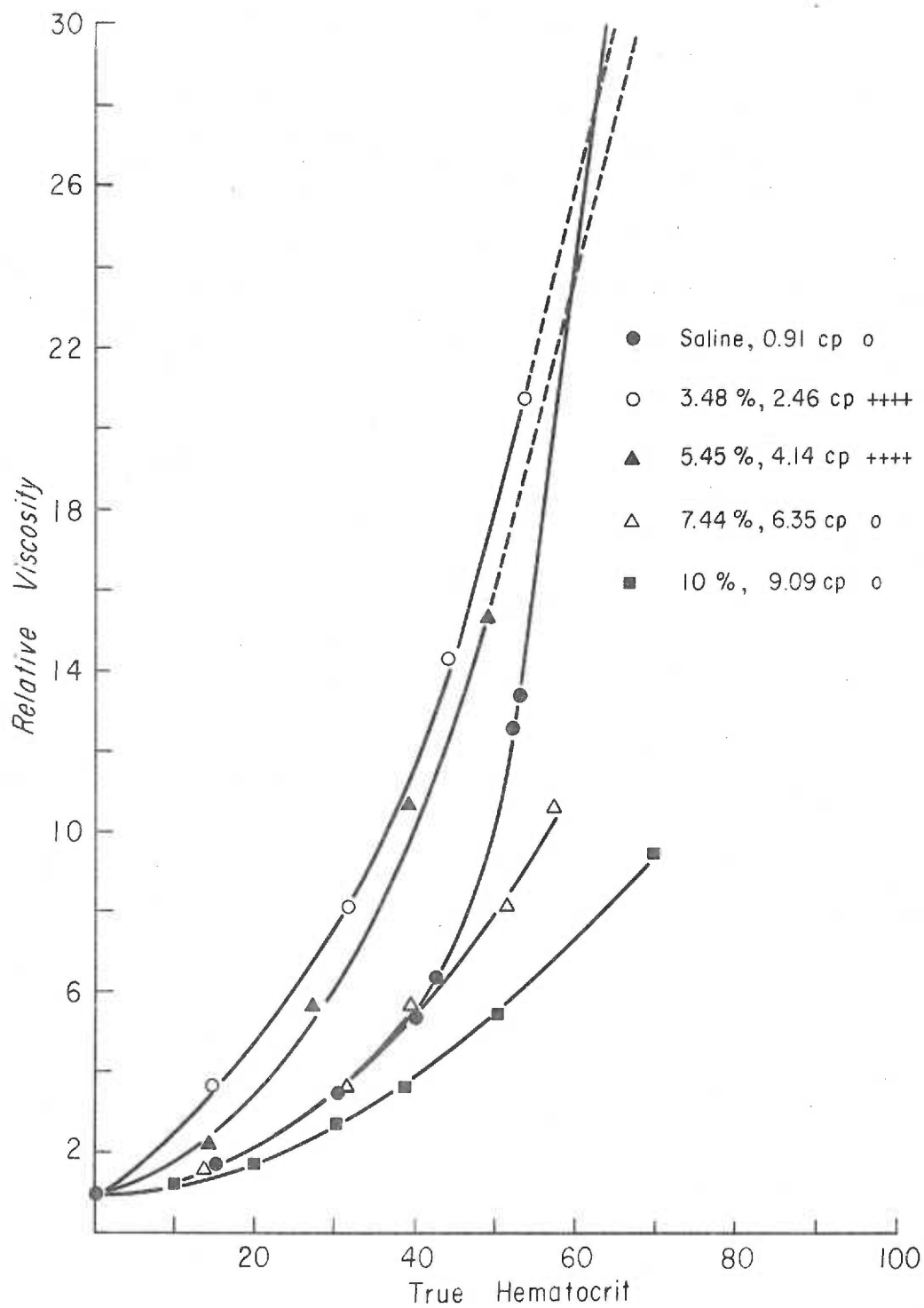


Figure 6-24. Relative viscosity vs. hematocrit at  $\dot{\gamma} = 0.68 \text{ sec}^{-1}$  for erythrocytes in saline/EDTA/dextran 110.

Chapter 1, reported in the literature several years ago (2, 163). The question at hand is what connection, if any, is there between the increased or decreased relative viscosities associated with the addition of dextran to the suspending media, and the increased cellular zeta potentials found in these systems.

A convenient measure of the relative differences between the dextran and saline suspensions of cells is provided by the ratio,  $R$ , of the relative viscosity in saline/EDTA to the relative viscosity in saline/EDTA/dextran at constant hematocrit and shear rate, i. e.:

$$R = \frac{(\eta/\eta_o)_{\text{sal}}}{(\eta/\eta_o)_{\text{dex}}} \Big|_{H, \dot{\gamma}} \quad (6-7)$$

where  $(\eta/\eta_o)_{\text{sal}}$  is the viscosity of a cell suspension in saline at fixed  $H$  and  $\dot{\gamma}$  divided by the viscosity of saline, and  $(\eta/\eta_o)_{\text{dex}}$  is the viscosity of a cell suspension in saline/dextran at the same  $H$  and  $\dot{\gamma}$ , divided by the viscosity of the saline/dextran solution.

Hence,  $R > 1$  implies that the presence of the dextran has reduced the relative viscosity of the suspension, while  $R < 1$  implies the dextran has increased it. Since it is particularly the cell-cell interactions that are of interest here,  $R$  is evaluated at a relatively high hematocrit,  $H = 50\% \text{ v/v}$  (similar to that of whole blood) and at a low shear rate,  $\dot{\gamma} = 0.68 \text{ sec}^{-1}$ . These values are of course arbitrary, but serve to illustrate the properties of interest.

To examine the factors which cause changes in the high relative viscosity of 50% cell suspensions in saline, the factors which have been proposed to be responsible for this high viscosity must be considered. One explanation is that as the shear rate is lowered, cellular deformation due to cell-cell collisions is reduced and the cells behave more and more like rigid cells which have higher suspension viscosities. Adding dextran to the medium increases its viscosity. This would either increase the deformability by increasing the local shear stresses around the cell, and therefore decrease the suspension viscosity, or if the the deformation due to cell-cell collisions was not dependent on shear transmitted through the medium, the relative viscosity would be unaffected. Increasing the zeta potential of the cells should have no effect in this model.

The second explanation for the high viscosity of concentrated suspensions is that intercellular collisions allow penetration and entanglement of surface structures on adjacent cells. The entanglement results in effectively a frictional interaction between the cells which dissipates energy and increases the viscosity. The entanglements are increasingly broken down at higher shear rates, so the viscosity decreases with increasing  $\dot{\gamma}$ . Adding dextran increases the zeta potential and intercellular repulsions, reduces surface interpenetrations both through these repulsions and through the coating of the cell surfaces by adsorbed polymer, and therefore reduces

the relative viscosity.

Both these proposed explanations require that the cells remain dispersed in the presence of dextran. Hence, they would apply only to suspensions for which  $R > 1$ , since Figures 6-21 to 6-24 show that all dextran suspensions with 0 aggregation have relative viscosities less than those of saline suspensions. Any correlations between  $R$  and the properties of the dextran suspensions proposed to affect the flow behavior, namely, the continuous phase viscosities and the relative zeta potentials in the presence of dextran, can be examined by plotting  $R$  against  $Z$  and  $\eta_o / \eta_{sal}$  (to render the continuous phase viscosity dimensionless). The correlations are illustrated in Figures 6-25 and 6-26 where the  $R$  vs  $\eta_o / \eta_{sal}$  and  $R$  vs  $Z$  curves are given for the systems in which no aggregation occurs. It is seen that both the correlations are quite good. Linear regression analyses of the data give regression coefficients of 0.92 and 0.91 respectively. Hence, it would seem that it is not possible to distinguish between the two proposed explanations on this basis.

In those cases in which the dextran induced aggregation in the suspensions, the arguments given above for the effect on the relative viscosity obviously have to be modified, since as stated both would predict decreased relative viscosities where increases are observed. Given that the increased relative viscosities are due to the aggregation, however, which seems relatively well established, the arguments

can still be applied to the variations of  $R$  in the dextran solutions for which  $R < 1$ . One can enquire, then, given that the suspensions are aggregated, whether the zeta potential or suspension viscosity correlates with the changes in  $R$  as the suspending medium is changed. That is, are local shear stresses proportional to  $\eta_0$  breaking down the aggregates, decreasing the relative viscosities and increasing  $R$ , or are the increased zeta potentials making the aggregates more susceptible to break down and dispersion.

Linear regression analysis between  $R$  and  $\eta_0$  indicated no correlation between these parameters (regression coefficient  $r = -0.03$ ). Furthermore, it is clear from the microscopic examinations of the suspensions, made at zero shear rate, that shear stresses are not necessary to vary the degree of aggregation of these systems. As discussed in Chapter 5, the aggregation is almost certainly a function of the relative zeta potential of the cells, since critical zeta potentials for disaggregation were found for each dextran fraction, in spite of the strong polymer-induced tendencies towards aggregation. It is not surprising, then, that no correlation is found between  $R$  and  $\eta_0$ .

Since it has been proposed that the zeta potential controls the degree of aggregation in these systems, some correlation between  $Z$  and  $R$  might be expected if indeed the degree of aggregation is being measured by this latter parameter. The absolute value of  $Z$



is not the appropriate value to use in the correlation since it has been shown previously that greater values of  $Z$  are required to disaggregate cells linked by the higher molecular weight dextrans. The effect of the molecular weight of the fraction can be normalized out, however, by dividing  $Z$  by the critical zeta potential,  $Z_{crit}$ , necessary to disaggregate the suspensions in each molecular weight fraction. In this way, differential effects of the increased strength of intercellular links associated with higher molecular weight fractions may be removed.

The correlation between  $R$  and  $Z/Z_{crit}$  for aggregated suspensions is seen from Figure 6-27 to be quite good for all molecular weights, the regression coefficient being  $r = 0.83$ . Hence, it would seem that for these aggregated suspensions the flow behavior is quite strongly affected by the zeta potential of the cells. One can observe in these systems, then, what can be considered to be in one sense an electroviscous effect.

The results and arguments outlined above are relevant to a recent publication of Chien (259) in which it is suggested that the effective cell volume is the dominant factor in the rheology of erythrocyte suspensions. Basing his suggestion on early work done on rigid, non-aggregating dilute suspensions, Chien has proposed that the relative viscosity of cell suspensions is determined only by the ratio of the effective to true particle volume,  $V_E/V_P$ . This

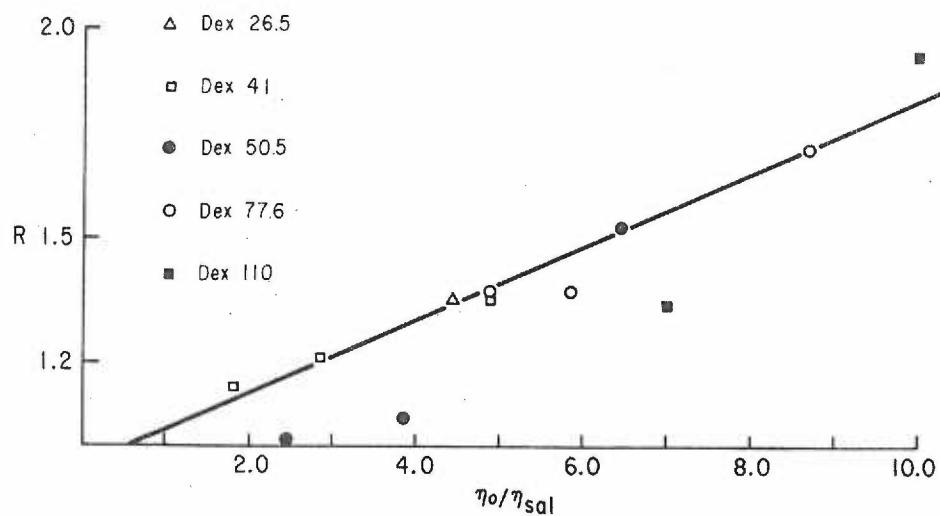


Figure 6-25.  $R$  vs.  $\eta_0/\eta_{sal}$  for disaggregated suspensions in various dextran fractions at  $H = 50$ ,  $\dot{\gamma} = 0.68 \text{ sec}^{-1}$ .

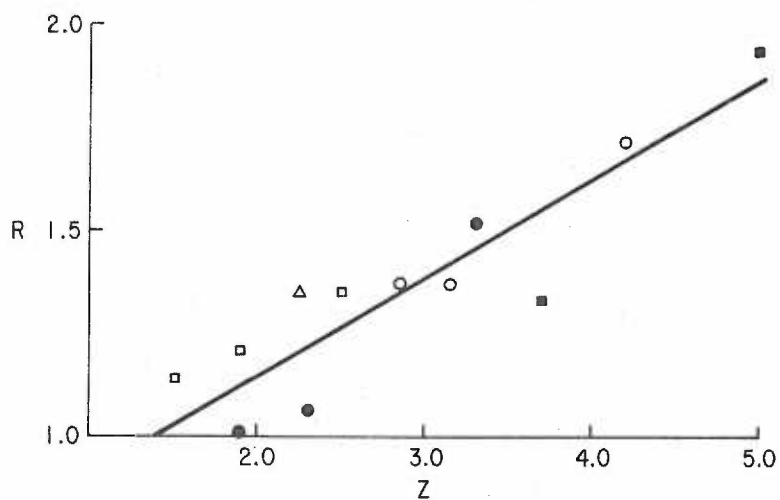


Figure 6-26

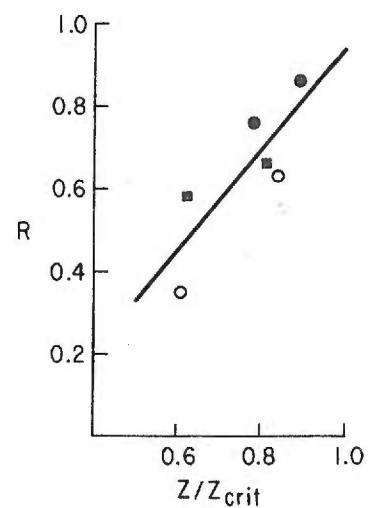


Figure 6-27

Figure 6-26.  $R$  vs.  $Z$  for disaggregated suspensions in various dextran fractions at  $H = 50$ ,  $\dot{\gamma} = 0.68 \text{ sec}^{-1}$ .

Figure 6-27.  $R$  vs.  $Z/Z_{crit}$  for aggregated suspensions in various dextran fractions at  $H = 50$ ,  $\dot{\gamma} = 0.68 \text{ sec}^{-1}$ .

parameter, in turn, varies with the axial ratio,  $R_A = \text{length}/\text{radius}$ , of the particle in suspension in such a way that increased  $R_A$ , and therefore increased assymetry, results in higher values of  $V_E/V_P$  and therefore higher values of relative viscosity. The shear dependent decrease in  $R_A$  for rouleaux subjected to increasing rates of shear is proposed to explain the shear thinning behavior of whole blood. Applying these arguments to the results of the present study, since a globular aggregate is more symmetrical than a single red cell, aggregation of the type described in this work as +++ should result in a decreased relative viscosity compared to a monodisperse suspension of equal hematocrit. Increasing the degree of aggregation from ++ (linear aggregates) to +++ (large, roughly symmetrical blobs) should likewise decrease the relative viscosities measured. Since these predictions are so clearly at variance with the results just discussed, where increased aggregation increases  $\eta/\eta_0$ , it would seem that Chien's hypothesis does not explain the rheological properties of all cell suspensions.

Although the correlations between  $R$  and  $\eta_0/\eta_{sal}$ , and  $R$  and  $Z$  were both good for the monodisperse systems at low shear rate, there is an argument that can be made in favor of the hypothesis that the decreased relative viscosities are functions of the suspending medium viscosity and not of the cellular zeta potential. The argument is based on the behavior of the aggregated suspensions at high

hematocrits. Examination of Figures 6-21 to 6-24 shows that at hematocrits greater than 50% v/v, several of the  $(\eta/\eta_0) - H$  curves for aggregated suspensions cross the saline curve. That is, even though these suspensions are heavily aggregated, at very high hematocrits their relative viscosities are lower than that of saline. Disaggregation could not have arisen from an increase in zeta potential of the cells at high cell concentrations, since  $Z$  is not a function of hematocrit. The most reasonable explanation for the observation seems to be that the extreme cellular deformation and shearing induced by close packing of the cells is sufficiently strong to break down the aggregates and deform the cells into units which flow with relatively less energy dissipation than either the aggregated cells or the cells in saline. The deformation at these very high cell concentrations and low shear rates is evidently enhanced by higher viscosity media, since the suspensions in high viscosity media have lower relative viscosities under these conditions. In this case the observed effect cannot be explained by a zeta potential argument. Thus it would seem that the decreases in relative viscosity associated with the presence of dextran in disaggregated cell suspensions are due to the elevated continuous phase viscosities.

The above evidence does not rule out the possibility that the zeta potential plays a role in the low shear viscosity of disperse cell systems. However, the analogy to the mechanism of non-Newtonian

flow in polymer solutions, on which the proposal was based, may not be a good one. The mechanism of non-Newtonian flow referred to is believed to lie in the entanglement of interacting polymer molecules (115, 260). As the fluid is sheared, entanglements are reduced both due to the shearing action, tending to separate the polymers, and due to thermal motion. On the other hand, thermal motion will also tend to cause the formation of new entanglements. If the shear rate is so high that the entanglements can be broken by shearing faster than they can reform under the influence of Brownian motion, the net number of entanglements will decrease as  $\dot{\gamma}$  increases, and the viscosity will fall. It was proposed that in an analogous manner the diffuse glycoproteins on the surfaces of colliding cells could interpenetrate and entangle, ultimately producing the same shear thinning behavior. The difficulty with this analogy is the range of shear rates over which the shear dependence is seen. Strong shear dependence is found for erythrocytes in saline only below  $100 \text{ sec}^{-1}$ , while the shear thinning region for polymer melts appears to be somewhat higher than this (126). Bueche's theory predicts (correctly for polymer melts) that shear-thinning commences when  $\dot{\gamma}\eta_0 M > T \times 10^8$ , where  $M$  is the molecular weight of the entangling species and  $T$  is the absolute temperature. Hence, if the surface region is highly viscous with  $\eta_0 \sim 1 \text{ poise}$  and the molecular species have  $M \sim 10^5$ , shear thinning will not commence until  $\dot{\gamma} > 3 \times 10^5 \text{ sec}^{-1}$ . It would seem,

then, that the shear rates at which non-Newtonian flow is pronounced in cell suspensions are orders of magnitude lower than the entanglement theory would predict. On this basis, entanglement might seem to be an inappropriate mechanism for the shear thinning observed in concentrated red cell/saline suspensions. If such entanglement is not significant, there would seem to be no obvious way in which electrostatic interactions could affect the flow behavior in these systems. The cellular zeta potential, therefore probably does not act to decrease the relative viscosity of dispersed erythrocyte suspensions in the manner originally proposed.

One cannot rule out the possibility that the zeta potential affects the flow behavior in these systems by some mechanism which has not yet been considered. The correlation in Figure 6-26 may in fact indicate a true causal relationship between  $\eta/\eta_0$  and  $Z$ . However, an explanation for the possibly fortuitously high regression coefficient in the  $R - Z$  plot can be found in the definition of  $Z$ . The relative zeta potential was defined as  $Z = (\eta U)_{\text{dex}} / (\eta U)_{\text{sal}}$ , and hence is proportional to  $\eta_{\text{dex}} / \eta_{\text{sal}}$ , the ratio of the continuous phase viscosities, as well as to the apparent mobility ratio ( $\eta_0$  is written as  $\eta_{\text{dex}}$  here for clarity). It was observed experimentally that  $U_{\text{dex}} / U_{\text{sal}}$  was roughly independent of molecular weight for a given dextran concentration. At least as far as the molecular weight dependence is concerned, then, the correlations of  $R$  with  $Z$  and

$\eta_{\text{dex}}/\eta_{\text{sal}}$  will be identical, since the variation in  $Z$  is due only to variations in  $\eta_{\text{dex}}/\eta_{\text{sal}}$ . The decreases in  $U_{\text{dex}}/U_{\text{sal}}$  with increasing concentration must be such that the correlation is maintained as the concentration is varied.

Considering only variations in  $\eta/\eta_0$  at constant dextran concentration makes this relationship more obvious. The low shear rate relative viscosities of suspensions all made 10% w/v in the various dextran fractions are shown in Figure 6-28. The correlations between  $R$  and  $Z$  or  $R$  and  $\eta_{\text{dex}}/\eta_{\text{sal}}$  are extremely good for this data, both having regression coefficients of  $r = 0.99$ . In this case, the high correlation of  $R$  with  $Z$  is entirely due to the variation in  $\eta_{\text{dex}}/\eta_{\text{sal}}$ . The correlation of  $R$  with  $Z$  in Figure 6-26, then, need not necessarily be taken as evidence for a connection between the relative viscosity of the suspensions and the cellular zeta potential. The satisfactory explanation of the low shear behavior in terms of the suspending media viscosities, the apparent inapplicability of the proposed mechanism of this behavior in terms of the cellular zeta potential, and the explanation of the  $R$ - $Z$  correlation given seem to indicate that there is no necessity at present to invoke cellular zeta potentials when explaining the low shear flow characteristics of the monodisperse cell suspensions studied.

The arguments presented above have considered the interactions among the elements of the suspensions believed to be important in

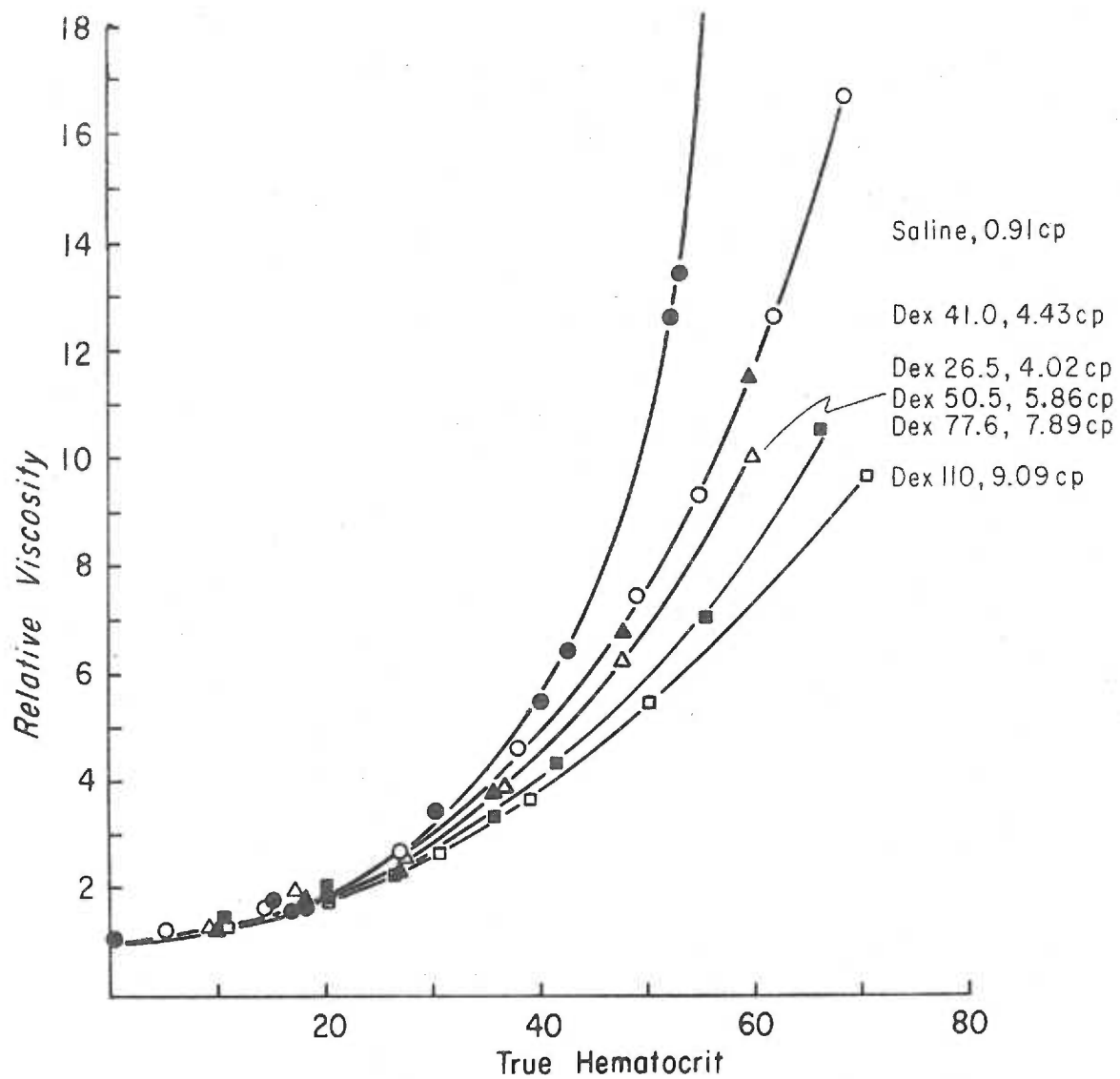


Figure 6-28. Relative viscosity vs. hematocrit at  $\dot{\gamma} = 0.68 \text{ sec}^{-1}$  for erythrocytes in 10% dextran solutions in saline/EDTA.



determining their viscous characteristics at low rates of shear. It was shown that at  $\dot{\gamma} = 0.68 \text{ sec}^{-1}$  the presence and degree of aggregation in the samples, determined partly by the zeta potential, were important factors in their rheological behavior. At higher shear rates, however, the aggregation present at low and zero rates of shear can be expected to be broken down by the local shear stresses in the suspensions. Once aggregates are broken down and the cells rendered monodisperse, it would appear that the relative viscosity, at fixed  $H$  and  $\dot{\gamma}$ , is determined only by the viscosity of the suspending medium (assuming the membrane rigidity remains unchanged).

The relative viscosities of the saline/EDTA/dextran suspensions described above are given at an intermediate ( $\dot{\gamma} = 17 \text{ sec}^{-1}$ ) and high ( $\dot{\gamma} = 680 \text{ sec}^{-1}$ ) shear rate in Figures 6-29 to 6-36. It is seen, as anticipated from the behavior of plasma suspensions (152), that even at the relatively low shear rate of  $\dot{\gamma} = 17 \text{ sec}^{-1}$  none of the suspensions exhibit relative viscosities greater than that of the saline suspensions at any hematocrit. In almost all cases, the relative viscosity is lower, the higher the suspending medium viscosity. This correlation is more apparent in Figure 6-37 where the parameter  $R$ , calculated at  $H = 50$  and  $\dot{\gamma} = 17 \text{ sec}^{-1}$ , is again plotted as a function of the suspending medium viscosity relative to saline. It is seen that the data fall quite nicely on a smooth curve which is

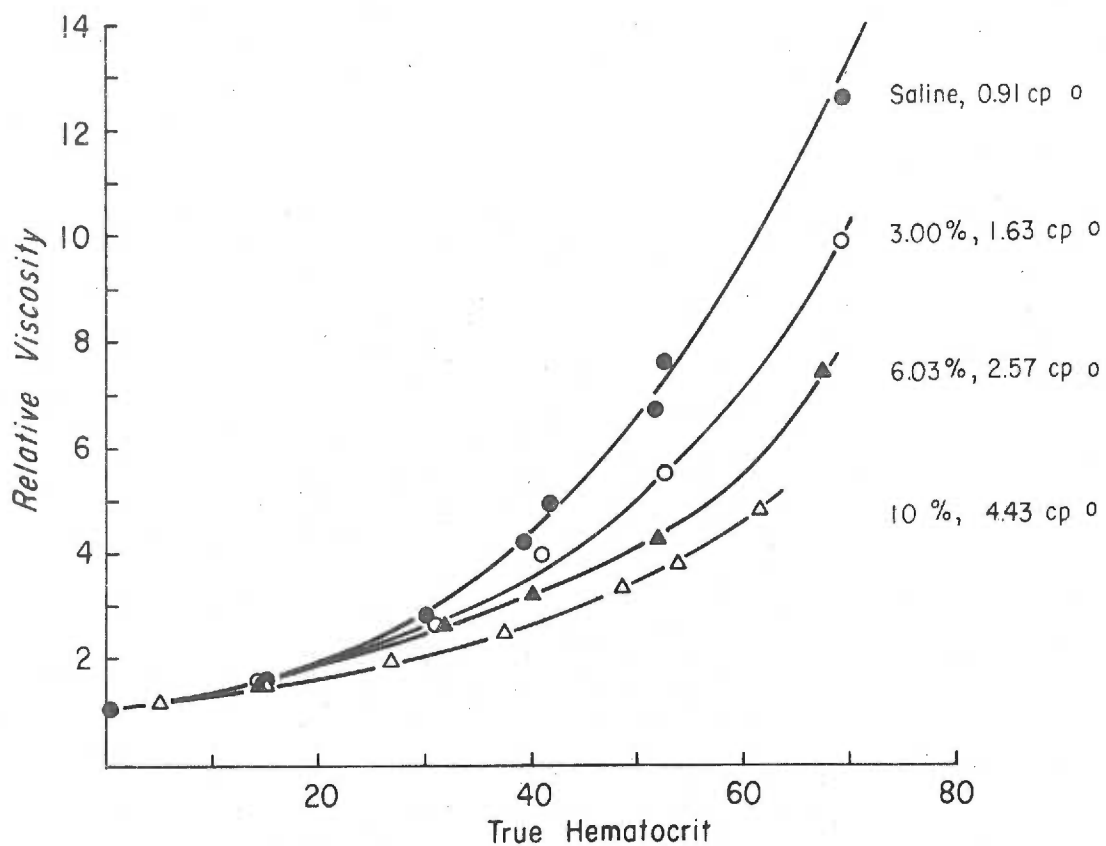


Figure 6-29. Relative viscosity vs. hematocrit at  $\dot{\gamma} = 17 \text{ sec}^{-1}$  for erythrocytes in saline/EDTA/dextran 4l.

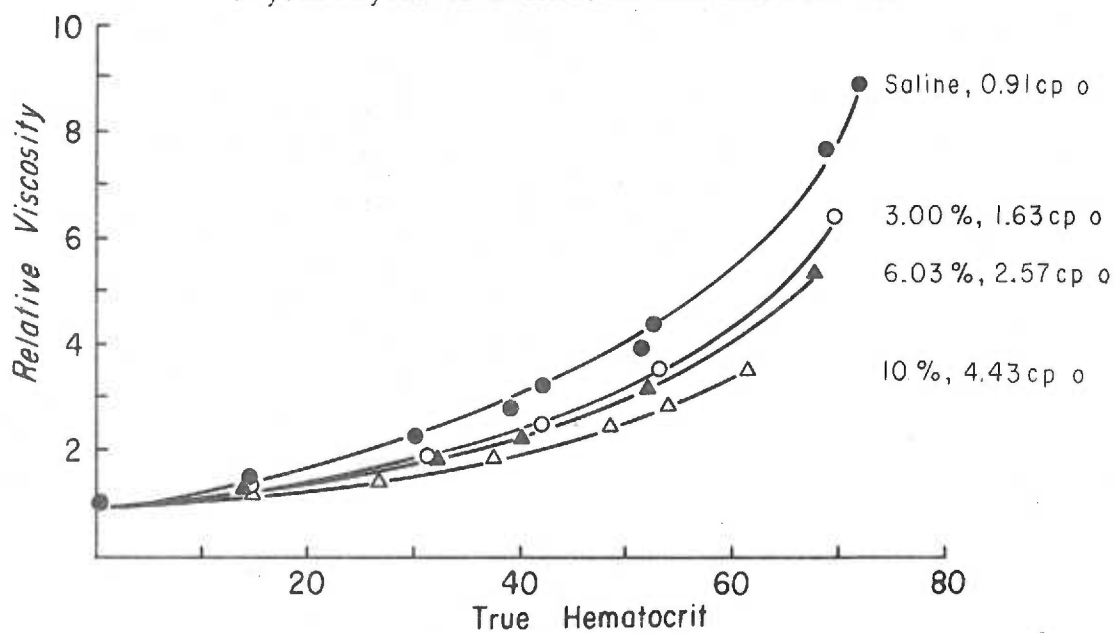


Figure 6-30. Relative viscosity vs. hematocrit at  $\dot{\gamma} = 680 \text{ sec}^{-1}$  for erythrocytes in saline/EDTA/dextran 4l.

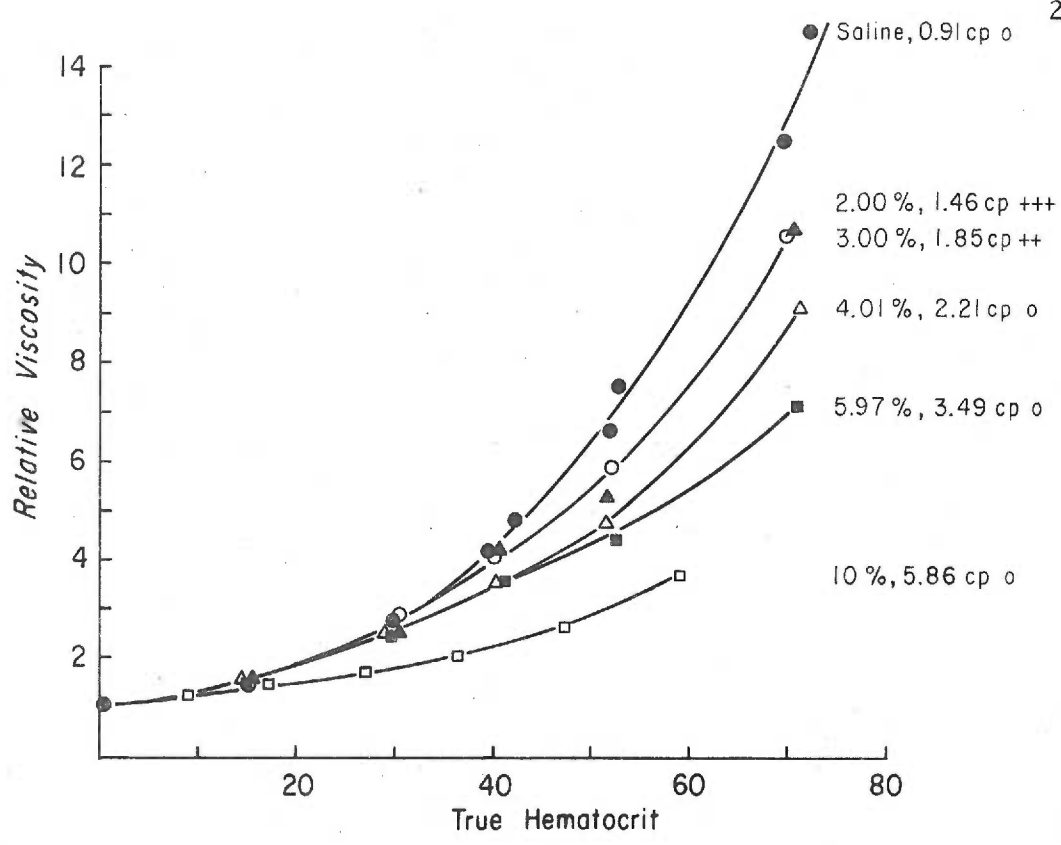


Figure 6-31. Relative viscosity vs. hematocrit at  $\dot{\gamma} = 17 \text{ sec}^{-1}$  for erythrocytes in saline/EDTA/dextran 50.5.

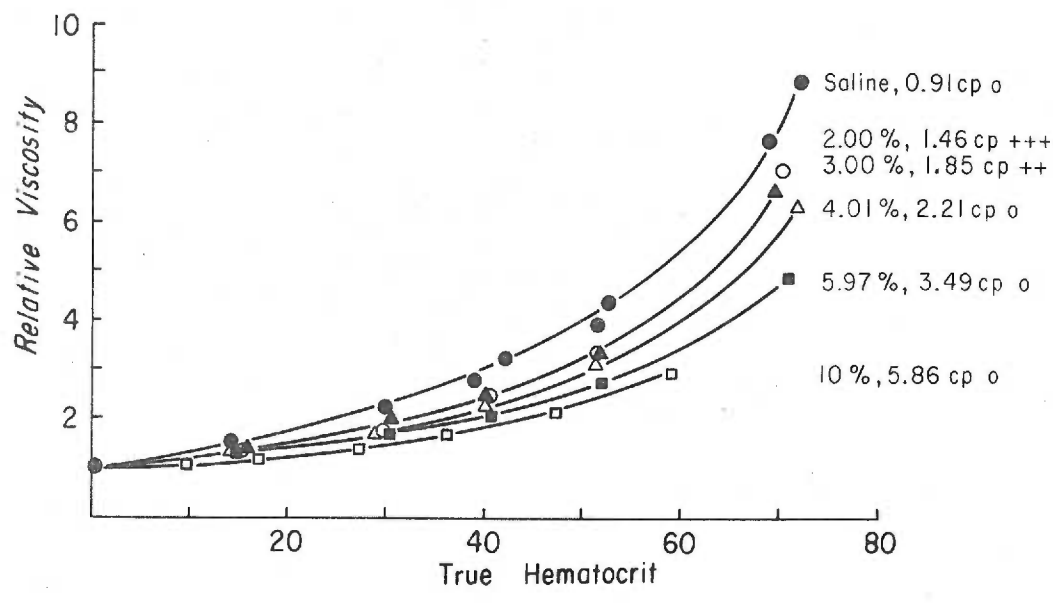


Figure 6-32. Relative viscosity vs. hematocrit at  $\dot{\gamma} = 680 \text{ sec}^{-1}$  for erythrocytes in saline/EDTA/dextran 50.5.

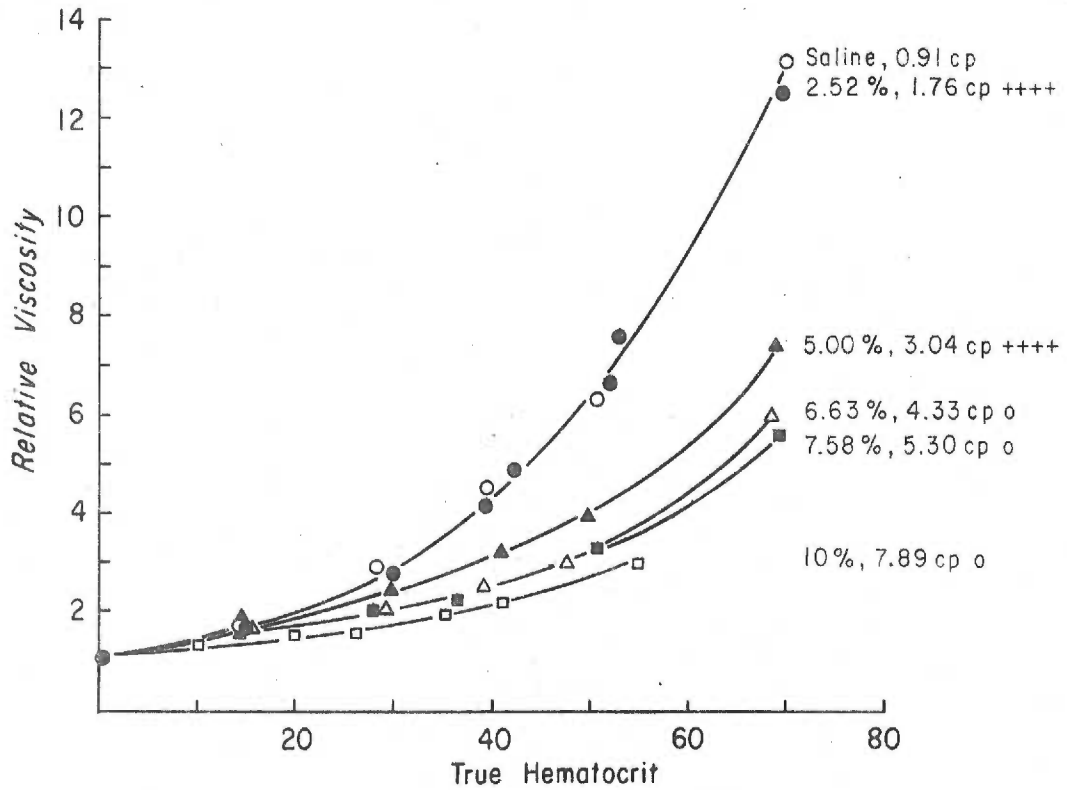


Figure 6-33. Relative viscosity vs. hematocrit at  $\dot{\gamma} = 17.1 \text{ sec}^{-1}$  for erythrocytes in saline/EDTA/dextran 77.6.

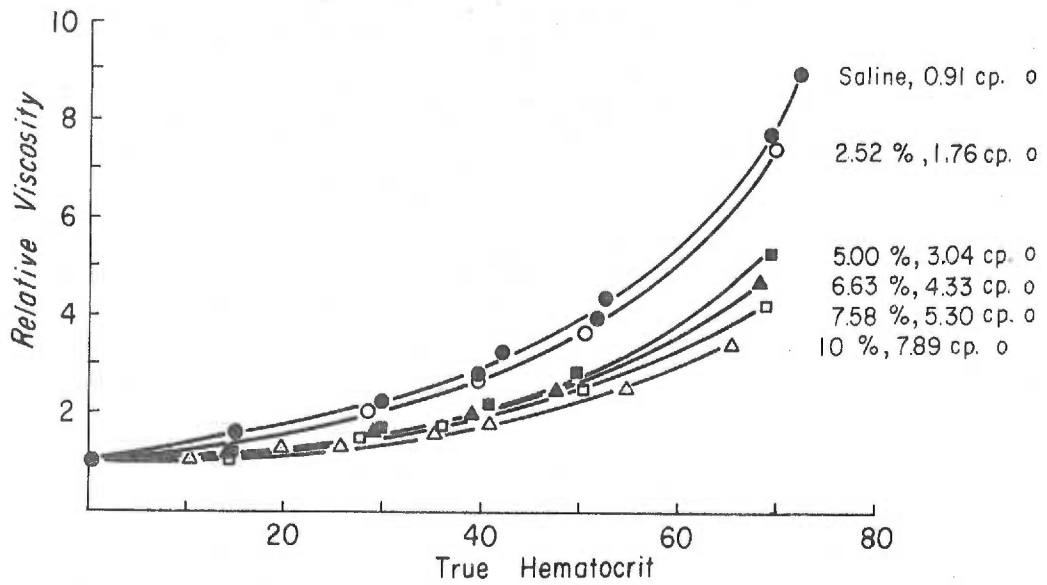


Figure 6-34. Relative viscosity vs. hematocrit at  $\dot{\gamma} = 680 \text{ sec}^{-1}$  for erythrocytes in saline/EDTA/dextran 77.6.

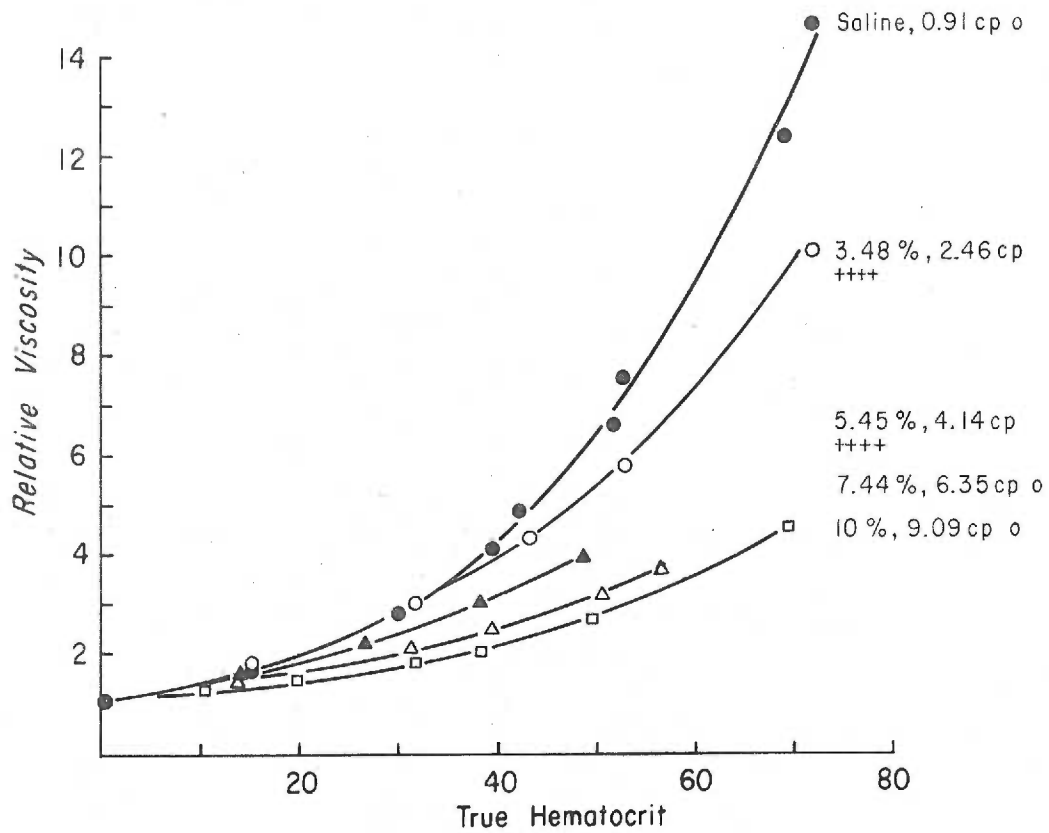


Figure 6-35. Relative viscosity vs. hematocrit at  $\dot{\gamma} = 17.1 \text{ sec}^{-1}$  for erythrocytes in saline/EDTA/dextran 110.

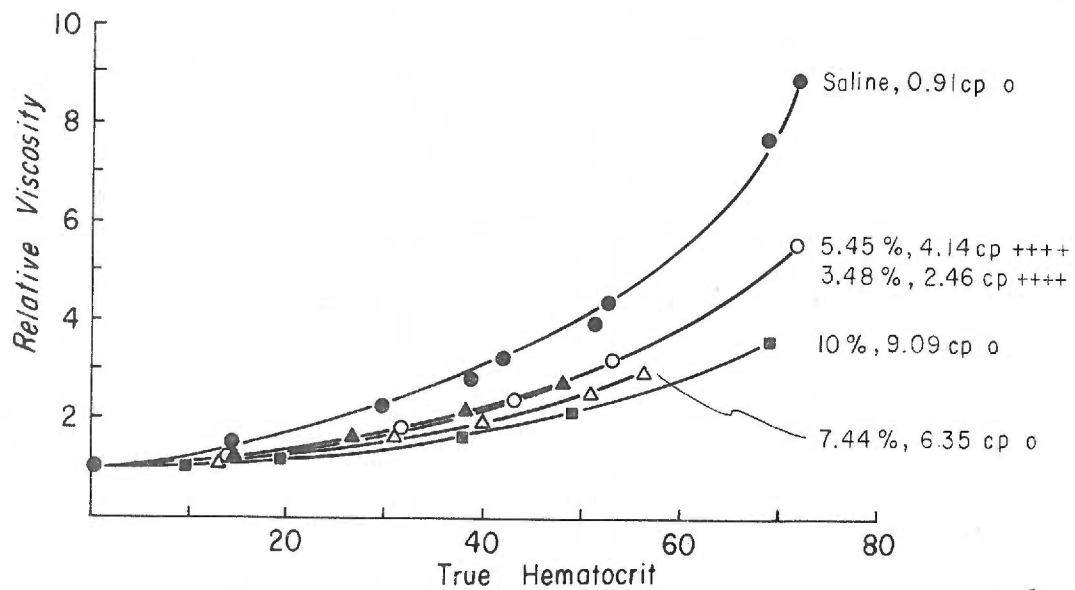


Figure 6-36. Relative viscosity vs. hematocrit at  $\dot{\gamma} = 680 \text{ sec}^{-1}$  for erythrocytes in saline/EDTA/dextran 110.

essentially linear over most of the viscosity range. There is some indication of a plateau at high suspension viscosities, however.

The decreases in relative viscosity of all the suspensions in dextran are even more evident at  $\dot{\gamma} = 680 \text{ sec}^{-1}$ . The concentration dependence of  $\eta/\eta_0$  is also much weaker at this high shear rate. Again, the decreases below the saline curve are more pronounced for the more viscous suspending media, although the differences do not appear to be as great as those seen at  $\dot{\gamma} = 17 \text{ sec}^{-1}$ . Another point of divergence between the high and intermediate shear rate curves is found in the concentration dependence of the relative viscosity difference between the saline and dextran suspensions. At  $\dot{\gamma} = 680 \text{ sec}^{-1}$  the dextran suspensions have a lower  $\eta/\eta_0$  than the saline suspensions at all hematocrits, while at  $\dot{\gamma} = 17 \text{ sec}^{-1}$  the decrease is seen in some of the samples only at high cell concentrations.

The dependence of the parameter  $R$  on  $\eta_{\text{dex}}/\eta_{\text{sal}}$  at  $H = 50$  and  $\dot{\gamma} = 680 \text{ sec}^{-1}$  is given in Figure 6-38. It is seen that there is much less variation in  $R$  than at  $\dot{\gamma} = 17 \text{ sec}^{-1}$ . The curve seems to level off at high values of the continuous phase viscosity. These tendencies of the  $R - \eta_{\text{dex}}/\eta_{\text{sal}}$  curves to plateau, implying that only a finite relative decrease in  $\eta/\eta_0$  may be achieved at a given shear rate no matter how great the suspending medium viscosity, are illustrated in the plots of Figure 6-39 and 6-40. These figures give the relative viscosities of all the suspensions in 10% dextran, as

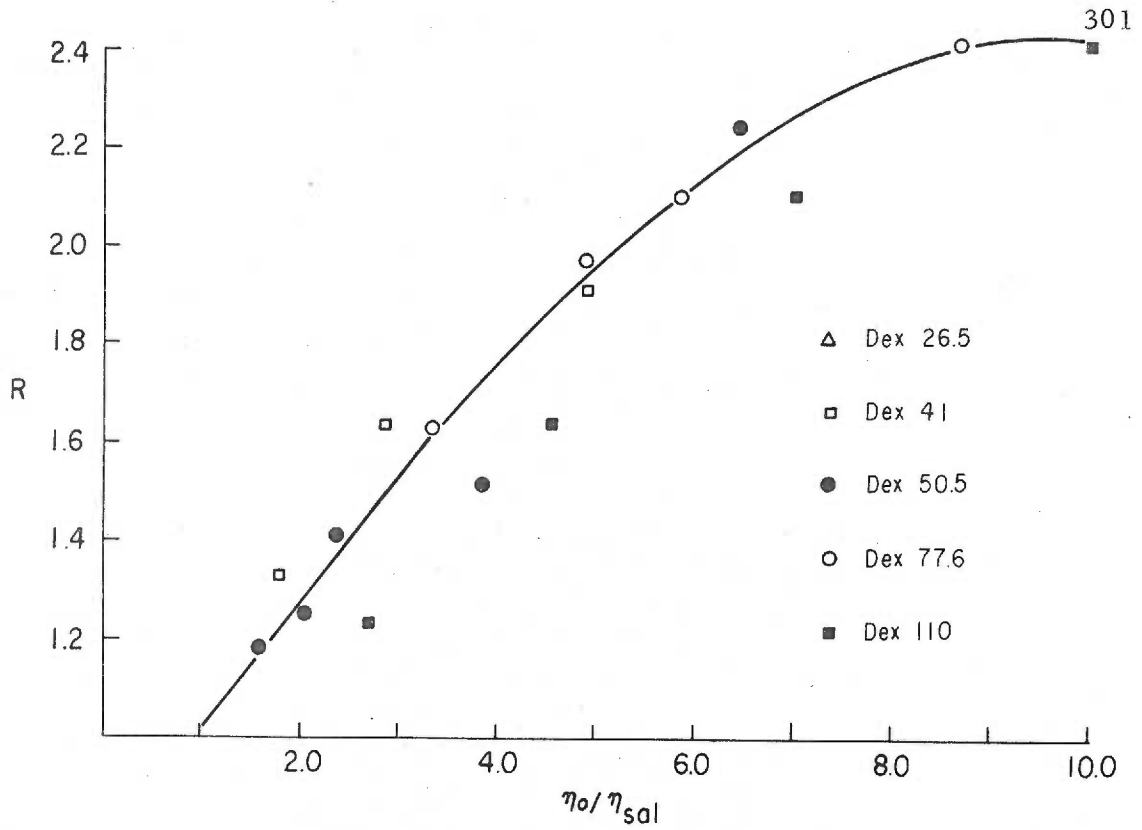


Figure 6-37.  $R$  vs  $\eta_0/\eta_{sal}$  for disaggregated suspensions in various dextran fractions at  $H = 50$ ,  $\dot{\gamma} = 17 \text{ sec}^{-1}$ .

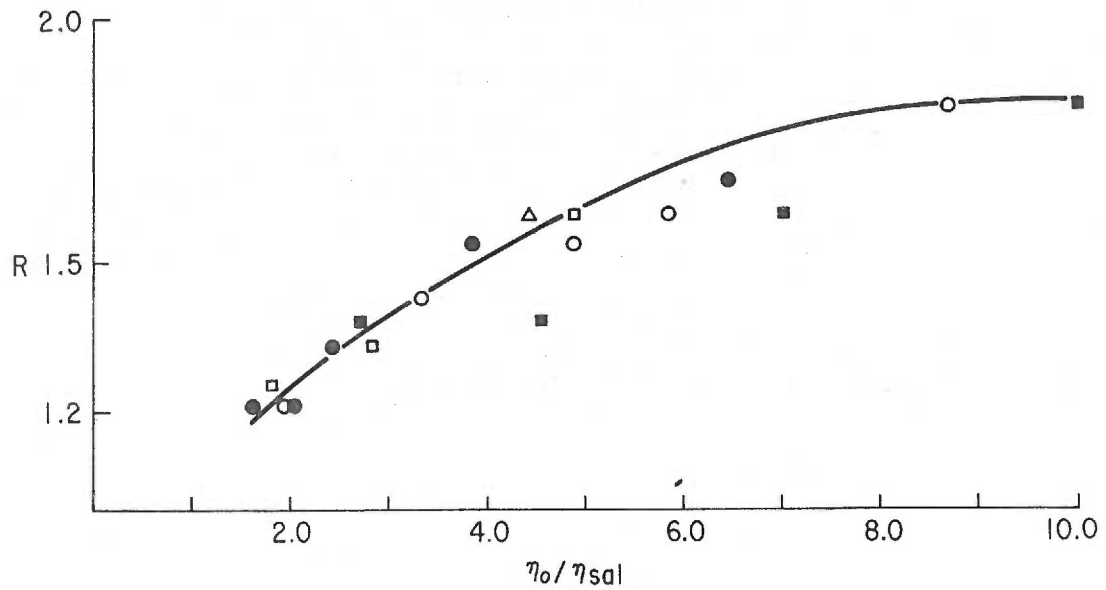


Figure 6-38.  $R$  vs.  $\eta_0/\eta_{sal}$  for disaggregated suspensions in various dextran fractions at  $H = 50$ ,  $\dot{\gamma} = 680 \text{ sec}^{-1}$ .

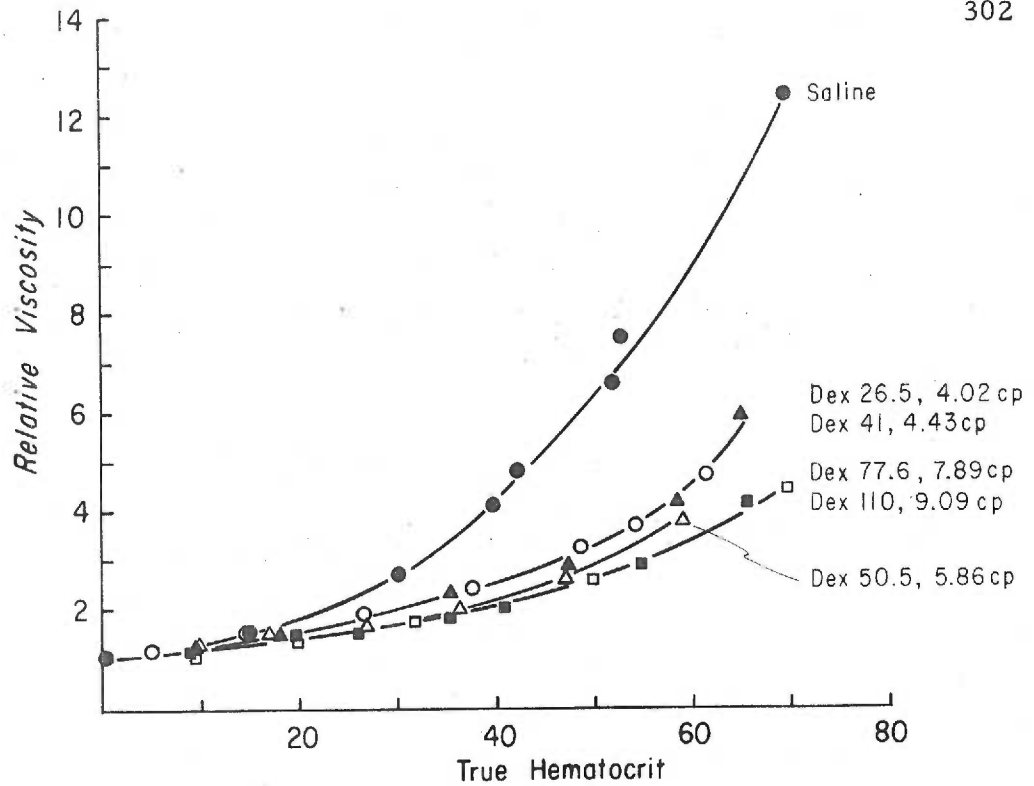


Figure 6-39. Relative viscosity vs. hematocrit at  $\dot{\gamma} = 17 \text{ sec}^{-1}$  for erythrocytes in 10% dextran solutions in saline/EDTA.

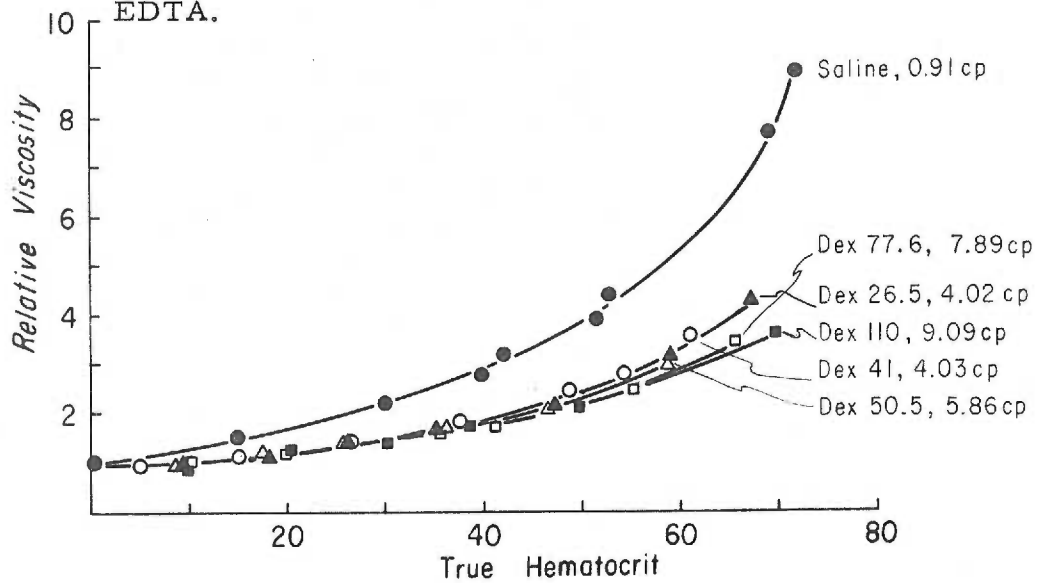


Figure 6-40. Relative viscosity vs. hematocrit at  $\dot{\gamma} = 680 \text{ sec}^{-1}$  for erythrocytes in 10% dextran solutions in saline/EDTA.



a function of  $H$ , at shear rates of 17 and 680  $\text{sec}^{-1}$  respectively.

It is apparent from these last two figures that for suspensions which are completely disaggregated at all shear rates there is little dependence of  $\eta/\eta_0$  on the continuous phase viscosity, even at shear rates as low as 17  $\text{sec}^{-1}$ .

All of the relative viscosity data at intermediate and high shear rates seems to be consistent with the following qualitative explanation. At high shear rates all aggregates are broken down and the dispersed cells are deformed by shear stresses imparted to them through the medium. Deformations due to cell-cell interactions are of little importance here, as may be seen by the weak hematocrit dependence of  $\eta/\eta_0$ , and the fact that the high shear rate dextran curves fall below the saline curve at even very low cell concentrations. The apparent plateau in Figure 6-38, reflecting the lack of dependence of the relative viscosity on  $\eta_0$  evident in Figure 6-40, suggests that the deformation induced by local shear stresses around the cells reaches a maximum. It has been reported (231) that the maximally deformed configuration of a red cell at high shear stress is an elongated prolate ellipsoid. Under these conditions, the membrane has been observed to rotate around the cell contents in a tank tread movement. Presumably such rotation is occurring under the conditions described above for which  $\eta/\eta_0$  is independent of  $\eta_0$ .

At the intermediate shear rate of 17  $\text{sec}^{-1}$ , the relative viscosity

of the suspensions is apparently subject to the influence of cellular aggregation, cellular deformation induced by cell-cell collisions, and cellular deformation due only to cell-medium interactions. In Figure 6-33, for instance, the relative viscosity of the 2.52% dextran 77.6 suspension is indistinguishable from that of saline, in spite of the fact that the continuous phase viscosity is roughly twice that of saline. The aggregation present in this suspension at low shear rates must therefore still be present to some degree, or the cellular deformation attendant with the higher medium viscosity would cause a reduced relative viscosity. In some of the dextran 41 suspensions, Figure 6-29, the presence of cellular deformation induced by cellular collisions is indicated. The 3% dextran 41 sample, for instance, is not aggregated at any shear rate, yet it is only at hematocrits greater than about 25% v/v that a decrease in  $\eta/\eta_0$  is seen relative to saline. The hematocrit dependence of the relative viscosity difference here indicates that deformation resulting from cell-cell contact is an operative factor in the flow behavior. Finally, it is seen that in 10% dextran solutions cellular deformation due only to the applied shear stress is a contributing factor to the relative viscosities at  $17 \text{ sec}^{-1}$ , since the differences in  $\eta/\eta_0$  are apparent at all hematocrits. The presence of interacting cells is not necessary to produce the relative viscosity decreases observed in these samples. As might be expected, then, the factors which dominate the rheological behavior of the

suspensions at low and high rates of shear all contribute to the flow characteristics at intermediate shear rates.

### Summary

The viscosities of washed human erythrocytes suspended in saline solutions containing various concentrations of dextrans of differing molecular weights have been measured as functions of hematocrit and shear rate. The results have been analyzed in terms of the variations in relative viscosities of the suspensions as functions of hematocrit at low, intermediate and high rates of shear. In those systems in which the cells were aggregated, the rheological behavior at low shear rate was shown to be controlled to some extent by the electrostatic interactions between the cells. For disaggregated systems, the low shear flow characteristics probably do not depend on the cellular zeta potentials. Rather, cellular deformations which result from intercellular collisions and which are increased in more viscous suspending media are probably the dominant factors in low shear rheology of monodisperse suspensions. At high rates of shear, cellular deformation induced by cell-medium interactions is the most important determinant of the relative viscosity. At intermediate rates of shear, cellular aggregation, cell deformation due to intercellular interactions, and deformation due to cell-medium interactions are all indicated as playing a role in flow behavior of the systems studied.

## CHAPTER 7

## CONCLUSIONS

1. The zeta potentials of all cells tested were increased when measured in the presence of the neutral polymers used in this study.
2. The increased zeta potentials measured could not be due to bulk properties of the polymer solutions, such as the dielectric constant.
3. Dextran solutions of up to 10% w/v concentration have a dielectric constant indistinguishable from that of water at measurement frequencies down to 10 kHz.
4. The zeta potential increase is not restricted to particles susceptible to interfacial rearrangement. Exposure of charge groups by adsorbed polymer cannot in general be the cause of the phenomenon.
5. The solubility of NaCl is significantly higher per ml of water in the presence of dextran than in its absence, suggesting that NaCl is effectively bound to the polymer at saturating concentrations.
6. The increased relative zeta potential can not be due to anion adsorption to a layer of polymer adsorbed to the cell.
7. Dextran adsorbs to human erythrocytes from simple salt solutions. Under the conditions of measurement, the adsorption was found to be strongly concentration dependent between  $6.8 \times 10^{-6} \text{ gm ml}^{-1}$

and  $0.15 \text{ gm ml}^{-1}$ , showing no evidence of saturation. The binding of dextran to the cell surface was apparently quite weak, since the equivalent of only about 2 close-packed monolayers was adsorbed at a dextran concentration of 10% w/v. If the dextran uptake was actually measured under equilibrium conditions, the isotherm obtained is unique in its concentration dependence.

8. At least 99.9% of the interstitial fluid in a normal erythrocyte pellet can be removed by spinning the pellet at  $3.68 \times 10^5 \text{ xg}$  for 30 min under a layer of organic phase whose density is between that of the cells and the medium in which they are suspended.
9. The presence of dextran stabilizes the normal human erythrocyte between pH 9 and 11.5 with respect to the reversibility of electrophoretic measurements made in this pH region. The range of acid stability is unaffected by the presence of dextran.
10. Dextran may be able to displace anions adsorbed at the surface of quartz particles.
11. Red cells obtained from ACD blood stored for 48 days at  $4^\circ \text{C}$  apparently retain adsorbed polyethylene glycol more tenaciously than do fresh cells.
12. The relative zeta potential of red cells in dextran does not depend on the monovalent anion present, but it is significantly higher when  $(\text{C}_3\text{H}_7)_4\text{N}^+$ , rather than  $\text{Na}^+$ ,  $\text{Li}^+$  or  $(\text{CH}_3)_4\text{N}^+$ , is the cation in the ionic suspending medium.

13. A simplified thermodynamic treatment is given of the effect a concentrated neutral surface phase would have on the chemical potentials of counterions in a double layer. This analysis predicts that the presence of neutral polymers adsorbed to a charged surface should increase the thickness of the counterion double layer adjacent to that surface, thus increasing the zeta potential. The electrokinetic data obtained for erythrocytes suspended in neutral polymer solutions fit the equations derived from the model. The proposed model gives a reasonable explanation of the observed phenomenon.
14. The presence of an impermeable, rigid neutral layer external to a fixed charge system is impossible to detect electrokinetically.
15. The dependence on polymer concentration of the relative zeta potential predicted by the proposed model is supported by the  $H^3$ -dextran uptake measurements.
16. Information regarding the density and depth of the neutral polymer layer adsorbed to cells and particles may be obtained by applying the equations developed to electrokinetic data for such systems. The total depth and the depth of the free draining portion of the adsorbed layer may be obtained from this treatment. There would appear to be no other way to obtain such data on particles of this size.
17. Layers of neutral polymers adsorbed to cells are completely or

partially free draining at the shear rates found in cell electrophoresis measurements.

18. The depth of the layers of dextran adsorbed from 7.5% solutions to erythrocytes as estimated electrokinetically increases linearly with the square root of the dextran molecular weight between  $\overline{M}_n = 26,000$  and  $\overline{M}_n = 114,000$ .
19. Neutral polymers of sufficiently high molecular weights induce cellular aggregation.
20. The mechanism of dextran-induced aggregation of cells is probably through the simultaneous adsorption of individual molecules to adjacent cell surfaces.
21. The forces responsible for dextran induced erythrocyte aggregation can be stronger than those which maintain normal red cell shape.
22. The presence of adsorbed layers of neutral polymers should increase the electrostatic repulsions between charged surfaces to which they are adsorbed.
23. Above a critical zeta potential for each dextran fraction, cells aggregated by polymer bridging are disaggregated by the increased electrostatic repulsions associated with the presence of adsorbed polymer. This is believed to be the first example reported of this mechanism of suspension stabilization by neutral polymers.

24. The relative viscosities of normal red cell suspensions aggregated by dextrans have been shown to correlate well with the zeta potentials of the cells. In these suspensions, electrostatic interactions appear to be a significant determinant of flow behavior at low rates of shear.
25. The flow properties of monodisperse red cell suspensions probably do not depend on the cellular zeta potentials.
26. At low shear rates cellular deformation which results from intercellular collisions, and which is increased in more viscous suspending media is probably the dominant factor in the rheology of concentrated non-aggregated cell suspensions. The decreased relative viscosities of normal red cells in high concentrations of dextran seem to be due to such deformation.
27. At high shear rates, cellular deformation induced by cell-medium interactions is the most important determinant of the relative viscosities of normal erythrocyte suspensions.
28. At intermediate rates of shear, cellular aggregation, cell deformation due to intercellular collisions, and deformation due to cell-medium interactions all appear to affect the rheological properties of the systems studied.
29. Chien's hypothesis, that the effective cell volume is the major determinant in the flow behavior of erythrocyte suspensions, cannot explain the results obtained in this work.



## REFERENCES

1. Ponder, E. Revêtement des plaquettes humaines et des globules rouges par les dextrans. *Revue d'Hématologie*, 1957. 12, 11-15.
2. Goodwin, J.W., Seaman, G.V.F., & Brooks, D.E. Deformation and aggregation in the rheology of erythrocyte suspensions. *Bibl. Anat.*, 1969. No. 10, 124-131.
3. Von Smoluchowski, M. In Graetz (Ed.) *Handbuch der Elektrizität und des magnetismus*. Leipzig: Barth, 1914. 2, 366.
4. Overbeek, J. Th. Electrokinetic phenomena. In H.R. Kruyt (Ed.) *Colloid science*. Vol. 1. Amsterdam: Elsevier, 1952. (pages 194-243)
5. Abramson, H.A., Moyer, L.S., & Gorin, M.H. *Electrophoresis of proteins and the chemistry of cell surfaces*. New York: Hafner, 1964. (pages 105-142)
6. Davies, J.T., & Rideal, E.K. *Interfacial phenomena*. New York: Academic Press, 1963. (pages 108-151)
7. Shaw, D.J. *Electrophoresis*. London: Academic Press, 1969. (pages 4-15)
8. Whitmer, R.M. *Electromagnetics* (2nd Ed.) Englewood Cliffs, N.J.: Prentice-Hall, 1962. (page 42)
9. Lyklema, J., & Overbeek, J. Th. G. On the interpretation of electrokinetic potentials. *J. Coll. Sci.*, 1961. 16, 501-512.
10. Stigter, D. On the viscoelectric effect in colloidal solutions. *J. Phys. Chem.*, 1964. 68, 3600-3602.
11. Hunter, R.J. The interpretation of electrokinetic potentials. *J. Coll. Interface Sci.*, 1966. 22, 231-239.
12. Henry, D.C. The cataphoresis of suspended particles. Part I. The equation of cataphoresis. *Proc. Roy. Soc. (London)*, 1931. A133, 106-129.

13. Carstensen, E. L., Fuhrmann, G. R., Smearing, R. W., & Klein, L. A. The influence of conductivity on the electrophoretic mobility of red blood cells. *Biochim. Biophys. Acta*, 1968. 156, 394-402.
14. Morrison, F. A., Jr. Electrophoresis of a particle of arbitrary shape. *J. Coll. Interface Sci.*, 1970. 34, 210-214.
15. Gouy, G. L. Constitution of the electric charge at the surface of an electrolyte. *J. Phys.*, 1910. 9, 457-467.
16. Chapman, D. L. A contribution to the theory of electrocapillarity. *Phil. Mag. (6)*, 1913. 25, 475-481.
17. Coddington, E. A. An introduction to ordinary differential equations. Englewood Cliffs, N.J.: Prentice-Hall, 1961. (page 50)
18. Langmuir, I. The role of attractive and repulsive forces in the formation of tactoids, thixotropic gels, protein crystals and coacervates. *J. Chem. Phys.*, 1938. 6, 873-93.
19. Derjaguin, B. Repulsive forces between charged colloid particles and the theory of slow coagulation and stability of lyophobic sols. *Trans. Far. Soc.*, 1940. 36, 203-215.
20. Overbeek, J. Th. The interaction between colloidal particles. In H. R. Kruyt (Ed.) *Colloid sciences*. Vol. 1. Amsterdam: Elsevier, 1952. (page 255)
21. Seaman, G. V. F., & Heard, D. H. The surface of the washed human erythrocyte as a polyanion. *J. Gen. Physiol.*, 1960. 44, 251-268.
22. Mitchell, P. The osmotic barrier in bacteria. In A. A. Miles & N. W. Pirie (Eds.) *The nature of the bacterial surface*. Oxford: Blackwell, 1949. (pages 55-75)
23. Heard, D. H., & Seaman, G. V. F. The influence of pH and ionic strength on the electrokinetic stability of the human erythrocyte membrane. *J. Gen. Physiol.*, 1960. 43, 635-654.
24. Haydon, D. A. The surface charge of cells and some other small particles as indicated by electrophoresis. I. The zeta potential-surface charge relationships. *Biochim. Biophys. Acta.*, 1961. 50, 450-457.

25. Haydon, D. A. , & Seaman, G. V. F. An estimation of the surface ionogenic groups of the human erythrocyte and of Escherichia coli. Proc. Roy. Soc. (London), 1962. B156, 533-549.
26. Haydon, D. A. The electrical double layer and electrokinetic phenomena. In J. F. Danielli, K. G. A. Pankhurst, and A. C. Riddiford (Eds.) Recent progress in surface science. Vol. 1. New York: Academic Press, 1964. (pages 94-158)
27. Brinton, C. C. , Jr. , & Lauffer, M. A. The electrophoresis of viruses, bacteria, and cells, and the microscope method of electrophoresis. In M. Bier, (Ed.) Electrophoresis. New York: Academic Press, 1959. (pages 427-492)
28. Seaman, G. V. F. , & Pethica, B. A. A comparison of the electrophoretic characteristics of the human normal and sickle erythrocyte. Biochem. J. , 1964. 90, 573-578.
29. Tenforde, T. Microelectrophoretic studies on the surface chemistry of erythrocytes. In T. Hayes (Ed.) Advances in biological and medical physics. Vol. 13. New York: Academic Press, 1970. In Press.
30. James, A. M. The electrochemistry of the bacterial surface. In J. A. V. Butler & B. Katz (Eds.) Progress in biophysics and biophysical chemistry. London: Pergamon Press, 1957. 8, 95-142.
31. Ambrose, E. J. Electrophoretic behaviour of cells. In J. A. V. Butler & H. E. Huxley (Eds.) Progress in biophysics and molecular biology. Oxford: Pergamon, 1966. 16, 243-265.
32. Ambrose, E. J. (Ed.) Cell electrophoresis. London: J. & A. Churchill, 1965.
33. Haydon, D. A. , & Seaman, G. V. F. Electrokinetic studies on the ultrastructure of the human erythrocyte. I. Electrophoresis at high ionic strengths - the cell as a polyanion. Arch. Biochem. Biophys. , 1967. 122, 126-136.
34. Heard, D. H. , & Seaman, G. V. F. The action of lower aldehydes on the human erythrocyte. Biochim. Biophys. Acta, 1961. 53, 366-374.

35. Cook, G. M. W., Heard, D. H., & Seaman, G. V. F. Sialic acids and the electrokinetic charge of the human erythrocyte. *Nature*, 1961. 191, 44-47.
36. Eylar, E. H., Madoff, M. A., Brody, O. V., & Oncley, J. L. The contribution of sialic acid to the surface charge of the erythrocyte. *J. Biol. Chem.*, 1962. 237, 1992-2000.
37. Furchgott, R. L., & Ponder E. Electrophoretic studies on human red blood cells. *J. Gen. Physiol.*, 1941. 24, 447-457.
38. Silberberg, A. The adsorption of flexible macromolecules. Part II. The shape of the adsorbed molecule; the adsorption isotherm surface tension, and pressure. *J. Phys. Chem.*, 1962. 66, 1884-1907.
39. Rowland, F., Bulas, R., Rothstein, E., & Eirich, F. R. Structure of macromolecules at liquid-solid interfaces. In *Chemistry and physics of interfaces*. Washington, D. C.: American Chemical Society Publications, 1965. (pages 110-116)
40. Hughes, R. E., & von Frankenberg, C. A. High polymers. *Ann. Rev. Phys. Chem.*, 1963. 14, 291-312.
41. Black, A. P., Birkner, F. B., & Morgan, J. J. Destabilization of dilute clay suspensions with labeled polymers. *J. American Water Works Association*, 1965. 57, 1547-1560.
42. Fontana, B. J., & Thomas, J. R. The configuration of adsorbed alkyl methacrylate polymers by infrared and sedimentation studies. *J. Phys. Chem.*, 1961. 65, 480-487.
43. French, R. O., Wadsworth, Milton E., Cook, Melvin A., & Cutler, Ivan B. The quantitative application of infrared spectroscopy to studies in surface chemistry. *J. Phys. Chem.*, 1954. 58, 805-811.
44. Stromberg, R. R., & Smith, L. E. Conformation of polystyrene adsorbed on liquid mercury. *J. Phys. Chem*, 1967. 71, 2470-2474.
45. Peyser, P., & Stromberg, R. R. Conformation of adsorbed polystyrene measured by attenuated total reflection in the ultraviolet region. *J. Phys. Chem.*, 1967. 71, 2066-2074.

46. Doroszkowski, A., & Lambourne, R. A viscometric technique for determining the layer thickness of polymer adsorbed on titanium dioxide. *J. Coll. Interface Sci.*, 1968. 26, 214-221.
47. Oehr, O. E. Preliminary report on the influence of adsorption on capillary dimensions of viscometers. *J. Polymer Sci.*, 1955. 17, 137-140.
48. Silberberg, A. Regulatory effects of macromolecular surface layers on flow through tubes. In A. L. Copley (Ed.) *Hemorheology, proceedings of the first international conference*. Oxford: Pergamon, 1968. (pages 225-230)
49. Frisch, H. L., Simha, R., & Eirich, F. R. Statistical mechanics of polymer adsorption. *J. Chem. Phys.*, 1953. 21, 365-366.
50. Simha, R., Frisch, H. L., & Eirich, F. R. The adsorption of flexible macromolecules. *J. Phys. Chem.*, 1953. 57, 584-589.
51. Roe, R. J. Conformation of an isolated polymer molecule at an interface. II. Dependence on molecular weight. *J. Chem. Phys.*, 1965. 43, 1591-1598.
52. DiMarzio, E. A., & McCrackin, F. L., Jr. One-dimensional model of polymer adsorption. *J. Chem. Phys.*, 1965. 43, 539-547.
53. Hove, C. A. J., DiMarzio, E. A., & Peyser, P. Adsorption of polymer molecules at low surface coverage. *J. Chem. Phys.*, 1965. 42, 2558-2563.
54. Rubin, R. J. Random-walk model of chain-polymer adsorption at surface. *J. Chem. Phys.*, 1965. 43, 2392-2407.
55. Hove, C. A. J. Density distribution of polymer segments in the vicinity of an adsorbing surface. *J. Chem. Phys.*, 1965. 43, 3007-3008.
56. Silberberg, A. Adsorption of flexible macromolecules. IV. Effect of solvent-solute interactions, solute concentration, and molecular weight. *J. Chem. Phys.*, 1968. 48, 2835-2851.

57. Derjaguin, B. V., & Landau, L. D. Theory of the stability of strongly charged lyophobic sols and of the adhesion of strongly charged particles in solutions of electrolytes. *Acta Physicochim. U.S.S.R.*, 1941. 14, 633-662.
58. Verwey, E. J. W., & Overbeek, J. Th. G. Theory of the stability of lyophobic colloids. Amsterdam: Elsevier Publishing Co., 1948.
59. Gregory, J. Flocculation of polystyrene particles with cationic polyelectrolytes. *Trans. Far. Soc.*, 1969. 65, 2260-2268.
60. Black, A. P., Birkner, F. B., & Morgan, J. J. The effect of polymer adsorption on the electrokinetic stability of dilute clay suspensions. *J. Coll. Interface Sci.*, 1966. 21, 626-648.
61. La Mer, V. K. Coagulation symposium introduction. *J. Coll. Sci.*, 1964. 19, 291-293.
62. Ruehrwein, R. A., & Ward, D. W. Mechanism of clay aggregation by polyelectrolytes. *Soil Sci.*, 1952. 73, 485-492.
63. La Mer, V. K., & Smellie, R. H., Jr. Flocculation, subsidence, and filtration of phosphate slimes. I. General. *J. Coll. Sci.*, 1956. 11, 704-709.
64. La Mer, V. K., & Smellie, R. H., Jr. Flocculation, subsidence, and filtration of phosphate slimes. II. Starches as agents for improving flocculation, subsidence, and filtration of phosphate slimes. *J. Coll. Sci.*, 1956. 11, 710-719.
65. Smellie, R. H., Jr., & La Mer, V. K. Flocculation, subsidence, and filtration of phosphate slimes. III. Subsidence behavior. *J. Coll. Sci.*, 1956. 11, 720-731.
66. Smellie, R. H., Jr., & La Mer, V. K. Flocculation, subsidence and filtration of phosphate slimes. VI. A quantitative theory of filtration of flocculated suspensions. *J. Coll. Sci.*, 1958. 13, 589-599.
67. Healy, T. W., & La Mer, V. K. The adsorption-flocculation reactions of a polymer with an aqueous colloidal dispersion. *J. Phys. Chem.*, 1962. 66, 1135-1138.

68. Slater, R. W., & Kitchener, J. A. Characteristics of flocculation of mineral suspensions by polymers. *Disc. Far. Soc.*, 1966. 42, 267-275.
69. La Mer, V. K. Filtration of colloidal dispersions flocculated by anionic and cationic polyelectrolytes. *Disc. Far. Soc.*, 1966. 42, 248-254.
70. Griot, O., & Kitchener, J. A. Role of surface silanol groups in the flocculation of silica suspensions by polyacrylamide. I. Chemistry of the adsorption process. *Trans. Far. Soc.*, 1965. 61, 1026-1031.
71. Healy, T. W. Flocculation-dispersion behavior of quartz in the presence of a polyacrylamide flocculant. *J. Coll. Sci.*, 1961. 16, 609-617.
72. Ries, Herman E., Jr., & Meyers, Bernard L. Flocculation mechanism: Charge neutralization and bridging. *Science*, 1968. 160, 1449-1450.
73. Dixon, J. J. K., La Mer, V. K., Cassian, L., Messinger, S., & Linford, H. B. Effect of the structure of cationic polymers on the flocculation and the electrophoretic mobility of crystalline silica. *J. Coll. Interface Sci.*, 1967. 23, 465-473.
74. Heller, W., & Pugh, T. L. Steric protection of hydrophobic colloidal particles by adsorption of flexible macromolecules. *J. Chem. Phys.*, 1954. 22, 1778.
75. van der Waarden, M. Stabilization of carbon-black dispersions in hydrocarbons. *J. Coll. Sci.* 1950. 5, 317-325.
76. Mackor, E. L. A theoretical approach to the colloid-chemical stability of dispersions in hydrocarbons. *J. Coll. Sci.*, 1951. 6, 492-495.
77. Mackor, E. L., & van der Waals, J. H. The statistics of the adsorption of rod-shaped molecules in connection with the stability of certain colloidal suspensions. *J. Coll. Sci.*, 1952. 7, 535-550.

78. Mathai, K.G., & Ottewill, R.H. Stability of hydrophobic sols in the presence of non-ionic surface-active agents. II. Stability of silver iodide sols in the presence of non-ionic surface-active agents. *Trans. Far. Soc.*, 1966. 62, 759-769.
79. Ottewill, R.H., & Walker, T. The influence of non-ionic surface active agents on the stability of polystyrene latex dispersions. *Kolloid-Zeitschrift & Zeitschrift für Polymere*, 1968. 227, 108-116.
80. Napper, D.H. Flocculation studies of non-aqueous sterically stabilized dispersions of polymer. *Trans. Far. Soc.*, 1968. 64, 1701-1711.
81. Napper, D.H. The steric stabilization of hydrosols by nonionic macromolecules. *J. Coll. Interface Sci.*, 1969. 29, 168-170.
82. Napper, D.H. Flocculation studies of sterically stabilized dispersions. *J. Coll. Interface Sci.*, 1970. 32, 106-114.
83. Flory, P.J. Principles of polymer chemistry. Ithaca: Cornell University Press, 1953. (pages 495-639)
84. Meier, D.J. Theory of polymeric dispersants. Statistics of constrained polymer chains. *J. Phys. Chem.*, 1967. 71, 1861-1868.
85. Ottewill, R.H. Effect of nonionic surfactants on the stability of dispersions. In M. J. Schick (Ed.) *Nonionic surfactants*. New York: Marcel Dekker, 1967. (pages 627-682)
86. Vold, M.J. The effect of adsorption on the van der Waals interaction of spherical colloid particles. *J. Coll. Sci.*, 1961. 16, 1-12.
87. La Mer, V.K., & Healy, T.W. Adsorption-flocculation reactions of macromolecules at the solid-liquid interface. *Rev. of Pure & Appl. Chem.*, 1963. 13, 112-133.
88. Nevo, A., De Vries, A., & Katchalsky, A. Interaction of basic polyamino acids with the red blood cell. I. Combination of polylysine with single cells. *Biochim. Biophys. Acta*, 1955. 17, 536-547.



89. Katchalsky, A., Danon, D., Nevo, A., & De Vries, A. Interactions of basic polyelectrolytes with red blood cell. II. Agglutination of red blood cells by polymeric bases. *Biochim. Biophys. Acta*, 1959. 33, 120-138.
90. von Hummel, K., & Szczepanski, L. V. Quantitative Untersuchungen über die Bindung von Polyvinylpyrrolidon an die Erythrozytenoberfläche. I. Experimente und Ergebnisse. *Blut*, 1963. 9, 145-164.
91. von Hummel, K. Quantitative Untersuchungen über die Bindung von Polyvinylpyrrolidon an die Erythrozytenoberfläche. II. Weitere Auswertung und Besprechung der Versuchsergebnisse. *Blut*, 1963. 9, 215-237.
92. Squire, J. B., Bull, J. P., Maycock, W. d'A., & Ricketts, C. R. Dextran. Springfield: Charles C. Thomas, 1955.
93. Gronwall, A. Dextran and its use in colloidal infusion solutions. New York: Academic Press, 1957.
94. Rothman, S., Adelson, E., Schwebel, A., & Langdell, R. D. Adsorption of carbon-14 dextran to human blood platelets and red blood cells, *in vitro*. *Vox Sanguinis*, 1957. 2, 104-109.
95. Bloom, W. L., Harmer, D. S., Bryant, M. F., & Brewer, S. S. Coating of vascular surfaces and cells. A new concept in prevention of intravascular thrombosis. *Proc. Soc. Exp. Biol. Med.*, 1964. 115, 384-386.
96. Håkansson, B. A. S., Östling, S. G., & Zade-Oppen, A. M. M. The non-affinity of the red cell surface for dextran. *Acta Physiol. Scand.*, 1969. Supp. 330, 146. (Abstract)
97. Engeset, J., Stalker, A. L., & Matheson, N. A. Effects of dextran 40 on erythrocyte aggregation. *The Lancet*, May 21, 1966. 1124-1127.
98. Engeset, J., Stalker, A. L., & Matheson, N. A. Objective measurement of the dispersing effect of dextran 40 on red cells from man, dog, and rabbit. *Cardiovasc. Res.*, 1967. 1, 385-388.
99. Richter, Wolfgang. Normalizing effect of low molecular weight dextran fractions on the reduced suspension stability of human erythrocytes *in vitro*. *Acta Chir. Scand.*, 1966. 131, 1-8.

100. Thorsén, G., & Hint, H. Aggregation, sedimentation and intravascular sludging of erythrocytes. *Acta Chir. Scand.* 1950. Supp. 154, 1-50.
101. Laurent, T.C. The interaction between polysaccharides and other macromolecules. V. The solubility of proteins in the presence of dextran. *Biochem. J.*, 1963. 89, 253-257.
102. Dhall, D.P., & Matheson, N.A. In vitro clumping of human platelets by dextran. *Thromb. Diath. Haem.*, 1968. 19, 70-76.
103. Ross, S.W., & Ebert, R.V. Microelectrophoresis of blood platelets and the effects of dextran. *J. Clin. Invest.*, 1959. 38, 155-160.
104. Pollack, W., Hager, H.J., Reckel, R., Toren, D.A., & Singher, H.O. A study of the forces involved in the second stage of hemagglutination. *Transfusion*, 1965. 5, 158-183.
105. Seaman, G.V.F., Hissen, W., Lino, L., & Swank, R.L. Physico-chemical changes in blood arising from dextran infusions. *Clin. Sci.*, 1965. 29, 293-304.
106. Bernstein, F., & Castaneda, A.R. Alterations in erythrocyte electrical charge associated with mannitol, polyvinylpyrrolidone (PVP), dextrose, and various dextran compounds. In P.N. Sawyer (Ed.) *Biophysical mechanisms in vascular homeostasis and intravascular thrombosis*. New York: Appleton-Century-Crofts, 1965. (pages 103-110)
107. Gardner, B. The effect of dextrans on zeta potential. *Proc. Soc. Exp. Biol. Med.*, 1969. 131, 1115-1118.
108. Srinivasan, S., Aaron, R., Chopra, P.S., Lucas, T., & Sawyer, P.N. Effect of thrombotic and antithrombotic drugs on the surface charge characteristics of canine blood vessels: In vivo and in vitro studies. *Surgery*, 1968. 64, 827-833.
109. Allgén, L., & Roswall, S. A dielectric study of carboxymethylcellulose in aqueous solution. *J. Polymer Sci.*, 1954. 12, 229-236.
110. Scott Blair, G.W. *Elementary rheology*. London: Academic Press, 1969. (page 1)

111. Goldsmith, H. L., & Mason, S. G. The microrheology of dispersions. In: F. Eirich (Ed.) *Rheology*. Vol. 4. New York: Academic Press, 1967. (pages 85-250)
112. Blachford, J., Chan, F.S., & Goring, D.A.I. The secondary electroviscous effect. Paths of approach of two charged spheres in a viscous medium. *J. Phys. Chem.*, 1969. 73, 1062-1065.
113. Goodeve, C.F. A general theory of thixotropy and viscosity. *Trans. Far. Soc.*, 1939. 35, 342-358.
114. Conway, B.E., & Dobry-Duclaux, A. Viscosity of suspensions of electrically charged particles and solutions of polymeric electrolytes. In F.R. Eirich (Ed.) *Rheology, theory & application*. Vol. 3. New York: Academic Press, 1960. (pages 83-120)
115. Bueche, F. Viscosity of entangled polymers; theory of variation with shear rate. *J. Chem. Phys.*, 1968. 48, 4781-4784.
116. Einstein, A. Berichtigung zu meiner Arbeit: Eine neue Bestimmung der Molekuldimensionen. *Ann. Physik.*, 1911. 34, 591-592.
117. Jeffery, G.B. The motion of ellipsoidal particles immersed in a viscous fluid. *Proc. Roy. Soc. (London)*, 1922. A102, 161-179.
118. Ford, T.F. Viscosity-concentration and fluidity-concentration relationships for suspensions of spherical particles in Newtonian liquids. *J. Phys. Chem.*, 1960. 64, 1168-1174.
119. Rand, R.P., & Burton, A.C. Mechanical properties of the red cell membrane. I. Membrane stiffness and intracellular pressure. *Biophys. J.*, 1964. 4, 115-135.
120. Fung, Y.C.B., & Tong, P. Theory of the sphering of red blood cells. *Biophys. J.*, 1968. 8, 175-198.
121. Sirs, J.A. Structure of the erythrocyte. *J. Theor. Biol.*, 1970. 27, 107-115.
122. Canham, P.B. The minimum energy of bending as a possible explanation of the biconcave shape of the human red blood cell. *J. Theor. Biol.*, 1970. 26, 61-81.

123. Schowalter, W.R., Chaffey, C.E., & Brenner, H. Rheological behavior of a dilute emulsion. *J. Coll. Interface Sci.*, 1968. 26, 152-160.
124. Copley, A.L. Some problems in hemorheology. In S. Onogi (Ed.) *Proceedings of the fifth international congress of rheology*. Tokyo: Univ. Tokyo Press & Univ. Park Press, 1970. (pages 3-25)
125. Ree, T., & Eyring, H. The relaxation theory of transport phenomena. In F.R. Eirich (Ed.) *Rheology, theory and applications*. Vol. 2. New York: Academic Press, 1958. (pages 83-143)
126. Merrill, E.A. Non-Newtonianism in thin liquids: molecular and physical aspects. In A. Acrivos (Ed.) *Modern chemical engineering*. Vol. 1. Physical operations. New York: Reinhold Publ. Co., 1963. (pages 141-195)
127. Sherman, P. Rheology of emulsions. In P. Sherman (Ed.) *Emulsion Science*. New York: Academic Press, 1968. (pages 217-351)
128. Booth, F. The electroviscous effect for suspensions of solid spherical particles. *Proc. Roy. Soc.*, 1950. A123, 533-551.
129. Chan, F.S., & Goring, D.A.I. The primary electroviscous effect in a sulfonated polystyrene latex. *J. Coll. Interface Sci.*, 1966. 22, 371-377.
130. Stone-Masui, J., & Watillon, A. Electroviscous effects in dispersions of monodisperse polystyrene latices. *J. Coll. Interface Sci.*, 1968. 28, 187-201.
131. Chan, F.S., Blachford, J., & Goring, D.A.I. The secondary electroviscous effect in a charged spherical colloid. *J. Coll. Interface Sci.*, 1966. 22, 378-385.
132. Casson, N. A flow equation for pigment-oil suspensions of the printing ink type. In C.C. Mill (Ed.) *Rheology of disperse systems*. London: Pergamon Press, 1959. (pages 84-102)
133. Hunter, R.J., & Nicol, S.K. The dependence of plastic flow behavior of clay suspensions on surface properties. *J. Coll. Interface Sci.*, 1968. 28, 250-259.

134. Cokelet, G.R. The rheology of human blood. Unpublished doctor's dissertation. Massachusetts Institute of Technology, 1963.
135. Merrill, E.W., Margetts, W.G., & Cokelet, G.R. Influence of plasma proteins on the rheology of human blood. In A.L. Copley (Ed.) Proceedings of the fourth international congress on rheology, Part 4. Symposium on biorheology. New York: Interscience, 1965. (pages 601-611)
136. Merrill, E.W., Cheng, C.S., & Pelletier, G.A. Yield stress of normal human blood as a function of endogenous fibrinogen. *J. Appl. Physiol.*, 1969. 26, 1-3.
137. Chien, S., Usami, S., Dellenback, J., & Gregersen, M.I. Shear-dependent interaction of plasma proteins with erythrocytes in blood rheology. *Am. J. Physiol.*, 1970. 219, 143-153.
138. Whitmore, R.L. Rheology of the circulation. Oxford: Pergamon Press, 1968.
139. Merrill, E.W. Rheology of blood. *Physiol. Rev.*, 1969. 49, 863-888.
140. Cokelet, G.R. The rheology of human blood. In Y.C. Fung (Ed.) Biomechanics; Its foundation and objectives. Prentice-Hall. In Press.
141. Cokelet, G.R., Merrill, E.W., Gilliland, E.R., Shin, H., Britten, A., & Wells, R.E. The rheology of human blood - measurement near and at zero shear rate. *Trans. Soc. Rheology*, 1963. 7, 303-317.
142. Chien, S., Usami, S., Taylor, H.M., Lundberg, J.L., & Gregersen, M.I. Effects of hematocrit and plasma proteins on human blood rheology at low shear rates. *J. Appl. Physiol.*, 1966. 21, 81-87.
143. Benis, A.M., & Lacoste, J. Study of erythrocyte aggregation by blood viscometry at low shear rates using a balance method. *Circulation Res.*, 1968. 22, 29-41.
144. Charm, S.E., & Kurland, G.S. Static method for determining blood yield stress. *Nature*, 1967. 216, 1121-1123.

145. Replogle, R.L., Meiselman, H.J., & Merrill, E.W. Clinical implications of blood rheology studies. *Circulation*, 1967. 36, 148-160.
146. Schmid-Schönbein, H., Gaehtgens, P., & Hirsch, H. On the shear rate dependence of red cell aggregation in vitro. *J. Clin. Invest.*, 1968. 47, 1447-1454.
147. Goldstone, J., Schmid-Schönbein, H., & Wells, R. The rheology of red blood cell aggregates. *Microvascular Res.*, 1970. 2, 273-286.
148. Scott Blair, G.W. An equation for the flow of blood, plasma, and serum through glass capillaries. *Nature*, 1959. 183, 613-614.
149. Merrill, E.W., Margetts, W.G., Cokelet, G.R., & Gilliland, E.R. The Casson equation and rheology of blood near zero shear. In A.L. Copley (Ed.) *Proceedings of the fourth international congress on rheology, Part 4. Symposium on biorheology*. New York: Interscience, 1965. (pages 135-143)
150. Seaman, G.V.F., & Swank, R.L. The influence of electrokinetic charge and deformability of the red blood cell on the flow properties of its suspensions. *Biorheology*, 1967. 4, 47-59.
151. Chien, S., Usami, S., Dellenback, R.J., & Gregersen, M.I. Blood viscosity: Influence of erythrocyte deformation. *Science*, 1967. 157, 827-829.
152. Brooks, D.E., Goodwin, J.W., & Seaman, G.V.F. Interactions among erythrocytes under shear. *J. Appl. Physiol.*, 1970. 28, 172-177.
153. Chien, S., Usami, S., Dellenback, R.J., & Gregersen, M.I. Shear-dependent deformation of erythrocytes in rheology of human blood. *Am. J. Physiol.*, 1970. 219, 136-142.
154. Meiselman, H.J. Some physical and rheological properties of human blood. Unpublished doctor's dissertation. Massachusetts Institute of Technology, 1965.
155. Gelin, L.E., & Ingleman, B. Rheomacrodex - a new dextran solution for rheological treatment of impaired capillary flow. *Acta Chir. Scand.*, 1961. 122, 294-302.

156. Cullen, C.F., & Swank, R.L. Intravascular aggregation and adhesiveness of the blood elements associated with alimentary lipemia and injections of large molecular substances. Effect on blood-brain barrier. *Circulation*, 1954. 9, 335-346.
157. Meiselman, H.J., Merrill, E.W., Salzman, E.W., Gilliland, E.R., & Pelletier, G.A. Effect of dextran on rheology of human blood: low shear viscometry. *J. Appl. Physiol*, 1967. 22, 480-486.
158. Meiselman, H.J. The influence of dextran on the sedimentation behavior of human red cells: macro and micro studies. Fifth europ. conf. microcirculation, Gothenburg, 1968. *Bibl. Anat.*, 1969. No. 10, 20-31.
159. Groth, C.G., & Lofstrom, B. Some aspects of the use of dextrans as erythrocyte stabilizers. *Bibl. Anat.*, 1964. 4, 166-173.
160. Ricketts, C.R. Interaction of dextran and fibrinogen. *Nature*, 1952. 169, 970.
161. Kroll, J., & Dybkaer, R. In vitro precipitations in plasma by low molecular weight dextran. *Scand. J. Clin. Lab. Invest.*, 1964. 16, 31-38.
162. Thompson, W.L. Interactions of hydroxyethyl starch and dextran with plasma proteins and erythrocyte envelopes. *Biorheology*, 1966. 3, 49-58.
163. Dintenfass, L. Internal viscosity of the red cell and a blood viscosity equation. *Nature*, 1968. 219, 956-958.
164. Cox, H.A., Jr., & Su, G-J. The influence of electrokinetic charge on the rheological properties of red blood cell suspensions. In A.L. Copley (Ed.) *Symposium on biorheology*. New York: Interscience Publ., 1965. (pages 337-350)
165. Seaman, G.V.F. The role of electrical charge in the stability and flow properties of red cell suspensions. In A.L. Copley (Ed.) *Hemorheology*. Oxford: Pergamon Press, 1968. (pages 551-564)
166. Oncley, J.L. The investigation of proteins by dielectric measurements. *Chem. Reviews*, 1942. 30, 433-450.

167. Takashima, S. Dielectric properties of macromolecules. In H. Peeter (Ed.) *Protides of biological fluids*. Amsterdam: Elsevier Publishing Co., 1966. (pages 393-401)
168. Oncley, J.L. Electric moments and relaxation times of protein molecules. *J. Phys. Chem.*, 1940. 44, 1103-1113.
169. O'Konski, C.T. Electric properties of macromolecules. V. Theory of ionic polarization in polyelectrolytes. *J. Phys. Chem.*, 1960. 64, 605-619.
170. Langmuir, R.V. *Electromagnetic fields and waves*. New York: McGraw-Hill, 1961. (page 60)
171. Haydon, D.A., & Seaman, G.V.F. Unpublished results.
172. Seaman, G.V.F. Personal communication. 1970.
173. Seaman, G.V.F., & Cook, G.M.W. Modification of the electrophoretic behaviour of the erythrocyte by chemical means. In E.J. Ambrose (Ed.) *Cell electrophoresis*. London: J.A. Churchill Ltd., 1965. (pages 48-65)
174. Seaman, G.V.F., & Uhlenbruck, G. The action of proteolytic enzymes on the red cells of some animal species. *Biochem. Biophys. Acta*, 1962. 64, 570-572.
175. Seaman, G.V.F., & Vassar, P.S. Changes in the electrokinetic properties of platelets during their aggregation. *Arch. Biochem. Biophys.*, 1966. 117, 10-17.
176. Robertson, A.L. Discussion. In P.N. Sawyer (Ed.) *Biophysical mechanisms in vascular homeostasis and intravascular thrombosis*. New York: Meredith Publ. Co., 1965. (page 109)
177. Sieh, J.B., & Sterling, C. Charging of glycogen in salt solutions. *Biochim. Biophys. Acta*, 1969. 184, 281-286.
178. Diamond, J.M., & Wright, E.M. Biological membranes: the physical basis of ion and nonelectrolyte selectivity. *Ann. Rev. Physiol.*, 1969. 31, 581-646.
179. Pedersen, C.J. Cyclic polyethers and their complexes with metal salts. *J. Am. Chem. Soc.*, 1967. 89, 7017-7036.



180. Kilbourn, B. T., Dunitz, J. D., Pioda, L. A. R., & Simon, W. Structure of the  $K^+$  complex with nonactin, a macrotetrolide antibiotic possessing highly specific  $K^+$  transport properties. *J. Mol. Biol.*, 1967. 30, 559-563.
181. Ponder, E., & Ponder, R. V. The interaction of dextran with serum albumin, gamma globulin and fibrinogen. *J. Gen. Physiol.* 1960. 43, 753-758.
182. Bloom, W. L. Personal communication. 1970.
183. Dyar, M. T. Electrokinetic studies on bacterial surfaces. *J. Bact.*, 1948. 56, 821-834.
184. Marsden, N. V. B. Solute behaviour in tightly cross-linked dextran gels. *Ann. N.Y. Acad. Sci.*, 1965. 125, 428-457.
185. Seaman, G. V. F. Microelectrophoresis of red blood cells. Unpublished doctor's dissertation, University of Cambridge, 1958. (page 78)
186. Klotz, I. M., & Sloniewsky, A. R. Macromolecule-small molecule interactions: a synthetic polymer with greater affinity than serum albumin for small molecules. *Biochem. Biophys. Res. Comm.*, 1968. 31, 421-426.
187. Baldwin, W. H., Raridon, R. J., & Kraus, K. A. Properties of organic-water mixtures. X. Activity coefficients of sodium chloride at saturation in water mixtures of polyglycols. *J. Phys. Chem.*, 1969. 73, 3417-3420.
188. Granath, K. Solution properties of branched dextrans. *J. Coll. Sci.*, 1958. 13, 308-328.
189. Washburn, E. W. (Ed.) International critical tables, Vol. 4. New York: McGraw-Hill, 1928. (page 235)
190. Edmond, E., & Ogston, A. G. An approach to the study of phase separation in ternary aqueous systems. *Biochem. J.*, 1968. 109, 569-576.
191. Couper, A., & Stepto, R. F. T. Diffusion of low-molecular weight poly(ethylene oxide) in water. *Trans. Far. Soc.*, 1969. 65, 2486-2496.

192. Haug, A., & Smidsrød, O. The solubility of polysaccharides in salt solutions. In *Solution properties of natural polymers*. London: The Chemical Society, 1968. (pages 273-282)
193. Hint, H., & Thorsén, G. A micro method for determination of dextran in blood. *Acta Chem. Scand.*, 1947. 1, 808-812.
194. Bombardieri, G., Rotilio, G., Crifò, C., & DeMarco, C. Studies on dextran and dextran derivatives. XIV. Metal binding properties of succinyl- and phythaly-dextrans. *Arch. Biochem. Biophys.*, 1968. 127, 766-769.
195. Egan, B.Z. Selectivity of polyacrylamide and dextran gels for simple cations and anions. *J. Chromatog.*, 1968. 34, 382-388.
196. Hjertén, S. Thermodynamic treatment of partition experiments with special reference to molecular-seive chromatography. *J. Chromatog.*, 1970. 50, 189-208.
197. Albertsson, P. Å. *Partition of cell particles and macromolecules*. New York: Wiley, 1960.
198. Mehrishi, J.N., & Seaman, G.V.F. Electrokinetic properties of dispersions of model compounds of biological interest. *Trans. Far. Soc.*, 1968. 64, 3152-3157.
199. Seaman, G.V.F., & Brooks, D.E. Unpublished experiments.
200. Bull, H.B. *An introduction to physical biochemistry*. Philadelphia: F.A. Davis, Co., 1964. (page 125)
201. Huggins, M.L. *Physical chemistry of high polymers*. New York: Wiley, 1958.
202. Bikerman, J.J. Structure and capacity of the electrical double layer. *Phil. Mag.* (7), 1942. 33, 384-397.
203. Eigen, M., & Wicke, E. The thermodynamics of electrolytes at higher concentration. *J. Phys. Chem.*, 1954. 58, 702-714.
204. Schlogl, R. Zur Statistik idealer Mischungen unter Berücksichtigung des Raumbedarfs der Teilchen. *Zeit. Physik, Chemie*, 1954. 202, 379-389.

205. Ohlenbusch, H. D. Adsorption on boundaries between liquid phases. II. Electrolyte adsorption and the structure of the electrical double layer. *Zeit. Elektrochem.*, 1956. 60, 607-616.
206. Haydon, D. A., & Taylor, F. H. On adsorption at the oil/water interface and the calculation of electrical potentials in the aqueous surface phase. I. Neutral molecules and a simplified treatment for ions. *Phil. Trans. Roy. Soc. (London)*, 1960. A252, 225-248.
207. Hart, W. L. *College Trigonometry*. Boston: D. C. Heath and Co., 1951. (page 172)
208. Clayfield, E. J., & Lumb, E. C. A theoretical approach for polymer dispersant action. I. Calculation of entropic repulsion exerted by random polymer chains terminally adsorbed on plane surfaces and spherical particles. *J. Coll. Interface Sci.*, 1966. 22, 269-284.
209. Smyth, C. P. *Dielectric behavior and structure*. New York: McGraw-Hill, 1955. (page 203)
210. Schwan, H. P. Electrode polarization impedance and measurements in biological materials. *Ann. New York Acad. Sci.*, 1968. 148, 191-209.
211. Schwan, H. P. Determination of biological impedances. In W. L. Nastuk (Ed.) *Physical techniques in biological research*. Vol. 6. *Electrophysiological methods*. New York: Academic Press, 1963. (pages 323-407)
212. Hodgman, C. D. (Ed.) *Handbook of chemistry and physics*. (44th Ed.). Cleveland: Chemical Rubber Publishing Co., 1962. (page 2611)
213. General Radio Co. *Instruction manual type 1620A capacitance measuring assembly*. West Concord, Mass., 1968.
214. Pollack, W. Personal communication. January 29, 1968.
215. Grant, E. H. Dielectric dispersion in bovine serum albumin. *J. Mol. Biol.*, 1966. 19, 133-139.

216. Masouredis, S.P. Quantitative isotopic immunohematology. *Transfusion*, 1964. 4, 69-76.
217. Chien, S., Dellenback, J. Usami, S., & Gregersen, M.I. Plasma trapping in hematocrit determination. Differences among animal species. *Proc. Soc. Exp. Biol. Med.*, 1965. 119, 1155-1158.
218. Chien, S., Dellenback, R.J., Usami, S. Seaman, G.V.F., & Gregersen, M.I. Centrifugal packing of suspensions of erythrocytes hardened with acetaldehyde. *Proc. Soc. Exp. Biol. Med.*, 1968. 127, 982-985.
219. Dubois, M., Gilles, K.A., Hamilton, J.K., Rebers, P.A., & Smith, F. Colorimetric method for determination of sugars and related substances. *Anal. Chem.*, 1956. 28, 350-356.
220. Laurent, T.C., & Killander, J. A theory of gel filtration and its experimental verification. *J. Chromatog.* 1964. 14, 317-330.
221. Hendry, E.B. Osmolarity of human serum and of chemical solutions of biologic importance. *Clin. Chem.*, 1961. 7, 156-164.
222. Reznikoff, P. A method for the determination of the specific gravity of red blood cells. *J. Exp. Med.*, 1923. 38, 441-444.
223. Ponder, E. Hemolysis and related phenomena. New York: Grune & Stratton, 1948. (page 56)
224. Parpart, A.K., & Ballantine, R. Hematocrit determination of relative cell volume. *Science*, 1943. 98, 545.
225. Ponder, E. Hemolysis and related phenomena. New York: Grune & Stratton, 1948. (page 14)
226. Bull, H.B. An introduction to physical biochemistry. Philadelphia: F.A. Davis, 1964. (page 217)
227. Hardwicke, J., & Squire, J.R. The basis of the erythrocyte sedimentation rate. *Clin. Sci.*, 1952. 11, 333-355.

228. Seaman, G. V. F. Electrophoresis using a cylindrical chamber. In E. J. Ambrose (Ed.) *Cell Electrophoresis*. London: J. & A. Churchill Ltd., 1965. (pages 4-21)
229. Seaman, G. V. F., & Heard, D. H. A microelectrophoresis chamber of small volume for use with biological systems. *Blood*, 1961. 18, 599-604.
230. Bangham, A. D. Electrophoretic characteristics of ram and rabbit spermatozoa. *Proc. Roy. Soc.*, 1961. B155, 292-305.
231. Schmid-Schönbein, H., & Wells, R. Fluid drop-like transition of erythrocytes under shear. *Science*, 1969. 165, 288-291.
232. Ottewill, R. H., & Shaw, J. N. Studies on the preparation and characterisation of monodisperse polystyrene latices. Part 2: Electrophoretic characteristics of surface groupings. *Koll-Zeit. & Zeit. Polymere*, 1967. 218, 34-40.
233. Davies, J. T., & Rideal, E. K. *Interfacial phenomena*. (2nd Ed.) New York: Academic Press, 1963. (page 85)
234. Bishop, C. Overall red cell metabolism. In C. Bishop & D. M. Surgenor (Eds.) *The red blood cell*. New York: Academic Press, 1964. (pages 147-188)
235. West, E. S., & Todd, W. R. *Textbook of Biochemistry* (3rd Ed.) New York: The MacMillan Co., 1961. (page 416)
236. Lacko, L., & Burger, M. Interaction of some disaccharides with the carrier system for aldoses in erythrocytes. *Biochem. J.*, 1962. (pages 622-625)
237. Whittam, R. *Transport and diffusion in red blood cells*. London: Edward Arnold Ltd., 1964. (pages 155-158)
238. Pardoe, G. I. Perspectives in blood group research. *Brit. J. Hospital Med.*, 1970. 3, 393-410.
239. Christophers, S. R. The mixture reaction in haemolysis by acids and bases. *Ind. J. Med. Res.*, 1929-30. 17, 533-543.
240. Thamsen, J. The acidic dissociation constants of glucose, mannitol and sorbitol, as measured by means of the hydrogen electrode and the glass electrode at 0° and 18°C. *Acta Chem. Scand.*, 1952. 6, 270-384.

241. Robinson, R. A., & Stokes, R. H. Electrolyte solutions. (2nd Ed. Rev.) London: Butterworths, 1959. (pages 125-126)
242. Hoeve, C. A. J. Adsorption isotherms for polymer chains adsorbed from  $\theta$  solvents. *J. Chem. Phys.*, 1966. 44, 1505-1509.
243. Seaman, G. V. F., Jackson, L. J., & Brooks, D. E. Unpublished experiments.
244. Dimarzio, E. A., & Rubin, R. J. Adsorption of a chain polymer between two plates. Preprint of paper presented to Division of Colloid and Surface Chemistry of the American Chemical Society, Chicago Ill., Sept. 1970.
245. Chien, S., Jan, K. M., Usami, S., Luse, S. A., Miller, L. H., & Fremont, H. Effects of macromolecules on the rheology and ultrastructure of red cell suspensions. Abstract for VI European Conference on Microcirculation, Aalborg, Denmark, June, 1970.
246. Levine, S., & Bell, G. M. Theory of a modified Poisson-Boltzmann equation. I. The volume effect of hydrated ions. *J. Phys. Chem.*, 1960. 64, 1188-1195.
247. Van Wazer, J. R., Lyons, J. W., Kim, K. Y., & Colwell, R. E. Viscosity and flow measurement. New York: Interscience, 1963. (page 272)
248. Tanford, C. Physical chemistry of macromolecules. New York: Wiley, 1961. (page 343)
249. Weed, R. I., LaCelle, P. L., & Merrill, E. W. Metabolic dependence of red cell deformability. *J. Clin. Invest.*, 1969. 48, 795-809.
250. Weed, R. I. The importance of erythrocyte deformability. *Am. J. Med.*, 1970. 49, 147-150.
251. Van Wazer, J. R., Lyons, J. W., Kim, K. Y., & Colwell, R. E. Viscosity and flow measurement. New York: Interscience Publ., 1963. (pages 113-116)
252. Mooney, M., & Ewart, R. H. The conicylindrical viscometer. *J. Appl. Physics*, 1934. 5, 350-354.

253. Kind, R.G., & Copley, A.L. Modifications to the Weissenberg Rheogoniometer for hemorheological and other biorheological studies. *Biorheology*, 1970. 7, 1-4.
254. Van Wazer, J.R., Lyons, J.W., Kim, K.Y., & Colwell, R.E. Viscosity and flow measurement. New York: Interscience Publ., 1963. (page 75)
255. Krieger, I.M., & Elrod, H. Direct determination of the flow curves of non-Newtonian fluids. II. Shearing rate in the concentric cylinder viscometer. *J. Appl. Physics*, 1953. 24, 134-136.
256. Merrill, E.W., Gilliland, E.R., Cokelet, G., Shin, H., Britten, A., & Wells, R.E., Jr. Rheology of human blood, near and at zero flow. *Biophysical J.*, 1963. 3, 199-213.
257. Schott, H. Deflocculation of swelling clays by nonionic and anionic detergents. *J. Coll. Interface Sci.*, 1968. 26, 133-139.
258. Shotton, E., & Davis, S.S. The influence of emulsifier concentration on the rheological properties of an oil-in-water emulsion stabilized by an anionic soap. *J. Pharm. Pharmac.*, 1968. 20, 439-449.
259. Chien, S. Shear dependence of effective cell volume as a determinant of blood viscosity. *Science*, 1970. 168, 977-979.
260. Graessley, W.W. Molecular entanglement theory of flow behavior in amorphous polymers. *J. Chem. Phys.*, 1965. 43, 2696-2703.
261. Coddington, E.A. An introduction to ordinary differential equations. Englewood Cliffs: Prentice-Hall, 1961. (page 126)
262. Sokolnikoff, J.S., & Redheffer, R.M. Mathematics of physics and modern engineering. New York: McGraw-Hill, 1958. (page 125)

APPENDICES



## APPENDIX I

THE USE OF ELECTROKINETIC MEASUREMENTS TO STUDY  
THE PROPERTIES OF NEUTRAL ADSORBED LAYERS

In Chapter 2, Section IV-B-3, an expression (equation 2-66) was derived which described the variation of the relative zeta potential,  $Z$ , as a function of electrolyte concentration,  $c$  for fixed charge systems to which permeable neutral layers of constant density were adsorbed. The form of  $Z(c)$  was shown to depend strongly on the location of the shear plane within the adsorbed layer; the greater the degree of free draining within the layer, the greater was  $Z(c)$  at a given electrolyte concentration. Within the context of the model described in Chapter 2, then, values for the polymer adsorption factor  $\beta$ , total thickness  $d$ , and thickness of the free draining region  $d_F$ , may be obtained by fitting equation (2-66) to curves of relative zeta potential vs electrolyte concentration for the particle-polymer system under study. The derivation applies equally to zeta potential measurements using electroosmosis. This method of examination, however, is limited to systems for which either the polymer has no effect on the surface charge density, or the charge density in the presence of polymer can be determined by an independent method.

In general, given the  $Z(c)$  curve, one can always obtain values

for the parameters  $\beta$ ,  $d$  and  $d_F$  using curve fitting techniques. However, the calculations involved rapidly become tedious, particularly if computing facilities are unavailable. It is desirable, then, to have analytical expressions relating features of the curve to the required parameters. To this end, we now consider various approximate forms of equation (2-39) and (2-66) for a variety of experimental conditions.

Totally Free Draining Layer ( $d_F = d$ )

At high electrolyte concentration, (2-39) becomes:

$$Z_{\max} \sim \frac{1}{\sqrt{1-\beta}}$$

Hence  $\beta$  may be obtained from:

$$\beta \sim 1 - Z_{\max}^{-2} \quad (\text{A1-1})$$

At low enough  $c$ , since  $\kappa = 0.329\sqrt{c}$ , we may write

$$\sinh \kappa\sqrt{1-\beta} d \sim \kappa\sqrt{1-\beta} d \quad (\text{A1-2})$$

$$\cosh \kappa\sqrt{1-\beta} d \sim 1 \quad (\text{A1-3})$$

If  $Z_{\min}$  is a value of  $Z$  measured at low electrolyte concentration, equation (2-39) becomes:

$$Z_{\min} \sim \frac{1}{\sqrt{1-\beta}} \left[ \frac{\kappa_{\min} \sqrt{1-\beta} d + \sqrt{1-\beta}}{\kappa_{\min} (1-\beta) d + 1} \right]$$

Solving for  $d$ :

$$d = \frac{1}{\kappa_{\min}} \left[ \frac{Z_{\min} - 1}{1 - Z_{\min} (1-\beta)} \right] \quad (\text{A1-4})$$

Therefore, for a completely free draining layer (one with no maximum in the  $Z(c)$  curve), both  $\beta$  and  $d$  may be approximately obtained from the values of  $Z(c)$  at high and low electrolyte concentration.

#### Partially Free Draining Layer

Equation 2-66 may be written:

$$\begin{aligned} & Z\sqrt{1-\beta} [\sqrt{1-\beta} \sinh \kappa\sqrt{1-\beta} d + \cosh \kappa\sqrt{1-\beta} d] \\ &= \sinh(\kappa\sqrt{1-\beta} d_F) + \sqrt{1-\beta} \cosh(\kappa\sqrt{1-\beta} d_F) \end{aligned}$$

For the value of  $\kappa$  at which  $Z = 1$ , ( $\kappa_1$ ), we have

$$\begin{aligned} & \sqrt{1-\beta} [\sqrt{1-\beta} \sinh \kappa_1 \sqrt{1-\beta} d + \cosh \kappa_1 \sqrt{1-\beta} d] \\ &= \sinh(\kappa_1 \sqrt{1-\beta} d_F) + \sqrt{1-\beta} \cosh(\kappa_1 \sqrt{1-\beta} d_F) \quad (\text{A1-5}) \end{aligned}$$

In the cases where  $\kappa_1 \sqrt{1-\beta} d_F \gtrsim 2$  (for maximum of 5% error):

$$\sinh \kappa_1 \sqrt{1-\beta} d_F \sim \cosh \kappa_1 \sqrt{1-\beta} d_F \sim \frac{\exp(\kappa_1 \sqrt{1-\beta} d_F)}{2}$$

$$\sinh \kappa_1 \sqrt{1-\beta} d \sim \cosh \kappa_1 \sqrt{1-\beta} d \sim \frac{\exp(\kappa_1 \sqrt{1-\beta} d)}{2}$$

(A1-5) then gives:

$$\sqrt{1-\beta}(1+\sqrt{1-\beta}) \exp \kappa_1 \sqrt{1-\beta} d = (1+\sqrt{1-\beta}) \exp \kappa_1 \sqrt{1-\beta} d_F \quad (\text{A1-6})$$

which may be solved for  $(d-d_F)$ :

$$d - d_F = \frac{-\ln \sqrt{1-\beta}}{\kappa_1 \sqrt{1-\beta}} \quad (\text{A1-7})$$

At low  $c$ , when  $\kappa \sqrt{1-\beta} d < 0.3$  (for maximum of 5% error),

(A1-2) and (A1-3) apply. If  $Z_{\min}$  and  $\kappa_{\min}$  are the values of  $Z$  and  $\kappa$  at some sufficiently low  $c$ , (2-66) may be solved for  $d$  to give:

$$d = \frac{1 - Z_{\min} + \kappa_{\min} d_F}{\kappa_{\min} Z_{\min} (1-\beta)} \quad (\text{A1-8})$$

If the value of  $\beta$  is known, (A1-7) and (A1-8) may be used to find  $d$  and  $d_F$ . However, an explicit expression for  $\beta$  is not in all cases available.

It is apparent that if  $d$  and  $d_F$  are both large so that  $\kappa \sqrt{1-\beta} d_F \gtrsim 2$ , then  $\sinh(\kappa \sqrt{1-\beta} d_F) \sim \cosh(\kappa \sqrt{1-\beta} d_F)$ ,  $\sinh \kappa \sqrt{1-\beta} d \sim \cosh \kappa \sqrt{1-\beta} d$ , and (2-66) becomes:

$$Z\sqrt{1-\beta} \sim \frac{\sinh(\kappa\sqrt{1-\beta} d_F)}{\sinh(\kappa\sqrt{1-\beta} d)}$$

Under these conditions,  $\sinh(\kappa\sqrt{1-\beta} d_F) \sim \exp(\kappa\sqrt{1-\beta} d_F)/2$ , which gives, when applied to the numerator also:

$$Z\sqrt{1-\beta} = \exp[-\kappa\sqrt{1-\beta} (d-d_F)]$$

Providing that  $(d-d_F)$  is sufficiently small,

$\exp[-\kappa\sqrt{1-\beta} (d-d_F)] \sim 1 - \kappa\sqrt{1-\beta} (d-d_F)$  and the expression in  $Z$  becomes, after some rearrangement:

$$\sqrt{1-\beta} = \frac{1}{Z + \kappa(d-d_F)} \quad (\text{A1-9})$$

For each of the two approximations which led to (A1-9) to hold to within 5%,  $\kappa$ ,  $\beta$ ,  $d$  and  $d_F$  must be such that:

$$\kappa\sqrt{1-\beta} d_F \gtrsim 2$$

$$\kappa\sqrt{1-\beta} (d-d_F) \lesssim 0.3$$

which means that for (A1-9) to apply, the parameters must obey:

$$2 < \kappa\sqrt{1-\beta} d_F > 0.3 \kappa\sqrt{1-\beta} d \quad (\text{A1-10})$$

If  $\beta$  and  $d$  are such that the highest  $c$  at which  $Z$  can be measured fulfills (A1-10), then (A1-10), (A1-7) and (A1-8) may be used to estimate  $\beta$ ,  $d$  and  $d_F$  for the system under study without

employing a curve fitting procedure.

A further relationship between the parameters, which applies under slightly less stringent conditions, may be obtained from the conditions which maximize  $Z(c)$ . Setting the first derivative of  $Z$  with respect to  $\kappa$  equal to zero, and applying the identities involving the hyperbolic functions of sums, we find:

$$\begin{aligned} & \sqrt{1-\beta}(d-d_F) \sinh[\kappa_{\max} \sqrt{1-\beta}(d+d_F)] + (d-d_F) \cosh[\kappa_{\max} \sqrt{1-\beta}(d+d_F)] \\ & - \frac{\beta d}{2} [\cosh(\kappa_{\max} \sqrt{1-\beta}(d+d_F)) + \cosh(\kappa_{\max} \sqrt{1-\beta}(d-d_F))] \\ & + \frac{\beta d_F}{2} [\cosh \kappa_{\max} \sqrt{1-\beta}(d+d_F) - \cosh \kappa_{\max} \sqrt{1-\beta}(d-d_F)] = 0 \quad (\text{A1-11}) \end{aligned}$$

If the location of the maxima is such that  $\kappa_{\max} \sqrt{1-\beta}(d-d_F) \lesssim 0.3$ ,  $\cosh \kappa_{\max} \sqrt{1-\beta}(d-d_F) \sim 1$ , and if  $\kappa_{\max}$ ,  $d$  and  $d_F$  are such that  $\kappa_{\max} \sqrt{1-\beta}(d+d_F) \gtrsim 2$ , then

$$\cosh[\kappa_{\max} \sqrt{1-\beta}(d+d_F)] \sim \sinh[\kappa_{\max} \sqrt{1-\beta}(d+d_F)] \sim \frac{\exp[\kappa_{\max} \sqrt{1-\beta}(d+d_F)]}{2}$$

Applying these approximations to (A1-11) and solving for  $\kappa_{\max}$  gives:

$$\kappa_{\max} = \frac{1}{\sqrt{1-\beta}(d+d_F)} \ln \left[ \frac{\beta(d+d_F)}{(d-d_F)(1+\sqrt{1-\beta}-\beta/2)} \right] \quad (\text{A1-12})$$

The thicker the free draining portion of the layer, then, the higher will be the electrolyte concentration at which the maxima in the  $Z(c)$

$\beta$  and  $d$  are known. Unfortunately, however, there appear to be no other relationships available which may be used to compute  $\beta$ ,  $d$  and  $d_F$ . Equation (A1-8) may be used in conjunction with (A1-14), but no third equation seems available which would allow the complete determination of  $\beta$ ,  $d$  and  $d_F$  for thin layers which are only partially free draining. Applying to (A1-5) the approximations which led to (A1-14) gives an expression for  $d$  which is independent of  $\kappa_1$ , and incompatible with (A1-13).

#### Adsorbed Layers in Which No Free Draining Occurs

If no free draining occurs within the adsorbed layer, the relative zeta potential will be less than one at cell electrolyte concentrations. Under these conditions, equation (2-63) applies:

$$Z = \frac{1}{\sqrt{1-\beta} \sinh(\kappa\sqrt{1-\beta}d) + \cosh(\kappa\sqrt{1-\beta}d)} \quad (2-63)$$

At high electrolyte concentrations,  $c_h$ , when  $[\kappa_h\sqrt{1-\beta}d] \gtrsim 2$ ,  $\sinh(\kappa_h\sqrt{1-\beta}d) \sim \cosh(\kappa_h\sqrt{1-\beta}d) \sim \exp(\kappa_h\sqrt{1-\beta}d)/2$ , (2-63) becomes:

$$-\kappa_h\sqrt{1-\beta}d \sim \ln\left[\frac{Z_h}{2}(1+\sqrt{1-\beta})\right] \quad (A1-15)$$

Under conditions of very dense adsorption, we may write

$\ln(1+\sqrt{1-\beta}) \sim \sqrt{1-\beta}$ , and (A1-15) yields:

$$\sqrt{1-\beta} = \frac{-\ln(Z_h/2)}{1+\kappa_h d} \quad (\text{A1-16})$$

where  $Z_h$  is the value of  $Z$  measured at the highest concentration  $c_h$  available ( $\kappa_h = 0.329\sqrt{c_h}$ ). At a very low electrolyte concentration,  $c_s$ , (A1-2) and (A1-3) apply, and (2-63) gives providing  $(\kappa_s \sqrt{1-\beta} d) < 0.3$ :

$$d = \frac{1-Z_s}{Z_s \kappa_s (1-\beta)} \quad (\text{A1-17})$$

where  $Z_s = Z(c_s)$  and  $\kappa_s = 0.329\sqrt{c_s}$ .

Hence, the values of  $Z$  and  $\kappa$  at the extremes of electrolyte concentration employed may be used to estimate the thickness and polymer adsorption factor for an adsorbed layer in which no free draining occurs.



## APPENDIX 2

THE EFFECT ON THE ZETA POTENTIAL OF A VARIABLE  
POLYMER ADSORPTION FACTOR

We wish to find a solution to the ordinary linear second order differential equation:

$$\psi''(x) = \kappa^2 [1 - \beta(x)] \psi(x) \quad (2-27)$$

For positive  $x$ , where:

$$\beta(x) = 1 - x/d \quad 0 \leq x \leq d \quad (\text{region 1})$$

$$\beta(x) = 0 \quad d \leq x \quad (\text{region 2})$$

The solution will describe the potential distribution adjacent to a charged infinite plane interface to which is adsorbed a neutral layer whose polymer adsorption factor,  $\beta(x)$ , decreases linearly from one to zero over a distance  $d$  from the charged surface.

Calling the potentials in regions 1 and 2  $\psi_1(x)$  and  $\psi_2(x)$  respectively, and assuming that the presence of the adsorbed layer does not affect the dielectric constant, the boundary conditions to be fulfilled are:

$$\text{at } x = d \quad \psi_1(d) = \psi_2(d) \quad (2-30)$$

$$\text{and} \quad \psi_1'(d) = \psi_2'(d) \quad (2-31)$$

$$x \rightarrow \infty \quad \psi(x) \rightarrow 0$$

and  $\psi'(x) \rightarrow 0$

Considering first the region inside the adsorbed layer:

$$\psi_1''(x) = \frac{\kappa^2 x}{d} \psi_1(x) \quad 0 \leq x \leq d \quad (\text{A2-1})$$

Since the coefficients of (A2-1) are analytic in the regions of interest, the equation has a power series solution (261).

Let

$$\phi(x) = \sum_{n=0}^{\infty} a_n x^n \quad (\text{A2-2})$$

be such a solution. Substituting in (A2-1) and differentiating gives:

$$\sum_{n=0}^{\infty} (n+1)(n+2)a_{n+2}x^n - \frac{\kappa^2}{d} \sum_{n=1}^{\infty} a_{n-1}x^n = 0 \quad (\text{A2-3})$$

$$\therefore 2a_2 + \sum_{n=1}^{\infty} \left[ (n+1)(n+2)a_{n+2} - \frac{\kappa^2}{d} a_{n-1} \right] x^n = 0 \quad (\text{A2-4})$$

This can only be true if all the coefficients are zero:

$$2a_2 = 0 \quad (\text{A2-5})$$

$$(n+1)(n+2)a_{n+2} - \frac{\kappa^2}{d} a_{n-1} = 0 \quad (\text{A2-6})$$

(A2-5) and (A2-6) can be solved for all the  $a_n$  in terms only of  $a_0$  and  $a_1$ , by solving (A2-6) for successive values of  $n$ :

$$a_2 = 0$$

$$a_3 = \frac{(\kappa^2/d)a_0}{2 \cdot 3}$$

$$a_4 = \frac{(\kappa^2/d)a_1}{3 \cdot 4}$$

$$a_5 = 0$$

$$a_6 = \frac{(\kappa^2/d)^2 a_0}{2 \cdot 3 \cdot 5 \cdot 6}$$

$$a_7 = \frac{(\kappa^2/d)^2 a_1}{3 \cdot 4 \cdot 6 \cdot 7}$$

and we see that in general:

$$a_{3m} = \frac{(\kappa^2/d)^m a_0}{2 \cdot 3 \cdot 5 \cdot 6 \dots (3m-1)3m} \quad m = 1, 2, 3, \dots \quad (\text{A2-7})$$

$$a_{3m+1} = \frac{(\kappa^2/d)^m a_1}{3 \cdot 4 \cdot 6 \cdot 7 \dots 3m(3m+1)} \quad m = 1, 2, 3, \dots \quad (\text{A2-8})$$

$$a_{3m+2} = 0 \quad m = 0, 1, 2, \dots \quad (\text{A2-9})$$

$$\therefore \phi(x) = a_0 \left[ 1 + \frac{(\kappa^2/d)}{2 \cdot 3} x^3 + \frac{(\kappa^2/d)^2}{2 \cdot 3 \cdot 5 \cdot 6} x^6 + \dots \right]$$

$$+ a_1 \left[ x + \frac{(\kappa^2/d)}{3 \cdot 4} x^4 + \frac{(\kappa^2/d)^2}{3 \cdot 4 \cdot 6 \cdot 7} x^7 + \dots \right] \quad (\text{A2-10})$$

Let:

$$F_1(x) = 1 + \sum_{m=1}^{\infty} \frac{(\kappa^2/d)^m x^{3m}}{2 \cdot 3 \cdot 5 \cdot 6 \dots (3m-1)3m} = 1 + \sum_{m=1}^{\infty} d_m(x) \quad (\text{A2-11})$$

$$F_2(x) = x + \sum_{m=1}^{\infty} \frac{(\kappa^2/d)^m x^{3m+1}}{3 \cdot 4 \cdot 6 \cdot 7 \dots 3m(3m+1)} = x + \sum_{m=1}^{\infty} f_m(x) \quad (\text{A2-12})$$

Then:

$$\phi(x) = a_0 F_1(x) + a_1 F_2(x) \quad (\text{A2-13})$$

Providing that the infinite series  $F_1(x)$  and  $F_2(x)$  converge, either may be a solution to (A2-1). Testing for convergence using the ratio test (262):

(i) For  $F_1(x)$ :

$$\begin{aligned} \left| \frac{d_{m+1}(x)}{d_m(x)} \right| &= \left| \frac{(\kappa^2/d)x^{3m+3}}{2 \cdot 3 \dots (3m-1)3m(3m+2)(3m+3)} \cdot \frac{2 \cdot 3 \dots (3m-1)3m}{(\kappa^2/d)^m x^{3m}} \right| \\ &= \frac{|(\kappa^2/d)x^3|}{(3m+2)(3m+3)} \end{aligned}$$

$$\therefore \lim_{m \rightarrow \infty} \left| \frac{d_{m+1}}{d_m} \right| = 0 \quad \text{for } (\kappa^2/d)x^3 \text{ finite}$$

$\therefore F_1(x)$  converges for finite  $x$  and  $d \neq 0$ .

$$(ii) \text{ For } F_2(x): \left| \frac{f_{m+1}(x)}{f_m(x)} \right| = \frac{|(\kappa^2/d)x^3|}{(3m+2)(3m+3)} \quad \text{and again}$$

$\lim_{m \rightarrow \infty} \left| \frac{f_{m+1}}{f_m} \right| = 0$  for finite  $x$  and  $d \neq 0$ . Therefore both series converge, (A2-13) is the general solution to (A2-1), and we may

write  $\psi_1(x) = \phi(x)$ . To apply the boundary conditions, we need

$\psi_1'(x)$ :

$$\psi_1'(x) = a_0 F_1'(x) + a_1 F_2'(x) \quad (\text{A2-14})$$

where

$$F_1'(x) = \sum_{m=1}^{\infty} \frac{(\kappa^2/d)^m x^{3m-1}}{2 \cdot 3 \cdot 5 \cdot 6 \dots (3m-1)} \quad (\text{A2-15})$$

$$F_2'(x) = 1 + \sum_{m=1}^{\infty} \frac{(\kappa^2/d)^m x^{3m}}{3 \cdot 4 \cdot 6 \cdot 7 \dots 3m} \quad (\text{A2-16})$$

In region 2, (2-27) becomes:

$$\psi_2''(x) = \kappa^2 \psi_2(x) \quad x \geq d \quad (\text{A2-17})$$

which has the solution:

$$\psi_2(x) = b_1 \exp(-\kappa x) + b_2 \exp \kappa x$$

Applying the boundary conditions for  $x \rightarrow \infty$  implies  $b_2 = 0$ , so

$$\psi_2(x) = b_1 \exp(-\kappa x) \quad (\text{A2-18})$$

The boundary conditions (2-30) and (2-31) are now used to calculate

$a_0$ ,  $a_1$  and  $b_1$  in terms of  $\psi(0)$ . Since from (A2-11) and (A2-12)  $F_1(0) = 1$  and  $F_2(0) = 0$ ,  $\psi(0)$  is just given by, from (A2-13):

$$\psi(0) = \psi_1(0) = a_0 \quad (\text{A2-19})$$

Some algebra gives for the remaining coefficients:

$$a_1 = -\psi(0) \left[ \frac{F_1'(d) + \kappa F_1(d)}{F_2'(d) + \kappa F_2(d)} \right] \quad (\text{A2-20})$$

$$b_1 = \psi(0) \left[ \frac{F_1(d)F_2'(d) - F_1'(d)F_2(d)}{F_2'(d) + \kappa F_2(d)} \right] \quad (\text{A2-21})$$

Now, the zeta potential in the presence of the adsorbed layer is related to the zeta potential in its absence through the expression for the charge density:

$$\sigma = -\frac{\epsilon}{4\pi} \psi'(0) \quad (1-16)$$

From (A2-14), (A2-15) and (A2-16), we see that:

$$\psi'(0) = a_1 = -\psi(0) \left[ \frac{F_1'(d) + \kappa F_1(d)}{F_2'(d) + \kappa F_2(d)} \right] \quad (\text{A2-22})$$

since  $F_1'(0) = 0$  and  $F_2'(0) = 1$ . Assume now that the adsorbed layer is essentially free draining, so that  $\zeta = \psi(0)$ . Substituting in (1-16), rearranging, and recognizing that  $\frac{4\pi\sigma}{\kappa\epsilon} = \zeta_0$  gives for the

Z, the relative zeta potential in the presence of the adsorbed layer:

$$Z = \frac{\zeta}{\zeta_0} = \kappa \left[ \frac{F_2'(d) + \kappa F_2(d)}{F_1'(d) + \kappa F_2(d)} \right] \quad (\text{A2-23})$$

where

$$F_1(d) = 1 + \sum_{m=1}^{\infty} \frac{(\kappa d)^{2m}}{2 \cdot 3 \cdot 5 \cdot 6 \dots (3m-1)3m} \quad (\text{A2-24})$$

$$F_1'(d) = \sum_{m=1}^{\infty} \frac{\kappa^{2m} d^{2m-1}}{3 \cdot 4 \cdot 6 \cdot 7 \dots 3m(3m+1)} \quad (\text{A2-25})$$

$$F_2(d) = d + \sum_{m=1}^{\infty} \frac{\kappa^{2m} d^{2m-1}}{3 \cdot 4 \cdot 6 \cdot 7 \dots 3m(3m+1)} \quad (\text{A2-26})$$

$$F_2'(d) = 1 + \sum_{m=1}^{\infty} \frac{(\kappa d)^{2m}}{3 \cdot 4 \cdot 6 \cdot 7 \dots 3m} \quad (\text{A2-27})$$

which is the result quoted in Section (IV-B-4) of Chapter 2.

In order to compute values for (A2-23), the expression was simplified algebraically somewhat to:

$$Z = \kappa \left[ \frac{1 + \kappa d + \sum_{m=1}^{\infty} \left(1 + \frac{\kappa/d}{3m+1}\right) \left(\frac{(\kappa d)^{2m}}{3 \cdot 4 \cdot 6 \cdot 7 \dots 3m}\right)}{\kappa + \sum_{m=1}^{\infty} (3m + \kappa d) \left(\frac{\kappa^{2m} d^{2m-1}}{2 \cdot 3 \cdot 5 \cdot 6 \dots (3m-1)3m}\right)} \right] \quad (\text{A2-28})$$

This expression was programmed on a Hewlett-Packard 9100B calculator. The two series were each calculated for a given  $\kappa$  and  $d$ , then divided, for successive values of  $m$  until  $|Z_{m+1} - Z_m| < 10^{-6}$ . Under this criterion of convergence, the values in Table A2-1 were obtained. It is from this table that the plot on Figure 2-5 was derived. The oscillation seen in this curve may be due to an oscillation in  $Z(m)$  about the series limit which was slow enough to satisfy the convergence criterion, or it may represent a true property of the solution. Changing the convergence criterion to  $|Z_{m+1} - Z_m| < 10^{-9}$  did not affect the results, however. No examination of the derivatives of  $Z(c)$  was made to investigate this question, as only the qualitative character of the behavior of  $Z$  as a function of  $c$  was required here.



